

Copyright

by

Emmanouil Karantinos

2019

The Dissertation Committee for Emmanouil Karantinos Certifies that this is the approved version of the following dissertation:

Choke Management and Production Optimization in Oil and Gas Fields

Committee:

Mukul M. Sharma, Supervisor

Larry W. Lake

Paul M. Bommer

Quoc P. Nguyen

Michael Baldea

Choke Management and Production Optimization in Oil and Gas Fields

by

Emmanouil Karantinos

Dissertation

Presented to the Faculty of the Graduate School of

The University of Texas at Austin

in Partial Fulfillment

of the Requirements

for the Degree of

Doctor of Philosophy

The University of Texas at Austin

August 2019

Dedication

To my parents,
Georgia and Akis

Acknowledgements

This dissertation would not have been possible to accomplish without the guidance from my supervisor, Dr. Sharma, the contribution of industry experts and the continuous support from family and friends. Firstly, my sincere gratitude goes Dr. Sharma for providing me with the opportunity to join UT Austin and his Research Group. Over the course of the program and despite his busy schedule he was always there to provide insight, share experiences and openly discuss interesting topics. His encouragement and constant belief in my skills were of primary importance in accomplishing the technically challenging second part of this dissertation. I would also like to thank the committee members, Dr. Lake, Dr. Bommer, Dr. Nguyen and Dr. Baldea for the constructive feedback on this work.

This project would not have been possible without Joseph Ayoub and Mehmet Parlar who furnished the initiative for this project as well as the member companies of the JIP on Hydraulic Fracturing and Sand Control for providing funding along with technical feedback on a yearly basis.

In addition, I would like to thank all the members of our Research group for sharing their perspectives and technical knowledge and the entire community of UT Austin for transforming these years into a joyful experience.

Finally, my sincere gratitude goes to my family and girlfriend for their unconditional love and encouragement.

Abstract

Choke Management and Production Optimization in Oil and Gas Fields

Emmanouil Karantinos, Ph.D.

The University of Texas at Austin, 2019

Supervisor: Mukul M. Sharma

When a well is brought on production, the selection of the optimum choke management strategy should aim towards maximizing well productivity and minimizing the risk of completion or wellbore failures. Until recently, ramp-up practices were based on liquid rate recommendations or empirical guidelines on choke sizes for the early life of a well. The objective of this dissertation is to establish a systematic method for the design of choke management strategies and flowback operations under wellbore completion and reservoir constraints. In order to account for multi-well pressure interference through the surface facilities, an integration scheme is proposed for the effective coupling of the well models with the surface gathering network. Finally, an optimization framework is deployed to maximize the daily operating income by properly adjusting well and network controls.

In the first part of the dissertation, we study choke management on an individual well basis. A general framework is introduced for comparing drawdown strategies for conventional and unconventional wells. Using analytical and numerical reservoir models we conclude that in conventional open-hole completions no more than 70% of the

drawdown should be applied in less than 30% of the ramp-up period. In formations characterized by high diffusivity (e.g. high permeability gas formations), the bottom-hole-pressure should be reduced linearly with time. Using nodal analysis, a systematic method is proposed for translating a set of wellbore, completion and reservoir constraints into a choke management schedule. Illustrative examples are presented both for conventional and unconventional wells. For hydraulically fractured wells, we introduced a coupled rate-stress criterion for mitigating proppant flowback and fracture closure near the wellbore. Application of the method suggests drawdown rates which are in agreement with successfully implemented field practices (5-10 psi/hour).

In order to capture well interference through the surface network, a multiphase (black-oil) pipeline network model has been developed. The network solver is formulated using fractional-flow theory, assuming steady state flow and concurrent flow of oil, water and gas phases. Using network topology, closed pipeline loops are unified into clusters where loop equations are solved using the Fletcher-Reeves conjugate gradient method. The network solver is validated using published network solutions, compared with field data and benchmarked against commercial network solvers. The well models are integrated with the surface gathering network using an explicit scheme that performs multi-point surface nodal analysis using fixed-point iteration. The integration scheme converges linearly and accurately captures well interference both for naturally flowing wells and wells on artificial lift. The integration scheme (forward model) is combined with various gradient based and derivative free optimization routines to optimize the well and network controls for a synthetic field. We observe that the use of integrated modeling can achieve significant

improvements in terms of daily operating income (by up to 30%). Finally, we introduce a reduced variable range approach which can accelerate the performance of sampling and global search methods in complex production systems.

This work introduces a systematic method for the design of choke management practices and presents new methods for integrating well models with the surface pipeline network.

Table of Contents

| | |
|--|----------|
| List of Tables | xvi |
| List of Figures | xix |
| List of Algorithms | xxv |
| Chapter 1: Introduction | 1 |
| 1.1 Research Motivation | 1 |
| 1.2 Research Objectives | 2 |
| 1.3 Dissertation Outline | 3 |
| MAJOR SECTION I: CHOKE MANAGEMENT FOR OIL AND GAS WELLS | 5 |
| Chapter 2: A General Method for the Selection of the Optimum Choke Management Strategy ^{1,2} | 6 |
| 2.1 Introduction | 6 |
| 2.2 Choke Management Considerations | 7 |
| 2.3 A General Framework for Comparing Bean-up Operations | 9 |
| 2.4 Numerical Simulation | 18 |
| 2.5 The Influence of Skin and Multiphase Flow | 28 |
| 2.6 Producing from multiple layers | 29 |
| 2.7 Conclusions | 32 |
| 2.8 Nomenclature | 36 |
| Chapter 3: Choke Management Strategies in Hydraulically Fractured Wells and Frac-Pack completions in Vertical Wells ¹ | 37 |
| 3.1 Introduction | 37 |
| 3.2 Factor Affecting Proppant Flowback | 39 |
| 3.3 Previous Studies in Unconventional Wells | 42 |

| | |
|--|----|
| 3.4 A General Framework for Defining and Comparing and Bean-up operations... | 44 |
| 3.5 Bean-up Strategies in Hydraulically Fractured Wells | 47 |
| 3.6 Bean-up Strategies in Frac-Pack Completions | 55 |
| 3.7 Summary and Conclusions | 64 |
| 3.7.1 Hydraulically fractured wells..... | 64 |
| 3.7.2 Frac-Pack Completions..... | 66 |
| 3.8 Nomenclature..... | 68 |
| Chapter 4: A Coupled Wellbore-Reservoir Model for Well Management ¹ | 69 |
| 4.1 Previous Studies on Choke Management | 69 |
| 4.1.1 Conventional Wells..... | 69 |
| 4.1.2 Unconventional Wells..... | 70 |
| 4.2 Design Considerations | 71 |
| 4.2.1 Wellbore Constraints | 71 |
| 4.2.2 Completion & Reservoir Constraints..... | 71 |
| 4.3 Model Description | 72 |
| 4.3.1 Reservoir Model..... | 72 |
| 4.3.2 Wellbore Model | 74 |
| 4.3.2.1 Pressure Drop along a Pipe Segment for three-phase flow ... | 75 |
| 4.3.3 Dynamic Nodal Analysis | 82 |
| 4.4 Choke Selection Algorithm | 85 |
| 4.5 Model Application | 86 |
| 4.5.1 Vertical Cased-Hole Well..... | 86 |
| 4.5.2 Hydraulically Fractured Horizontal Wells..... | 90 |

| | |
|---|------------|
| 4.6 Discussion and Conclusions | 97 |
| 4.7 Nomenclature..... | 98 |
| MAJOR SECTION II: FIELD-WIDE MODELING OF PETROLEUM FIELDS..... | 100 |
| Chapter 5: Modeling of Three-Phase Pipeline Networks | 100 |
| 5.1 Introduction..... | 100 |
| 5.2 Pertinent Literature Review | 101 |
| 5.2.1 Elements of Graph Theory | 101 |
| 5.2.2 Governing Equations | 102 |
| 5.2.3 Pipeline network solvers | 103 |
| 5.2.4 Phase split models..... | 105 |
| 5.2.5 Limitations of Numerical Models in Pipeline Networks | 107 |
| 5.3 Model Formulation for Three-Phase Branched Networks..... | 110 |
| 5.3.2 Analysis of Equations/ Unknowns..... | 111 |
| 5.3.3 Model Assumptions | 112 |
| 5.3.4 Conventions | 112 |
| 5.3.5 Formulation..... | 113 |
| 5.3.6 Workflow Summary..... | 115 |
| 5.4 Model Formulation for Three-Phase Looped Networks..... | 116 |
| 5.4.1 Assumptions and Conventions..... | 116 |
| 5.4.2 Analysis of equations/ unknowns | 117 |
| 5.4.3 Network Topology and Loop Clustering | 117 |
| 5.4.4 Solution for a Cluster of Loops..... | 122 |
| 5.4.4.2 Individual Cluster Topology and Tearing Variables..... | 123 |

| | | |
|------------|--|-----|
| 5.4.4.3 | Definition of Relative Residuals | 125 |
| 5.4.4.4 | Minimization of Loop Residuals..... | 130 |
| 5.4.4.5 | Termination Conditions..... | 132 |
| 5.4.4.6 | Initial Guess..... | 132 |
| 5.4.4.7 | Evaluation of the Cluster Solution | 134 |
| 5.4.5 | Solution of Networks containing loops..... | 135 |
| 5.4.6 | Workflow Summary..... | 138 |
| 5.5 | Handling multiple pressure boundary conditions | 140 |
| 5.6 | Modeling of gas injection networks..... | 142 |
| 5.7 | Validation and Benchmarking | 143 |
| 5.7.1 | Incompressible, Single-Phase Network Flows – Case 1..... | 143 |
| 5.7.2 | Incompressible, Single-Phase Network Flows – Case 2..... | 146 |
| 5.7.3 | Compressible, Single-Phase Network Flows..... | 147 |
| 5.7.4 | Benchmarking – Three phase network flows..... | 152 |
| 5.8 | Summary..... | 157 |
| 5.9 | Nomenclature..... | 159 |
| Chapter 6: | Integration of Well Models with Surface Facilities | 160 |
| 6.1 | Introduction..... | 160 |
| 6.2 | Components of the Integrated System..... | 163 |
| 6.2.1 | Well Models..... | 164 |
| 6.2.1.1 | Naturally Flowing Wells | 165 |
| 6.2.1.2 | Wells produced with an ESP..... | 166 |
| 6.2.1.3 | Gas-injected Oil Wells | 168 |

| | | |
|------------|--|-----|
| 6.2.2 | The surface production and gas injection networks..... | 171 |
| 6.3 | Integration Scheme | 173 |
| 6.3.1 | Coupling of the well models with the production network..... | 173 |
| 6.3.2 | Coupling the production with the gas injection network | 178 |
| 6.4 | Application of the Coupling Scheme..... | 179 |
| 6.4.1 | Description of Synthetic Field | 179 |
| 6.4.2 | Convergence Speed..... | 182 |
| 6.4.3 | Understanding Well Interference | 183 |
| 6.4.4 | Satisfying the gas injectivity condition..... | 187 |
| 6.5 | Conclusions..... | 188 |
| 6.6 | Nomenclature..... | 190 |
| Chapter 7: | Optimization of Well and Network Controls | 191 |
| 7.1 | Introduction..... | 191 |
| 7.2 | Review of Optimization Methods in Oilfield Management | 193 |
| 7.3 | Statement of the Optimization Problem..... | 195 |
| 7.4 | Optimization Framework..... | 197 |
| 7.4.1 | The Dakota Framework | 197 |
| 7.4.2 | Design of Experiment Methods (Sampling) | 201 |
| 7.4.3 | Local Search Methods..... | 204 |
| 7.4.3.1 | Newton and Quasi-Newton Methods | 204 |
| 7.4.3.2 | Mesh Adaptive Direct Search | 206 |
| 7.4.4 | Global Search Methods..... | 207 |
| 7.4.4.1 | Evolutionary Algorithms..... | 207 |

| | | |
|--------------|--|-----|
| 7.4.4.2 | Division of Rectangles | 208 |
| 7.4.4.3 | Surrogate Based Optimization | 209 |
| 7.5 | Objective Function and Constraint Evaluation | 210 |
| 7.5.1 | Evaluation of Objective Function for Gradient Based Optimization Methods | 211 |
| 7.5.2 | Evaluation of Objective Function for Derivative-Free Optimization Methods | 212 |
| 7.6 | Optimization Workflows | 213 |
| 7.7 | Application to Synthetic Field | 215 |
| 7.8 | Summary and Conclusions | 224 |
| 7.9 | Nomenclature | 226 |
| Chapter 8: | Summary, Key Findings and Future Work | 227 |
| 8.1 | Summary | 227 |
| 8.2 | Key Findings | 229 |
| 8.3 | Future Work | 231 |
| Appendices | | 233 |
| Appendix A1 | - Solution of Radial-Diffusion Equation | 233 |
| Appendix A2 | - Transient Model for Hydraulically Fractured Wells..... | 235 |
| Appendix B | – Choke Models..... | 238 |
| Single Phase | Incompressible Liquid..... | 238 |
| Single Phase | Gas Flow | 239 |
| Two Phase | Flow..... | 240 |
| Appendix C | – Fluid Properties | 241 |
| Gas | Properties | 241 |

| | |
|--|-----|
| Calculation of the Gas Deviation Factor, z | 242 |
| Calculation of Gas Density | 243 |
| Calculation of the Gas-Formation-Volume factor | 243 |
| Gas Viscosity | 244 |
| Oil Properties | 244 |
| Calculation of the Solution Gas-Oil Ratio | 245 |
| Calculation of the Oil compressibility, c_o | 246 |
| Calculation of the Oil formation Volume Factor | 247 |
| Calculation of the Oil Density | 248 |
| Calculation of Oil Viscosity | 249 |
| Appendix D – Material Balance Equation | 251 |
| References | 253 |

List of Tables

| | |
|--|-----|
| Table 2.1 Reservoir Properties..... | 12 |
| Table 2.2 Simulation Parameters | 23 |
| Table 3.1 Simulation Parameters for Hydraulically Fractures Wells. | 51 |
| Table 3.2 Comparing choke management strategies for a prolonged bean-up in a hydraulically fractured gas well..... | 55 |
| Table 3.3 Anticipated failure mechanisms and design criteria for frac-pack completions..... | 58 |
| Table 3.4 Pressure gradient of the instantaneous drawdown case for various fracture conductivities. Drawdown equals 500 psi. | 59 |
| Table 3.5 Simulation Parameters for frac-pack completions..... | 61 |
| Table 3.6 Frac-Pack Properties..... | 63 |
| Table 4.1 Velocity and pressure constraints for various types of completions | 72 |
| Table 4.2a Reservoir and wellbore properties for vertical cased-hole well..... | 87 |
| Table 4.2b Constraints imposed for vertical cased-hole well. | 87 |
| Table 4.3 System properties and constraints imposed for the design of clean-up operation | 93 |
| Table 4.4 Sample calculations for selecting choke sizing at early time | 94 |
| Table 5.1 Analysis of equations/unknowns for three-phase network flows | 108 |
| Table 5.2 Analysis of equations/ unknowns for three-phase branched networks..... | 111 |
| Table 5.3 Underdetermined system of equations/ unknowns for three-phase network flows..... | 117 |
| Table 5.4 Underdetermined system of equations/ unknowns for three-phase network flows..... | 123 |
| Table 5.5 Pipeline Properties for Validation Case 1 - Jeppson (1976)..... | 144 |

| | |
|---|-----|
| Table 5.6 Sinks/Sources for Validation Case 1 – Jeppson (1976)..... | 145 |
| Table 5.7 Pipelines Properties of Consumer Power Co. gas distribution network..... | 150 |
| Table 5.8 Sink/Sources and field pressure measurements for Consumer Powers Co. gas network | 151 |
| Table 5.9 Pipeline properties | 154 |
| Table 5.10 External volumetric flowrates entering the network..... | 154 |
| Table 5.11 Calculated nodal pressures using the proposed model and PIPESIM | 155 |
| Table 5.12 Calculated pipeline flowrates and pressure drops using the proposed model and PIPESIM | 156 |
| Table 5.13 Comparison of Loop Residuals..... | 156 |
| Table 6.1 Well controls for Base Case scenario | 180 |
| Table 6.2 Reservoir and Wellbore properties for producing wells..... | 181 |
| Table 6.3 Allocated compressor power for base case..... | 181 |
| Table 6.4 Surface nodal pressure per iteration step, k | 182 |
| Table 6.5 Comparison of controls and production rates for Base Case and Case A. | 184 |
| Table 6.6 Comparison of controls and production rates for Base Case and Case B..... | 185 |
| Table 6.7 Comparison of controls and production rates for Case B and Case C..... | 187 |
| Table 6.8 Provided versus required gas injection pressure..... | 188 |
| Table 7.1 Statement of the Field-Wide Production Optimization Problem..... | 196 |
| Table 7.2 Description of upper bound values for control variables..... | 196 |
| Table 7.3 Sampling and Optimization routines available in the DAKOTA framework . | 200 |
| Table 7.4 Reservoir and wellbore properties of synthetic field | 216 |
| Table 7.5 Description and bounds for optimization variables | 217 |
| Table 7.6 Optimization workflow for synthetic field case | 218 |

| | |
|--|-----|
| Table 7.7 Reduced upper bounds for well controls | 221 |
| Table 7.8 Comparison of optimal solutions using a) Static gas-lift curves and b) integrated production modeling | 223 |
| Table C.1 Input parameter for Black-Oil PVT Correlations..... | 241 |
| Table C.2 Coefficients for the calculation of solution gas (Vasquez and Beggs, 1980) . | 246 |

List of Figures

| | |
|---|----|
| Figure 2.1 Pressure gradient decline for a single choke adjustment..... | 11 |
| Figure 2.2 Lattice discretization of BHP and bean-up duration. | 11 |
| Figure 2.3 Variation of pressure gradients (dashed lines) for the applied bean-up (continuous line). The dotted line is the pressure gradient of the instantaneous drawdown..... | 12 |
| Figure 2.4 Comparing choke management strategies with respect to pressure gradient reduction and cumulative production for a bean-up duration of 10 hr. Reservoir properties shown in Table 2.1. | 14 |
| Figure 2.5 Parameters λ and RCP for all 251 strategies. Bean-up duration is 10 hr and the reservoir properties are presented in Table 2.1. | 15 |
| Figure 2.6 Choke management strategies yielding the minimum pressure gradients..... | 16 |
| Figure 2.7 Ratio of pressure gradient versus bean-up duration for the three optimum strategies. Reservoir properties presented in Table 2.1. | 17 |
| Figure 2.8 Dimensionless graph of BHP and bean-up time for different values of parameter a | 21 |
| Figure 2.9 Bean-up operation defined from Eq.(2.6) for $a=-0.9$ and choke settings of 15 min each. | 21 |
| Figure 2.10 Pressure gradient ratio versus bean-up duration for the case of an oil well in a 1,400x1,400 ft square reservoir..... | 24 |
| Figure 2.11 Comparing choke management strategies for an oil well producing from a square reservoir of 1,400x1,400 ft drainage area..... | 26 |
| Figure 2.12 Comparing choke management strategies for a gas well producing from a square reservoir of 1,400x1,400 ft drainage area..... | 26 |

| | |
|---|----|
| Figure 2.13 Optimum bean-up strategy versus relative bean-up duration for homogeneous and isotropic reservoirs of square drainage area..... | 27 |
| Figure 2.14 Ratio of pressure gradients versus bean-up duration for different values of S . $k=1\text{md}$, $1,400 \times 1,400$ ft drainage area. | 29 |
| Figure 2.15 Simple model of vertical gas well producing from two layers of different permeabilities..... | 32 |
| Figure 2.16 Comparing choke management strategies in a gas well producing from two layers. Bean-up duration is 48 hr and the drainage area is $1,400 \times 1,400$ ft. | 32 |
| Figure 3.1 Percent of proppant mass removed with respect to confining stress and fracture pressure gradient for fracture width equal to two, three and four proppant diameters (Shor & Sharma 2014). | 41 |
| Figure 3.2 Dimensionless graph of BHP and bean-up time for different values of parameter a | 46 |
| Figure 3.3 Bean-up operation defined from Eq. (6) for $a=-0.9$ and choke settings of 15 min each. | 46 |
| Figure 3.4 Fracture regimes with respect to confining stress and fracture pressure gradient. Proppant flowback is most likely to occur during the clean-up phase when effective stress is low (Shor & Sharma 2014)..... | 48 |
| Figure 3.5 Pressure gradient ratio versus bean-up duration for the case of a gas well. Fracture width is 1 mm and fracture length equals 120 ft. | 52 |
| Figure 3.6 Comparing choke management strategies for a hydraulically fractured gas well. Fracture width is 1 mm and fracture length equals 120 ft. | 54 |
| Figure 3.7 Schematic representation of a frac-pack completion. | 58 |

| | |
|--|-----|
| Figure 3.8 Ratio of pressure gradients versus bean-up duration for vertical open-hole completions and frac-pack lengths of 4, 12, 16, 22 and 30 ft. | 62 |
| Figure 3.9 Comparing choke management strategies for a frac-pack completion in a gas well. Drainage area is 1,000 ft x1,000 ft and reservoir and fracture properties as in Table 3.5 and Table 3.6. | 63 |
| Figure 3.10 Optimum bean-up strategy versus relative bean-up duration for homogeneous and isotropic reservoirs of square drainage area (after Karantinos et al. 2015). | 64 |
| Figure 4.1 Discretization and boundary conditions of pipeline model | 75 |
| Figure 4.2 Divergence of fixed-point iteration for a small choke size | 83 |
| Figure 4.3 Convergence of fixed-point iteration for a large choke size | 83 |
| Figure 4.4 Graphical interpretation of the modified secant method | 84 |
| Figure 4.5 Logic diagram of choke selection algorithm | 85 |
| Figure 4.6 IPR and VLP curves at initial conditions | 88 |
| Figure 4.7 Output of choke selection algorithm | 89 |
| Figure 4.8 Choke sizing as a function of time for separator pressure of 1000psi and 500psi. | 90 |
| Figure 4.9 Mass fraction of proppant produced..... | 91 |
| Figure 4.10 Failure envelope for 30% proppant flowback | 91 |
| Figure 4.11 Output for the design of clean-up operation..... | 95 |
| Figure 4.12 Choke sizing for Sw in SRV of 0.5 and 0.6 | 96 |
| Figure 5.1 Illustrative example of directed graph..... | 102 |
| Figure 5.2 A) Side-arm, B) Symmetric impacting and C) Asymmetric impacting junctions (after Stewart 2015)..... | 105 |

| | |
|--|-----|
| Figure 5.3 Loop topology and external flows..... | 106 |
| Figure 5.4 Split Coefficient versus the ratio of external volumetric fluxes. Loop topology shown in Figure 5.3. | 107 |
| Figure 5.5 Branched network with external three-phase streams. | 110 |
| Figure 5.6 Minimum Spanning Tree (MST) and Chords Identified using Kruskal's Algorithm..... | 118 |
| Figure 5.7 Iterative approach for identifying the nodes enclosing a closed pipeline loop | 119 |
| Figure 5.8 Concept of loop clustering in networks..... | 122 |
| Figure 5.9 Illustrative example of a cluster comprising two loops..... | 123 |
| Figure 5.10 MST and chords for the cluster topology shown in Figure 5.9..... | 124 |
| Figure 5.11 Concept of tearing variables..... | 124 |
| Figure 5.12 Isolated cluster in gas network. | 128 |
| Figure 5.13 Cluster residual as a function of the tearing variables..... | 129 |
| Figure 5.14 Illustrative example for coupling individual cluster solutions | 136 |
| Figure 5.15 Tail of network with two separators..... | 140 |
| Figure 5.16 Addition of no-flow link S1-S2..... | 140 |
| Figure 5.17 Network Topology of Validation Case 1 – Jeppson (1976)..... | 144 |
| Figure 5.18 Comparison of model results with published network solution (Jeppson, 1976) | 145 |
| Figure 5.19 Network topology and external flows | 146 |
| Figure 5.20 Comparison of nodal pressures with EPANET..... | 147 |
| Figure 5.21 Network topology of Consumer Power Co. gas network (Stoner, 1972)..... | 149 |

| | |
|---|-----|
| Figure 5.22 Comparison of model results (solid line) with pressure measurements (data points). | 152 |
| Figure 5.23 Network topology for comparing the proposed model with PIPESIM. | 153 |
| Figure 6.1 Concept of "Well Model" for naturally flowing wells | 165 |
| Figure 6.2 Concept of "Well Model" for wells produced with an ESP | 166 |
| Figure 6.3 Concept of "Well Model" for gas-injected oil wells | 168 |
| Figure 6.4 VLP curves for various gas injection rates..... | 170 |
| Figure 6.5 Gas Lift Curve (GLV) under constant WHP..... | 170 |
| Figure 6.6 Superimposed surface production (green) and gas injection (red) surface networks..... | 171 |
| Figure 6.7 Concept of Surface Nodal Analysis for well i..... | 174 |
| Figure 6.8 Iterative process for coupling the well models with the surface pipeline network. | 176 |
| Figure 7.1 Sampling from a two-dimensional parameter space using a) Pseudo MC b) Stratified Monte-Carlo and c) Latin Hypercube Sampling (after Adams et al. 2019) | 202 |
| Figure 7.2 Orthogonal array sampling in a three-dimensional parameter space. There is exactly one sample per bin (index =1) in any two-dimensional projection (strength =2) (after Giunta et al. 2003)..... | 203 |
| Figure 7.3 Pattern search methods for local optimization: The stencil undergoes operations of a) displacement and b) contraction in search of the local optimum (after Adams et al. 2018)..... | 207 |
| Figure 7.4 Illustrative example of Division of Rectangles in a two-dimensional variable space (adjusted from Adams et al. 2018)..... | 209 |

| | |
|---|-----|
| Figure 7.5 Objective function and constraint evaluation for gradient based methods..... | 211 |
| Figure 7.6 Objective function and constraint evaluation for derivative free methods..... | 213 |
| Figure 7.7 Network topology of synthetic field. Field comprises 12 wells and 4 compressors..... | 215 |
| Figure 7.8 Evolution of optimal objective value versus function evaluations..... | 219 |
| Figure 7.9 Evolution of optimal objective value versus function evaluations using a) full parameter range and b) reduced parameter range | 222 |
| Figure 7.10a Static Gas-Lift Curve for Well W2..... | 223 |
| Figure 7.10b Static Gas-Lift Curve for Well W9 | 223 |
| Figure A-1 Transient and Steady-State Inflow Performance Relationship | 237 |

List of Algorithms

| | |
|--|-----|
| Algorithm 4.1 Pseudocode for calculating the pipeline inlet pressure | 81 |
| Algorithm 5.1 Algorithm for identifying the nodes of non-overlapping loops | 120 |
| Algorithm 5.2 Fletcher-Reeves direction search algorithm (Nocedal, 2006)..... | 130 |
| Algorithm 5.3 Proposed Step search algorithm for three-phase network flows..... | 132 |

Chapter 1: Introduction

1.1 RESEARCH MOTIVATION

When a well is brought on production, the selection of an optimum choke management strategy should be aimed towards maximizing well productivity and minimizing the risk of wellbore failure. For example, in unconventional resources, an improper choke management strategy may trigger the backflow of excessive amounts of proppant, resulting in fracture closure and possible wellbore damage and loss of production (Wilson, 2015; Crafton, 2008). In conventional wells, an aggressive production ramp-up could give rise to completion stability issues or excessive sand production resulting in the erosion of surface or downhole equipment which can add to the maintenance costs and increase the likelihood of a temporary shut-in (Tiffin, 2005, Economides, 2008). Due to the prohibitive costs of intervention, operators have shown an ever-increasing awareness in properly designing well startup and shutdown procedures and have documented the predominant failure mechanisms in conventional and unconventional formations.

In order to prevent wellbore failures and maximize present value (PV), operators tend to implement somewhat aggressive choke management strategies that are based on rules of thumb and trial and error approaches (Barree, 1995; Willberg, 1998). For example, in unconventional formations, wells may be choked back if excessive proppant flowback is observed (Asgian, 1994). In such cases, damage to the fracture network might be irreversible, with a negative impact on well productivity (Wilson, 2015). In addition, empirical guidelines are expressed in terms of maximum liquid rates and do not take into

consideration well-specific reservoir properties or completion designs. An informal survey conducted among operators at the Joint Industry Project of Hydraulic Fracturing and Sand Control indicated that ramp-up strategies vary significantly among operators and no systematic method exists for properly designing ramp-up or clean-up procedures, providing a strong motivation for this work. In addition, multi-well pressure interference through the surface pipeline network has been shown to be important (Dutta-Roy, 1999) furnishing additional incentives to study well management (i.e. choke and artificial lift management) in complex production systems.

1.2 RESEARCH OBJECTIVES

This dissertation is intended to establish a systematic approach for the design of ramp-up and flow-back operations. The study is intended to identify the factors affecting a successful production ramp-up and recommend a workflow for the design of choke management strategies suitable not only for individual well analysis but also applicable on a field-wide basis. More specifically, this work is intended to:

- a) Review current industry practices on choke management and summarize the predominant failure mechanisms both for conventional and unconventional resources.
- b) Propose a systematic workflow and develop a numerical scheme for the design of choke management strategies under wellbore, completion and reservoir constraints.

- c) Formulate a computationally efficient three-phase network solver for modeling complex production and gas injection pipeline networks.
- d) Develop an efficient method for integrating well models with the surface pipeline network in order to ensure rate and pressure continuity at each well head.
- e) Deploy optimization methods to maximize daily operating income by properly adjusting well and network controls.

1.3 DISSERTATION OUTLINE

The dissertation is presented in two major sections. The first section comprises Chapters 2 to 4 and focuses on choke management for single wells. The second part of this dissertation (Chapters 5 to 7) discusses the integration of surface and subsurface models for field-wide production modeling and optimization. More specifically:

Chapter 2 discusses industry practices for choke management for conventional open-hole completions and introduces a framework for comparing drawdown strategies using both analytical and numerical reservoir models.

Chapter 3 studies drawdown strategies in hydraulically fractured wells and frac-pack completions in vertical wells using numerical reservoir models.

Chapter 4 proposes a coupled wellbore- reservoir model for the selection of choke sizes under wellbore, completion and reservoir constraints. Illustrative examples of the method are presented for conventional and unconventional wells.

Chapter 5 proposed a computationally efficient three-phase pipeline network solver. The network solver is validated against published network solutions, compared with field data and benchmarked with commercial solvers.

Chapter 6 delineates the process of coupling the well models with the surface gathering and gas injection pipeline networks.

Chapter 7 applies optimization methods to maximize the daily hydrocarbon production and operating income by properly adjusting well controls.

Finally, Chapter 8 summarizes the conclusions of this study and suggests topics for future research.

MAJOR SECTION I: CHOKE MANAGEMENT FOR OIL AND GAS WELLS

This major section (Chapters 2, 3 and 4) discusses choke management strategies for single wells.

Chapter 2 is adapted from the following publications:

- Karantinos (2015), A General Method for the Selection of an Optimum Choke-Management Strategy, Masters Report, The University of Texas at Austin
- Karantinos, E., Sharma, M. M., Ayoub, J. A., Parlar, M., & Chanpura, R. A. A General Method for the Selection of an Optimum Choke-Management Strategy, SPE Production & Operations, Vol. 32, May 2017

Chapter 3 is adapted from the following SPE publication:

- Karantinos, E., Sharma, M. M., Ayoub, J. A., Parlar, M., & Chanpura, R. A. Choke Management Strategies for Hydraulically Fractured Wells and Frac-Pack Completions in Vertical Wells, SPE Production & Operations, Vol. 33, August 2018

Chapter 4 is adapted from the following SPE publication:

- Karantinos, E., Sharma, M. M., Choke Management under Wellbore, Completion and Reservoir Constraints. Paper SPE 187190 presented at the SPE Annual Technical Conference and Exhibition, San Antonio, TX, 9-11 October 2017

Chapter 2: A General Method for the Selection of the Optimum Choke Management Strategy ^{1,2}

2.1 INTRODUCTION

Choke management strategies vary significantly among operators, primarily with respect to the overall duration of the ramp up process. An improper production schedule, characterized by a rapid and excessive drawdown could trigger massive sand production or proppant flowback, possibly resulting in completion impairment and wellbore failure.

Previous studies on bean-up protocols and sand production (Weingarten & Perkins 1995; Tiffin et al. 2003; Wong et al. 2003) have focused primarily on suggesting the maximum allowable drawdown or upper bound limits for fluid velocities in the near wellbore region, with respect to different failure mechanisms and completion types. Such recommendations are either based on compilation of data or have been derived from conventional models of tensile and/or shear failure. The application of analytical models usually provides an overly conservative estimate for the maximum allowable drawdown since sand production is considered to be concomitant with sand failure. Additional parameters affecting sanding severity include reservoir depletion and water breakthrough, which significantly reduces tensile strength. Researchers have underlined the notion that sand failure is a necessary; however not a sufficient condition for sand production to occur. Sanding events will only be triggered upon the presence of favorable hydraulic conditions (i.e., substantial pressure gradients) capable of mobilizing the failed sand or causing direct tensile failure of the weakly consolidated formation (Vaziri et al. 2002).

¹ Karantinos (2015), A General Method for the Selection of an Optimum Choke-Management Strategy, Masters Report, The University of Texas at Austin

² Karantinos, E., Sharma, M. M., Ayoub, J. A., Parlar, M., & Chanpura, R. A. A General Method for the Selection of an Optimum Choke-Management Strategy, SPE Production & Operations, Vol. 32, May 2017
Author Contributions: Karantinos E. performed the simulations and documented the methodology. Sharma M., Ayoub J., Parlar M. and Chanpura R. provided guidance and technical advice.

Based on the previous observation, choke management strategies should be aimed towards minimizing the near-wellbore pressure gradients induced by the applied overall drawdown. This notion has also been adopted by Geilikman et al. (2005) who studied the effect of bean-up procedures on fines migration. Keeping these potential formation damage mechanisms in mind we have proposed a method to select a bean-up or choke management strategy that minimizes the pressure gradient in the near wellbore region. The approach is quite general and can be applied whether the well is unloaded for the first time, pushed toward a peak rate or re-started after a long shut-in period. Within this study we assess the performance of different choke management strategies for wells that operate under constant BHP, rather than increasing surface rate. More specifically, we provide a framework for selecting an optimum series of decreasing BHP that will yield the greatest reduction in pressure gradients in the well vicinity, thus minimizing the risk of formation tensile failure, sand fluidization or gravel pack destabilization. To this end, we deploy the available analytical solution for wells operating under constant BHP whereas, for a more detailed analysis, numerical simulation is performed. Additionally, we address how the overall drawdown and bean-up duration may affect the selection of the optimum choke management strategy as well as the potential benefits of prolonging the overall duration of the ramp-up process. Finally, we assess the performance of bean-up strategies in vertical wells characterized by positive or negative skin factors as well as for vertical wells producing from multiple layers.

2.2 CHOKE MANAGEMENT CONSIDERATIONS

Choke management strategies (or bean-up operations) refer to the process of gradually increasing the rate or drawdown towards achieving a target, stabilized rate. A bean-up operation can be described with respect to increasing production rates or levels of drawdown. However, since the rate is primarily controlled by the choke size and since most of the previous work has

focused on determining the maximum allowable drawdown, we adopt the latter approach. In order to simplify the study of bean-up operations, we assume that the wellbore provides adequate vertical lift performance to produce all the fluid the reservoir can deliver during the ramp-up process. Consequently, bean-up operations can be studied on the basis of increasing levels of drawdown or, equivalently, decreasing BHP. Taking the previous considerations into account, a bean-up process can be defined by the following parameters: duration (t_B), overall drawdown (DD), number of BHP configurations (N), duration and magnitude of each subsequent reduction in BHP. Even though the term bean-up operation usually refers to the process of bringing a well on production, choke management strategies should also be considered during shut-in cycles. In fact, frequent and harsh shut-downs followed by rapid bean-ups can severely harm cementation due to differential strain loading, causing premature formation failure and possibly sanding (Vaziri et al. 2004).

Among the different parameters characterizing a bean-up operation, drawdown has been studied the most. Several papers have been published for predicting the maximum allowable drawdown that a formation or completion can withstand (Nouri et al. 2006; Wong et al. 2003). Methods vary from purely empirical to analytical models and sophisticated numerical schemes. However, since the parameters associated with numerical modeling are not routinely measured, major operating companies typically deploy analytical models that are based on either shear or tensile failure criteria. Such analytical models typically capture a single failure mechanism and assume that formation or completion failure is concomitant with the onset of sand production. Vaziri et al. (2002) showed that analytical models generally provide a high level of conservatism in predicting the maximum allowable drawdown, especially in HP/HT wells. Additionally, massive reservoir depletion and/or water-breakthrough limit the applicability and reliability of analytical methods (Nouri et al. 2006).

As opposed to the maximum drawdown, bean-up duration is a parameter that has not been extensively studied. Vaziri et al. (2004) suggests that a new step of the ramp-up process should not be applied unless pore pressures from the previous adjustment have reached a state of equilibrium within a close region around the well. That implies that formations characterized by high diffusivity can be brought on production within relatively short bean-up durations (Geilikman et al. 2005). Later in this study we address how the duration of the ramp-up process can determine the selection of the optimum choke management strategy with respect to reservoir and fluid properties.

2.3 A GENERAL FRAMEWORK FOR COMPARING BEAN-UP OPERATIONS

In this section we present the foundation for comparing choke management strategies in reservoirs that satisfy the assumptions of the radial diffusivity equation. Bean-up operations will be evaluated with respect to minimizing pressure gradients near the wellbore. Even though the assumptions associated impose limitations in the applicability of the method in real-life reservoirs, useful observations and general conclusions may be drawn.

For a single choke adjustment (or reduction in BHP), the pressure transient solution can be obtained from the analytical solution of the radial diffusivity equation for wells produced under constant BHP. The well is located in the center of a circular reservoir and satisfies the assumptions inherited in the radial diffusivity equation: the formation is considered to be homogeneous and isotropic with constant thickness, porosity and permeability. Additionally, the pore space is occupied by a single phase fluid of constant viscosity which is assumed to be slightly compressible. A thorough overview of the analytical solution is provided by Economides (1979). The dimensionless pressure or rate decline solution is given in tabulated form as well as in the Laplace space. For a detailed analysis, the solution can be obtained in real time and space variables by

numerically inverting the Laplace transformation using a commercially available numerical package (see Appendix A1).

Figure 2.1 illustrates the rate (or pressure gradient decline) as a function of dimensionless time, t_D , for a single reduction in BHP. The dimensionless time is defined as:

$$t_D = \frac{kt}{\phi\mu cr_w^2} \quad (2.1)$$

The pressure gradient obtains its maximum value immediately after a decrease in BHP. The rate of decline depends on the diffusivity constant, D , which depends on both formation and fluid properties:

$$D = \frac{k}{\phi\mu c} \quad (2.2)$$

A reservoir with high diffusivity will result in a rapid decline in pressure away from the wellbore upon the implementation of a single, instantaneous drawdown.

Bean-up operations are intended to reduce the wellbore flowing pressure from an initial pressure (P_i) to a final pressure (P_f) over the duration of the rate ramp-up process. Pressure, P_i , can either be the initial reservoir pressure or the average pressure after a sufficiently long shut-in period. The difference between P_i and P_f equates the overall drawdown (DD) of the ramp-up process, which is user specified. In order to systematically define choke management strategies, we provide the discretization shown in Figure 2.2. Different strategies can be selected, allowing for a reduction of BHP in a stepwise manner. The BHP is considered to be constant during every step of the ramp-up process. This particular discretization yields a total of 252 strategies, including the instantaneous drawdown case.

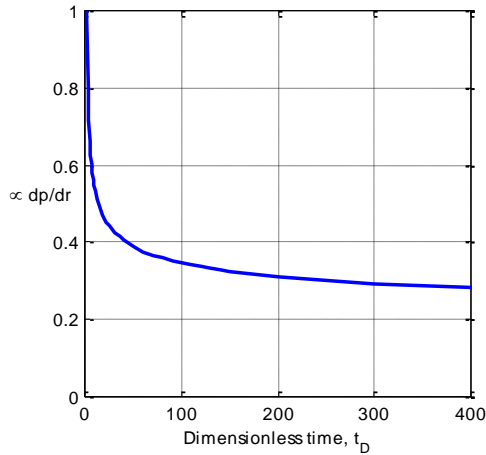


Figure 2.1 Pressure gradient decline for a single choke adjustment

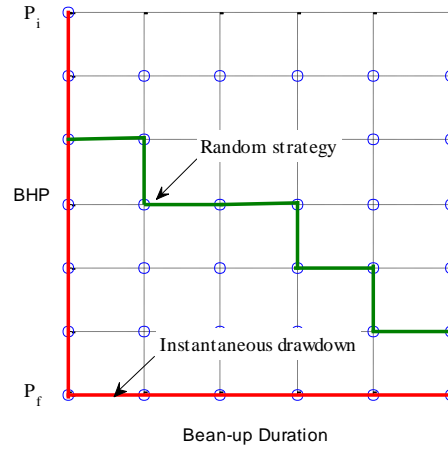


Figure 2.2 Lattice discretization of BHP and bean-up duration.

For a stepwise reduction in BHP, the pressure solution can be obtained by applying the principle of superposition with respect to the time variable. Several examples of the principle of superposition for wells producing under constant pressure are presented by Lee (1982). The principle of superposition allows us to calculate the pore pressure gradient near the wellbore after each choke adjustment. More specifically, the pressure gradient is calculated at the sandface 90 sec after a choke adjustment, for bean-up operations as well as for the instantaneous drawdown case. Prior to the passage of 90 sec, the pressure gradients will be greater compared to the calculated values however, the time frame of 90 sec is assumed to be representative of the maximum pressure gradient during a given choke adjustment and short enough to inhibit severe formation damage or sanding events of continuous nature.

Figure 2.3 illustrates the pressure gradient induced by a random bean-up operation. The reservoir properties are presented in Table 2.1. The BHP is gradually reduced until an overall drawdown of 1,200 psi is applied over a period of 10 hr. Figure 2.3 indicates that the maximum pressure gradient during the ramp-up process is smaller (by approximately 18%) compared to the

maximum pressure gradient induced by a single, instantaneous reduction in the BHP by 1,200 psi. Gradually reducing the BHP has a profound impact on pressure gradients near the wellbore.

Table 2.1 Reservoir Properties

| Reservoir Property | Value |
|--|--------------------|
| Permeability, k (md) | 100 |
| Porosity, ϕ | 0.2 |
| Total compressibility, c (psi^{-1}) | 5×10^{-5} |
| Fluid viscosity, μ (cp) | 1 |
| Drainage radius, r_e (ft) | 500 |
| Wellbore radius, r_w (ft) | 0.25 |

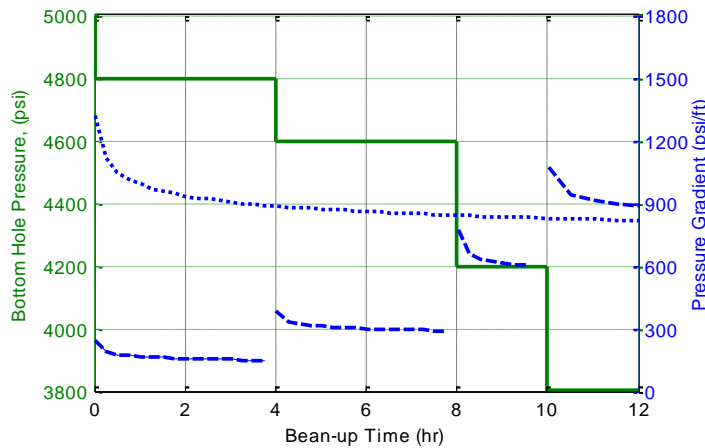


Figure 2.3 Variation of pressure gradients (dashed lines) for the applied bean-up (continuous line). The dotted line is the pressure gradient of the instantaneous drawdown.

In order to quantify the efficiency of a bean-up operation, we define the following two parameters:

- A) Lamda (λ) is the ratio of the maximum pressure gradient during the entire ramp-up process over the (maximum) pressure gradient of the instantaneous drawdown:

$$\lambda = \frac{(\text{dp}/\text{dr})_{\text{bean-up}}}{(\text{dp}/\text{dr})_{\text{inst. drawdown}}} \quad (2.3)$$

B) RCP (Ratio of Cumulative Production) is the ratio of the cumulative volume produced during the ramp-up process over the volume produced during the corresponding instantaneous drawdown for the same bean-up duration:

$$\text{RCP} = \frac{(\text{Volume Produced})_{\text{bean-up}}}{(\text{Volume Produced})_{\text{inst. drawdown}}} \quad (2.4)$$

Resulting from the definition, both parameters are smaller than one. We also need to reiterate that the smaller the parameter λ , the greater the efficiency of the ramp-up process with regard to pressure gradient reduction. A parametric analysis with respect to the applied drawdown proves that both ratios are independent of the overall drawdown. That implies that the efficiency of a strategy is not related to the magnitude of the drawdown.

It is important to note that the optimum strategy is not known a priori. Figure 2.4 illustrates three different strategies along with the corresponding parameters, λ and RCP. Intuition suggests that a stepwise strategy characterized by a linear-like reduction in BHP would be a good option (Figure 2.4a). However, an aggressive reduction in BHP during the early stage of the ramp-up process (Figure 2.4b) performs better, yielding lower pressure gradients (smaller value of parameter λ). On the contrary, poor performance is observed when a considerable reduction in BHP is applied toward the final stage of a bean-up operation (Figure 2.4c). The reservoir response to the aforementioned strategies can be explained as follows: applying a substantial drawdown during the early stage of the bean-up allows pressure gradients to dissipate with time, resulting in smaller gradients as additional drawdown is applied towards the final stage of the ramp-up process.

In other words, a large reduction in BHP has a smaller contribution to the pressure gradient if applied during the early stage of a bean-up operation.

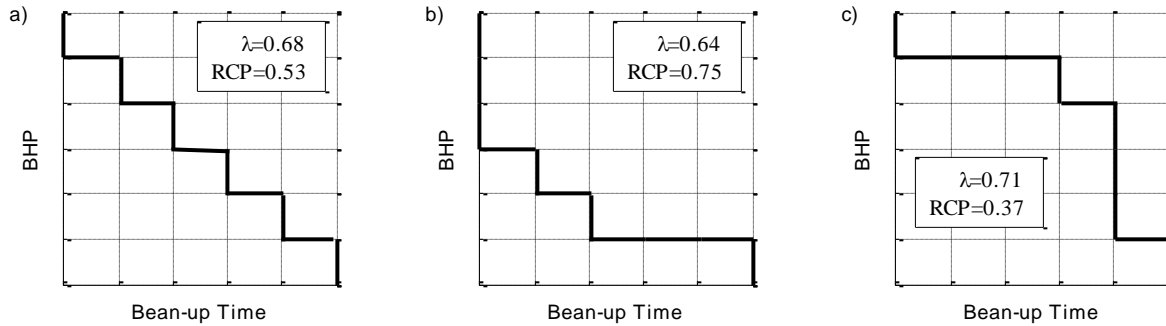


Figure 2.4 Comparing choke management strategies with respect to pressure gradient reduction and cumulative production for a bean-up duration of 10 hr. Reservoir properties shown in Table 2.1.

Figure 2.5 presents parameters λ and RCP for the entire set of 251 strategies, for a bean-up duration of 10 hr. Every point on this graph represents a different bean-up operation. Apart from minimizing pressure gradients near the wellbore, achieving a relatively high cumulative production during the ramp-up process could also be an additional objective, particularly in high-rate wells if a prolonged bean-up operation is applied. The graph illustrates that selecting a bean-up process from the upper-left part of the graph can accomplish both objectives (low pressure gradients and high cumulative production). Thus, low pressure gradients and high cumulative production are not mutually exclusive. On the other hand, selecting a bean-up strategy from the bottom-right part of the plot is expected to underperform, yielding high pressure gradients and small volumes of cumulative production. Such inefficient strategies are characterized by a significant reduction in BHP toward the mid/final stage of the ramp-up process (see Figure 2.4c).

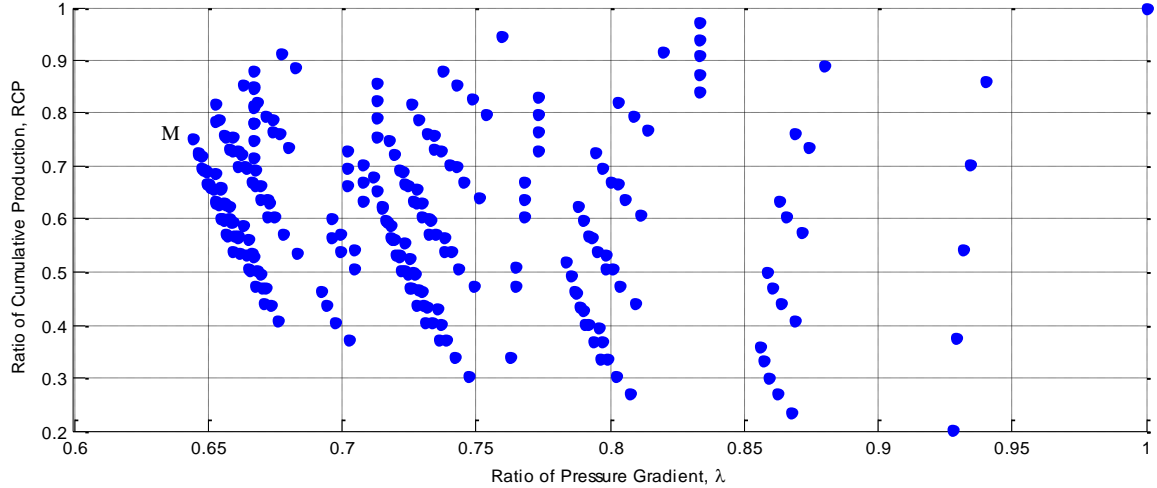


Figure 2.5 Parameters λ and RCP for all 251 strategies. Bean-up duration is 10 hr and the reservoir properties are presented in Table 2.1.

Nevertheless, minimizing pressure gradients during the bean-up operation is the primary objective of this study. To this end, we need to identify the strategy that yields the minimum value of λ . This strategy is considered to be the optimum choke management strategy. For example, in Figure 2.5, the optimum strategy corresponds to point M. To identify the optimum strategies, multiple comparisons were performed for a wide range of the following parameters: diffusivity constant, reservoir radial extent and bean-up duration. The runs indicate that among the 251 strategies, three of them consistently appear to be the optimum. The optimum strategies are presented in Figure 2.6. It is important to note that all three optimum strategies fall below the dashed diagonal.

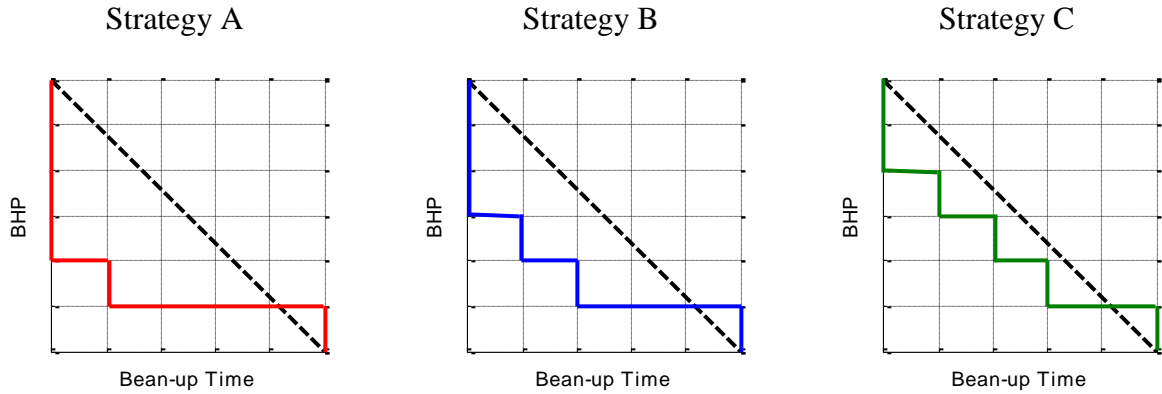


Figure 2.6 Choke management strategies yielding the minimum pressure gradients.

The performance of strategies A, B and C for various bean-up durations is presented in Figure 2.7. Any strategy other than A, B or C lies above the curves shown. Also, the vertical dashed line indicates the end of infinite acting period, t_{EIA} , calculated by the formula proposed by Earlougher (1977), in field units:

$$t_{EIA} \text{ (hr)} = 1200 \frac{\phi \mu c}{k} r_c^2 \quad (2.5)$$

We observe that for a short bean-up, lasting less than 5 hr, all three strategies have similar performance, with Strategy A performing slightly better. In this case, the fastest way to bring a well on production corresponds to strategy A. However, the performance of Strategy A reaches a plateau ($\lambda=0.67$) since 67% of the overall drawdown is applied instantaneously (see Figure 2.6a), which constitutes a limitation of the proposed discretization. For bean-up operations longer than 5 hr but shorter than the t_{EIA} , strategies B and C have similar performance. For prolonged bean-up operations strategy C is the optimum. The following trend is observed: increasing the bean-up duration causes the optimum bean-up strategy to shift towards a less aggressive reduction in BHP (gradually progressing from Strategy A to C).

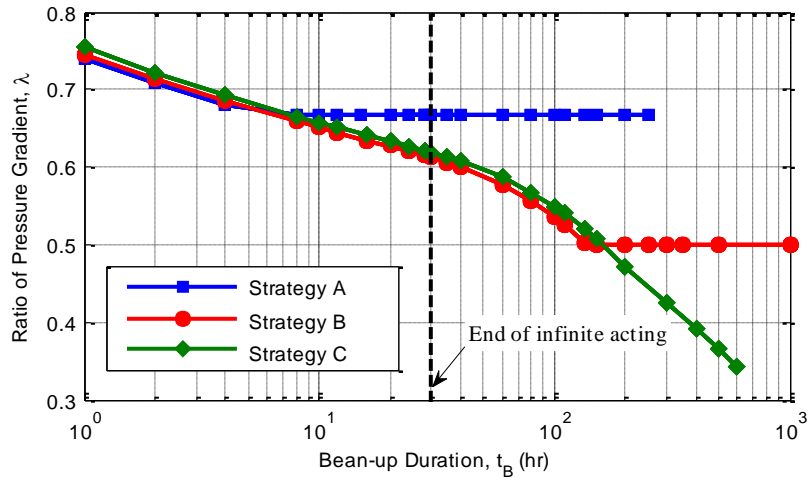


Figure 2.7 Ratio of pressure gradient versus bean-up duration for the three optimum strategies. Reservoir properties presented in Table 2.1.

Figure 2.7 also indicates that λ , which is proportional to the maximum pressure gradient, decreases logarithmically with bean-up duration, provided that the optimum choke strategy is selected. For durations lasting longer than t_{EIA} , pressure gradients rapidly decline, as a result of reservoir depletion. If reservoir depletion occurs before the end of the bean-up process, rate decline causes additional decrease in pressure gradients, which justifies the deviation from the original slope.

In this section, we performed a comparison of 251 bean-up operations derived from a lattice discretization. The discretization is rather coarse allowing for a maximum of six choke adjustments, with an initial reduction in BHP at the beginning of the process. Since we only used a maximum of six choke adjustments, this may pose limitations in the applicability of the method for prolonged bean-up operations. However, with the current analysis, the following conclusions can be drawn:

- The performance of bean-up operations is independent of the overall applied drawdown. Consequently, determining the maximum allowable drawdown and selecting a choke management strategy are two distinct tasks that should be conducted independently and iteratively to yield the optimum short-term production schedule.
- Low pressure gradients and relatively high volumes of cumulative production are not mutually exclusive, provided that an optimum strategy is selected. In general, a better performance is observed if a large reduction in BHP is applied during the early stage of the ramp-up process.
- The performance of a choke management strategy depends on the duration of the bean-up process as well as on reservoir properties. For relative short durations (i.e., infinite acting behavior), a large initial reduction in BHP is preferred (Figure 2.6a) whereas, for a prolonged bean-up operation a more gradual adjustment is suggested (Figure 2.6c).
- For relatively short bean-up operations (i.e., infinite acting behavior), pressure gradients reduce logarithmically with increasing duration. The impact of reservoir boundaries increases the performance bean-up operations due to reservoir depletion. Thus, prolonging the duration of the ramp-up process could prove beneficial in reservoirs characterized by high diffusivity.

2.4 NUMERICAL SIMULATION

The method described in the previous section is general and can be used for comparing choke management strategies in any reservoir of interest, provided that the transient pressure solution is known. For cases where the strict assumptions of the analytical solution are not satisfied, a reservoir simulator can be deployed to acquire the pressure solution and the

corresponding pore pressure gradients near the wellbore. This section describes the process of comparing bean-up operations in oil and gas wells using a reservoir simulator.

As mentioned previously, the objective is to minimize pressure gradients near the wellbore. A reservoir simulator provides the capability of calculating the pressure gradients at any point of interest, depending on the anticipated failure mechanism. For a slotted liner or open hole completion, pressure gradients may be calculated at the sandface or within the plastic zone whereas, for a cased and perforated well, emphasis should be placed on minimizing pressure gradients within the gravel pack or along the perforations. The near-wellbore region should be meshed accordingly in a refined manner. Data including spatially varying formation properties, phase behavior, reservoir shape and well location can be incorporated within the input file of the reservoir simulator in use.

In order to overcome the shortcomings of the previously presented coarse discretization of the choke settings, we introduce the following single-parameter dimensionless equation that describes the variation of BHP as a function of time:

$$P_D = \frac{P_{wf}(t_{BD}) - P_f}{P_i - P_f} = \frac{(a+1)(1-t_{BD})}{a(1-t_{BD})+1}, \quad (2.6)$$

where t_{BD} is the dimensionless bean-up time, defined as

$$t_{BD} = \frac{t}{t_B} \leq 1 \quad (2.7)$$

The left-hand side of Eq.(2.6) is the fraction of the cumulative drawdown applied at time, t_{BD} , of the ramp-up process. Parameter, a , represents different choke management strategies, as shown in Figure 2.8. The instantaneous drawdown case corresponds to $a=-1$, whereas for $a=0$, the BHP is linearly reduced with time. For positive values of a , the BHP configuration is located in

the upper-right triangular section of Figure 2.8. As discussed previously, the optimum BHP configuration falls under the diagonal, thus, from now on we will focus exclusively on negative values of a .

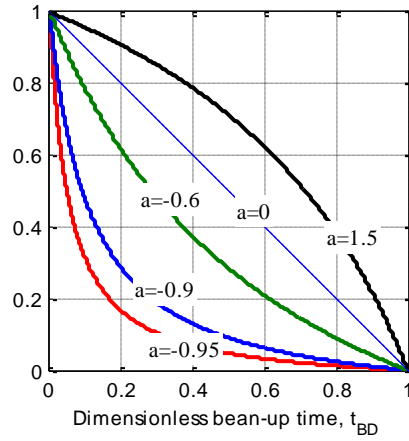


Figure 2.8 Dimensionless graph of BHP and bean-up time for different values of parameter a

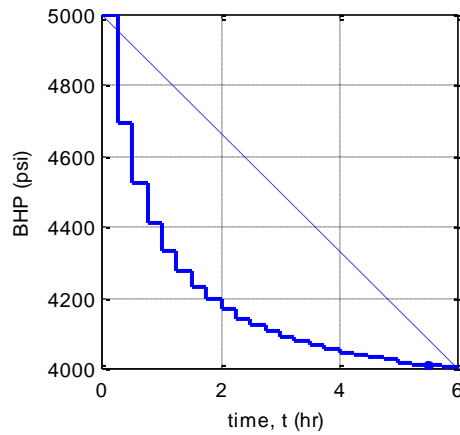


Figure 2.9 Bean-up operation defined from Eq.(2.6) for $a=-0.9$ and choke settings of 15 min each.

In order to simulate and ultimately compare choke management strategies, the continuously varying wellbore pressure, as calculated by Eq. (2.6) is converted into steps of constant BHP. The duration of each step is considered to be equal to 15 min. Figure 2.9 presents

a BHP schedule derived in this manner. The proposed steps of constant BHP can be implemented in the field with the use of a computer-adjusted choke.

Different bean-up scenarios (values of a) are compared for oil and gas wells located at the center of a homogeneous and isotropic square reservoir. The reservoir and bean-up properties are presented in Table 2.2. The combination of reservoir properties and bean-up parameters yields a pool of possible scenarios. Pressure gradients are calculated 0.2 ft away from the wellbore using a refined mesh of square elements (0.2 x 0.2 ft) in the well vicinity. The wellbore comprises of cells operating under constant BHP (i.e., infinite productivity index).

Table 2.2 Simulation Parameters

| Formation Properties | |
|---|-------------------------|
| Field dimensions (ft x ft) | 600x600; 1,400x1,400 |
| Porosity, ϕ | 0.15 |
| Permeability, k (md) | 1; 10; 100; 1000 |
| Temperature, T (F) | 250 |
| Initial Reservoir Pressure, P_i (psi) | 5,000 |
| Irreducible water saturation, S_{wr} | 0.25 |
| Rel. permeability exponent, n | 2.5 |
| Bean-up Properties | |
| Total drawdown (psi) | 1,000; 2,000; 3,200 |
| Duration, t_B (h) | 2; 4; 8; 12; 24; 48 |
| Bean-up strategy, a | -0.99 to 24 (20 values) |
| Oil Reservoir – Fluid Properties | |
| Oil density (API) | 30 |
| Specific gravity of gas (air =1) | 0.70 |
| Viscosity, μ (cp) | ~ 0.75 |
| Compressibility (psi ⁻¹) | $\sim 3 \times 10^{-5}$ |
| Bubble point pressure, P_b (psi) | 3,000 |
| Residual oil saturation, S_{or} | 0.25 |
| Gas Reservoir – Fluid Properties | |
| Specific gravity of gas (air =1) | 0.70 |
| Viscosity, μ (cp) | ~ 0.025 |
| Residual gas saturation, S_{gr} | 0.15 |

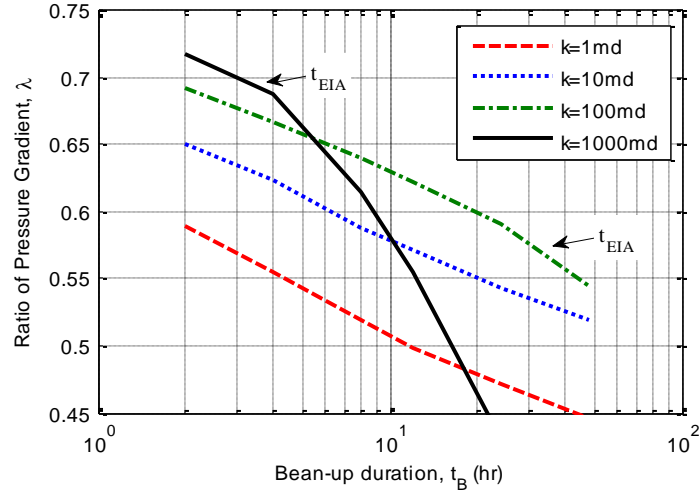


Figure 2.10 Pressure gradient ratio versus bean-up duration for the case of an oil well in a 1,400x1,400 ft square reservoir.

For each set of formation and fluid properties, choke management strategies (parameter a) are evaluated for bean-up durations (t_B) varying from 2 to 48 hr. For each t_B , the optimum strategy is selected. Figure 2.10 illustrates the reduction in pressure gradients with increasing bean-up duration for different values of formation permeability in an oil well producing from a 1,400x1,400 ft reservoir. For durations shorter than t_{EIA} (i.e., infinite acting behavior) pressure gradients reduce logarithmically with t_B . On the other hand, if the no-flow boundary is felt during the bean-up process, greater pressure gradient reduction can be achieved. This observation implies that bean-up operations are expected to be more efficient in fields characterized by high diffusivity, where t_{EIA} is limited to a couple of hours. Eq. (2.2) suggests that the fluid component of the diffusivity constant is the product of viscosity and compressibility which is greater by approximately an order of magnitude for the case of a gas hydrocarbon. Consequently, the effect of bean-up operations will be more pronounced in high permeability, gas fields.

Figures 2.11 and 2.12 present the performance (parameter λ , y-axis) of different choke settings (parameter a , x-axis) with respect to permeability and bean-up duration for oil and gas wells. Based on these plots, the following observations can be made:

- For infinite acting behavior (see Figures 2.11a, 2.11b, 2.11c, 2.12a, 2.12b), strategies between $a=-0.9$ to $a=0$ have similar performance. In fact a BHP setting with $a=-0.9$ performs slightly better. This observation is in agreement with the conclusions derived from the discretized model discussed in the previous section.
- For relatively short bean-up operations (i.e., infinite acting behavior), the best way to bring a well on production, even for a bean-up duration of 2 hr, corresponds to a parameter of -0.9 . Figure 2.8 suggests that such a strategy can be implemented in the field by applying no more than 70% of the overall drawdown during the initial 20% of the bean-up duration. On the contrary, values of parameter a smaller than -0.95 yield higher pressure gradients and should be avoided.
- For the case when reservoir boundary effects can be felt (see Figures 2.11d, 2.12c, 2.12d) the optimum choke strategy shifts from $a=-0.9$ to greater values, depending on the duration of the ramp-up process. More precisely, the longer the bean-up duration, the larger the value of parameter a .

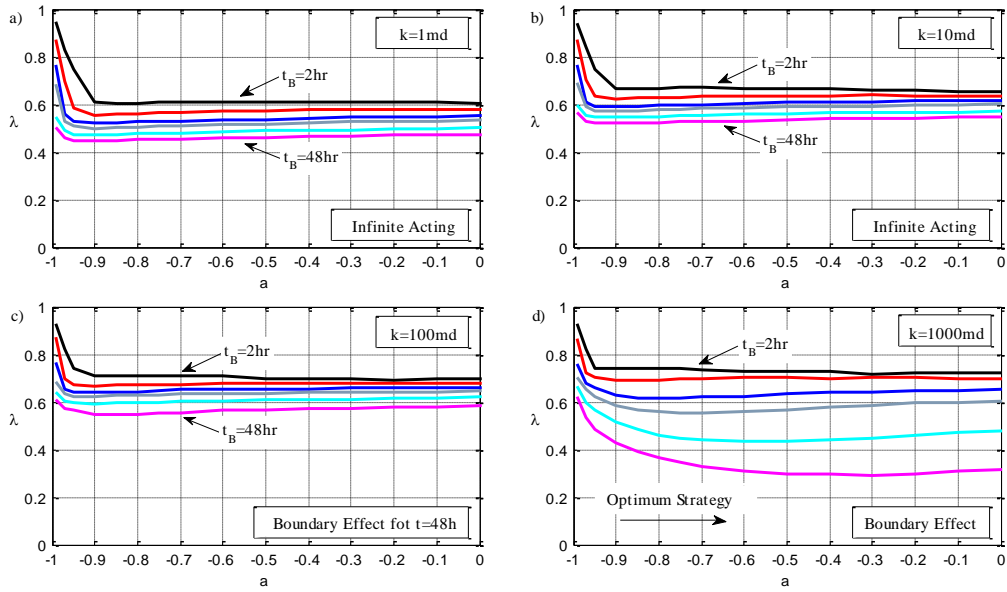


Figure 2.11 Comparing choke management strategies for an oil well producing from a square reservoir of 1,400x1,400 ft drainage area.

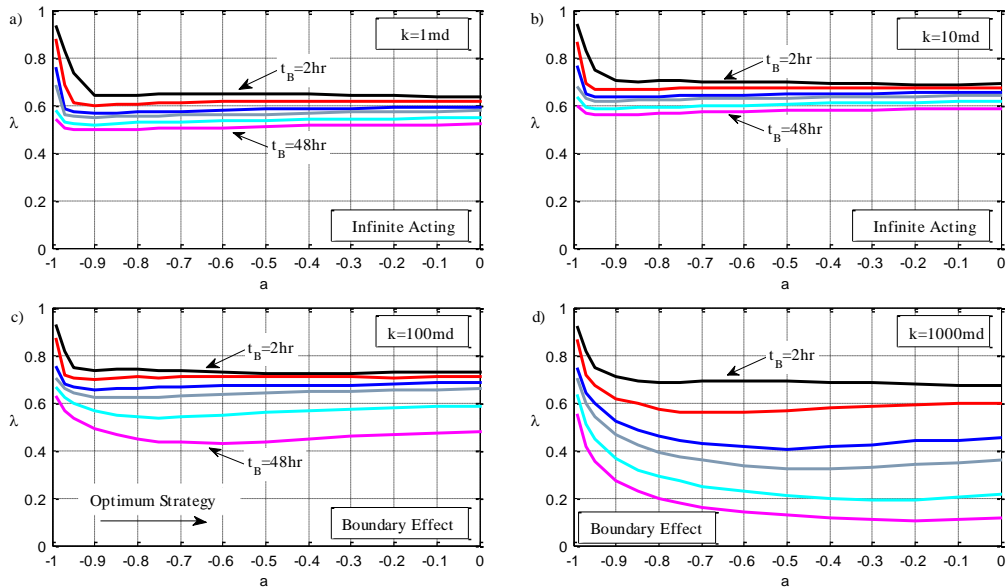


Figure 2.12 Comparing choke management strategies for a gas well producing from a square reservoir of 1,400x1,400 ft drainage area.

Simulation results were utilized to express the optimum strategy as a function of bean-up duration, formation and fluid properties. To this end, we define the relative duration t^* :

$$t^* = \frac{t_B}{t_{EIA}}, \quad (2.8)$$

which provides a relative measure of the bean-up duration with respect to reservoir properties and acreage. For a homogeneous and isotropic reservoir with square drainage area, the optimum strategy can be obtained from Figure 2.13. The points have been generated using Eq. (2.5) and approximate values from Table 2.2 for both oil and gas wells. The increasing trend between duration and parameter a indicates that a prolonged bean-up operation should be combined with a slower reduction in BHP.

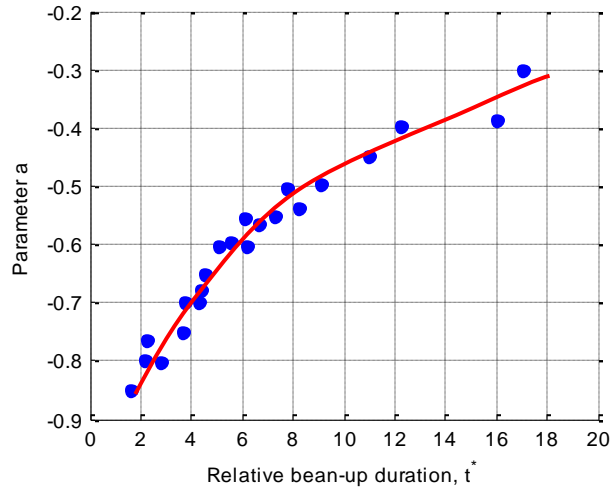


Figure 2.13 Optimum bean-up strategy versus relative bean-up duration for homogeneous and isotropic reservoirs of square drainage area.

2.5 THE INFLUENCE OF SKIN AND MULTIPHASE FLOW

In this section we assess the effect of skin and multiphase flow on the performance of choke management strategies. More specifically we investigate whether such conditions can boost or compromise the efficiency of bean-up operations with respect to reducing pressure gradients near the wellbore.

A positive or negative skin factor can be implemented in the model by assuming an impaired or stimulated zone of constant permeability k_{skin} near the wellbore. The permeability of the impaired (or stimulated) zone can be obtained from the following equation:

$$S = \left[\frac{k}{k_{skin}} - 1 \right] \ln \left[\frac{r_{skin}}{r_w} \right] \quad (2.9)$$

Using the reservoir properties of Table 2.2, the near-wellbore permeability was modified to account for an impaired zone of 3 ft. The methodology of the previous section is adopted with pressure gradients calculated within the impaired zone for the instantaneous drawdown case as well as for each candidate bean-up operation. Figure 2.14 illustrates the reduction in pressure gradients with respect to increasing bean-up duration for different values of skin. Positive values of skin negatively affect the performance of bean-up operations, yielding higher values of λ and thus larger pressure gradients, relative to the corresponding instantaneous drawdown. On the contrary, the presence of a stimulated zone increases diffusivity near the well, ultimately improving the performance of bean-up operations. We also observe that prolonging the duration of a ramp-up process has a more profound effect on a stimulated well. For $S=-2$, increasing the bean-up duration from 4 to 8 hr further reduces λ by 10% (from point A to point B) whereas for $S=3$ pressure gradients only reduce by an additional 4% (point C to point D).

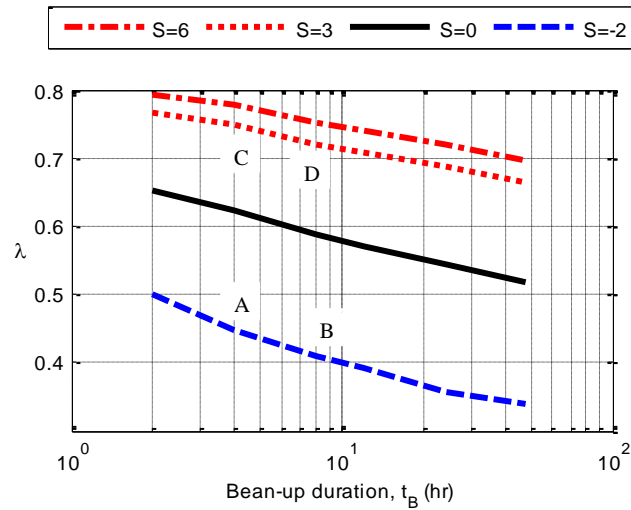


Figure 2.14 Ratio of pressure gradients versus bean-up duration for different values of S . $k=1\text{md}$, $1,400 \times 1,400$ ft drainage area.

Multiphase flow near the wellbore may occur due to various reasons including water coning, flow of condensate or BHP dropping below the bubble point. Multiphase flow near the wellbore gives rise to relative permeability, which reduces the effective permeability. The reduction in effective permeability is equivalent to the presence of a positive skin factor, with the implications presented previously. Choke management strategies were compared for wellbore pressures dropping below the bubble point and the results indicate an effect similar to that of a positive skin factor. The impact of multiphase flow appears to depend on the endpoint values as well as on the shape of the relative permeability curves.

2.6 PRODUCING FROM MULTIPLE LAYERS

So far, we have focused exclusively on vertical wells producing from a single horizontal layer. However, most wells are completed along multiple layers or produced from a combination of normally pressured and over pressured productive zones. In this section, we discuss in a

qualitative manner how the presence of multiple producing layers may affect the selection of an optimum bean-up strategy.

Figure 2.15 illustrates a well intersecting two layers of different permeabilities. Prior to initiating the ramp-up process, the pressure is hydrostatic. The vertical permeability of the formation is assumed to be spatially constant and equal to 1 md. Additionally, the BHP is considered to be constant along the vertical portion of the well since a wellbore model has not been incorporated.

The well is subjected to an instantaneous drawdown. The abrupt nature of the applied drawdown combined with low vertical permeability disrupts the hydrostatic pressure distribution near the wellbore. At the very early stage of production, both layers behave autonomously, as if the presence of the other is neglected. That causes pressure gradients to be different among the layers, giving rise to higher pressure gradients in the low permeability zone (point L1). However, with increasing time, vertical pressure equilibrium is restored and pressure gradients converge to an equal value.

Using a bean-up operation allows vertical pressure equilibrium to re-establish shortly after the first few choke adjustments. In this case, pore pressure gradients are approximately equal in both layers and the formation behaves like a medium with horizontal permeability equal to:

$$k_{av} = \frac{h_1 k_1 + h_2 k_2}{h_1 + h_2} \quad (2.10)$$

Figure 2.16 presents the performance of different choke management strategies applied on a gas well producing from both layers I and II. Bean-up operations are compared for a duration of 48 hr in a gas reservoir with drainage area of 1,400x1,400 ft. The graph includes the performance

of different choke management strategies for the sequence of layers as well as for the case where each layer is produced independently. From this graph, we may infer the following:

- The optimum choke management strategy for a well producing from both layers corresponds to a value of a equal to -0.85 (Points A and B). This strategy is different compared to the optimum strategy of $a=-0.6$ which should have been applied if Layer II was to be produced independently (Point C). Consequently, the optimum strategy for a well producing from a series of layers should not be approximated by using individual layer permeabilities, but rather the weighted average horizontal permeability.
- The coupling of both layers yields greater pressure gradients (Point A) in the high permeability layer compared to the anticipated pressure gradient if that layer was the only one to be produced (Point C). On the other hand, smaller pressure gradients are observed in the low permeability layer. Consequently, the coupling of layers proves to be beneficial for the low permeability layer and detrimental for the sand prone, high permeability layer. That implies that in order to limit the maximum pressure gradient under a threshold value, smaller overall drawdowns should be applied in multi-layered formations compared to fields comprising a single high-permeability layer of identical properties.

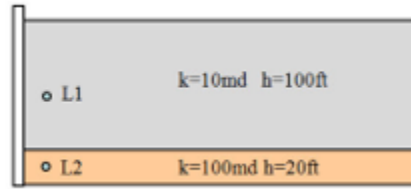


Figure 2.15 Simple model of vertical gas well producing from two layers of different permeabilities.

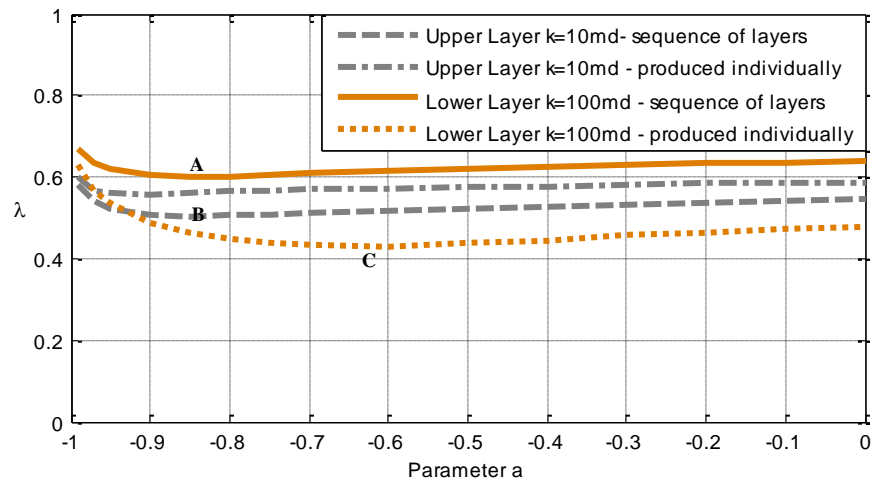


Figure 2.16 Comparing choke management strategies in a gas well producing from two layers. Bean-up duration is 48 hr and the drainage area is 1,400 x 1,400 ft.

2.7 CONCLUSIONS

In this study we provided a general framework and a systematic method for comparing and selecting choke management strategies. Examples were illustrated for vertical, openhole oil and gas wells located at the center of homogeneous and isotropic reservoirs of circular and square drainage area. The method is general and can be used in any real-life reservoir. The proposed

method is intended to be used in conjunction with either analytical pressure transient models or reservoir simulators that provide an estimate of the pressure transient response of wells with varying drawdowns. The process for selecting an optimum choke management strategy can be summarized in the following steps:

Step 1-Determine the maximum allowable drawdown

- a) In competent rocks, a conservative estimate can be obtained from analytical models that account for shear and/or tensile failure. Finite element modeling is suggested in cases where reservoir depletion and water cut limit the reliability of analytical models.
- b) In weakly consolidated formations, a proxy can be obtained from drawdown guidelines based on compilation of data and screen erosion criteria (Tiffin et al. 2003).

Step 2-Determine the maximum allowable pressure gradient

The maximum pressure gradient can be obtained from analytical models based on direct tensile or cavity failure. The critical pressure gradient can also be approximated through Darcy's Law from rate (or fluid velocity) limitations (Wong et al. 2003) and field specific formation properties. Laboratory experiments can provide additional verification to ensure that the selected pressure gradient will not cause massive fluidization of the disaggregated material.

Step 3-Determine the duration of the ramp-up process

Construct a graph of λ vs bean-up duration (t_B), similar to Figure 2.10, and use this to select a bean-up duration ensuring that the pressure gradient stays below the maximum pressure gradient obtained in Step 2.

Step 4-Select the optimum choke management strategy

For the selected drawdown and bean-up duration, select the optimum choke management strategy (value of a) by constructing a plot of λ vs a for the selected bean-up duration (t_B), similar to Figure 2.11.

Within this study we also evaluated the effect of skin and provided a qualitative assessment of how choke management strategies should be selected in multi-layered formations. The following practical conclusions may be drawn from this study:

- For relatively short durations (i.e., infinite active behavior), bean-up strategies have similar performance as far as no more than 70% of the overall drawdown is applied within the initial 20% of the bean-up process. This recommendation can be used as a rule of thumb to inhibit excessive pressure gradients near the wellbore.
- For longer bean-up operations (i.e., when the effect of the no-flow boundaries is felt), the BHP should be reduced more gradually. For a prolonged bean-up, the BHP should be reduced linearly with time.
- For relatively short bean-up operations (i.e., infinite acting behavior), pressure gradients reduce logarithmically with increasing bean-up duration. Boundary effects have a positive influence on the performance of bean-up operations as a result of reservoir depletion. That implies that in reservoirs of high diffusivity (high perm gas) we may prolong the duration to benefit from boundary effects.
- Positive skin factors and multiphase flow negatively affect the performance of bean-up operations since they limit diffusivity and thus the dissipation of pressure gradients near the wellbore.
- In multilayered formations, the optimum choke management strategy should be selected with respect to the weighted average horizontal permeability. The co-

existence of layers causes pressure gradients to be relatively elevated in the high-permeability, sand prone layers which may pose additional limitations to the maximum allowable drawdown.

2.8 NOMENCLATURE

a = parameter describing bean-up operations

BHP = Bottom Hole Pressure

D = diffusivity constant

DD = drawdown

h_i = thickness of layer i (ft)

k = horizontal permeability (md)

k_{av} = weighted averaged horizontal permeability

k_{skin} = horizontal permeability of the impaired/stimulated zone (md)

P_i = initial reservoir pressure (psi)

P_f = BHP at the end of the ramp-up process (psi)

P_{wf} = wellbore flowing pressure (psi)

RCP = cumulative production of bean-up operation over cumulative production of instantaneous drawdown

r_e = drainage radius (ft)

r_{skin} = radius of impaired or stimulated zone (ft)

r_w = well radius (ft)

s = skin factor

t = time (h)

t^* = relative bean-up duration

t_{EIA} = end of infinite acting period (h)

t_B = bean-up duration (h)

t_{BD} = dimensionless bean-up time

t_D = dimensionless time

λ = pressure gradient of bean-up operation over pressure gradient of instantaneous drawdown

Chapter 3: Choke Management Strategies in Hydraulically Fractured Wells and Frac-Pack completions in Vertical Wells¹

3.1 INTRODUCTION

Choke management strategies vary significantly among operators and no definite guidelines exist for properly designing clean-up procedures or drawdown schedules in hydraulically fractured wells and frac-pack completions. The clean-up phase is considered to be the most crucial time in the life of the well: the proppant is adjusted and packed in place, setting the foundation for short and long term productivity. Upon the completion of stimulation treatments, operators are sometimes tempted to apply aggressive drawdown schedules which may result in increased proppant back-production, reduced fracture conductivity and hence poor well performance. An abrupt decrease in bottom-hole-pressure (BHP) can also give rise to completion stability issues, with particularly severe implications in offshore developments. In addition, the destabilization of the annular pack due to high velocities through the perforations may cause a series of operating nuances such as the plugging of screens or flowlines, the erosion of surface or downhole equipment which add to the maintenance costs and increase the likelihood of a temporary shut-in. These factors have increased the awareness of properly designing flowback procedures in order to maximize fracture conductivity and improve long term performance.

Fracture conductivity may be compromised due to various mechanisms such as proppant crushing or removal, embedment, and plugging of proppant pore space by formation fines or gel residue (Robinson et al. 1992, Barree et al. 1995, Andrews et al. 1998). In order to improve well

¹ Karantinos, E., Sharma, M. M., Ayoub, J. A., Parlari, M., & Chanpura, R. A. Choke Management Strategies for Hydraulically Fractured Wells and Frac-Pack Completions in Vertical Wells, SPE Production & Operations, Vol. 33, August 2018

Author Contributions: Karantinos E. performed the simulations and documented the methodology. Sharma M., Ayoub J., Parlari M. and Chanpura R. provided guidance and technical advice.

productivity, several proppant flowback mitigation techniques are available in the industry. Among the most widely used methods is forced fracture closure, a controlled flowback technique where fracturing fluids are produced in a controlled manner, forcing the fracture to close and holding the proppant in place. Induced closure can improve the recovery of fracturing fluids and better results are expected when combined with aggressive proppant schedules. Ely et al. (1990) provided general guidelines for successfully implementing forced closure. Resin Coated Sand (RCS) has also been deployed with considerable success by increasing proppant pack cohesion, permeability and resistance to crushing, compared to conventional, uncured proppant. Further improvement can be achieved when used in conjunction with forced closure, in which case curing should not occur prior to closure. The use of RCS is typically associated with elevated costs, when operators use RCS in the tail-in stage of the stimulation process (Van Batenburg et al. 1999). The use of fibers or heat-sensitive plastic films can also improve the geomechanical properties of the propping agent, at considerably lower costs compared to RCS. Finally, in the case of excessive proppant back-production, the injection of curable resins or surface modification agents has been applied (Nguyen et al. 2006) with variable success, particularly in long intervals. It is important to note that no method can guarantee proppant-free production under all conditions.

Choke management strategies are intended to be used in conjunction with other proppant flowback mitigation techniques and provide an extra margin of safety in reducing proppant flowback, retaining post stimulation fracture conductivity and minimizing the risk of future well intervention. In this study, we compare and suggest choke management strategies for hydraulically fractured wells and frac-pack completions in vertical wells.

3.2 FACTOR AFFECTING PROPPANT FLOWBACK

In general, the production of proppant depends on the design and implementation of the fracturing treatment (proppant size, fracture width, rheology of fracturing fluids) as well as on the implemented flowback and production strategy. The flowback and production strategy is considered to be of primary importance since it determines the hydrodynamic or geomechanical loading on the proppant pack that keeps the fracture open once the stimulation job is complete.

A properly designed stimulation treatment is less likely to result in excessive amounts of proppant being produced once the well is brought on production. Various factors determine the effectiveness of proppant placement from fluid rheology and leak-off to slurry density gradients and crossflow between layers of varying effective stress (Barree et al. 1995). Gadde and Sharma (2005), Malhotra and Sharma (2012), and Blyton et al. (2015) provided a detailed documentation of the factors affecting proppant placement including fracturing fluid rheology, proppant type and concentration, formation leak-off, and pump rate. A careful selection of these parameters combined with a high concentration of proppant towards the tail-in stage can ensure that the proppant pack is tightly packed near the wellbore. A dense pack minimizes the effective stress acting on the particles and prevents proppant crushing, which could possibly result in connectivity loss with the wellbore. The stability of the pack can also be improved by gradually increasing the proppant size, using RCS and/or fibers, and preventing the over-flushing of the proppant during the very last stage of the treatment.

Once stimulation is complete, fracture conductivity is retained by arches of proppant that keep the fracture propped. The “arch effect” converts the hydrodynamic force acting on particles into shear stresses at the points of contact between particles and ultimately conveys this force to the fracture face. The fluid force acting on particles is a body force proportional to the pore pressure

gradient and the volume of the proppant. At some critical hydrodynamic force, shear failure occurs and the arch collapses, adding to the amount of proppant being produced. Numerical results and experimental data show that the critical parameters affecting the stability of the proppant pack are fracture closure stress, pore pressure gradient and proppant size relative to fracture width (Andrews et al. 1996).

Increasing pressure gradients during flowback tend to reduce the amount of proppant retained in the fracture and thus have a detrimental effect on the stability of the pack. On the contrary, increasing confining stress enhances the stability of the proppant pack (improved friction forces) unless the mechanical strength of the proppant is exceeded, in which case proppant crushing and fracture closure occur. Shor and Sharma (2014) conducted grain-scale Discrete Element Modeling (DEM) simulations to assess the combined effect of effective closure stress, pore pressure gradient and particle size on the amount of proppant being produced from a single planar fracture. Their results indicate that the destabilizing effect of pore pressure gradient is more pronounced in wide fractures (relative to proppant size) and/or low effective stress. Figure 3.1 illustrates the percentage of proppant mass removed as the effective closure stress and fracture pressure gradient are changed, for fracture widths equal to two, three and four proppant diameters.

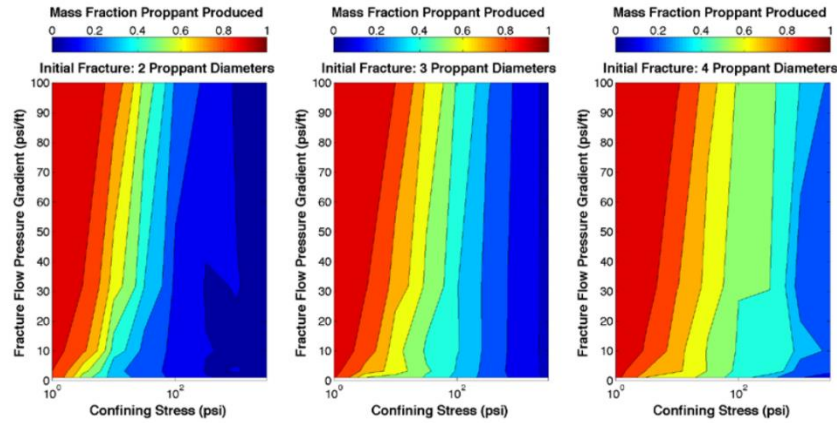


Figure 3.1 Percent of proppant mass removed with respect to confining stress and fracture pressure gradient for fracture width equal to two, three and four proppant diameters (Shor & Sharma 2014).

It can be observed that wider fractures produce more proppant under equivalent stress and flow conditions. A wide fracture will not allow stable bridges to form, resulting in more proppant being produced. Early experimental (Milton-Taylor 1992) and numerical studies (Asgian 1994) attest to the fact that fracture widths greater than 5-6 proppant diameters are inherently unstable and thus extremely susceptible to movement induced by pressure gradients. The use of poly-disperse proppant is associated with increased proppant back-production compared to mono-disperse proppant subject to similar conditions. The use of RCS or surface modification agents (SMA) can improve proppant cohesion and inter-granular friction thus increasing the critical pressure gradient at which arch failure occurs. Finally, additional parameters affecting the stability of the arches are proppant angularity and face roughness. However, these factors are thought to be of secondary importance compared to closure stress, pressure gradient and fracture width (Andrews et al. 1998). Although the concepts reviewed in this section apply to both hydraulically fractured wells and frac-pack completions, for proppant flowback to occur in a frac-pack completion screen has to fail. In the context of frac-pack, a potential cause for failure is incomplete

pack or not so tight annular pack that is re-arranged in the annulus right across the perforations, exposing the screens to formation sand at high velocities and possible screen erosion (Wong et al. 2003).

3.3 PREVIOUS STUDIES IN UNCONVENTIONAL WELLS

Choke management strategies vary significantly among operators, primarily with respect to the overall duration of the ramp-up process. An improper ramp-up schedule, could induce excessive hydrodynamic and geomechanical loading of the proppant resulting in conductivity loss or completion stability issues for the case of frac-packs. Due to the prohibitive costs of intervention, operators express an ever increasing awareness in properly designing clean-up schedules or production strategies in both conventional and unconventional formations.

Previous studies on choke management have focused primarily on high permeability, poorly consolidated formations with an emphasis on sand production. Drawdown guidelines and near-wellbore fluid velocity limitations have been suggested based on shear or tensile failure (Vaziri et al. 2002), screen erosion (Wong et al. 2003, Tiffin et al. 2003) or gravel pack destabilization (Economides et al. 2008). Geilikman et al. (2005) investigated the effect of bean-up protocols on fines migration on the principle of minimizing near wellbore pressure gradients. Using the same criterion, Karantinos et al. (2015) introduced a general framework for defining drawdown schedules and compared bean-up strategies for vertical, open-hole completions. They concluded that for short-lived bean-up operations (i.e., infinite acting behavior) no more than 70% of the overall drawdown should be applied during the initial 30% of the bean-up duration. On the other hand, for longer bean-up procedures (i.e., when the effect of reservoir boundaries can be felt) the optimum choke management strategy depends on the duration of the process as well as on formation and fluid properties.

For the case of unconventional formations, choke management strategies have so far not been studied in a systematic and consistent manner. The literature has rather focused on understanding the mechanisms affecting proppant flowback and providing qualitative or field specific recommendations for improving forced closure. The general consensus is that clean-up operations should be designed to inhibit proppant settling and ensure that closure stress is gradually increased to prevent proppant crushing. To this end, Robinson et al. (1988) and Ely et al. (1990) suggested that flowback operations should be initiated immediately after the cessation of stimulation treatments and before the breaking of the gel, ensuring that the proppant remains suspended within the target zone. In cases of various stress zones, clean-up rates should exceed intra-zone crossflow rates in order to avert the vertical overflushing of the proppant (Barree et al. 1995). The effect of leak-off has also been discussed in the literature and flowback rates should be greater compared to the overall leak-off in order to assist proppant migration towards the mouth of the fracture and enhance reverse screenout at the wellbore. Based on successful clean-up procedures, Robertson et al. (1988) suggested that clean-up operations should be initiated at low rates of 10-20 bbl/hr using choke increments of 2/64 in for several days or even weeks. On the contrary, the use of large chokes (or large choke increments) would abruptly reduce Bottom-hole-Pressure (BHP) resulting in rapid loading of the proppant beads, increasing the likelihood of proppant crushing and fracture pinching near the wellbore. Ely et al. (1990) recommended rates of 10-15 gallons per minute for up to 30 minutes after near-wellbore fracture closure has been identified based on surface pressure measurements, followed by flowback rates of 1-2 bpm. Using field data from the Barnett shale, Willberg et al. (1998) suggested that forced closure should be augmented using flowback rates in excess of 3 bpm. According to Crafton (2008), the industry has been using flowback rates ranging anywhere from five to a few tenths of barrels per minute. The

above recommendations indicate a lack of consensus among the industry and the implementation of such guidelines cannot guarantee a successful clean-up procedure. The sequence of increasing flowback rates or choke sizes is expected to be highly dependent on various field-specific parameters including fracture height, closure stress, pay interval, matrix permeability, proppant size, fracturing fluid rheology and wellbore/tubing properties.

In high-permeability formations, existing guidelines are exclusively applicable to open-hole gravel packs (OHGP), stand-alone-screens (SAS) or cased and perforated completions, with no particular recommendations found in the literature with respect to frac-pack completions. The fundamental difference between fractured wells in unconventional formations and frac-pack completions lies in the formation permeability, the fracture width relative to proppant size and formation leak-off, with all three parameters being substantially greater in frac-packs, in addition to presence of screens and an annular pack in frac-packs. High leak-off rates provide a natural mechanism of gradually building-up closure stress on proppant beads, making proppant crushing less likely to occur compared to forced closure applied in unconventional fractures. In addition, high leak-off rates allow the implementation of greater rates, reducing the time necessary to ramp-up production to a few hours or days. In this study, we examine whether the process of selecting choke management strategies in frac-packs differs from open-hole completions. We also assess the effect of fracture properties on the efficiency of bean-up operations.

3.4 A GENERAL FRAMEWORK FOR DEFINING AND COMPARING AND BEAN-UP OPERATIONS

Choke management strategies (or bean-up operations) refer to the process of gradually increasing the drawdown or production rate for recovering fracturing fluids or bringing a well on production after a long shut-in period. A bean-up operation is fully defined by three quantities: the overall drawdown (DD), the duration (t_B) and the sequence of reducing BHP with respect to time.

Karantinos et al. (2015) introduced a general method for defining and comparing bean-up operations. For completeness, as well as for ease of understanding, the method is briefly discussed below. Bean-up strategies can be defined using the following, single-parameter dimensionless equation that describes the variation of BHP as a function of time:

$$\frac{P_{wf}(t_{BD}) - P_f}{P_i - P_f} = \frac{(a+1)(1-t_{BD})}{a(1-t_{BD})+1}, \quad (3.1)$$

where t_{BD} is the dimensionless bean-up time, defined as

$$t_{BD} = \frac{t}{t_B} \leq 1 \quad (3.2)$$

The left-hand side of Eq. (3.1) is the fraction of the cumulative drawdown applied at time, t_{BD} , of the ramp-up process. Parameter, a , represents different choke management strategies, as shown in Figure 3.2. The instantaneous drawdown case corresponds to $a=-1$, whereas for $a=0$, the BHP is linearly reduced with time. For positive values of a , the BHP reduction is located in the upper-right triangular section of Figure 3.2.

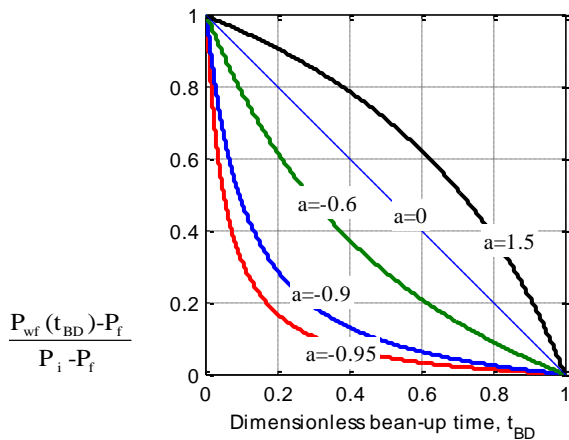


Figure 3.2 Dimensionless graph of BHP and bean-up time for different values of parameter a .

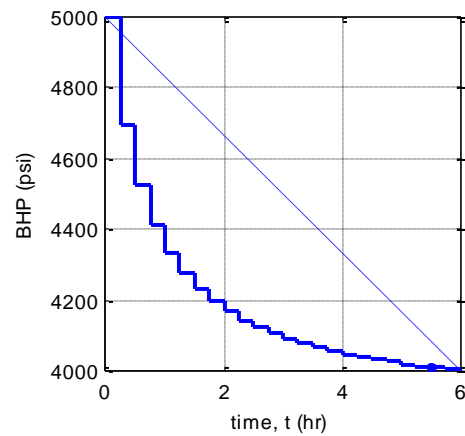


Figure 3.3 Bean-up operation defined from Eq. (6) for $a=-0.9$ and choke settings of 15 min each.

In order to simulate and ultimately compare choke management strategies, continuously varying wellbore pressure, as calculated by Eq. (3.1) is converted into steps of constant BHP. The duration of each step is considered to be equal to 15 min. Figure 3.3 presents a BHP schedule derived in this manner. The proposed steps of constant BHP can be implemented in the field with the use of a computer-adjusted choke.

Depending on the anticipated failure mechanisms, bean-up operations should focus on minimizing pressure gradients at critical points of interest. In an open hole completion, near wellbore pressure gradients should be minimized in order to inhibit fines migration or mobilization of the disaggregated material. Using the principle of minimizing pressure gradients, Karantinos et al. (2015) introduced a ratio, λ . This ratio is defined as the maximum pressure gradient observed during a specific bean-up operation over the maximum pressure gradient that corresponds to the instantaneous drawdown case ($a=-1$) at a specific point of interest:

$$\lambda = \frac{(\text{dp/dr})_{\text{bean-up}}}{(\text{dp/dr})_{\text{inst. drawdown}}} \quad (3.3)$$

This ratio λ , expresses the efficiency of a strategy in terms of reducing pressure gradients relative to the hypothetical case in which the drawdown is applied instantaneously. Using the principle of superposition and the analytical solution for wells operating under constant BHP, Karantinos et al. (2015) concluded that the optimum strategy corresponds to negative values of parameter a (i.e., the optimum strategy lies in the lower left part of Figure 3.2). Comparisons of bean-up operations in vertical open-hole completions indicate that λ is independent of the applied drawdown and thus, the process of selecting bean-up strategies is decoupled from determining the overall drawdown.

3.5 BEAN-UP STRATEGIES IN HYDRAULICALLY FRACTURED WELLS

Choke management strategies are implemented either at the clean-up phase, once the stimulation job is complete, or when a well is brought back on production after a long shut-in period. Between these cases, it is important to underline the following:

- Upon the cessation of stimulation treatments, fluid pressure along the fracture creates a low effective stress environment on the proppant, making proppant arches highly susceptible to pressure gradients. On the other hand, when a well is producing for a long time, the reservoir pressure has depleted and the corresponding effective stress has a stabilizing effect.
- During the initiation of the clean-up process, fractures are saturated with fracturing fluid which can retain significant viscosity depending on the additives and the efficiency of the gel breakers. A fracture saturated with a viscous fluid is expected to exert greater forces on

the proppant pack due to the combined effect of elevated pressure gradients and viscous drag.

The above observations lead to the conclusion that from a bean-up standpoint, the clean-up phase is considerably more crucial for retaining fracture conductivity. Simulations by Shor and Sharma (2014) indicate that complete fracture evacuation may occur in case of low effective stress and high pressure gradients, typical for the case of clean-up operations. Figure 3.4 illustrates the possible regimes based on the combined effect of effective stress and pore pressure gradient.

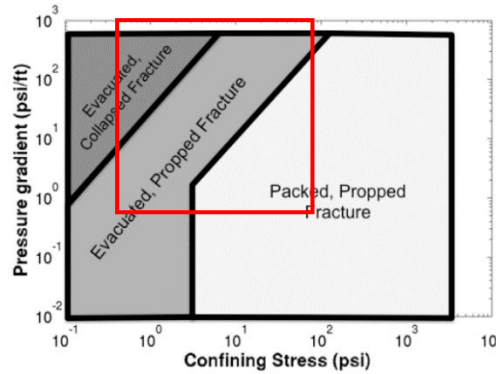


Figure 3.4 Fracture regimes with respect to confining stress and fracture pressure gradient. Proppant flowback is most likely to occur during the clean-up phase when effective stress is low (Shor & Sharma 2014).

For the clean-up process, a conservative estimate for the maximum allowable drawdown can be determined by accounting for proppant crushing. The effective stress acting on proppant grains should not exceed the mechanical strength of the pumped proppant, $\sigma_{proppant}$, typically varying between 3,000 to 8,000 psi:

$$\sigma' \leq \sigma_{proppant} \rightarrow \sigma_H - P_{wf} \leq \sigma_{proppant} \rightarrow \sigma_H - (P_i - DD) \leq \sigma_{proppant} \rightarrow DD \leq \sigma_{proppant} + P_i - \sigma_H \quad (3.4)$$

Accounting for pressure dependent horizontal stress, Eq. (3.4) can be written as:

$$DD \leq \frac{\sigma_{proppant}}{a_B} \frac{1-\nu}{\nu} + P_i - \frac{\rho_o g(TVD)}{a_B} \quad (3.5)$$

where ν is Poisson's ratio, a_B is Biot's constant and ρ_o is the density of the overburden.

In cases where embedment is likely to occur (i.e., when the matrix has a low elastic modulus), a proppant embedment test can provide additional limitations on the selected maximum drawdown. Wilson (2015) studied bean-up operations from a geomechanics standpoint and showed that a stepwise reduction in BHP can drastically reduce the maximum effective stress on the fracture, minimizing the risk of embedment or proppant crushing.

The next step involves the selection of a critical pressure gradient that should not be exceeded throughout the bean-up operation. Based on the design parameters of the fracturing treatment (fluid rheology, proppant size, pump rate, etc.) and pre-job simulations, an estimate of the fracture width can be obtained. Using this fracture width along with the horizontal stress (obtained from DFIT analysis, mini-frac tests or well log-correlations) and the proppant size, DEM simulations can assess the percent of proppant mass removed relative to the applied pressure gradient. Depending on the selected margin of safety (i.e., the percent of proppant removed) engineers can determine an upper bound for the fracture pressure gradient (see Figure 3.1).

In order to properly design bean-up operations for hydraulically fractured wells, it is essential to identify the optimum bean-up strategy (if any) and also assess the benefit of prolonging bean-up operations. We assume that the well is intersected by a single planar fracture of constant width and height equal to the perforating and producing interval. Under these assumptions, the well is considered to be a line source and 2-D simulations can be performed. Bean-up operations

(different values of a) were compared for a wide range of formation, fluid and fracture properties, presented in Table 3.1.

A refined mesh was used in the well vicinity in order to obtain an accurate estimate of the pressure distribution close to the wellbore and along the fracture. The selection of the grid is in agreement with the recommendations by Bennett et al. (1986) for minimizing truncation error. Based on the pressure solution, pressure gradients were calculated along the fracture, at a distance of 0.4 ft from the wellbore. The wellbore was discretized with a refined mesh of infinite productivity cells so that the induced BHP matches the local cell pressure. Simulations were performed with the Computer Modelling Group (CMG) IMEX, a commercial black-oil reservoir simulator.

Table 3.1 Simulation Parameters for Hydraulically Fractures Wells.

| Formation Properties | |
|---|-----------------------------|
| Field dimensions (ft x ft) | 1,000x1,000 |
| Porosity, ϕ | 0.10 |
| Permeability, k (mD) | 1; 0.1; 0.01; 0.001; 0.0001 |
| Temperature, T (F) | 250 |
| Initial Reservoir Pressure, P_i (psi) | 5,000 |
| Irreducible water saturation, S_{wr} | 0.25 |
| Rel. permeability exponent, n | 2.5 |
| Fracture Properties | |
| Fracture Half-Length, L_f (ft) | 60; 120; 180; 220 |
| Fracture Width, w_f (mm) | 1; 2 |
| Permeability, k (mD) | 1,000; 3,000 |
| Porosity, ϕ | 0.40 |
| Irreducible oil saturation, S_{or} | 0.10 |
| Irreducible gas saturation, S_{gr} | 0.10 |
| Irreducible water saturation, S_{wr} | 0.10 |
| Rel. permeability exponent, n | 1 |
| Bean-up Properties | |
| Total drawdown (psi) | 1,000; 2,000 |
| Duration, t_B (hr) | 2; 4; 8; 12; 24; 48 |
| Bean-up strategy, α | -0.99 to 24 (20 values) |
| Oil Reservoir – Fluid Properties | |
| Oil density (API) | 30 |
| Specific gravity of gas (air =1) | 0.70 |
| Viscosity, μ (cP) | ~ 0.75 |
| Compressibility (psi^{-1}) | ~ 3×10^{-5} |
| Bubble point pressure, P_b (psi) | 3,000 |
| Residual oil saturation, S_{or} | 0.25 |
| Gas Reservoir – Fluid Properties | |
| Specific gravity of gas (air =1) | 0.70 |
| Viscosity, μ (cP) | ~ 0.025 |
| Residual gas saturation, S_{gr} | 0.15 |

In the matrix, water was assumed to be immobile. However, the initial conditions depend on the nature of the problem. If a bean-up process is intended to be used in a clean-up operation, then the fracture should be simulated as initially saturated with fracturing fluid, the properties of which are obtained from the treatment design. In order to account for fracturing fluid imbibition, a zone of gradually varying saturation between the fracture and formation matrix was assumed.

Similarly, if a well is brought back on production after a long shut-in period then it is reasonable to assume that the fracture is saturated with hydrocarbon. Simulations were run for both cases and results indicate that the pressure gradient at the mouth of the fracture greatly depends on the viscosity of the fracture-occupying fluid. It was also observed that pressure gradients are approximately proportional to the magnitude of the drawdown applied, as for the case of vertical, open-hole wells.

In unconventional formations, clean-up operations typically last from a few hours to 2-3 days. For this reason, choke management strategies were compared for various durations ranging from 2 to 48 hours. For every bean-up duration, all strategies were simulated and the corresponding pressure gradients and ratios λ were assessed. The strategy yielding the smallest ratio λ was selected as the optimum for each bean-up duration. Figure 3.5 illustrates the performance (ratio λ) of the (optimum) choke management strategies for different ramp-up durations. Ratio λ reduces in a logarithmic fashion with increasing bean-up duration.

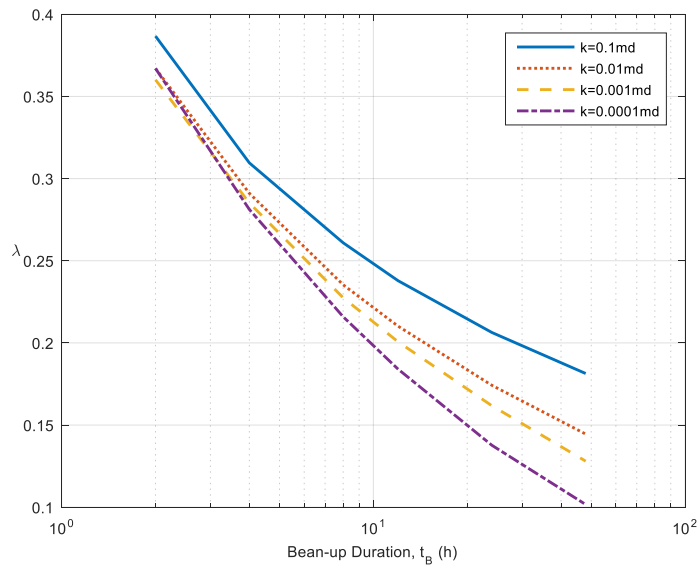


Figure 3.5 Pressure gradient ratio versus bean-up duration for the case of a gas well. Fracture width is 1 mm and fracture length equals 120 ft.

We observe that for short bean-up durations, ratio λ is independent of formation permeability which can be attributed to the early time linear flow along the fracture when the matrix contribution is insignificant. The purpose of this chart is to assist engineers in selecting the minimum duration of the ramp-up process, as follows:

- 1) For the selected overall drawdown, obtain the (maximum) pressure gradient of the instantaneous drawdown case: $(dP/dr)_{instantaneous}$
- 2) Using the critical pressure gradient determined from DEM simulations (Shor and Sharma 2014), calculate the critical ratio λ^* as follows:

$$\lambda^* = \frac{(dP / dr)_{critical}^{DEM}}{(dP / dr)_{instantaneous}} \quad (3.6)$$

- 3) Construct a graph similar to Figure 3.5 and select the bean-up duration that corresponds to the critical ratio λ^* .

Figure 3.6 presents the performance (ratio λ , y-axis) of various bean-up strategies (parameter a , x-axis) for different durations for a hydraulically fractured gas well. We observe that for the cases where the matrix permeability equals 0.1 md or less, the optimum strategy appears for values of parameter a between -0.75 and -0.65. This observation holds true for entire gamut of simulations performed, for both oil and gas wells. The simulations performed cover a wide range of dimensionless fracture conductivity, C_{fd} , from 0.02 to 300. In order to inhibit excessive pressure gradients, values of parameter a smaller than -0.8 should generally be avoided, particularly in bean-up operations lasting 8 hours or less (Figure 3.6 a, b & c). For the case of $k=1$ md or larger, flow contribution from the matrix directly to the wellbore is significant and the selection of the optimum strategy resembles that of open-hole completions as discussed by Karantinos et al. (2015). The

difference between the optimum strategies in low permeability fractured wells and open-hole completions can be attributed to dominant flow regimes: linear or bilinear flow for fractured wells and radial flow for open-hole completions.

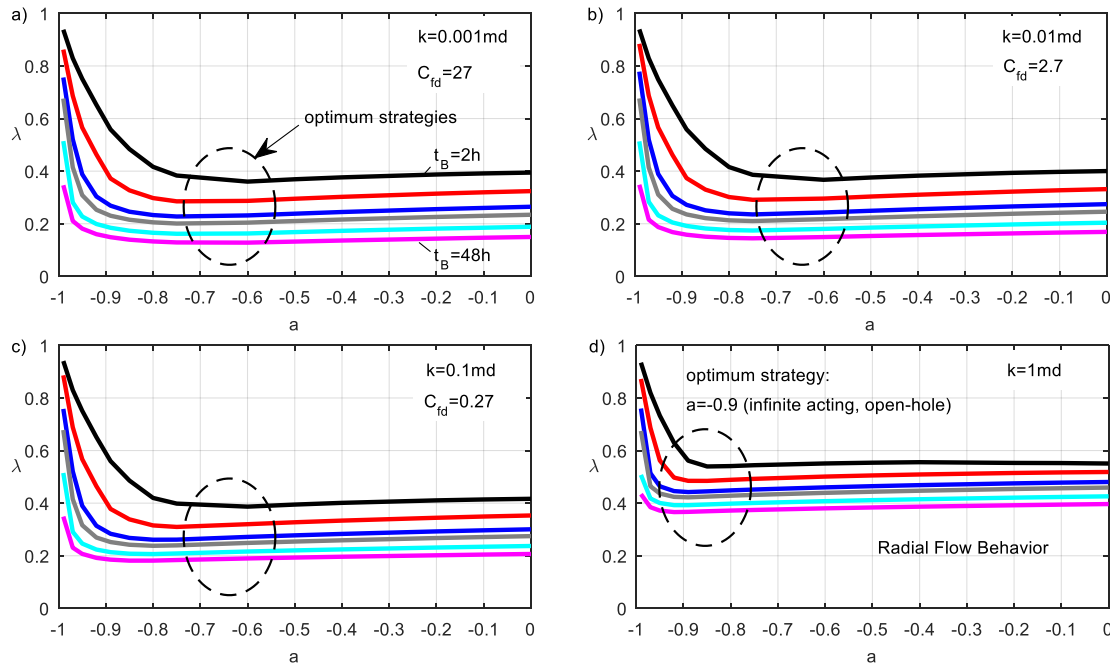


Figure 3.6 Comparing choke management strategies for a hydraulically fractured gas well.

Fracture width is 1 mm and fracture length equals 120 ft.

A sensitivity analysis was performed with respect to the viscosity of the fracturing fluid. The viscosity of the fracturing fluid greatly affects the maximum pressure gradient and should be taken into consideration in the design of clean-up operations. The previous analysis was also applied to suggest an optimum long term depletion schedule. The objective here is to identify the optimum strategy for a significantly larger drawdown applied over the course of months upon the cessation of stimulation treatments. For this purpose an overall drawdown of 3,000 psi was selected to be implemented over a period of 6 months on a gas well ($k=0.001$), initially saturated with a fracturing fluid of viscosity, 10 and 50 cP, respectively. Since this is a long-term depletion

schedule, adjustments in BHP take place every 12 h, compared to the 15 min intervals for the case of short-lived clean-up operations. The pressure gradients corresponding to different bean-up scenarios are presented in Table 3.2.

Table 3.2 Comparing choke management strategies for a prolonged bean-up in a hydraulically fractured gas well.

| Frac-Fluid Viscosity (cP) | 50 | | | | | 10 | | | | |
|---------------------------------|-------|------|------|------|------|-------|------|------|------|------|
| Strategy, a | -0.95 | -0.9 | -0.7 | -0.4 | -0.1 | -0.95 | -0.9 | -0.7 | -0.4 | -0.1 |
| Max. Pressure Gradient (psi/ft) | 42 | 34 | 28 | 33 | 35 | 40 | 33 | 27 | 30 | 32 |

We observe that for a depletion schedule lasting several months, the optimum strategy lies in the vicinity of -0.7, as for the case of clean-up procedures. Such a strategy performs significantly better compared to an abrupt ($a=-0.9$) or linear ($a=-0.10$) reduction in BHP providing an extra margin of safety. Additionally, in a long-term drawdown schedule, the fracturing fluid viscosity has a minor effect since load recovery occurs primarily during the early stage of production.

3.6 BEAN-UP STRATEGIES IN FRAC-PACK COMPLETIONS

Frac-pack completions have long been used in weakly consolidated formations providing large surface area and delivering high production rates. Compared to cased hole gravel packs and high rate water packs, frac-packs achieve lower skin factors and improved long-term reliability. The efficiency of the technique is highly dependent on achieving tip-screen-out and maintaining fracture conductivity. As mentioned previously, proppant flow-back may occur due to excessive pressure gradients or low effective stress environment, typical of overpressured turbidite formations where frac-packs have become commonplace. Additional parameters that may

compromise the productivity of frac-packs include fines migration or screen erosion and should thus be considered from a choke management standpoint.

The study of choke management strategies on frac-packs is notably more complicated compared to fractured wells since additional failure mechanisms need to be considered. Figure 3.7 provides a schematic representation of a frac-pack completion. Fluid enters the wellbore both from the fracture (Point A) and the formation sandface perpendicular to the wellbore (Point B). The following failure mechanisms need to be considered when designing a bean-up operation:

- Excessive pressure gradients along the fracture (Point A) in combination with low effective stress can destabilize the proppant in cases of incomplete (or not tight) packing of perforations and/or the annulus between the screen and the casing.
- High pressure gradients perpendicular to the fracture face (Point C) are expected to enhance formation fines migration into the fracture and ultimately to the gravel pack. In this case, fines may plug the annular pore space or cause screen erosion, if allowed to flow towards the screen under high velocities.
- Excessive fluid velocities along the perforations (Points A and B) may fluidize the gravel pack, leaving the screen exposed to formation sand or fine particles.
- Aggressive drawdowns are expected to enhance shear/tensile failure at Point B and/or mobilize the disaggregated material towards perforations and into the wellbore.

The above mechanisms should be superimposed and combined with literature recommendations on maximum fluid velocities or drawdown. Table 3.3 provides a brief description of the dominant failure mechanisms in the well vicinity.

Keeping these failure mechanisms in mind, bean-up strategies were compared for a wide range of formation and fracture properties. Ratios λ were assessed at all three points of interest (A: along the fracture, B: perpendicular to the well face, C: perpendicular to the fracture face). Based on simulation results, the following observations can be made:

- λ does not depend on the point of calculation: For a specific bean-up operation and formation/fracture properties, λ will be the same at points A & B. This is an important observation that simplifies the study and design of choke management strategies.
- The pressure gradient of the instantaneous drawdown case does not depend on fracture half-length, L_f . Indeed, at the instantaneous drawdown, the fracture tip has zero effect near the well and the corresponding pressure gradients are independent of fracture length.
- The pressure gradient of the instantaneous drawdown depends heavily on fracture conductivity, k_{fwf} . A highly conductive fracture will allow more fluid to flow through the fracture conduit and provide greater relief at point B.
- The instantaneous pressure gradient is proportional to the drawdown applied.

Table 3.3 Anticipated failure mechanisms and design criteria for frac-pack completions.

| | Point A | Point B | Point C |
|---------------------------------------|---|--|--|
| Anticipated Failure Mechanisms | Screen Erosion Proppant Pack Destabilization | Screen Erosion Drawdown induced Shear / Tensile Failure | Fines migration into the fracture |
| Establish Design Criteria | <p>Perforation Velocity¹: $V_{fr} < 10 \text{ ft/s}$ for oil wells $V_{fr} < 20 \text{ ft/s}$ for gas wells</p> <p>Fracture velocity limitations may be obtained from perforation velocity by accounting for perforation to fracture flow area. Based on fracture conductivity and Darcy's law, a pressure gradient limitation can be obtained $(dp/dr)_{A,Vc}$</p> <p>To ensure the stability of the proppant pack, DEM simulations can provide a critical pressure gradient $(dp/dr)_{A,DEM}$ based on horizontal stress, proppant size and fracture width.²</p> | <p>Perforation Velocity¹: $V_{fr} < 10 \text{ ft/s}$ for oil wells $V_{fr} < 20 \text{ ft/s}$ for gas wells</p> <p>Sandface velocity limitations may be approximated from the ratio of perforated to sandface area. Using these limitations along with the matrix permeability and Darcys Law, a maximum pressure gradient $(dp/dr)_{B,Vc}$ for Point B may be obtained</p> <p>Analytical or numerical models accounting for shear or tensile can provide additional limitation on the maximum allowable pressure gradient at point B, $(dp/dr)_{shear,B}$³</p> | <p>Minimize (dp/dr): fines mobilization depends on pressure gradients and chemical compatibility</p> |
| References | <p>*1: Wong (2003), Tiffin (2003), Economides (2008)</p> <p>*2: Shor & Sharma (2014)</p> | <p>*1: Wong (2003), Tiffin (2003), Economides (2008)</p> <p>*4: Weingarten (1995), van den Hoek (2000), Vaziri (2002)</p> | |
| Determine Critical Pressure Gradients | $\left[\frac{dP}{dr} \right]_A \leq \min \left[\frac{dP}{dr} \Big _{A,Vc}^{crit}, \frac{dP}{dr} \Big _{A,DEM} \right]$ | $\left[\frac{dP}{dr} \right]_B \leq \min \left[\frac{dP}{dr} \Big _{B,Vc}, \frac{dP}{dr} \Big _{B,shear} \right]$ | |

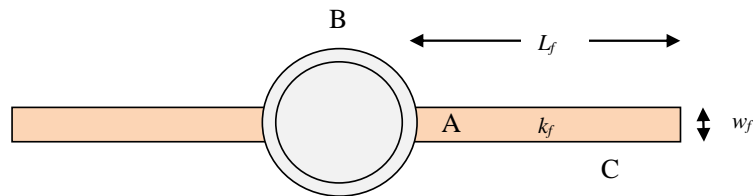


Figure 3.7 Schematic representation of a frac-pack completion.

Table 3.4 illustrates the effect of fracture conductivity on the instantaneous pressure gradient for the case of a gas reservoir and a drawdown of 500 psi.

Table 3.4 Pressure gradient of the instantaneous drawdown case for various fracture conductivities. Drawdown equals 500 psi.

| Formation Permeability | 250 md | | | | 500 md | | | |
|----------------------------------|-------------|-------------|--------------|-----------|-------------|-------------|--------------|-----------|
| Fracture conductivity, $k_f w_f$ | 4,200 md-ft | 8,400 md-ft | 12,500 md-ft | Open-hole | 4,200 md-ft | 8,400 md-ft | 12,500 md-ft | Open-hole |
| (dp/dr)instantaneous, A | 21.8 | 13.3 | 9.6 | 150 | 32 | 20.2 | 15 | 161 |
| (dp/dr)instantaneous, B | 23 | 16.21 | 13.4 | | 27.44 | 20.2 | 16.72 | |

It is obvious that increasing fracture conductivity reduces pressure gradients and thus the likelihood of proppant flowback at point A or shear/tensile failure at point B, especially compared to open-hole completions. Achieving better fracture conductivity is the key for improving productivity in frac-packs and as shown, improved conductivity minimizes one of the components that determine the maximum pressure gradient of a bean-up operation, that of the instantaneous pressure gradient.

Choke management strategies (values of λ) were compared for various reservoir and fracture properties as presented in Table 3.5. For every bean-up duration, the strategy yielding the minimum λ was selected as the optimum strategy. Figure 3.8 illustrates the reduction in pressure gradients (parameter λ) with increasing bean-up duration for the case of a gas well with fracture conductivity equal to 8,400 md-ft and various fracture lengths (4, 12, 16, 22 and 30 ft). The following observations can be made:

- Frac-pack completions significantly improve the performance of bean-up operations (lower λ) compared to vertical open-hole completions.

- Increasing the fracture length improves the performance of bean-up operations (reduces λ). A frac-pack length of ~12 ft is sufficient to provide a generous reduction in pressure gradients, although perforated interval length will typically necessitate longer fracture lengths for vertical coverage.
- Improvement reaches a plateau for $C_{fd}=1$. Consequently, from a bean-up standpoint, fracture lengths greater than k_{fwf}/k offer no additional improvement in minimizing pressure gradients.
- Field practice suggests that in high permeability formations, values of C_{fd} are typically smaller than one, indicating that current industry practices are typically favorable for maximizing bean-up performance.
- For short bean-up operations (i.e., infinite acting behavior), pressure gradients reduce logarithmically with duration, as for the case of vertical open-hole completions (Karantinos et al. 2015).
- For prolonged bean-up operations (i.e., boundary effects) pressure gradients (parameter λ) rapidly decline as a result of reservoir depletion.

Table 3.5 Simulation Parameters for frac-pack completions

| Formation Properties | |
|---|--------------------------|
| Field dimensions (ft x ft) | 1,000x1,000;2,000x2,000 |
| Porosity, ϕ | 0.20 |
| Permeability, k (mD) | 250;500;1,000 |
| Temperature, T (F) | 250 |
| Initial Reservoir Pressure, P_i (psi) | 5,000 |
| Irreducible water saturation, S_{wr} | 0.25 |
| Rel. permeability exponent, n | 2.5 |
| Fracture Properties | |
| Fracture Half-Length, L_f (ft) | 4; 12; 16; 22; 30 |
| Fracture Width, w_f (in) | 1; 2 |
| Permeability, k_f (D) | 50; 100; 150 |
| Porosity, ϕ | 0.20 |
| Irreducible oil saturation, S_{or} | 0.10 |
| Irreducible gas saturation, S_{gr} | 0.10 |
| Irreducible water saturation, S_{wr} | 0.10 |
| Rel. permeability exponent, n | 1 |
| Bean-up Properties | |
| Total drawdown (psi) | 400; 600 |
| Duration, t_B (hr) | 2; 4; 8; 12; 24; 48 |
| Bean-up strategy, a | -0.99 to 0.1 (20 values) |
| Oil Reservoir – Fluid Properties | |
| Oil density (API) | 30 |
| Specific gravity of gas (air =1) | 0.70 |
| Viscosity, μ (cP) | ~ 0.75 |
| Compressibility (psi ⁻¹) | ~ 3x10 ⁻⁵ |
| Bubble point pressure, P_b (psi) | 3,000 |
| Residual oil saturation, S_{or} | 0.25 |
| Gas Reservoir – Fluid Properties | |
| Specific gravity of gas (air =1) | 0.70 |
| Viscosity, μ (cP) | ~ 0.025 |
| Residual gas saturation, S_{gr} | 0.15 |

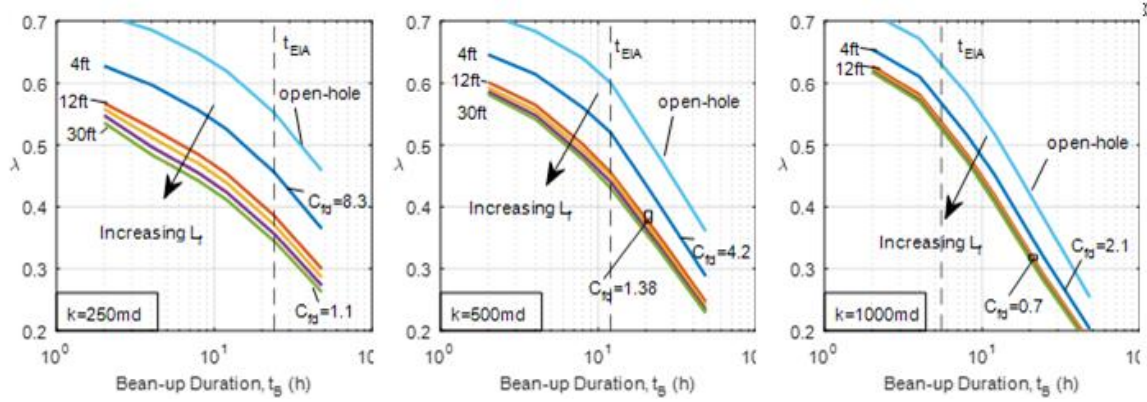


Figure 3.8 Ratio of pressure gradients versus bean-up duration for vertical open-hole completions and frac-pack lengths of 4, 12, 16, 22 and 30 ft.

A figure similar to Figure 3.8 can assist engineers determine the duration of the process:

- 1) For a selected overall drawdown, obtain the (maximum) pressure gradient of the instantaneous drawdown case for points A and B: $(dP/dr)_{\text{instantaneous, A}}$, $(dP/dr)_{\text{instantaneous, B}}$
- 2) Using the critical pressure gradients defined in Table 3.3, calculate the critical ratios λ_A and λ_B :

$$\lambda_A = \frac{(dP/dr)_A}{(dP/dr)_{\text{instantaneous, A}}} \quad (3.7)$$

$$\lambda_B = \frac{(dP/dr)_B}{(dP/dr)_{\text{instantaneous, B}}} \quad (3.8)$$

- 3) Calculate the combined critical ratio λ^*

$$\lambda^* = \min(\lambda_A, \lambda_B) \quad (3.9)$$

- 4) Construct a chart similar to Figure 3.8 and using the combined critical ratio, obtain the duration of the process.

Figure 3.9 illustrates the performance (ratio λ) of various choke management strategies (values of a) for different bean-up durations for the case of a gas well. We observe that the optimum

strategy (value of a yielding the lowest λ) depends on the duration of the process. For infinite acting behavior, the optimum strategy corresponds to $a=-0.9$, whereas for the case of boundary effects the optimum strategy shifts towards greater values of parameter a , as for the case of vertical open-hole completions (Karantinos et al. 2015).

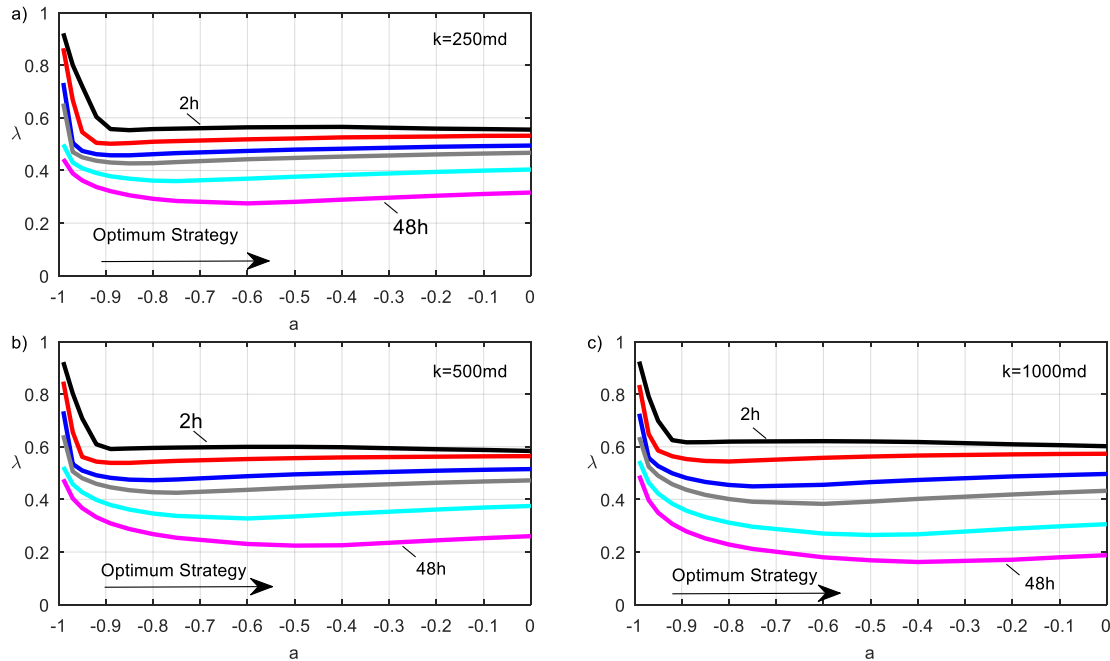


Figure 3.9 Comparing choke management strategies for a frac-pack completion in a gas well. Drainage area is 1,000 ft x1,000 ft and reservoir and fracture properties as in Table 3.5 and Table 3.6.

Table 3.6 Frac-Pack Properties.

| | |
|------------|-----|
| k_f (D) | 100 |
| w_f (in) | 1 |
| L_f (ft) | 22 |

Since frac-packs are typically implemented in high-permeability formations, characterized by short infinite-acting behavior, special emphasis should be placed on properly selecting the optimum strategy with respect to the duration of the process and the reservoir and fluid properties.

To reduce computational effort, an approximation for the optimum strategy can be obtained by Figure 3.10 that suggests the optimum strategy for vertical open-hole completions in homogeneous reservoir of square drainage area.

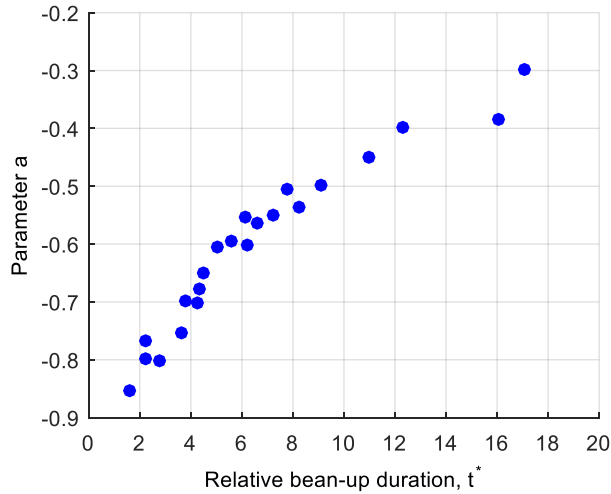


Figure 3.10 Optimum bean-up strategy versus relative bean-up duration for homogeneous and isotropic reservoirs of square drainage area (after Karantinos et al. 2015).

3.7 SUMMARY AND CONCLUSIONS

In this study choke management strategies were compared for vertically fractured wells and frac-pack completions. A general framework was introduced to assist engineers in selecting the duration of the ramp-up process by accounting for the predominant failure mechanisms. For each case, a methodology for selecting the optimum strategy was presented and additional factors affecting the efficiency of bean-up operations were discussed.

3.7.1 Hydraulically fractured wells

The design of bean-up operations involves the following steps:

1. Determine the maximum allowable drawdown

The well drawdown should be smaller than or equal to the maximum allowable drawdown as suggested by proppant crushing criteria or laboratory embedment tests.

2. Suggest a critical value for the fracture pressure gradient

Use the results presented by Shor and Sharma (2014) and suggest a maximum pressure gradient based on the effective horizontal stress, proppant size used and fracture width, an estimate of which can be obtained from pre-job simulations.

3. Calculate the pressure gradient of the instantaneous drawdown

Using a reservoir simulator and a properly refined mesh, obtain the pressure solution for the instantaneous drawdown and calculate the pressure gradient along the fracture. Special attention should be given to the viscosity of the fracture-occupying fluid.

4. Calculate the critical ratio λ

The critical ratio is defined as the ratio of Step (2) / Step (3).

5. Assume an optimum strategy of $a=-0.6$ and prepare a chart of λ vs t_B

Numerical simulations for a wide range of dimensionless fracture conductivity and typical durations of clean-up operations suggest that the optimum choke management strategy corresponds to a value of $a=-0.6$. For longer bean-up durations an extensive comparison of choke management strategies may be performed.

6. Determine the duration of the ramp-up process

Using the critical ratio λ (Step 4) and the chart of λ vs t_B (Step 5), obtain the duration of the ramp-up process.

7. Calculate the optimum BHP sequence

Using the selected overall drawdown, the duration of the ramp-up process and the optimum strategy (parameter a), obtain the sequence of BHP with respect to time using Eq. (3.1).

8. Implement the BHP sequence

The calculated BHP sequence can be implemented in the field with the use of a computer-adjusted choke or with a wellbore model that suggests the most appropriate choke size with respect to time. We have built such a model and this has been used for choke selection as a function of time.

3.7.2 Frac-Pack Completions

The design of bean-up operations involves the following steps:

1. Determine the overall drawdown

An upper bound for the overall drawdown may be obtained from analytical models that account for shear and/or tensile failure of drawdown guidelines based on compilation of data and screen erosion criteria.

2. Prepare a list of the anticipated failure mechanisms and set the design criteria

Depending on the completion properties, prepare a table similar to Table 3.3. Identify the anticipated failure mechanisms and the corresponding literature recommendations on fluid velocities or pressure gradients.

3. For the instantaneous drawdown case, calculate the pressure gradients at the points of interest

Using a reservoir simulator and a properly refined mesh, obtain the pressure solution for the instantaneous drawdown case and calculate the instantaneous pressure gradients at the (failure-prone) points of interest. Special attention should be given to the viscosity of the fracture-occupying fluid.

4. Calculate the critical ratio λ_i for every failure mechanism considered

The critical ratio is defined as the ratio of the critical pressure gradient suggested in step (2) over the corresponding pressure gradient calculated in step (3).

5. Calculate the combined critical ratio λ^*

The combined critical ratio is defined as the minimum critical ratio λ_i .

6. Select the optimum strategy and the duration of the ramp-up process

Calculate the optimum ratio λ for various durations and prepare a plot of λ vs t_B .

Using this chart and the combined critical ratio λ^* , determine the duration of the ramp-up process.

7. Calculate the optimum BHP sequence

Using the selected drawdown, the duration of the ramp-up process and the optimum strategy (parameter a), obtain the sequence of BHP with respect to time using Eq. (3.1).

8. Implement the BHP sequence

The calculated BHP sequence can be implemented in the field with the use of a computer-adjusted choke or with a wellbore model that suggests the most appropriate choke size with respect to time.

For the case of frac-pack completions, the performance of bean-up operations is maximized for a dimensionless conductivity less than or equal to one. In high permeability formations, current completion practices typically achieve values of $C_{fd} < 1$, thus taking full advantage of the potential of choke management strategies. In high permeability formations, the selection of the optimum choke management is highly dependent on duration and should be selected based on the steps described herein.

3.8 NOMENCLATURE

a = parameter describing bean-up operations

a_B = Biot's constant

BHP = Bottom Hole Pressure

C_{fd} = Dimensionless fracture conductivity, defined as $(k_f w_f)/(k L_f)$

c_t = total compressibility (psi^{-1})

DD = drawdown (psi)

g = gravitational acceleration (m/s^2)

k = horizontal permeability (md)

k_f = fracture permeability (md)

L_f = fracture half-length (ft)

P_i = initial reservoir pressure (psi)

P_f = BHP at the end of the ramp-up process (psi)

P_{wf} = wellbore flowing pressure (psi)

r_e = drainage radius (ft)

t = time (h)

t^* = relative bean-up duration

t_{EIA} = end of infinite acting period (h)

t_B = bean-up duration (h)

t_{BD} = dimensionless bean-up time

t_D = dimensionless time

TVD = True Vertical Depth (ft)

w_f = fracture width

λ = pressure gradient of bean-up operation over pressure gradient of instantaneous drawdown

μ = viscosity (cp)

ν = Poisson's ratio

ρ_o = overburden density (kg/m^3)

σ_H = horizontal stress

$\sigma_{proppant}$ = proppant crushing strength (psi)

ϕ = porosity

Chapter 4: A Coupled Wellbore-Reservoir Model for Well Management¹

4.1 PREVIOUS STUDIES ON CHOKE MANAGEMENT

Choke management strategies vary significantly among operators and no definite guidelines exist for properly designing clean-up procedures or drawdown schedules in conventional and unconventional formations. Previous studies have shown that aggressive ramp-up strategies have caused completion failures in offshore wells (Tiffin et al. 2003) or productivity impairment/loss of production in shale formations (Wilson, 2015). Due to the prohibitive costs of intervention, operators have shown an ever-increasing awareness of properly designing well startup and shutdown procedures and schedules in both conventional and unconventional formations.

4.1.1 Conventional Wells

Previous studies on conventional wells have focused primarily on the geomechanical aspects of sand production. Drawdown guidelines and near-wellbore fluid velocity limitations have been suggested based on shear or tensile failure (Vaziri et al. 2002), screen erosion (Wong et al. 2003, Tiffin et al. 2003) or gravel pack destabilization (Economides et al. 2008). Geilikman et al. (2005) investigated the effect of bean-up protocols on fines migration.

Minimizing pressure gradients near the wellbore can often lead to less sand and fines production, lower proppant flowback and less screen erosion, among other benefits. With the primary goal of minimizing pressure gradients near the wellbore, Karantinos et al. (2015)

¹ Karantinos, E., Sharma, M. M., Choke Management under Wellbore, Completion and Reservoir Constraints, paper SPE-187190, presented at the SPE Annual Technical Conference and Exhibition, San Antonio, TX, 9-11 October 2017

Author Contributions: Karantinos E. documented the methodology and performed the numerical simulations. Sharma M. provided guidance and technical advice.

introduced a general framework for defining drawdown schedules and compared bean-up strategies for vertical, open-hole completions. They provided the sequence of choke sizes that minimizes near-wellbore pressure gradients and concluded that for short-lived bean-up operations (i.e., infinite acting behavior) no more than 70% of the overall drawdown should be applied during the initial 30% of the bean-up duration. On the other hand, for longer bean-up procedures (i.e., when the effect of reservoir boundaries can be felt) the optimum choke management strategy depends on the duration of the process as well as on formation and fluid properties. Andrews et al. (2016) provided an overview of sanding criteria for open-hole completions and suggested an approach for selecting choke sizes which ensures that the transient pressure gradients during bean-up do not exceed the stabilized pressure gradients observed during normal production operations.

4.1.2 Unconventional Wells

For the case of unconventional formations, choke management strategies have so far not been studied in a systematic and consistent manner. Numerical studies have shown that constrained choke management can significantly reduce the peak effective stress on the fractures and improve EUR by up to 40% in formations with upropped natural fractures (Wilson 2016). The general consensus is that clean-up operations should be designed to inhibit proppant settling and ensure that closure stress is gradually increased to prevent proppant crushing. Based on successful clean-up procedures, Robinson et al. (1998) suggested that clean-up operations should be initiated at low rates of 10-20 bbl/hr using choke increments of 2/64 in for several days or even weeks. Ely et al. (1990) recommended rates of 10-15 gallons per minute for up to 30 minutes after near-wellbore fracture closure has been identified based on surface pressure measurements, followed by flowback rates of 1-2 bpm. Using field data from the Barnett shale, Willberg et al. (1998) suggested that forced closure should be augmented using flowback rates in excess of 3 bpm. According to

Crafton (2008), the industry has been using flowback rates ranging anywhere from 5 to a few tenths of barrels per minute. The above recommendations indicate a lack of consensus among the industry and the implementation of such guidelines cannot guarantee a successful clean-up procedure, especially if one accounts for the variation of permeability, number of stages and fracture properties among the various formations.

4.2 DESIGN CONSIDERATIONS

It is clear that if no constraints are placed on the production system, choke management would be of no importance and wells should be allowed to flow with an open choke at their absolute flow potential. To mitigate the risk of productivity impairment or failures associated with the completion or other equipment, production engineers should take into consideration existing guidelines for allowable values of flow velocities or drawdown limits. These recommendations can be classified into three major categories: wellbore, completion or reservoir constraints.

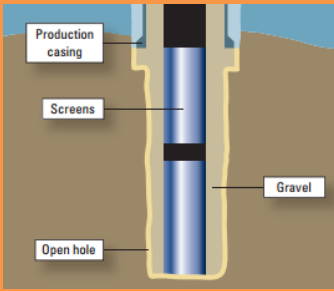
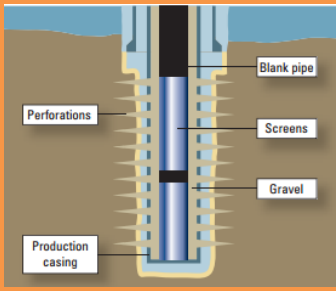
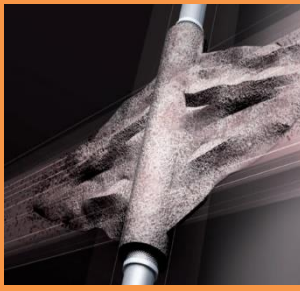
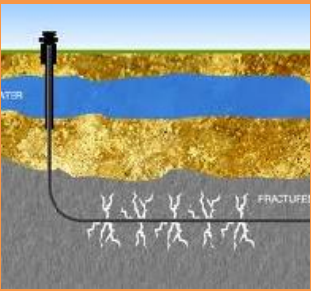
4.2.1 Wellbore Constraints

Wellbore constraints include, but are not limited to, the maximum pressure drop across the choke to prevent hydrate or wax / asphaltene formation downstream of the choke, the maximum fluid velocity in the surface flowlines to *prevent* erosion and the minimum fluid velocity along the wellbore trajectory to ensure effective proppant transport during flowback operations.

4.2.2 Completion & Reservoir Constraints

These constraints depend on the completion type in place. Table 4.1 presents several completion and reservoir constraints along with their maximum allowable values reported in the literature.

Table 4.1 Velocity and pressure constraints for various types of completions

| OPEN HOLE | CASED HOLE | FRAC-PACK | UNCONVENTIONAL |
|---|---|--|---|
|  |  |  |  |
| Annular Fluid Velocity $\leq 1\text{ft/s}$ (SPE 84495/ 84497) | Annular Fluid Velocity $\leq 1\text{ft/s}$ (SPE 84495/ 84497) | Annular Fluid Velocity | Peak Effective stress |
| Pressure Gradients $\leq \text{UCS}/r$ (SPE 63108/ 78235/ 185906) | Perforation Velocity $\leq 10\text{ft/s}$ (SPE 84495/84497) | Perforation Velocity | Pressure Gradient Along Fracture |
| Drawdown Limit (SPE 77683/ 78235) | C-Factor (Kinetic Energy) ≤ 60 (SPE 84495) | C-Factor (Kinetic Energy) | Combined effective stress/ pressure gradient |
| Incremental Drawdown (SPE 185906) | ΔP across perforations | Pressure gradient along fracture | Conductivity of upropped fractures |
| Critical water conning rate | Drawdown Limit (SPE 776863/ 782335/ 84495) | Completion ΔP | Total Drawdown |

4.3 MODEL DESCRIPTION

To properly design a flowback operation or a choke management strategy, reservoir, wellbore, completion, and choke flow models must be combined. The method presented comprises two major entities: the reservoir and the wellbore. Both entities are modeled separately and this modularity allows any commercially available reservoir simulation or wellbore model to be deployed by the algorithm presented herein.

4.3.1 Reservoir Model

The reservoir model contains all the properties used in a reservoir simulator (i.e. reservoir geometry, formation properties, initial conditions etc.) along with a grid capable of accurately

delineating the near wellbore region and/or the fracture geometry. For a given set of initial conditions (i.e. pressure and saturation distribution) and flowing Bottom-Hole-Pressure (BHP), the reservoir model provides the production rates and the final distribution of pressure and fluid saturations. It is important to note that the reservoir entity accounts for the reservoir only, excluding any completion model. Consequently, the BHP used as input to the reservoir model is the pore pressure at the completion/reservoir interface, P_{cr} .

An attractive alternative to a numerical reservoir simulator is the use of a proxy model, namely an Inflow-Performance-Relationship (IPR) model. For undersaturated reservoir conditions (i.e. when the average pressure in the well vicinity is greater than the bubble point pressure), the reservoir influx into the wellbore, Q^{liq} , can be obtain using the definition of productivity index, J

$$Q^L = J(P_{av} - P_{wf}) \quad (4.1)$$

Where

- J The well productivity index for undersaturated reservoir conditions (STBD/psi)
- P_{av} The average reservoir pressure
- P_{wf} The flowing bottom-hole-pressure at the sandface or perforations

For saturated conditions (i.e. when the average pressure in the well vicinity is lesser than the bubble point pressure, in which case free gas enters the wellbore) the liquid rate can be approximate using either Vogel's equation (Bommer, 2012; Ahmed, 2006):

$$Q^L = Q_{\max} \left[1 - 0.2 \frac{p_{wf}}{p_{av}} - 0.8 \left(\frac{p_{wf}}{p_{av}} \right)^2 \right] \quad (4.2)$$

Where

- Q_{\max} The maximum liquid rate
- P_{av} The average reservoir pressure

P_{wf} The flowing bottom-hole-pressure at the sandface or perforations (completion-reservoir interface)

The oil, water and gas rates can be obtained using the appropriate phase ratios such as the Water-Oil-Ratio (WOR) or Gas-Oil-Ratio (GOR) at the current reservoir conditions. It is important to note that the use of an IPR model imposes the assumption that phase ratios at saturated conditions are insensitive to the drawdown (e.g WOR is independent to the flowing BHP). On the contrary, the use of a numerical reservoir can capture the variation of phase ratios with respect to the flowing BHP, providing a more accurate estimate of the reservoir flowrates.

4.3.2 Wellbore Model

For a given choke size, the wellbore model provides the flowing bottom-hole pressure as a function of the liquid rates and the choke size. The wellbore model comprises the surface equipment (i.e. separator and surface flowlines), the selected choke size and the wellbore trajectory. The flowing Bottom-Hole-Pressure, p_{wf} , is the pressure inside the wellbore and is calculated using the following equation:

$$p_{wf,w} = WM(Q, c) = P_{sep} + \Delta P_{flowline} + \Delta P_{choke} + \Delta P_{wellbore} \quad (4.3)$$

Where

- Q The oil, water and gas flowrates
- c The well control (i.e. the choke size)
- P_{sep} The separator pressure
- $\Delta P_{flowline}$ The pressure drop across the surface flowline
- ΔP_{choke} The pressure drop across the choke
- $\Delta P_{wellbore}$ The pressure drop (frictional and hydrostatic) along the wellbore

Depending on the fluid system under consideration (black-oil, dry gas etc.) the appropriate choke flow model should be used (see Appendix B). The following paragraphs present the numerical model deployed for calculating the pressure drop along a pipeline segment.

4.3.2.1 Pressure Drop along a Pipe Segment for three-phase flow

In this section we present a numerical scheme for calculating the pipeline inlet pressure, given the outlet pressure and the oil, water and gas rates in standard conditions $\mathbf{q} = (q_{sc}^o, q_{sc}^w, q_{sc}^g)$. To this end, we utilize the fractional flow theory as introduced by Nagoo (2013). The proposed formulation assumes steady state flow (i.e. stabilized flow rates and pressures) and isothermal conditions. Additionally, we consider a black-oil PVT model where the inputs required are the Oil API density and the gas specific gravity, γ_g . The fluid properties are a function of pressure and are approximated using the PVT correlations presented in Appendix C. Figure 4.1 illustrates a horizontal pipeline of constant cross-section and known outlet pressure, P_{outlet} .

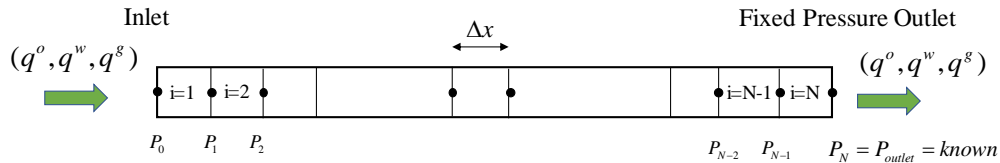


Figure 4.1 Discretization and boundary conditions of pipeline model

Equation (4.4) represents the macroscopic phase-averaged momentum balance equation along the x-direction for steady-state conditions.

$$\frac{\Delta P_{mix}}{\Delta L} = \frac{4}{D_H} \sum_{j=1}^{N_p=3} \tau_{j \rightarrow wall} + \rho_{mix} g \cos \theta \quad (4.4)$$

where

| | |
|--------------------------|---|
| ΔP_{mix} | The pressure drop along a pipe element of length ΔL |
| D_H | The hydraulic radius of the pipe element |
| $t_{j \rightarrow wall}$ | The momentum flux (shear stress of phase j to the wall of the pipe) |
| ρ_{mix} | The average density of the mixture |
| g | The gravitational acceleration |
| θ | The inclination angle |

The pipeline is discretized into N pipeline elements of equal length, Δx . The pressure drop, ΔP_i , along each discretized element i is defined as the pressure at the upstream node minus the pressure at the downstream node:

$$\Delta P_i = P_{i-1} - P_i \quad (4.5)$$

Where P_i is the pressure at node i . Consequently, P_N corresponds to the known outlet pressure (boundary condition) and P_0 corresponds to the sought inlet pipeline pressure. The pressure drop along a discretized element is a strong function of the average element pressure since fluid properties are a function of pressure. In order to obtain the pressure profile along the pipeline (and hence the pressure at the inlet node), we iteratively solve the system of pressure equations:

$$\begin{array}{l}
 \text{Element 1} \\
 \text{Element 2} \\
 \dots \\
 \text{Element N-1} \\
 \text{Element N}
 \end{array}
 \begin{bmatrix}
 1 & -1 & 0 & & 0 & 0 & 0 \\
 0 & 1 & -1 & & 0 & 0 & \\
 & & \dots & & 0 & 0 & \\
 & & & \dots & & 0 & \\
 0 & & & & \dots & & \\
 0 & 0 & & & 1 & -1 & \\
 0 & 0 & & & 1 & -1 & \\
 0 & 0 & 0 & & & 1 &
 \end{bmatrix}
 \begin{bmatrix}
 P_0^{k+1} \\
 P_1^{k+1} \\
 \dots \\
 P_{n-1}^{k+1}
 \end{bmatrix}
 =
 \begin{bmatrix}
 \Delta P_1^k \\
 \Delta P_2^k \\
 \dots \\
 \dots \\
 \Delta P_{n-1}^k \\
 \Delta P_n^k + P_{outlet}
 \end{bmatrix} \quad (4.6)$$

Where:

P_i^k The pressure at node i at iteration k

ΔP_i^k The pressure drop along element i at iteration k

The iteration terminates when convergence is achieved within a predetermined specified tolerance ε , typically set to 1.0E-3:

$$\max_{i=1,2,\dots,N-1} \left[\left| \frac{P_i^{k+1} - P_i^k}{P_i^k} \right| \right] \leq \varepsilon \quad (4.7)$$

In the system of equations (4.6), the pressure drop along each pipe element i at iteration k , ΔP_i^k , is calculated with the following procedure:

1. Calculate the average pressure \bar{P}_i in element i , defined as $\frac{P_{i+1} + P_i}{2}$, where P_i is the pressure at node i (i.e. the interface between elements $i + 1$ and i)
2. Calculate the oil, water and gas fluid properties. More specifically, calculate the solution gas (R_s), the gas deviation factor (z), the oil and gas formation volume factors (B_o, B_g) and gas density using Black-Oil correlations (see Appendix C).
3. Using the solution gas ratio, perform a black-oil flash and evaluate the volumetric flowrate of free gas in standard conditions. The black-oil flash is performed with the following steps:
 - i. Calculate the soluble gas (i.e. the gas that can be dissolved in the oil phase at the current pressure and temperature)

$$q_{SC, \text{soluble}}^g = q_{SC}^o R_s \quad (4.8)$$

Where q_{SC}^o is the oil rate expressed in standard conditions (STBO/day) and R_s the solution gas-oil ratio expressed in Scf/STBO

- ii. If the total flowing gas rate, q_{SC}^g is greater than the soluble gas calculated from equation (4.8) then gas will be flowing as a separate phase (referred to as free gas). The volumetric flowrate of free gas, $q_{SC}^{g,free}$ is equal to the excess amount of gas that may not be dissolved in the oil phase:

$$q_{SC}^{g,free} = q_{SC}^g - q_{SC}^o R_s \quad (4.9)$$

- iii. If the total flowing gas rate, q_{SC}^g is lesser than the soluble gas calculated from equation (4.8) then the gas is completely dissolved in the oil phase and the volumetric flowrate of free gas equals zero:

$$q_{SC}^{g,free} = 0 \quad (4.10)$$

4. Calculate the in-situ volumetric flowrates for the oil phase, the water phase and the free gas using the corresponding formation volume factors:

$$q_{in-situ}^o = \frac{q_{SC}^o}{B_o} \quad (4.11)$$

$$q_{in-situ}^w = \frac{q_{SC}^w}{B_w} \quad (4.12)$$

$$q_{in-situ}^{g,free} = \frac{q_{SC}^{g,free}}{B_g} \quad (4.13)$$

5. Calculate the in-situ fractional flow for each of the flowing phases, j. The fractional flow, f_j , is defined as the fraction of the in-situ volumetric flowrate of phase j over the total in-situ volumetric flowrate

$$f_o = \frac{q_{in-situ}^o}{q_{in-situ}^o + q_{in-situ}^w + q_{in-situ}^g} \quad (4.14)$$

$$f_w = \frac{q_{in-situ}^w}{q_{in-situ}^o + q_{in-situ}^w + q_{in-situ}^g} \quad (4.15)$$

$$f_g = \frac{q_{in-situ}^{g,free}}{q_{in-situ}^o + q_{in-situ}^w + q_{in-situ}^g} \quad (4.16)$$

6. Convert the fractional flow of phases into fluid saturations using the appropriate slip model. If no slip occurs then the saturation of phase j , S_j , is equal to the fractional flow of phase j . Nagoo (2013), introduced the ANSLIP model and showed that it provides a significantly better estimate of pressure drop over a wide range of scenarios and flow patterns. Using the ANSLIP model, the gas saturation is obtained from the following equation:

$$S_{g,free} = \frac{f_g + 1 - [(f_g + 1)^2 - 4(f_g)^2]^{1/2}}{2f_g} \quad (4.17)$$

The water and oil saturations can be evaluated from the equations:

$$S_o = (1 - S_{g,free}) \frac{q_{in-situ}^o}{q_{in-situ}^o + q_{in-situ}^w} \quad (4.18)$$

$$S_w = (1 - S_{g,free}) \frac{q_{in-situ}^w}{q_{in-situ}^o + q_{in-situ}^w} \quad (4.19)$$

7. Calculate the in-situ, v_j , and superficial u_j velocities, for each phase j =oil, water and gas:

$$u_j = \frac{q_{in-situ}^j}{A_{pipe}} \quad (4.20)$$

$$v_j = \frac{q_{in-situ}^j}{S_j A_{pipe}} \quad (4.21)$$

8. Calculate the Reynolds Number, $N_{RE,j}$ for each phase j:

$$N_{RE,j} = \frac{\rho_j |v_j| D}{\mu_j} \quad (4.22)$$

9. Calculate the Fanning friction factor for each phase j:

$$ff_j = \begin{cases} \frac{16}{N_{RE,j}} & N_{RE,j} \leq 2300 \\ \frac{7.05 \times 10^{-8}}{(N_{RE,j})^{-1.5}} & 2300 \leq N_{RE,j} \leq 2900 \\ \left\{ -3.6 \log_{10} \left[\frac{6.9}{N_{RE,j}} + \left(\frac{1}{3.7} \frac{k_{wall}}{D_H} \right)^{10/9} \right] \right\}^{-2} & N_{RE,j} > 2900 \end{cases} \quad (4.23)$$

10. Calculate the momentum flux (shear stress of phase j to the wall of the pipe):

$$\tau_{j \rightarrow wall} = \frac{1}{2} f_j \rho_j |v_j| v_j \quad (4.24)$$

11. Calculate the total friction component, F_f of the momentum balance equation

$$F_f = \frac{4}{D_H} \sum_{j=1}^{N_p=3} \tau_{j \rightarrow wall} \quad (4.25)$$

12. Calculate the in-situ mixture density, ρ_{mix}

$$\rho_{mix} = S_o \rho_o + S_w \rho_w + S_g \rho_g \quad (4.26)$$

13. Calculate the hydrostatic component, F_H of the momentum balance equation

$$F_H = \rho_{mix} g \cos \theta \quad (4.27)$$

14. Calculate the pressure drop along the element i:

$$\Delta P_i = (F_c + F_H)\Delta x \quad (4.28)$$

The calculation of the inlet pressure can also be evaluated, in a more efficient manner, using the following process: The pressure drop is calculated for each pipe element of length Δx starting with the element closest to the outlet and heading towards the inlet (upstream calculation). The pressures at the interfaces between elements are updated as soon as the downstream pressure drops have been evaluated and the process continues until convergence is achieved with regard to the inlet pressure. This procedure is illustrated in the form of pseudocode in Algorithm 4.1.

Algorithm 4.1 Pseudocode for calculating the pipeline inlet pressure

```
//PN=Poutlet= known
k=0
while (true)
    for i=N to 1
        Calculate  $\Delta P_i$ 
        Update  $P_{i-1}=P_i-\Delta P_i$ 
    end
     $P_0^k = P_0$ 
     $\varepsilon = |P_0^k - P_0^{k-1}|$ 
    if ( $\varepsilon < 0,001$ )
        break;
    k=k+1
end
```

4.3.3 Dynamic Nodal Analysis

In order to match the pore pressure at the reservoir/completion interface, a dynamic nodal analysis scheme was deployed. The objective is to find the equilibrium rate and BHP for a given Well-Head-Pressure (WHP) and well controls (choke size). The reservoir model (either a numerical simulator or an Inflow-Performance-Relationship) provides the oil, water and gas volumetric flowrates $\mathbf{Q} = (Q^{oil}, Q^{water}, Q^{gas})$, as a function of the flowing BHP:

$$\text{Reservoir Model:} \quad \bar{Q} = g_r(BHP) = g_r(p_{wf}) \quad (4.29)$$

The wellbore model provides the BHP as a function of the flowrates and the well controls (i.e. choke size) and separator pressure (see equation 4.3 for a detailed description of the wellbore model). The wellbore model can be represented by equation (1.6)

$$\text{Wellbore Model:} \quad BHP = p_{wf,w} = g_w(\bar{Q}) \quad (4.30)$$

Combining equations (4.26) and (4.27) we obtain the following expression for the flowing BHP:

$$p_{wf} = BHP = g_w(g_r(BHP)) = g_{NA}(BHP) \quad (4.31)$$

Equation (4.28) is in the form of $x=f(x)$ and can be solved using fixed point iteration. Fixed point iteration converges to a solution provided that the gradient of the function f is smaller than unity near the solution. This condition is generally not satisfied for the case of small choke sizes where a miniscule increase in the rate can greatly affect the BHP. Figure 4.2 illustrates the divergence of fixed-point iteration method for a steep VLP curve (i.e. small choke size).

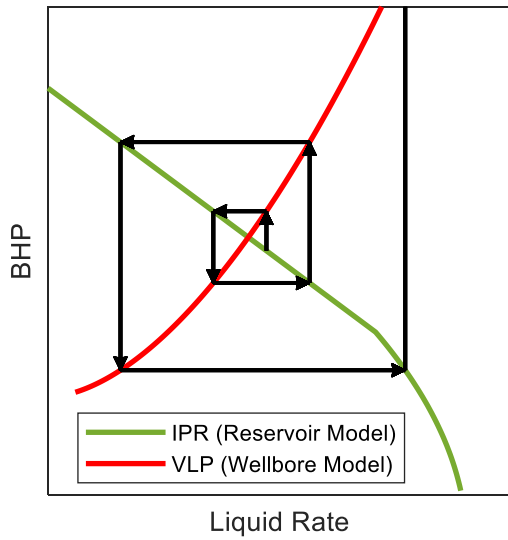


Figure 4.2 Divergence of fixed-point iteration for a small choke size

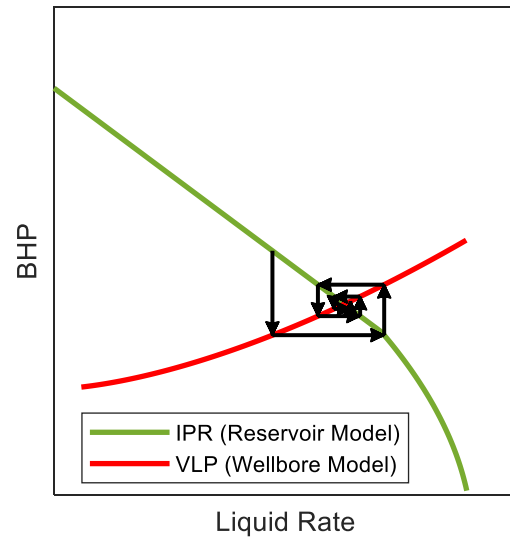


Figure 4.3 Convergence of fixed-point iteration for a large choke size

We observe that fixed point iteration fails to converge for small choke sizes which are of particular importance for choke management, especially during the early life of a well. Consequently, we investigate the potential of alternate root-finding algorithms such as the secant method. To perform nodal analysis using the secant method, the new guess for the BHP is obtained with the following equation:

$$P_{wf}^k = \frac{P_{wf}^{k-2} P_{wf,w}^{k-1} - P_{wf}^{k-1} P_{wf,w}^{k-2}}{P_{wf}^{k-2} - P_{wf}^{k-1} + P_{wf,w}^{k-1} - P_{wf,w}^{k-2}}, k \geq 2 \quad (4.32)$$

P_{wf}^k : The BHP at iteration k

$P_{wf,w}^k$: The BHP as calculated using the wellbore model at iteration k

The method requires two initial guesses for the BHP (i.e. k=0 and k=1). The method can be interpreted graphically in the following manner: Using the last two approximations for the BHP,

the IPR and VLP curves are linearized and their intersection is used to obtain the new estimate for the BHP, as shown in Figure 4.4.

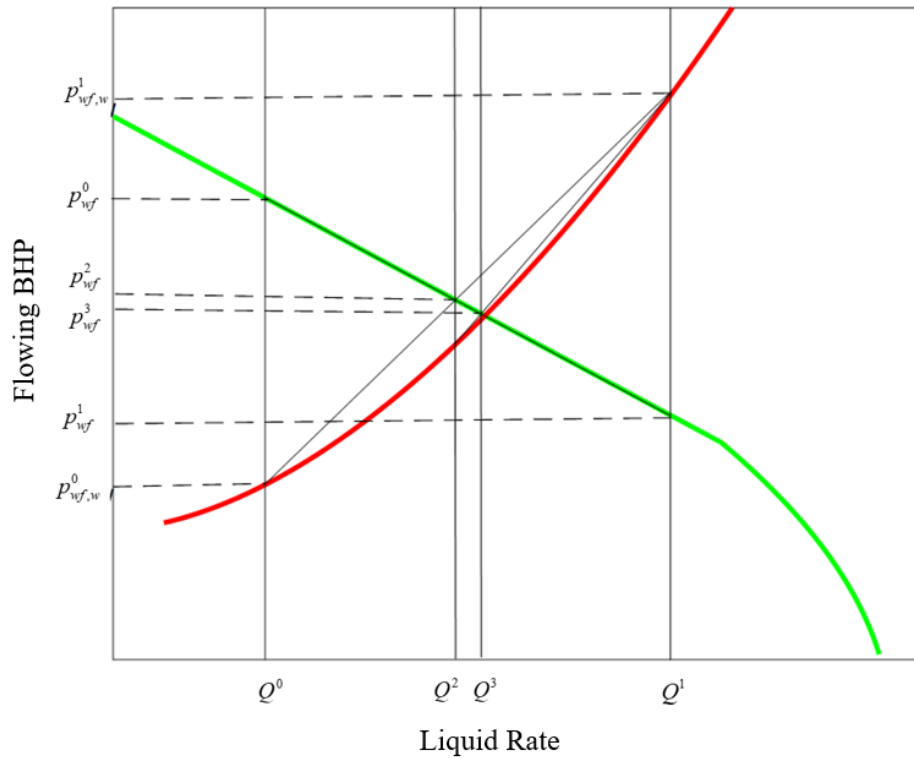


Figure 4.4 Graphical interpretation of the modified secant method

The secant method converges both for the cases of small and large choke sizes. To reduce computational effort and minimize the number of expensive reservoir simulations, the secant method is selected in lieu of the, otherwise faster, Newton-Raphson Method. In order to solve for the BHP with an accuracy of 0.1 psi, the tolerance is set to 2×10^{-5} or smaller. Using the secant method, convergence is typically achieved within 4-5 iterations.

4.4 CHOKE SELECTION ALGORITHM

The primary objective of the algorithm is to select, at all times, the largest choke size that satisfies the entire set of constraints placed on the system. In other words, the algorithm maximizes production while ensuring that wellbore, completion and reservoir constraints are met. Figure 4.5 presents the logic diagram of the choke selection algorithm.

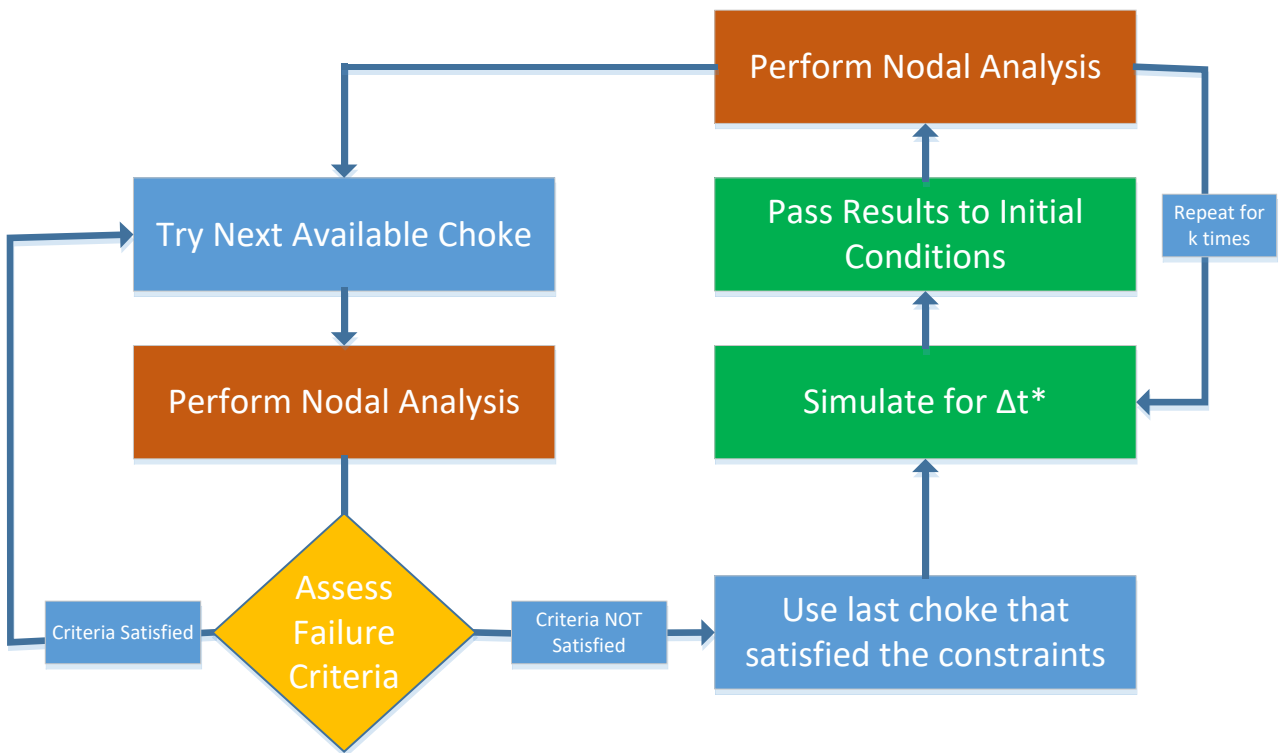


Figure 4.5 Logic diagram of choke selection algorithm

The assessment of the failure criteria requires that all the necessary calculations and checks must be made until all constraints are met. When all constraints are met, the algorithm proceeds with testing the next larger available choke size. On the other hand, if one or more constraints are not satisfied, the currently tested choke size is considered unsuitable and the algorithm reverts to the previous smaller choke size that satisfied all constraints.

After a choke size has been selected, the algorithm will simulate the reservoir domain for a user specified time of Δt^* , update the reservoir conditions (pressure and fluid saturations) and the BHP through nodal analysis. If an IPR curve is utilized instead of a numerical reservoir simulator, the new reservoir pressure may be obtained by solving the material balance equation as described in Appendix D. The process will terminate once the simulation time has been exceeded or the maximum choke has been selected.

4.5 MODEL APPLICATION

The suggested choke selection algorithm was applied to a conventional vertical well and a hydraulically fractured horizontal well. In both cases, reservoir simulations were performed with a commercial black-oil reservoir simulator. Fractional-flow theory (Nagoo, 2013) was used to simulate fluid flow along the wellbore.

4.5.1 Vertical Cased-Hole Well

In this example application, we seek the choke management strategy that satisfies a set of constraints for a given formation and production system. The properties and of the system are presented in Table 4.2a. The well is subject to the constraints shown in Table 4.2b. It is important to note that we do not know, a priori, which of the three constraints will be crucial in the selection of choke size as a function of time.

Table 4.2a Reservoir and wellbore properties for vertical cased-hole well.

| Formation Properties | | Available Choke Sizes | |
|---|-----------|---|--------|
| Field dimensions (ft x ft) | 1000x1000 | Minimum Choke Diameter (/64") | 6 |
| Thickness (ft) | 100 | Maximum Choke Diameter (/64") | 40 |
| Porosity, ϕ | 0.25 | Diameter Increments (2/64in) | 2 |
| Permeability, k (md) | 1000 | Surface Facilities | |
| Temperature, T (F) | 250 | Separator Pressure (psi) | 750 |
| Initial Reservoir Pressure, P_i (psi) | 8000 | Flowline Length (ft) | 300 |
| Initial Oil Saturation, S_{oi} | 0.60 | Flowline Inner Diameter (in) | 2.98 |
| Initial Water Saturation, S_{wi} | 0.40 | Wellbore Properties | |
| Irreducible Oil Saturation, S_{or} | 0.25 | Wellbore MD (ft) | 8000 |
| Connate Water, S_{wc} | 0.25 | Wellbore TVD (ft) | 8000 |
| Rel. permeability exponent, n | 2.2 | Tubing Inner Diameter (in) | 4.88 |
| Completion Properties | | Oil Reservoir – Fluid Properties | |
| Perforated Length (ft) | 30 | Oil density (API) | 30 |
| Perforation Density (SPF) | 10 | Specific gravity of gas (air =1) | 0.70 |
| Perforation Diameter (in) | 0.4 | Viscosity, μ (cp) | ~ 0.75 |
| % of Active Perforations | 50 | Bubble point pressure, P_b (psi) | 3000 |
| Gravel Permeability (D) | 100 | Oil Compressibility (psi^{-1}) | ~5E-5 |

Table 4.2b Constraints imposed for vertical cased-hole well.

| Design Criterion | Critical Value |
|----------------------------------|-----------------------|
| Pressure drop along perforations | 1000 psi |
| Perforation velocity | 8 ft/s |
| Annular velocity | 1 ft/s |

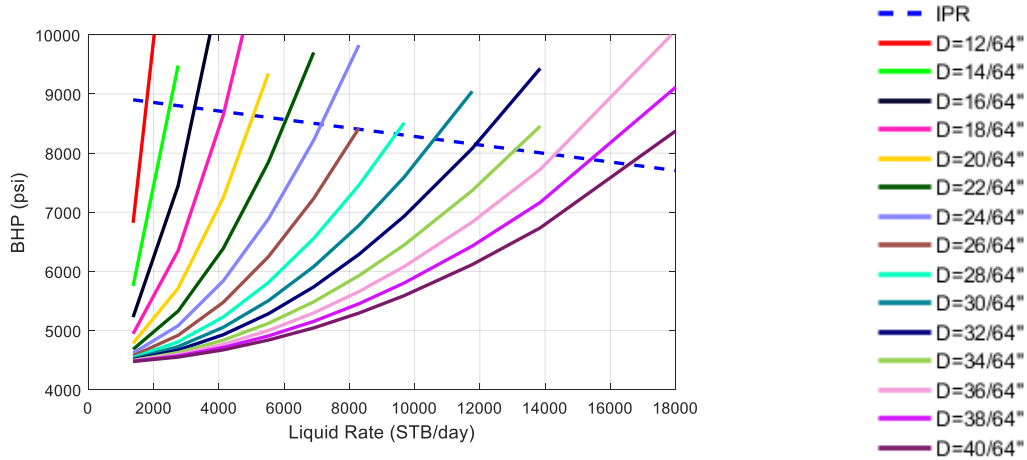


Figure 4.6 IPR and VLP curves at initial conditions

Figure 4.6 presents the IPR and VLP curves for the reservoir/ production system at initial conditions. The smallest choke size that may be used is 12/64". The choke selection algorithm was run for this case and the recommended choke management strategy, along with the full profile of the operation are presented in Figure 4.7. At t=0, instead of using the smallest compatible diameter (12/64"), the algorithm selects the largest choke diameter (26/64") that satisfies all three constraints placed on the system. Comparing Figure 4.7 (d,e,f) we observe that, for this particular case, perforation velocity is the crucial factor that determines the choke size as a function of time.

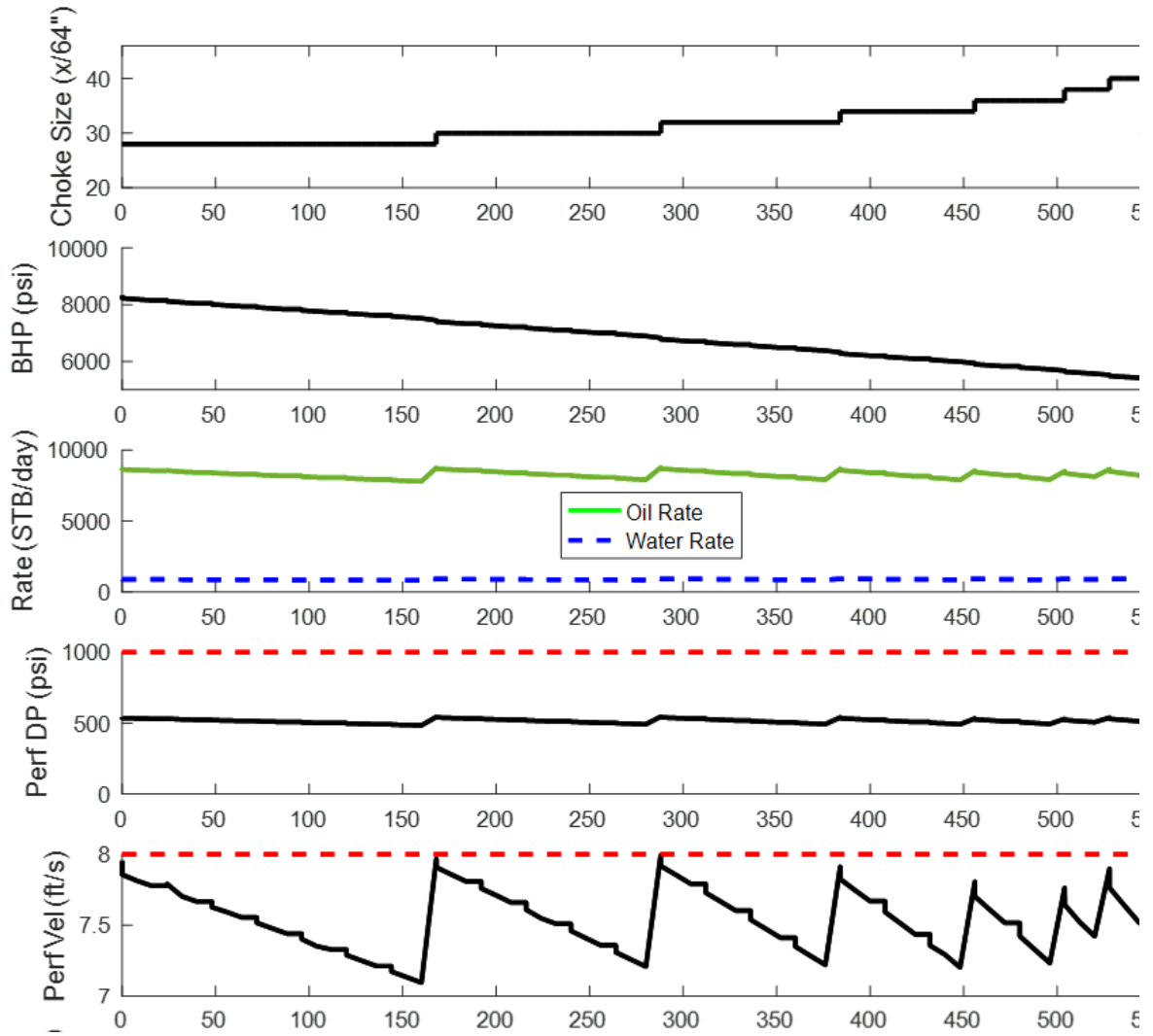


Figure 4.7 Output of choke selection algorithm

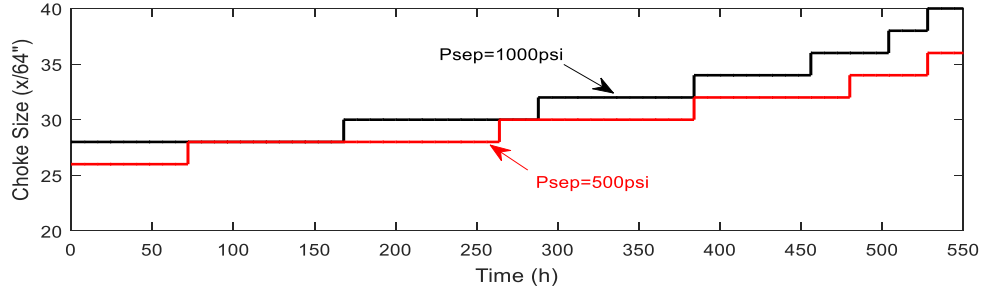


Figure 4.8 Choke sizing as a function of time for separator pressure of 1000psi and 500psi.

Figure 4.8 illustrates the optimum choke management strategy for the case of a smaller separator pressure. We observe that for the same set of constraints, a smaller separator pressure requires a smaller choke diameter: the pressure difference should now be provided as friction loss across the choke. This simple, yet important, observation proves that the selection of the choke sizing depends on various components of the system such as the separator pressure.

4.5.2 Hydraulically Fractured Horizontal Wells

In this example, we illustrate how the method can be deployed for the design of a clean-up operation or production ramp-up in an unconventional oil well. More specifically, we seek a choke sequence that maximizes production and mitigates the risk of excessive proppant flowback. To quantify proppant flowback we utilize the numerical study by Shor and Sharma (2014) who performed grain-scale Discrete Element Modeling (DEM) simulations to assess the combined effect of effective closure stress, pore pressure gradient and particle size on the amount of proppant being produced from a single planar fracture. Figure 4.9 illustrates the mass fraction of the produced proppant as a function of pressure gradient and closure stress.

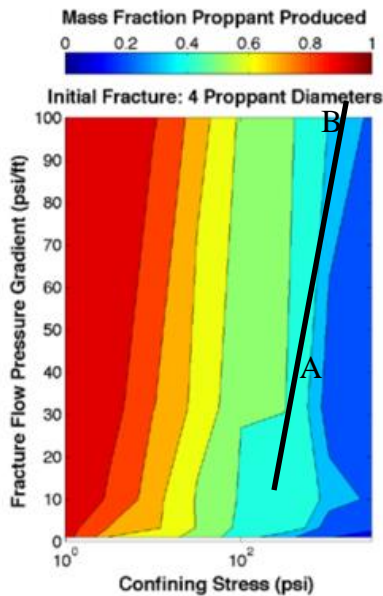


Figure 4.9 Mass fraction of proppant produced

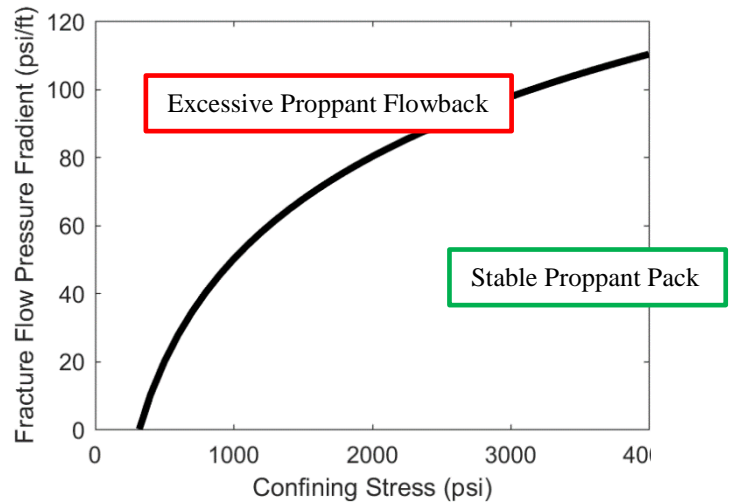


Figure 4.10 Failure envelope for 30% proppant flowback

At the beginning of the clean-up operation, the confining stress is low (Point A) and the proppant can tolerate a small of hydraulic pressure gradient. As the effective stress increases, a larger pressure gradient is required to destabilize the proppant pack. For simplicity, we may assume that the maximum (allowable) pressure gradient is a logarithmic function of the effective stress, σ' , acting on the proppant:

$$\left(\frac{dp}{dx}\right)_{\max} = a \log(\sigma') + b, \text{ where } \sigma' = \sigma_{H\min} - p_{\text{frac}} \quad \text{Eq-1} \quad (4.29)$$

For the design of the clean-up operation, we require that no more than 30% of the proppant flows back into the wellbore. Selecting points A (700psi, 30 psi/ft) and B (3500 psi, 100 psi/ft) as characteristic points, we obtain $a = 100$ and $b = -250$. Using these values, we construct the failure

envelope shown in Figure 4.10. For a given choke size, if the actual pressure gradient along the fracture is larger than the maximum allowable pressure gradient, calculated by Equation-1, then the choke is considered too big and a choke of a smaller diameter should be used.

The method is applied to an unconventional oil well in the Wolfcamp B formation. The reservoir properties were obtained from Wilson, 2015. A refined mesh was used in the well vicinity in order to obtain an accurate estimate of the pressure distribution close to the wellbore and along the fracture. The selection of the grid is in agreement with the recommendations by Bennett et al. (1986) for minimizing truncation error. To reduce computational effort, we simulate a quarter of a single planar fracture using symmetric element modeling. The “pinch points” where pressure gradients were calculated are in a radial distance of 1.5 ft from the mouth of the fracture.

Table 4.3 System properties and constraints imposed for the design of clean-up operation

| Formation Properties | | Available Choke Sizes | |
|--|-----------|---|--------|
| Field dimensions (ft x ft) | 1000x1000 | Minimum Choke Diameter (/64") | 6 |
| Thickness (ft) | 250 | Maximum Choke Diameter (/64") | 40 |
| Minimum Horizontal Stress (psi) | 7250 | Diameter Increments (/64") | 2 |
| Porosity, ϕ | 0.05 | Surface Facilities | |
| Matrix Permeability, k (nd) | 200 | Separator Pressure (psi) | 150 |
| Temperature, T (F) | 170 | Flowline Length (ft) | 300 |
| Initial Reservoir Pressure, P_i (psi) | 5600 | Flowline Inner Diameter (in) | 3 |
| Initial Oil Saturation, So_i | 0.8 | Wellbore Properties | |
| Initial Water Saturation, Sw_i | 0.20 | Wellbore MD (ft) | 14000 |
| Irreducible Oil Saturation, Sor | 0.25 | Wellbore TVD (ft) | 9800 |
| Connate Water, Swc | 0.20 | Tubing Inner Diameter (in) | 3.6 |
| Rel. permeability exponent, n | 2.0 | Fluid Properties | |
| Fracture Properties | | Frac Fluid Viscosity (cp) | 0.5 |
| Fracture Pore Pressure (psi) | 6100 | Oil density (API) | 40 |
| Half-Length (ft) | 200 | Specific gravity of gas (air =1) | 0.70 |
| Fracture Conductivity (md-ft) | 200 | Viscosity, μ (cp) | ~ 0.50 |
| Fracture Height (ft) | 250 | Bubble point pressure, P_b (psi) | 2750 |
| Fracture Spacing (ft) | 175 | Oil Compressibility, (psi ⁻¹) | ~5E-5 |
| Number of Fractures | 60 | Constraint | |
| Stimulated Reservoir Volume (SRV) | | $\left(\frac{dp}{dx}\right)_{\max}^{fracture} \leq 100 \log(\sigma') - 250$ | |
| Permeability (nd) | 1000 | | |
| Pore Pressure (psi) | 5800 | | |
| Water Saturation | 0.5 | | |
| Oil Saturation | 0.5 | | |

The algorithm will check whether the choke size can be increased every 8 h hours. This time schedule depends on the availability of personnel. Table 4.4 shows the calculated values for the choke selection and Figure 4.11 provides the choke sequence along with the full profile or the operation (BHP, liquid rates and fracture pore pressure gradient).

Table 4.4 Sample calculations for selecting choke sizing at early time

| Time (h) | Choke (/64") | BHP | Confining Stress x=1.5ft (psi) | Allowable dp/dr (psi/ft) | Actual dp/dr (psi/ft) | Compatibility |
|----------|--------------|--------|--------------------------------|--------------------------|-----------------------|---------------|
| 0 | 8 | 5333.5 | 1646 | 71.65 | 69.82 | OK |
| | 10 | 5271.1 | 1690 | 72.79 | 87.00 | - |
| 24 | 10 | 5221 | 1962 | 79.29 | 74.66 | OK |
| | 12 | 5105 | 1999 | 80.09 | 88.89 | - |

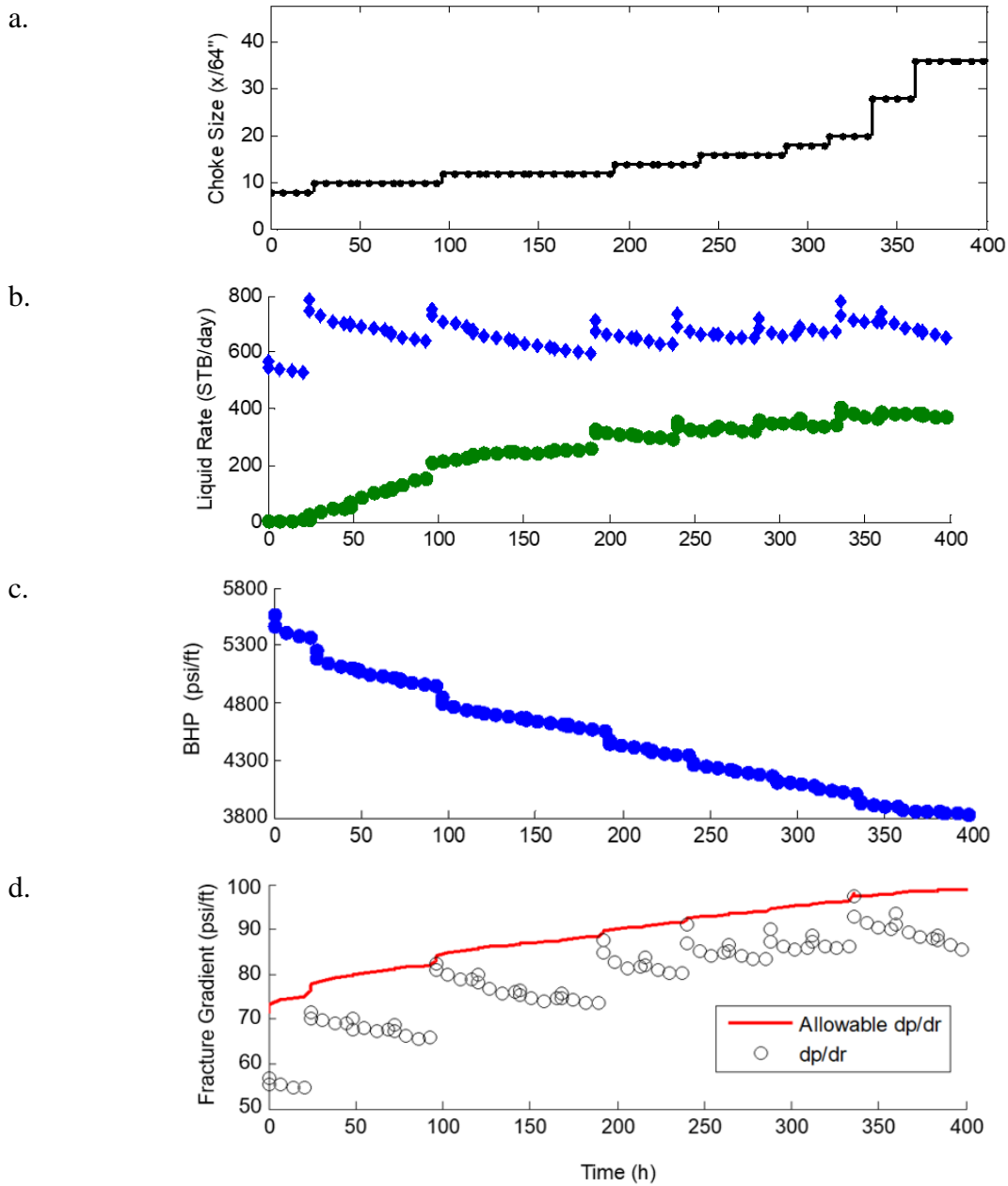


Figure 4.11 Output for the design of clean-up operation

The algorithm selects the choke size so that that the actual pressure gradient along the fracture does not exceed the allowable pressure gradient (Figure 4.11d), assuming that no more

than 30% of the proppant flows back. The model nicely captures the decline of WOR as a function of time as well as the increase of the total liquid rate when a choke of a larger diameter is applied. The controlled BHP management over the span of 250 hours corresponds to an average drawdown rate of 6psi/hour which is similar to conservative clean-up operations deployed in the field (Wilson 2015). The algorithm was run for various reservoir parameters and a relationship between choke size and WOR was observed. Figure 4.12 compares the previous choke management strategy with the one that corresponds to a formation with a higher leak-off volume. Larger water saturation in the SRV delays the onset of hydrocarbon production yet allows choke sizes to be increased at a faster pace. This is attributed to the compressibility of the fluid produced: as incompressible, frac-water is produced, pore pressure rapidly declines, ultimately providing higher confining stresses and allowing the implementation of aggressive choke management strategies. Operators should closely track WOR during clean-up operations and slow down on aggressive choke management strategies as soon as OWR exceeds an approximate value of 0.03.

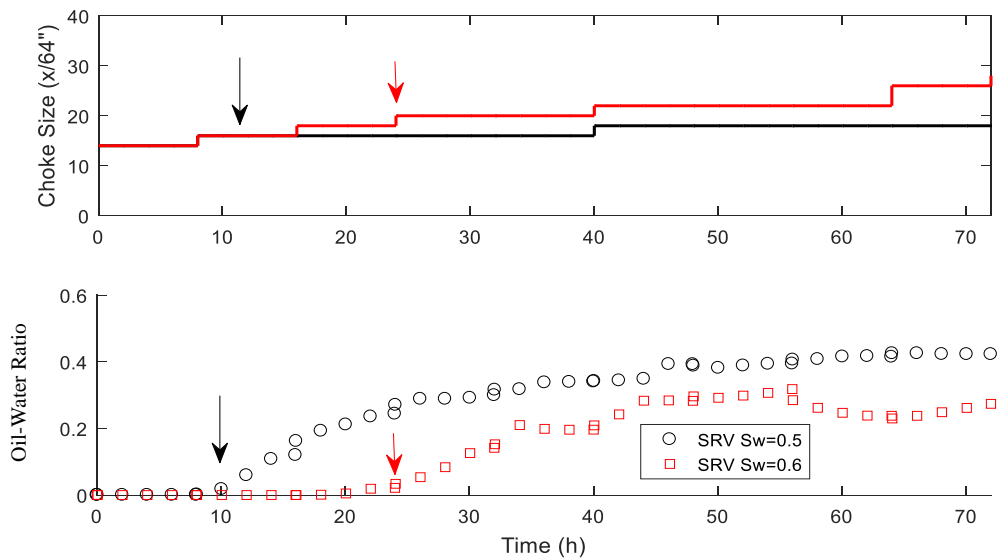


Figure 4.12 Choke sizing for Sw in SRV of 0.5 and 0.6

4.6 DISCUSSION AND CONCLUSIONS

A systematic and logical method was presented for the selection of a choke management strategy in conventional and unconventional wells. Applications of the method illustrate that the selection of a choke management strategy depends on various factors such as the separator pressure or the water saturation in the SRV. Consequently, general guidelines on choke sizes or rate constraints may not always guarantee a successful production ramp up.

In addition, as stress dependent rate constraint has been proposed for the design of flowback operations in hydraulically fractured wells. Implementing this constraint in the choke selection algorithm yields drawdown rates which are in agreement with successful field practices (in the range of 5-10 psi/hr), as proposed by Wilson (2015). A simple application in unconventional oil wells showed that choke sizes can be increased aggressively until the onset of hydrocarbon production, if, for example, proppant flowback is an issue of concern.

Due to the high uncertainty associated with reservoir parameters, this algorithm can be deployed with a history matching scheme that utilizes real-time sensor data to better assess reservoir properties and improve recommendations for future choke adjustments.

Finally, the method presented here is expected to provide insight on whether current practices are too aggressive or conservative and assist operators in properly selecting choke sizes to improve well performance and mitigate the risk of wellbore or completion failures.

4.7 NOMENCLATURE

D_H = hydraulic diameter

ff_j = friction factor of phase j

f_j = fractional flow of phase j

g = gravitational acceleration

J = productivity index (STBD/psi)

$N_{RE,j}$ = Reynolds number for phase j

p_{cr} = pressure at the completion/reservoir interface

P_{av} = average reservoir pressure (psi)

P_{frac} = pore pressure at the mouth of the fracture

P_{outlet} = pipeline outlet pressure

P_{sep} = separator pressure

p_{wf} = Flowing Bottom-Hole-Pressure (psi)

q^j = volumetric flowrate of phase j in standard conditions

$q_{in-situ}^j$ = volumetric flowrate of phase j

Q^L = liquid rate (STBLD)

Q_{max} = maximum liquid rate (STBLD)

S_j = saturation (hold-up) of phase j

u_j = superficial velocity of phase j

v_j = in-situ velocity of phase j

ΔP_{choke} = pressure drop across surface flowline

$\Delta P_{completion}$ = pressure drop across surface flowline

$\Delta P_{flowline}$ = pressure drop across surface flowline

ΔP_i = pressure drop across element i

$\Delta P_{wellbore}$ = pressure drop across surface flowline

ε = tolerance

θ = inclination

μ_j = viscosity of phase j

ρ_j = density of phase j

ρ_{mix} = average mixture density

σ' = effective (closure) stress

σ_{Hmin} = minimum horizontal stress

τ^j = shear stress of phase j to wall

MAJOR SECTION II: FIELD-WIDE MODELING OF PETROLEUM FIELDS

This major Section (Chapters 5, 6 and 7) discusses production modeling and optimization on a field-wide basis. It integrates single well models developed in Section 1 with complex surface production facilities (flowlines, chokes, valves etc.) that connect multiple wells in an oil or gas field to optimize production from the entire field.

Chapter 5: Modeling of Three-Phase Pipeline Networks

5.1 INTRODUCTION

In the previous chapters a systematic method was presented for the selection of the optimum production strategy for a single well under a given set of wellbore, completion and reservoir constraints. For a given set of constraints, the optimum strategy is a function of the various components of the system such as the separator pressure and the tubing diameter which determine the overall pressure drop and ultimately, the total backpressure applied to the reservoir. In real life oil and gas fields, individual well rates are fed into complex surface flowline networks which establish pressure communication between the wells and other components of the system. Pressure losses along the components of a surface flowline network (such as valves, manifolds, regulators etc.) can be significant and may greatly affect both wellhead and bottom-hole pressures and hence production rates, especially in wells characterized by high productivity. In order to capture the effects of multi-well pressure interference and accurately estimate surface pressures, production engineers should properly model and monitor the surface flowline network. In this chapter we present a computationally efficient model for solving three-phase flowline networks under isothermal and steady state conditions. The proposed model is validated with published

network solutions, compared versus field measurements and benchmarked against commercial network solvers used in the oil and gas industry.

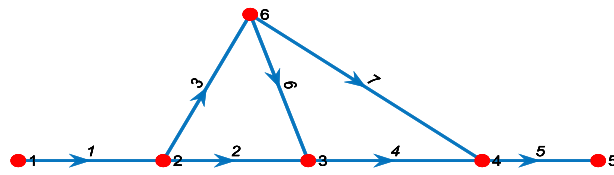
5.2 PERTINENT LITERATURE REVIEW

Network problems are an active research topic in various disciplines including chemical engineering, electrical engineering, traffic engineering and urban hydraulics works. In order to solve a network problem, graph theory is utilized to represent the topology of the network and convert a complex set of nodes and pipelines into a well-defined system of equations. The focus of this section is to briefly discuss the fundamental elements of graph theory, define the set of equations that need to be satisfied and provide an overview of the various models that have traditionally been deployed for solving network flow problems.

5.2.1 Elements of Graph Theory

The topology of a network can be represented with a use of a graph which consists of nodes and branches. A directed graph is graph in which branches have an associated directionality that denotes the flow direction for each branch (Jeppson, 1976). A directed graph (or digraph) may be mathematically described with an oriented incidence matrix where each row represents a node and each column represents a branch. Figure 5.1 illustrates a directed graph and the corresponding oriented incidence matrix. In the oriented incidence matrix, a cell value of +1 indicates the node where the branch originates and cell a value of -1 indicates the node where the branch terminates.

Oriented Incidence Matrix



| | Pipelines | | | | | | |
|-------|-----------|----|----|----|----|----|----|
| Nodes | 1 | 0 | 0 | 0 | 0 | 0 | 0 |
| | -1 | 1 | 1 | 0 | 0 | 0 | 0 |
| | 0 | -1 | 0 | 1 | 0 | -1 | 0 |
| | 0 | 0 | 0 | -1 | 1 | 0 | -1 |
| | 0 | 0 | 0 | 0 | -1 | 0 | 0 |
| | 0 | 0 | -1 | 0 | 0 | 1 | 1 |

Figure 5.1 Illustrative example of directed graph

The incidence matrix conveniently represents the coefficients for the mass balance equations and the transpose of the incidence matrix relates the pressure drop equations with the upstream and downstream nodal pressures for each of the branches (Zhou, 1995).

5.2.2 Governing Equations

As for the case of electric circuits, fluid flow in networks is governed by two physical laws:

- Kirkoff's First Law which dictates that at every node in the network, the algebraic sum of mass flowrates should add up to zero (equivalent to mass balance or continuity equations). In a network of N nodes there are N-1 linearly independent node equations since a global mass balance equation may be applied to the entire network (Jeppson, 1977). This set of equations is usually referred to as the set of node equations. For the case of single-phase flow of incompressible fluids, the node equation at node k has the following form:

$$\sum_i (q_i)_{out} - \sum_i (q_i)_{in} = Q_{ext,k} \quad (5.1)$$

Where q_i is the volumetric flowrate in pipeline i and $Q_{ext,n}$ the external flow at node j . The subscripts *out* and *in* indicate the sets of pipelines originating and terminating at node j , respectively.

- Kickoff's Second Law which dictates that along every closed network loop, the algebraic sum of pressure losses equals zero. This set of equations is commonly referred to as the loop or mesh equations. In a network of N nodes and L branches, there are $L-N+1$ linearly independent loop equations, as are the number of loops (Dolan & Aldous, 1993).

This work focuses on solving the previously mentioned set equations in order to calculate the pressure at the nodes given the outlet pressure (separator pressure) and production rates on the wellheads. However, before proceeding to the three-phase model formulation we briefly discuss the models that have traditionally been used in solving single phase network flows.

5.2.3 Pipeline network solvers

Early approaches to solving network problems adopted the Hardy Cross Method which was originally developed for structural analysis in complex truss structures and large reinforced concrete buildings. With regard to network flows, the method was initially deployed for solving large scale water distribution systems assuming a hydraulic resistance equation that relates single phase flow rates with pressure drop along a pipe element. In order to solve for the node and loop equations, the Cross method requires that the node equations are satisfied and then proceeds with correcting the flowrates in order to satisfy the loop equations. That Hardy-Cross method requires that the initial guess of flowrates satisfies the mass balance equations at every node, including the loops. The correction of flowrates is performed in an iterative manner, in which every loop

equation is solved independently, without having to solve the entire system of equations (Jeppson, 1977). According to Wood et al. (1972), in certain cases, the Cross method converges very slowly or does not converge at all because of the dependency of the solution on the initial guess. In the absence of computers, the method provided an efficient way of solving pipeline networks but was then made obsolete by computer systems that utilized the Newton-Raphson method for solving the entire set of loop and node equations (Dolan & Aldous, 1996).

A significant milestone in network solvers was the introduction of the Linear Theory Method (LTM) by Wood et al. (1972). The LTM linearizes the hydraulics equations and converts the nodal and loop equations into a simple linear system which is then solved iteratively. The LTM has many advantages over the Cross Method such as improved convergence and no requirement for an accurate initial guess. Mucharam and Adewumi (1990) utilized LTM to solve a two-phase pipeline network and observed fast convergence using the Beggs and Brill's PVT correlations.

In the early 1960's, the multivariate Newton-Raphson method was introduced for simultaneously solving the loop and node equations for steady state flows in urban hydraulic works (Martin & Peters, 1963) and natural gas distribution networks (Stoner, 1968). Recently, Stewart (2015), suggested a workflow for solving liquid-gas flow in pipeline networks and characterized the system of equation to make the problem well-posed. The solution of two-phase pipeline networks necessitates the use of empirical correlations on phase splitting and the efficiency of the method is sensitive to the initial conditions. In the numerical scheme suggested by Stewart (2015), fluid properties and saturations in each pipeline are calculated implicitly, an approach which significantly increases the number of unknowns and hence the computational effort for the calculation of the partial derivatives in the Jacobian matrix. Stewart (2015), observed that in large

pipeline networks, the calculation of the Jacobian may be computationally expensive, and a good initial guess might be hard to obtain.

5.2.4 Phase split models

In multi-phase networks, the presence of diverging junctions causes the unequal splitting of gas/liquid phases. This problem is known as the manifold or phase-splitting problem. The unequal splitting of the phases is attributed to the following:

- a) As the lighter phase segregates on top of the heavier phase, it tends to divert towards the branch of higher inclination, and,
- b) As the lighter phase has less inertia, it preferentially flows into the more angled branch of the junction.

Researchers (Saba & Lahey, 1994; Azzopardi et al, 1999; Isaa & Oliveira, 1993) have studied the manifold problem both experimentally and numerically and various models exist for calculating the quality of the mixture (mass flux of air over total flux) in the outlet and branch pipes. The existing phase-split models are specific to different types of junction configurations (Figure 5.2) and are only applicable when a maximum of three pipelines intersect at a junction.

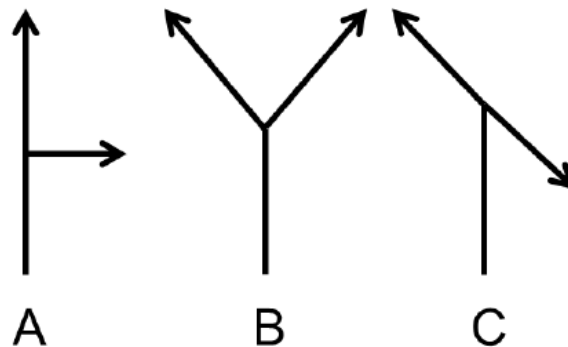


Figure 5.2 A) Side-arm, B) Symmetric impacting and C) Asymmetric impacting junctions
(after Stewart 2015)

Azzopardi (1999) and Muller (1991) provided an overview of the available analytical and empirical phase-separation models that take into account the junction geometry and the fluid properties. These models have focused on two phase water-air and water-gas systems at low pressures and require the inclination and azimuth angles for each of the impacting pipelines - azimuth angles may not always be well documented in complex pipeline networks of the oil and gas industry. Additionally, incorporating the phase split equations in a multiphase network solver requires a priori knowledge of the junctions where phase splitting really occurs. This is not always known, as illustrated by the following example.

A loop comprising three pipelines is shown in Figure 5.3. Single phase streams Q_A and Q_B enter the loop at nodes A and B respectively and the flow exits the loop at node C. Splitting can either take place in node A or B. Assuming a split coefficient, a_s , splitting occurs in node A for $0 < a_s < 1$ and splitting occurs in node B for $a_s < 0$. For various ratios $\beta = Q_A/Q_B$ we solve the loop equation for the split ratio, a_s , using a hydraulic resistivity type of constitutive equation ($\Delta P_i = K|q_i|q_i$).

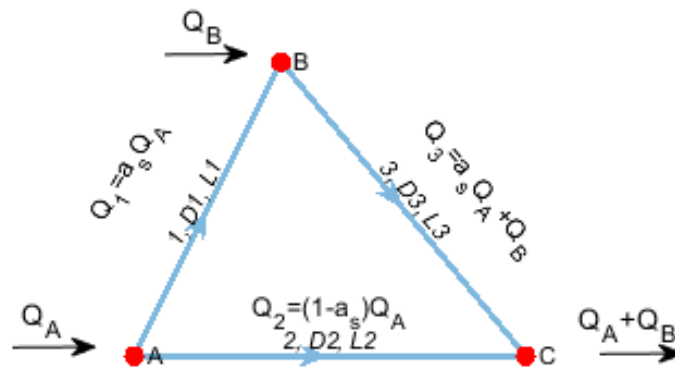


Figure 5.3 Loop topology and external flows

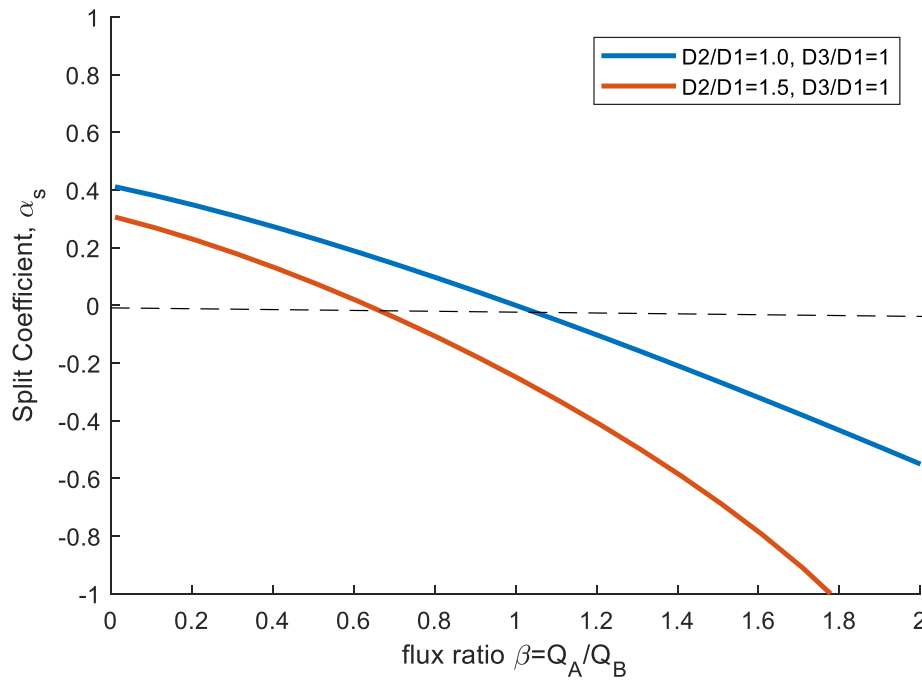


Figure 5.4 Split Coefficient versus the ratio of external volumetric fluxes. Loop topology shown in Figure 5.3.

In Figure 5.4 we observe that the sign of the split coefficient depends both on the flow ratio β and the diameter of the pipelines. Consequently, in a complex pipeline network, and for any user-specified rates, the nodes where splitting really occurs is not known a priori.

5.2.5 Limitations of Numerical Models in Pipeline Networks

Previously in this section, we presented an overview of the available models for solving single and multi-phase pipe networks. Expanding the model by Stewart (2015) into three-phase pipeline networks and assuming an explicit calculation of the PVT properties, yields the set of unknowns / equations presented in Table 5.1.

Table 5.1 Analysis of equations/unknowns for three-phase network flows

| Unknowns | | Equations | |
|-------------------------|-------------|-----------------------------|-------------|
| Nodal Pressures | N | Pressure Boundary Condition | 1 |
| Rates in each Pipelines | 3L | Phase Continuity Equations | 3(N-1) |
| | | Loop Equations | L-N+1 |
| | | Phase Split Equations | 2(L-N+1) |
| | | Pressure Drop Definitions | L-(L-N+1) |
| SUM | N+3L | | N+3L |

Solving the aforementioned set of equations for three-phase network flows, one faces the following challenges:

- In order to simultaneously solve the entire system of equations, two equations for phase-splitting are required per closed network loop. One phase split equation is required for the lighter-phase (gas) and one for the intermediate phase (oil). The currently available phase split models have been developed and validated for water-gas and water-air systems at low pressure conditions which questions their suitability in oil-water-gas systems at higher pressures.
- The implementation of the phase split models requires knowledge of the exact geometry of the junctions such as the inclination and azimuth angles, locally at the intersection. Azimuth angles may not always be documented and maintained in large pipeline networks of the oil and gas industry.
- Current models on phase splitting can only handle the intersection of three pipelines. If more than three pipelines intersect at a single node, these models fail to provide an answer.

- As previously illustrated, the nodes at which a phase split occurs is not known a priori. Consequently, using a Newton-Raphson formulation with phase splitting equations should assume the nodes where splitting occurs and then validate the feasibility of the solution based on that assumption. In the presence of multiple loops, this approach can negatively impact the performance of the network solver and increase computational time.
- Implicitly solving for the Pressure-Volume-Temperature (PVT) properties (such as fluid densities) and fluid saturations for each pipeline increases the number of unknowns and the computational overhead for the calculation of the partial derivatives in the Jacobian Matrix. Consequently, an explicit calculation of PVT properties is suggested.
- Using a finite difference scheme for calculating the pressure drop along a pipeline significantly increases the computational effort in the evaluation of the Jacobian Matrix, should the Newton-Raphson method be used. More specifically, for each pipeline in the network, the partial derivatives of the pressure drop equation need to be calculated with respect to the variables that correspond to the downstream pressure and oil, water and gas rates. Consequently, using a computationally expensive pipeline model (such as the one presented in Chapter 4) can significantly impact the performance of the network solver.
- Finally, in the case of complex pipeline networks, the flow direction along a closed network loop is not known in advance. Consequently, a good initial guess on the sign of flowrates is not readily available.

5.3 MODEL FORMULATION FOR THREE-PHASE BRANCHED NETWORKS

This section describes the workflow for solving three-phase pipeline networks with a tree-like structure. The objective is to calculate the nodal pressures and the flowrates of oil, water and gas in each pipeline of the network given a) the external volumetric flowrates of oil, water and gas entering the network and b) a pressure boundary condition. An example of a branched network with external three-phase flowrates ($Q_{ext}^{o,w,g}$) is illustrated in Figure 5.5. In this particular example, external three-phase streams (sources $Q_{ext}^{(o,w,g)}$), enter the network at nodes #1, #3 and #5, respectively. Fluid exits the network at node #7 under constant pressure (boundary condition).

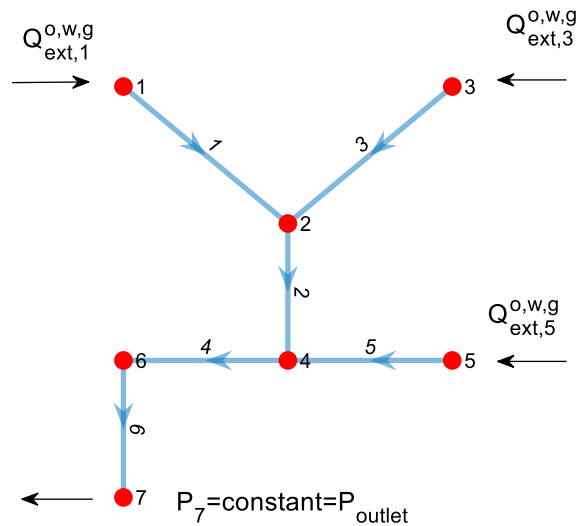


Figure 5.5 Branched network with external three-phase streams.

5.3.2 Analysis of Equations/ Unknowns

For the case of branched networks, no loops exist, and the network solution needs to satisfy the node equations for each phase j , j =oil, water gas. The analysis of equations and unknowns is presented in Table 5.2.

Table 5.2 Analysis of equations/ unknowns for three-phase branched networks

| Unknowns | | Equations | |
|--------------------|------------------|-----------------------------|--------------------|
| Nodal Pressures | N | Pressure Boundary Condition | 1 |
| Rates in Pipelines | 3L | Continuity Equations | 3(N-1) |
| | | Pressure Drops | L |
| SUM | N+3L=4N-3 | | 3N+L-2=4N-3 |

It is important to note that in the analysis presented herein the pressure drop along each pipeline is evaluated using the pipeline model presented in Chapter 4. Since a black-oil model is deployed, the node equations are translated as phase mass balance (or continuity) equations (instead of mass balance equations applied to individual components). For each phase j =oil, water, gas, the phase continuity equations at node k can be expressed in standard conditions as:

$$\sum_i (q_i^j)_{out} - \sum_i (q_i^j)_{in} = Q_{ext,k}^j \quad j=\text{oil, water, gas} \quad (5.2)$$

Where q_i^j is the volumetric flowrate of phase j in pipeline i and $Q_{ext,k}^j$ the external flow of phase j at node k , both at *standard conditions*. $Q_{ext,k}^j$ is positive if the stream enters and node and negative, otherwise. The subscripts *out* and *in* indicate the sets of pipelines originating and terminating at node k , respectively. Note that to convert the flow rates at a node to standard conditions the density of the fluid phase must be computed at a specific pressure and temperature (P, T). This makes the

problem non-linear. To linearize the problem an initial guess for the pressure and temperature is made and iterations are performed until the equations are satisfied to some tolerance and convergence is achieved. These PVT properties are computed as discussed in Appendix C.

In Table 5.2 we observe that for branched networks, the number of equations equals the number of unknowns. Additionally, since the continuity equations are linearized (see equation 5.2), the pipeline flowrates, q_i^j can be obtained by solving the set of node equations for each phase j .

5.3.3 Model Assumptions

The model assumes steady-state flow and isothermal conditions. Additionally, the proposed model does not account for lumping and de-lumping of the PVT properties at pipeline intersections, which imposes the assumption that hydrocarbon streams flowing into the network have similar black-oil properties (i.e. the oil API density and specific gas gravity, γ_g are equal for all external flows in the network). This is a reasonable assumption for wells being produced from the same field. Finally, the current formulation does not take into consideration local energy losses in pipeline bends or intersections and the nodal pressures are assumed to be equal for all pipelines adjoining the same junction.

5.3.4 Conventions

In the network analysis presented herein, the following conventions hold:

- a) For a pipeline connecting two nodes, a positive flowrate corresponds to flow along the assigned positive direction. A negative flowrate indicates that flow occurs against the assigned direction (i.e. from the downstream to the upstream node).

- b) The pressure drop along pipeline i , ΔP_i , is defined as the pressure at the upstream node minus the pressure at the downstream node. Consequently, for horizontal pipelines, a positive volumetric flowrate corresponds to a positive pressure drop.

5.3.5 Formulation

In the absence of loops, the network solution needs to satisfy the continuity equations for each phase. To this end, the pipeline flowrates are obtained by solving the continuity equations with all flow rates being at standard conditions for each phase j , j =oil, water and gas:

$$[A_r]q^j = B^j \quad (5.3)$$

Where

$[A_r]$: the reduced (node-pipeline) oriented incidence matrix. This matrix is obtained from the incidence matrix by omitting the row that corresponds to the node of known pressure.

q^j : is the column vector comprising the volumetric flowrates (at standard conditions) of phase j in pipeline i , q_i^j , for each pipeline in the network

B^j : is the column vector comprising the external flowrates, in standard conditions, of phase j at node i , B_i^j , for each node in the branched network. B_i^j is positive when phase j enters the network at node i and negative, otherwise.

The solution of the linear systems described by equation (5.3) (one linear system for each phase j) yields the oil, water and gas flowrates at standard conditions for each pipeline in the branched network. The nodal pressures can then be obtained by iteratively solving the linear system:

$$[A_r]^T P^{(k+1)} = \Delta P^k \quad (5.4)$$

Where:

$[A_r]^T$: the transpose of the reduced incidence matrix (see equation (5.1))

\mathbf{P}^{k+1} : the column vector comprising the nodal pressures at iteration k+1

$\Delta\mathbf{P}^k$: the column vector comprising the pressure drop along each pipeline i at iteration k, ΔP_i^k , evaluated using the corresponding downstream pressure of pipeline i from iteration k-1. $\Delta\mathbf{P}^k$ also encompasses the pressure boundary condition, the value of which is added to the row that represents the pipeline connected to the node of known pressure (i.e. the separator)

It is important to note that the linear system needs to be solved iteratively since the pressure drop in a pipeline and the fluid phase density are both strong functions of the downstream pressure which is updated per iteration. This formulation is an explicit formulation, implying that the PVT properties (density, fluid viscosity) are calculated using the pressures from the previous iteration (lagging). The iteration scheme terminates once the nodal pressures have stabilized, typically with an accuracy of 0.01psi. In other words, the convergence criterion for the iterative scheme is defined as:

$$\max_{i \in \text{Nodes}} |P_i^{(k+1)} - P_i^{(k)}| < 0.01 \text{ psi} \quad (5.5)$$

Where $P_i^{(k)}$ is the pressure at node i at iteration k. In gas networks or three-phase networks with high Gas Oil Ratios (GORs) the pressure drop in each pipeline is much more sensitive to the downstream flowing pressure and hence, it may take significantly more iterations for nodal pressures to stabilize as opposed to low compressibility or low GOR fluid networks. The following page provides an illustrative example of solving three-phase networks with a tree-like structure.

5.3.6 Workflow Summary

Figure 5.5 illustrates a branched network with external flows, $Q_{ext}^{o,w,g}$, entering the network at nodes #1, #3 and #5. Fluid exits the network at node #7 under constant pressure, P_{out} (pressure boundary condition). The objective is to find the flow rates of oil, water and gas in each pipeline as well as the pressure at the nodes.

Step A

Construct the (node-pipeline) Adjacency Matrix, $[A]$ of the Network and initialize the pressures at the nodes: $P_i^0 = P_{out}, i=1,2,..N$ where N is the number of nodes.

$$\text{Pipe: } \begin{matrix} 1 & 2 & 3 & 4 & 5 & 6 \end{matrix}$$

$$A = \begin{bmatrix} 1 & 0 & 0 & 0 & 0 & 0 \\ -1 & 1 & -1 & 0 & 0 & 0 \\ 0 & 0 & 1 & 0 & 0 & 0 \\ 0 & -1 & 0 & 1 & 1 & 0 \\ 0 & 0 & 0 & -1 & 0 & 0 \\ 0 & 0 & 0 & 0 & -1 & 1 \\ 0 & 0 & 0 & 0 & 0 & -1 \end{bmatrix} \begin{matrix} \text{Node 1} \\ \text{Node 2} \\ \text{Node 3} \\ \text{Node 4} \\ \text{Node 5} \\ \text{Node 6} \\ \text{Node 7} \end{matrix}$$

Step B

Solve the (N-1) node equations for each phase j , $[A_r]q^j = B^j$ to obtain the flowrate of phase j in each pipeline i , q_i^j . $[A_r]$ is obtained from $[A]$ by removing the row that corresponds to the outlet node. Column vector B contains the external flows of phase j for every node in the network.

Repeat for j =oil, water gas

$$\text{Pipe: } \begin{matrix} 1 & 2 & 3 & 4 & 5 & 6 \end{matrix}$$

$$\begin{matrix} \text{Node 1} \\ \text{Node 2} \\ \text{Node 3} \\ \text{Node 4} \\ \text{Node 5} \\ \text{Node 6} \end{matrix} \begin{bmatrix} 1 & 0 & 0 & 0 & 0 & 0 \\ -1 & 1 & -1 & 0 & 0 & 0 \\ 0 & 0 & 1 & 0 & 0 & 0 \\ 0 & -1 & 0 & 1 & 1 & 0 \\ 0 & 0 & 0 & -1 & 0 & 0 \\ 0 & 0 & 0 & 0 & -1 & 1 \end{bmatrix} \begin{bmatrix} q_1^j \\ q_2^j \\ q_3^j \\ q_4^j \\ q_5^j \\ q_6^j \end{bmatrix} = \begin{bmatrix} Q_{ex,1}^j \\ 0 \\ Q_{ex,3}^j \\ 0 \\ Q_{ex,5}^j \\ 0 \end{bmatrix}$$

Step C

Iteratively solve $[A_r]^T P^{k+1} = \Delta P^k$ until pressures stabilize. Pressure drops ΔP are calculated using the downstream pressures from the previous iteration and the flow rates from Step B. Iteration is required since ΔP_i depends on the outlet (downstream) pressure of pipeline i which is updated per each iteration.

$$\text{Node: } \begin{matrix} 1 & 2 & 3 & 4 & 5 & 6 \end{matrix}$$

$$\begin{matrix} \text{Pipe 1} \\ \text{Pipe 2} \\ \text{Pipe 3} \\ \text{Pipe 4} \\ \text{Pipe 5} \\ \text{Pipe 6} \end{matrix} \begin{bmatrix} 1 & -1 & 0 & 0 & 0 & 0 \\ 0 & 1 & 0 & -1 & 0 & 0 \\ 0 & -1 & 1 & 0 & 0 & 0 \\ 0 & 0 & 0 & 1 & -1 & 0 \\ 0 & 0 & 0 & 1 & 0 & -1 \\ 0 & 0 & 0 & 0 & 0 & 1 \end{bmatrix} \begin{bmatrix} P_1^{k+1} \\ P_2^{k+1} \\ P_3^{k+1} \\ P_4^{k+1} \\ P_5^{k+1} \\ P_6^{k+1} \end{bmatrix} = \begin{bmatrix} \Delta P_1^k \\ \Delta P_2^k \\ \Delta P_3^k \\ \Delta P_4^k \\ \Delta P_5^k \\ \Delta P_6^k + P_{outlet}^k \end{bmatrix}$$

5.4 MODEL FORMULATION FOR THREE-PHASE LOOPED NETWORKS

The model presented herein is intended to provide an efficient computational scheme for solving three-phase pipeline networks by overcoming some of the challenges discussed previously in this chapter (see paragraph 5.2.5). To this end, the model was formulated in order to:

- Perform mass balance calculations by using flow rates at standard conditions
- Decouple the node equations from the loop equations
- Explicitly calculate the PVT properties using Black-Oil Correlations
- Isolate and independently solve clusters of loops to minimize loop residuals
- Account for multiple (more than three) pipelines adjoining the same junction
- Require no information on the local azimuth angles at pipeline intersections

The proposed model adopts the approach of “Diakoptics” (Greek: dia–through +kopto–cut, tear) introduced by Kron (1963). Using network topology the network problem is decomposed into minor sub-problems (one for each cluster of loops) before independent solutions are joined together to obtain the solution of the entire network.

5.4.1 Assumptions and Conventions

The analysis presented herein adopts the entirety of assumptions and conventions previously discussed in the formulation of the branched network solver (see paragraphs 5.3.3 and 5.3.4).

5.4.2 Analysis of equations/ unknowns

For the reasons presented earlier in the chapter the phase split equations are excluded from the proposed model. Table 5.3 presents the unknowns and equations for a network comprising of N nodes and L links:

Table 5.3 Underdetermined system of equations/ unknowns for three-phase network flows

| Unknowns | | Equations | |
|-------------------------|-------------|---|---------------|
| Nodal Pressures | N | Pressure Boundary Condition | 1 |
| Rates in each Pipelines | 3L | Phase Continuity Equations (in standard conditions) | 3(N-1) |
| | | Loop Equations | L-N+1 |
| | | Pressure Drop Definitions | L-(L-N+1) |
| SUM | N+3L | | 3N+L-2 |

Omitting the phase split equations results in a deficit of $2(L-N+1)$ equations and hence the system is underdetermined. We seek solutions (i.e. pipeline flowrates) that satisfy the node continuity equations as well as the energy loop equations.

5.4.3 Network Topology and Loop Clustering

This section describes the approach for identifying the linearly independent loops in a complex pipeline network. In a network with N nodes and L pipelines, the number of linearly independent loops is given by the following equation:

$$N_{loops} = L - N + 1 \quad (5.6)$$

The first step towards identifying the linearly independent loops is to obtain the Minimum Spanning Tree (MST) of the network using Kruskal’s algorithm (Jeppson, 1976). The minimum spanning tree is a network that encompasses all nodes of the initial network, it has, however, a tree-like structure. Essentially, Kruskal’s algorithm excludes a number of N_{loop} pipelines from the initial network topology. The excluded pipelines are referred to as “chords”. A looped network and the corresponding MST are shown in Figure 5.6

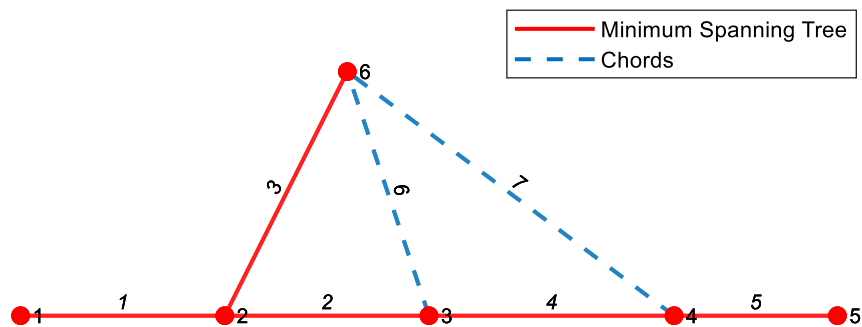


Figure 5.6 Minimum Spanning Tree (MST) and Chords Identified using Kruskal's Algorithm

Whenever a chord is added to MST, one loop is formed. For example, in the topology shown in Figure 5.6, if pipeline #6 is added to the Minimum Spanning Tree then the loop comprising pipelines 2-3-6 is formed. Similarly, if pipeline #7 is added to the MST, the loop 3-7-4-2 is formed. In order to find the algebraic equation of a linearly independent loop, one chord is added to the MST and then the nodes of the MST are pruned until that loop is isolated. This process can be accomplished with the use of the node-node connectivity matrix. By convention, we assign zero elements on the diagonal of the connectivity matrix. For the connectivity matrix, we remove, one at a time, rows and columns whose sum equals to one (i.e. nodes that are only connected to a single pipeline). When no more rows or columns can be removed, the loop has been isolated and

the nodes enclosing that loop have been identified. For example, the process for identifying the loop that corresponds to chord #6 is shown in Figure 5.7.

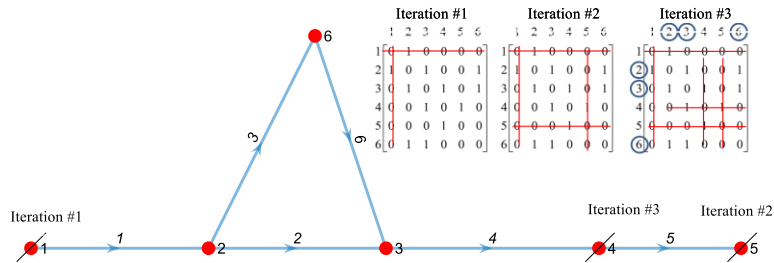


Figure 5.7 Iterative approach for identifying the nodes enclosing a closed pipeline loop

An alternative method for obtaining the loops of a graph is by implementing Algorithm 5.1 which identifies the linearly independent, non-overlapping loops that contain the least number of pipes:

Algorithm 5.1 Algorithm for identifying the nodes of non-overlapping loops

For each node i in the network

1. Select node i . Call it 'A'.
2. If less than 3 branches are connected to 'A', then go to step 8
3. Enumerate the pairs of links originating from 'A'.
4. Select one pair. Name the adjacent nodes 'B' and 'C'.
5. If B and C are connected, output the closed network loop ABC and proceed to step 4.
6. If B and C are not connected
 - i. Enumerate the set of nodes connected to B. Assume it is connected to nodes D, E, and F. Create the list of vectors CABD, CABE, CABF and for each of these vectors:
 - ii. If the last node of a vector is connected to any internal node except for C or B, discard that vector
 - iii. If the last node is connected to node C, output the vector as a loop and discard
 - iv. If it is not connected to node B or node C, create a new list of vectors and append all nodes to which the last node is connected.
 - v. Repeat until no more vectors exist
7. Repeat steps 4-6 for all pairs.
8. Continue

End

Once the nodes enclosing a loop have been identified, either with the MST approach or the heuristic algorithm, the equation for that loop can be obtained. The algebraic equation for a loop can be written in following generic form:

$$\sum_{j \in \Omega} s_j \Delta P_j = \mathbf{P}^T [A^{loop}] \mathbf{S} = 0 \quad (5.7)$$

Where

- Ω the set of pipelines contained in the loop
- ΔP_j The (signed) pressure drop along pipeline j
- s_j A constant (-1 or +1) indicating whether the assigned positive direction of pipeline j is clockwise or anticlockwise
- \mathbf{P} The row vector comprising the nodal pressure of the nodes enclosing the loop
- A^{Loop} The local oriented incidence matrix of the loop
- \mathbf{S} The column vector comprising constants s_j , for each pipeline j included in the loop

To determine the sign coefficients, s_j for each pipeline j in the loop, we arbitrarily determine the direction convention by postulating that $s_k=1, k \in \Omega$, and then solve the linear system:

$$[A^{loop}] \mathbf{S} = 0 \quad (5.8)$$

using backward substitution. For the loop in Figure 5.7 the linear system has the form:

$$\begin{array}{l} \text{Pipes:} \quad 2 \quad 3 \quad 6 \\ \text{Node 2} \quad \left[\begin{array}{ccc} 1 & 1 & 0 \end{array} \right] \left[\begin{array}{c} S_2 \\ S_3 \end{array} \right] = \left[\begin{array}{c} 0 \\ 0 \end{array} \right] \\ \text{Node 3} \quad \left[\begin{array}{ccc} -1 & 0 & -1 \end{array} \right] \\ \text{Node 6} \quad \left[\begin{array}{ccc} 0 & -1 & 1 \end{array} \right] \left[\begin{array}{c} S_6 \end{array} \right] = \left[\begin{array}{c} 0 \end{array} \right] \end{array}$$

By postulating that $S_2=1$, we obtain $S_3=-1$ and $S_6=-1$ and the corresponding loop equation is:

$$\Delta P_2 - \Delta P_3 - \Delta P_6 = 0 \quad (5.9)$$

To identify the loop equations for each loop in network, the process is repeated for all chords obtained from the MST algorithm. Once the loops have been identified, they are categorized into clusters. A cluster of loops is defined as a set H of loops in which for every loop

$L1 \in H$, there is another loop $L2 \in \Omega$ with at least a common pipeline. In addition, every loop must be a subset of a unique cluster. The concept of loop clustering is illustrated in Figure 5.8.

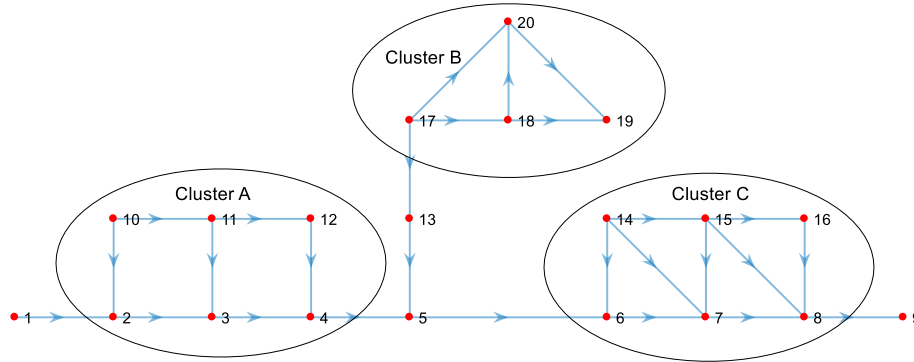


Figure 5.8 Concept of loop clustering in networks

5.4.4 Solution for a Cluster of Loops

This section delineates the process of solving an isolated cluster of loops given the external flowrates of oil, water and gas along with a pressure boundary condition. The pressure boundary condition is typically the pressure at the node where the fluid exits the cluster. The solution of the cluster is intended to provide:

- a) The volumetric flowrates of water, oil and gas for each pipeline in the cluster
- b) The pressure at the nodes forming the cluster

Table 5.4 presents the number of unknowns and number of equations for a cluster comprising N nodes and L links:

Table 5.4 Underdetermined system of equations/ unknowns for three-phase network flows

| Unknowns | | Equations | |
|-------------------------|-------------|-----------------------------|---------------|
| Nodal Pressures | N | Pressure Boundary Condition | 1 |
| Rates in each Pipelines | 3L | Phase Continuity Equations | 3(N-1) |
| | | Loop Equations | L-N+1 |
| | | Pressure Drop Definitions | L-(L-N+1) |
| SUM | N+3L | | 3N+L-2 |

In any given cluster there is a deficit of $2(L-N+1)$ equations and hence the system is underdetermined. We seek cluster solutions (i.e. pipeline flowrates) that satisfy both the node continuity equations and the energy loop equations, locally in the cluster.

5.4.4.2 Individual Cluster Topology and Tearing Variables

The topology of an isolated cluster is presented Figure 5.9. The cluster is connected with the external network at nodes #1, #2 and #4 which define the flows external to the cluster.

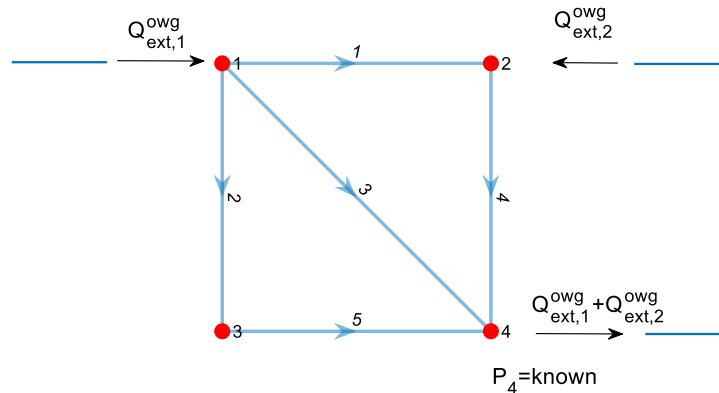


Figure 5.9 Illustrative example of a cluster comprising two loops.

In order to solve the cluster, we adopt the “tearing method” and the cluster is torn apart by replacing the chords with external flowrates, x which are referred to as tearing variables. The concept of tearing variables is illustrated in Figure 5.10 and Figure 5.11.

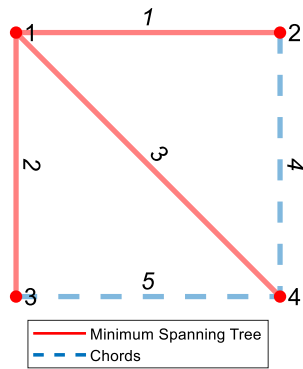


Figure 5.10 MST and chords for the cluster topology shown in Figure 5.9

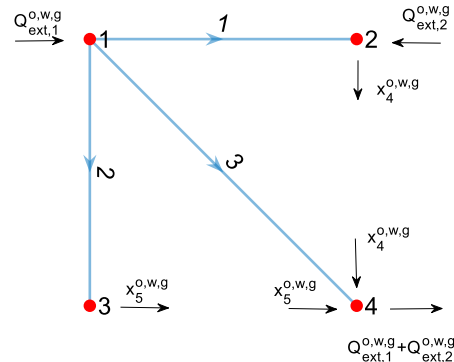


Figure 5.11 Concept of tearing variables

In an isolated cluster comprising N nodes and L pipelines there are $L-N+1$ chords which, for the case of three-phase flow, yield a total of $3(L-N+1)$ tearing variables. For given vector of tearing variables, \mathbf{x} , the oil water and gas flowrates in the pipelines composing the MST can be calculated by solving the node continuity equations for each phase j =oil, water, gas

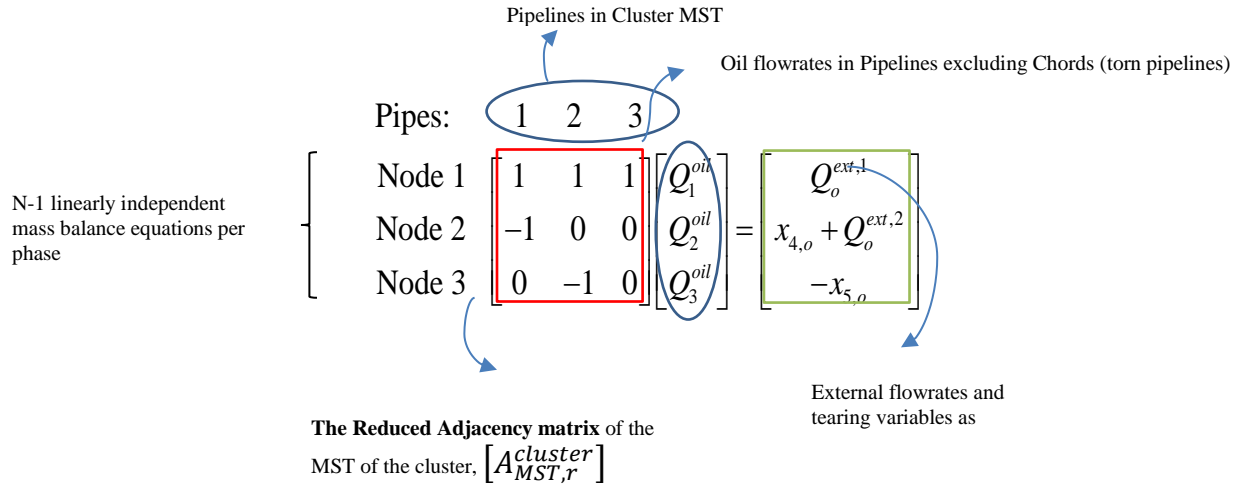
$$[A_{MST,r}^{cluster}] \mathbf{q}_{MST}^j = \mathbf{B}_x^j \quad (5.10)$$

where

- $[A_{MST,r}^{cluster}]$ The reduced local incidence matrix of the cluster Minimum Spanning Tree (MST). This matrix is obtained from the local incidence matrix of the MST by excluding the (outlet) node of known pressure
- \mathbf{q}_{MST}^j The column vector comprising the flowrates of phase j for each pipeline in the Minimum Spanning Tree of the Cluster

B_x^j The column vector comprising the j-phase external flowrates and tearing variables for each node in the cluster

For the example presented in Figure 5.11, the node equations for the oil phase have the following form:



5.4.4.3 Definition of Relative Residuals

We observe that for any selection of tearing variables, the phase balance equations are satisfied since the pipeline flow rates are obtained by solving a linear system (equation 5.10). The process of solving the cluster is associated with finding a vector of tearing variables, \mathbf{x} , that minimizes the residual of the loop equations contained in the cluster. In the proposed method, for a single loop, i , the relative residual, R_{loop}^i , is defined as:

$$R_{loop}^i = \frac{\sum_{j \in \Omega_i} (s_j^i \Delta P_j)}{\sum_{j \in \Omega_i} |\Delta P_j|} \quad (5.11)$$

where:

Ω_i : the set of pipelines contained in loop i

S_j^i : the sign constant (+1 or -1) for pipeline j in loop i, indicating clock wise or anti-clock direction

ΔP_i : The signed pressure drop along pipeline i defined as $P_{\text{upstream}} - P_{\text{downstream}}$

The relative loop residual is a dimensionless quantity that relates the absolute loop residual with the sum of the absolute pressure drops around a loop. This is a convenient way to quantify loop residuals both in systems with significant or miniscule frictional pressure losses. Following this definition, the residual of the cluster is defined as:

$$R(\bar{x}) = \sqrt{\frac{\sum_{i=1}^{N_{\text{Loops}}^c} (R_{\text{Loop}}^i)^2}{N_{\text{Loops}}^c}} \quad (5.12)$$

Where:

\mathbf{x} : the vector of the tearing variables (i.e. oil water and gas rates for each chord in the cluster)

N_{Loops}^c : the number of linearly independent loops contained in the cluster

R_{Loop}^i : the relative residual of loop i

In the proposed model and for a given vector of tearing variables, \mathbf{x} , the calculation of the relative cluster residual, $R(\mathbf{x})$ is performed in the following steps:

- a) For each phase, solve the node equations $[A_{MST,r}^{cluster}] \mathbf{q}^j = \mathbf{B}^j(x, Q_{ext}^j)$ treating both the external flows, $Q_{ext}^{o,w,g}$, and tearing variables, \mathbf{x} , as sinks/sources.
- b) For the flowrates obtained in step a, update the pressure drop, ΔP_i , in each pipeline i contained in the cluster using the pipeline model presented in Chapter 4 and the PVT correlations summarized in Appendix C.
- c) Obtain the pressures at the nodes of the cluster by solving the linear system:

$$[A_{MST,r}^{cluster}]^T \mathbf{P} = \Delta \mathbf{P} \quad (5.13)$$

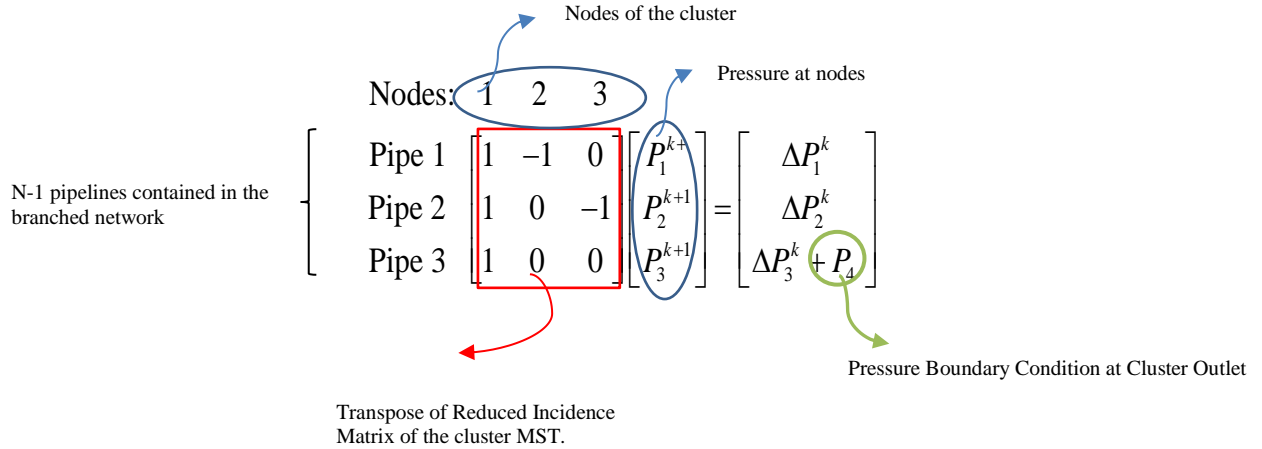
Where

$A_{MST,r}^{cluster}$ The reduced oriented incidence matrix of the Minimum Spanning Tree (MST) of the cluster

\mathbf{P} The column vector comprising the pressure at the nodes of the cluster

$\Delta \mathbf{P}$ The column vector comprising pressure drops (calculated from step b) for each of the pipelines included in the MST and the cluster pressure boundary condition

For the topology shown in Figure this linear system has the form:



d) Repeat steps b, c and d until pressures stabilize

e) Calculate the cluster residual using equation (5.12)

Before solving the cluster by identifying the vector of tearing variables that minimizes the cluster residual, it is important to understand the behavior of the residual function, given a vector of tearing variables. To this end we evaluate the value of the cluster residual, R , for the cluster topology shown in Figure 5.12. Gas enters the cluster at nodes #1 and #2 at a gas rate of 41 and 30 MMSCFD, respectively.

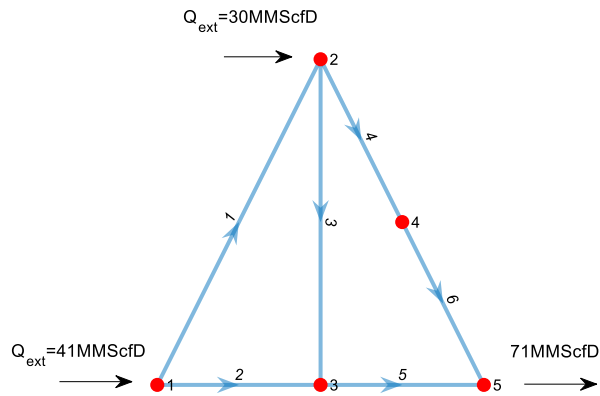


Figure 5.12 Isolated cluster in gas network.

For this example, the selected tearing variables are the gas rates in pipeline #2 and #6, respectively. The value of the cluster residual as a function of the tearing variables is shown in Figure 5.13. We observe that the average cluster residual is minimized for $q_2 \sim 31 \text{ MMScfD}$ and $q_6 = 26 \text{ MMScfD}$ which constitutes the solution for the cluster. In the next section we discuss how to find the minimum of the average cluster residual (i.e. solve the cluster) using a gradient based approach.

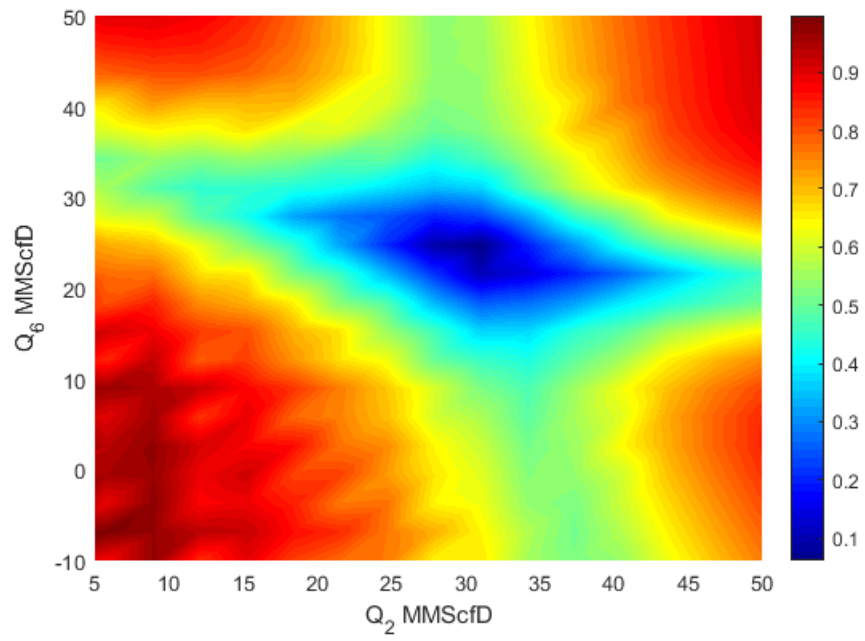


Figure 5.13 Cluster residual as a function of the tearing variables

5.4.4.4 Minimization of Loop Residuals

Given an initial guess (\mathbf{x}_0) for the vector of tearing variables, the cluster residual is minimized using the nonlinear Fletcher-Reeves Conjugate Gradient Method. The Fletcher-Reeves method is an iterative line search method where the new guess for the vector of tearing variables, \mathbf{x} , is given by:

$$\mathbf{x}_{k+1} = \mathbf{x}_k + a\mathbf{p}_k \quad (5.14)$$

Where:

\mathbf{x}_k : the vector of tearing variables at iteration k

a_k : the step length at iteration k

\mathbf{p}_k : the search direction

In the Fletcher-Reeves (FR) method, the search direction is a linear combination of the steepest descent and the search direction of the previous iteration (Nocedal, 2006). The FR method was slightly modified with the implementation of restarts to periodically refresh the algorithm (see Algorithm 5.2).

Algorithm 5.2 Fletcher-Reeves direction search algorithm (Nocedal, 2006)

```

Given  $\mathbf{x}_0$ 
Evaluate  $R(\mathbf{x}_0)$   $\nabla R(\mathbf{x}_0)$ 
Set  $\mathbf{p}_0 = \nabla R(\mathbf{x}_0)$  and  $k = 0$ 
while  $|\nabla R(\mathbf{x}_k)| > \varepsilon$ 
    Compute  $a_k$  using the backtracking algorithm
     $\mathbf{x}_{k+1} = \mathbf{x}_k + a_k * \mathbf{p}_k$ 
    Evaluate  $\nabla R(\mathbf{x}_{k+1})$ 
     $\beta_{k+1} = \frac{\nabla R_{k+1}^T \nabla R_{k+1}}{\nabla R_k^T \nabla R_k}$ 
    If  $(\text{mod}(k, 5) == 0)$   $\beta_{k+1} = 0$ ; //restart every 5 iterations
     $\mathbf{p}_{k+1} = -\nabla R_{k+1} + \beta_{k+1}\mathbf{p}_k$ 
     $k = k + 1$ 
end (while)

```

In typical gradient-based optimization algorithms, the step length, a_k , is obtained with a backtracking algorithm where the step length is reduced an arbitrary number of times by a factor of $\frac{1}{2}$ until the Armijo-Goldstein conditions are satisfied (Nocedal, 2006). In the proposed model, the pipeline model presented in Chapter 4 assumes concurrent flow of oil, water and gas in each pipeline of the network. This requirement imposes the constraint that the elements of \mathbf{x} which correspond to the same chord (torn pipeline) should have the same sign. For this reason, the backtracking algorithm is modified by incrementing, instead of decrementing, the step length by a factor of 2 (see Algorithm 5.3). The minimum (or starting) value for the step length, a_{min} , can be obtained from equation (5.15) based on the desired accuracy, ε :

$$a_{min} = \frac{1}{\varepsilon} \max \left\{ \frac{|\partial R / \partial x_i|}{|\nabla R|} \right\} \quad (5.15)$$

Where

- ε : The accuracy of the solution
- R : The cluster residual
- \mathbf{x} : The vector of tearing variables

For example, in a three-phase network, the desired accuracy of the solution might be set to 0.01STBOD or 0.01MMScfD. Starting from a_{min} , the value of a is being incremented by a factor of 2.0 until at least one chord comprises of flowrates with alternating signs in which case reverse flow occurs.

In each iteration, we select the step-length that yields the lowest value of the cluster residual. Then the new gradient is evaluated, using the Fletcher-Reeves algorithm. The process terminates when the cluster residual, R , is less than a user-specified value, typically 1.0E-3.

Algorithm 5.3 Proposed Step search algorithm for three-phase network flows

```
Given  $p_k, x_k$ 
Evaluate  $a_{\min} = \max \left\{ \frac{|VR_i|}{|VR|} \right\} / \varepsilon$   $R(x_k)$ 
 $\min R = R(x_k), a^* = a_{\min}, a = a_{\min}$ 
while (true)
     $x = x_k + a * p_k$ 
    Evaluate  $R(x)$ 
    If flow is unidirectional in all pipes
        If  $(R(x) < \min R)$ 
             $\min R = R(x);$ 
             $a^* = a;$ 
        end
         $a = 2a;$ 
    else
        return  $a^*;$ 
    end
end
```

5.4.4.5 Termination Conditions

The Fletcher-Reeves minimization algorithm terminates when one of the following occurs:

- a) The cluster residual is smaller than the specified tolerance in which case a solution has been found.
- b) The norm of the gradient is close to zero and the residual for the cluster is greater than the specified tolerance. This indicates that the Fletcher-Reeves method has identified a local minimum and a different initial guess should be evaluated.

5.4.4.6 Initial Guess

An initial guess for the tearing variables \mathbf{x} is acceptable if it satisfies the physical constraint that in all pipelines of the cluster, the j -phase volumetric flowrate cannot not exceed the total volumetric flowrate of that phase entering (or exiting) the cluster.

- a) The absolute value of a tearing variable cannot not exceed the total volumetric flowrate of that phase entering (or exiting) the cluster.

$$\max_{i \in \text{Chords}} |x_i^j| \leq \sum Q_{ext}^j \quad (5.16)$$

b) For the selected vector x , the solution of the linear system $[A_{tree,r}^{cluster}]q^j = B^j(x, Q_{ext}^j)$ must yield j -phase volumetric flowrates, q_i^j , the absolute value of which does not exceed the total volumetric flowrate of phase j exiting the cluster

$$\max_{i \in \text{Links}} |q_i^j| \leq \sum Q_{ext}^j \quad (5.17)$$

For cases where Gas-Oil-Ratios (GORs) and Oil-Water-Ratios (OWRs) are approximately the same for all incoming streams in the cluster, a good initial guess may be obtained by solving the cluster assuming single phase flow (preferably water) and then multiplying the single-phase solution with the given GWR and WOR to obtain the volumetric flowrate of gas and oil rates and hence, the corresponding values for the tearing variables. The single-phase problem can be solved using the Linear Theory Method (Wood, 1972). More specifically, the node equations are solved in tandem with the loop equations which are linearized using a hydraulic resistivity type of equation:

$$\Delta P_i = K_i |q_i| q_i \quad (5.18)$$

Where the hydraulic resistivity, K_i , can be approximated by

$$K_i = \frac{L_i}{D_i^5} |q_i^{(k-1)}| \quad (5.19)$$

Where L_i and D_i are the length and diameter of pipeline i and q_i^k is the single-phase flowrate in pipeline i at iteration k . In equation (5.19), the coefficient L/D^5 is obtained from the Darcy-

Weissbach equation which states that the head loss along a pipeline is proportional to its length and inversely proportional to the diameter. For the ease of calculations, the pipe roughness has been omitted from the hydraulic resistivity but is taken into account when minimizing the cluster residual using the pipeline model presented in Chapter 4. This approach appears to be working for WORs, GORs that vary up to 60-80% among different entry points. In cases where the GOR and WOR vary significantly (100% or more), random guesses are required for the components of \mathbf{x} until the previously mentioned constraints (equations 5.16 and 5.17) are satisfied.

5.4.4.7 Evaluation of the Cluster Solution

The methodology presented herein yields a solution that satisfies both the node and loop equations for the cluster. Once a candidate solution has been obtained, the following should be taken into account:

- a) The solution needs to be evaluated with respect to the residuals of the governing equations. In the formulation presented herein, the flowrates are obtained by solving linear systems and hence the residuals of the node equations are inherently zero. As for the loop equations, if the cluster residual is less than the specified tolerance (typically less than $10E-3$) then the solution obtained from the Fletcher-Reeves algorithm is said to be a feasible solution.
- b) The feasible solution then needs to be evaluated with respect to the stability of the numerical model. To this end, we compare the nodal pressures of the last iteration with the nodal pressures of the previous iteration. If the change is less than 0.001psi then the numerical model is considered stable.
- c) Finally, the solution needs to be vetted with regards to its stability at the initial conditions. This is typically performed by perturbing the initial conditions and re-

evaluating the cluster. If a small change in the initial conditions results in a solution with lower nodal pressures, then the candidate solution is said to be a solution of the transient problem and has to be discarded. Statistical approaches in network flows have shown that steady-state flows tend to maximize the entropy of the system, yielding solutions that minimize nodal pressure while satisfying Kirkoff's physical laws (Niven et al. 2016, Waldrip et al. 2016).

It is important to note that a solution obtained using the method presented herein is not necessarily a unique solution. In an illustrative example, Stewart (2015) showed that for a two-phase network, changing the initial conditions results in vastly different solutions. To illustrate this, Stewart (2015) solved the fully determined system of equations (number of unknowns equals the number of equations) using an iterative Newton-Raphson method. This observation justifies the approach used in this work to identify cluster solutions by solving the underdetermined system of equations using a minimization approach.

5.4.5 Solution of Networks containing loops

In the previous sections we outlined the workflow for modeling branched networks and illustrated the process for solving a cluster of loops given the incoming streams and a pressure boundary condition. In this section, we discuss how individual cluster solutions are combined in order to obtain solution for the entire network. Figure 5.14 illustrates a pipeline network comprising three clusters.

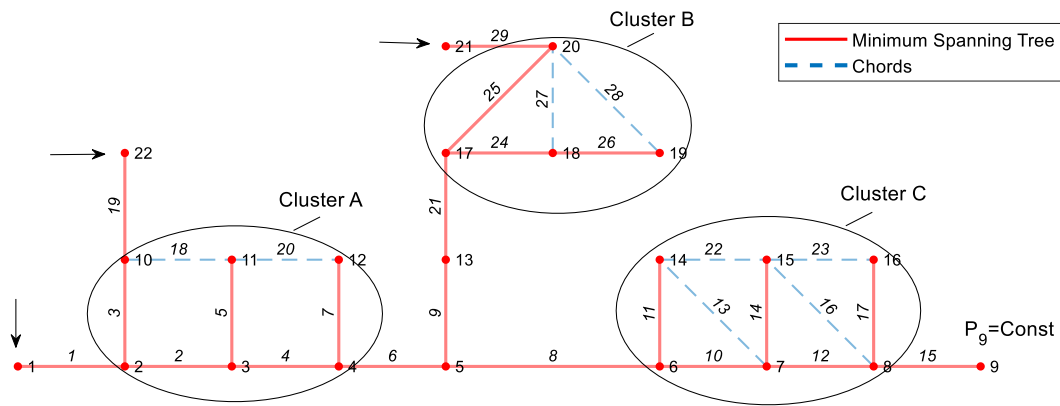


Figure 5.14 Illustrative example for coupling individual cluster solutions

The links in red color define the Minimum Spanning Tree (MST), obtained using Kruskal's algorithm. We represent the reduced incidence matrix of the MST with the square matrix $[A_{MST,r}^{network}]$, from which the node of constant pressure has been omitted (in this case node #9). Solving the nodal equations $[A_{MST,r}^{network}] \mathbf{q}^j = \mathbf{B}^j(Q_{ext}^j)$ for each phase j =oil, water, gas provides the flowrates for all the pipelines comprising the MST and hence, the incoming streams for each of the clusters. For example, the flowrates in pipelines #1 and #19 are external flows to Cluster A (see Figure 5.14). Similarly, the flow of pipeline #21 is external flow to Cluster B etc. The pressure at the node where fluids exit the cluster serves pressure boundary condition for that particular cluster. For example, in cluster A, node #4 is the outlet node and in cluster B, node #17 is the outlet node. It is important to note that if a cluster has two nodes of fluid exiting the cluster, then this cluster is a part of a larger cluster and has to be solved as such. Using the external streams and assuming an initial cluster outlet pressure equal to the separator pressure, the clusters can be solved. However, since the splitting of the phases and the pressure drops depend on the cluster outlet pressure, an iterative scheme must be deployed. The purpose of the iterative scheme is to

update the nodal pressures of the network (and hence the outlet pressure for each of the clusters) by solving the pressure equations $[A_{MST,r}^{network}]^T [\mathbf{P}^{(k+1)}] = \Delta \mathbf{P}^{(k)}$. It is important to note that the MST of the network comprises all the nodes and has a tree-like structure, consequently, solving this linear system conveniently updates all nodal pressures. Using the new outlet pressures at level $k+1$, the clusters can be re-evaluated. The process continues until convergence is achieved and the nodal pressures have stabilized. When formulating the linear system, the pressure drops on the right-hand side are calculated in the following manner:

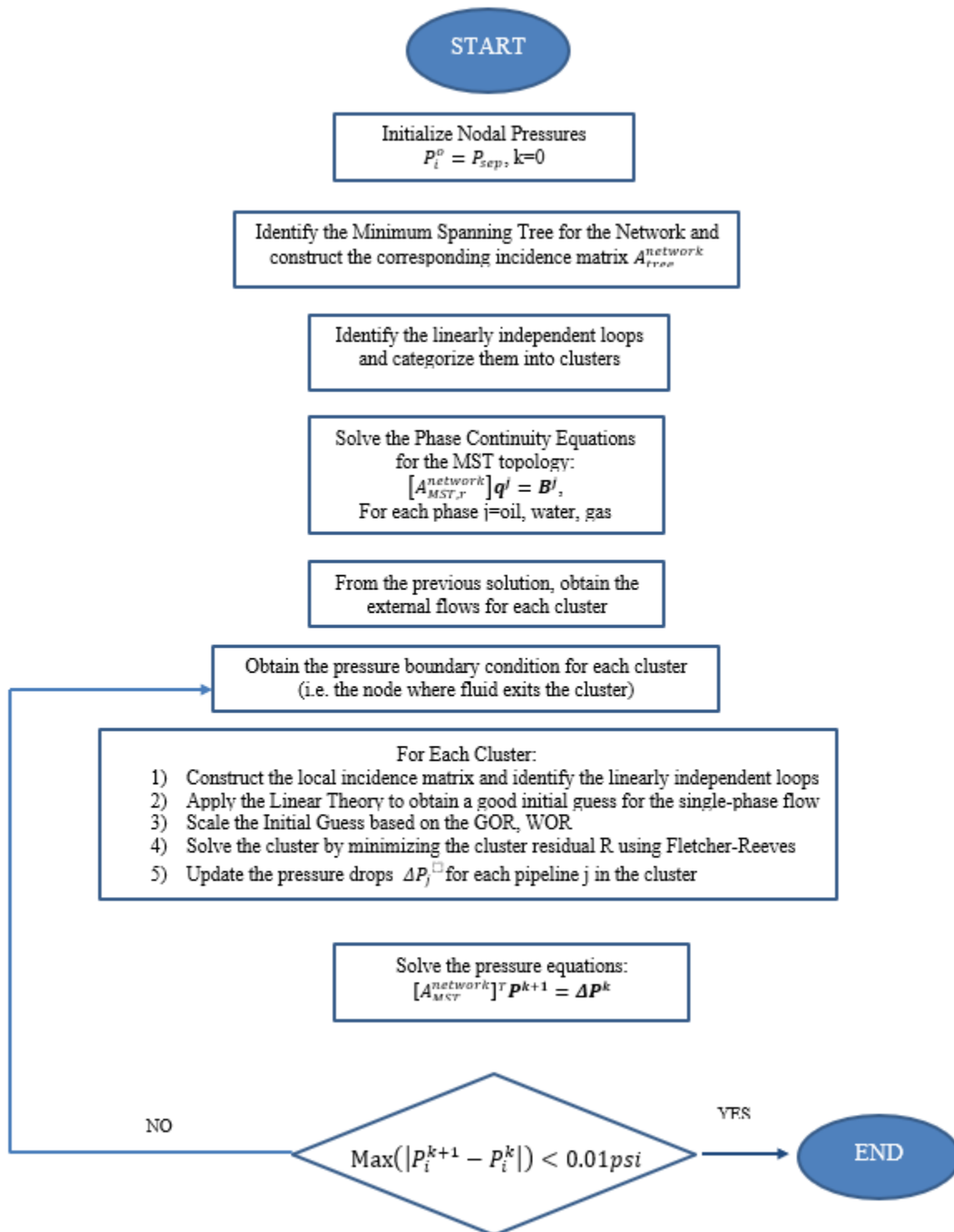
- a) For pipelines not included in clusters the pressure drop ΔP is calculated using the j -phase volumetric flowrates obtained from $[A_{MST,r}^{network}] \mathbf{q}^j = \mathbf{B}^j(Q_{ext}^j)$
- b) For pipelines included in clusters the pressure drop ΔP is calculated using the j -phase flowrates obtained from the solution of the corresponding cluster.

5.4.6 Workflow Summary

The proposed methodology is particularly efficient in large pipeline networks which comprise a significant number of manifolds that can be modelled as clusters. Since each manifold is solved separately, we only need to evaluate the gradients of the cluster residual with respect to the tearing variables. To evaluate the gradients of the cluster residual, the frictional pressure losses need to be calculated for all pipelines contained in loops, without the need to calculate frictional pressure losses for out-of-loop pipelines. On the contrary, in the case of the Newton-Raphson method, the formulation of the Jacobian matrix requires the derivatives of the pressure drop for each pipeline in the network. Assuming that the pressure drop only depends on the oil, water and gas rate as well as on the downstream pressure there would be 4 non-zero derivatives that should be evaluated for each pipeline per iteration step. In a large network and given the fact the frictional pressure losses are evaluated using a finite difference scheme, this is not a viable option, at least from a computational standpoint.

Additionally, solving the network with the fully determined Newton-Raphson iteration, requires the simultaneous solution of $3L+N$ equations whereas, in the proposed model, the solution of the network problem is translated into smaller minimization problems, one for each cluster of loops, with a total of $3(L-N+1)$ minimization variables. For example, in a three-phase network comprising 100 nodes and 120 pipelines, a Newton-Raphson iteration would comprise 460 variables whereas, in the proposed network analysis we only need to solve for 63 minimization variables. The logical diagram of the proposed three-phase network solver is presented in Algorithm 5.3.

Algorithm 5.3 - Logical diagram of the proposed three-phase network solver



5.5 HANDLING MULTIPLE PRESSURE BOUNDARY CONDITIONS

An interesting problem in network flows is the modeling of multiple pressure boundary conditions. For example, in a surface production network two or more separators may be installed to better handle and distribute the produced fluids. Figure 5.15 presents the tail of a network comprising two separators S1 and S2 with known pressures P_{s1} and P_{s2} , respectively.

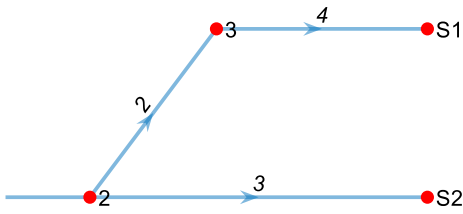


Figure 5.15 Tail of network with two separators

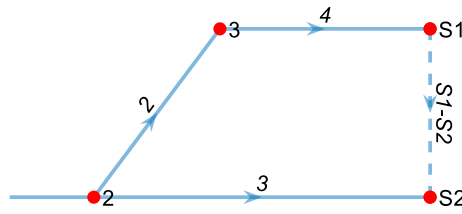


Figure 5.16 Addition of no-flow link S1-S2

The pressure at node #2 can either be calculated from the separator S1, by adding the pressure drops along the path S1-3-2 or from separator S2, by adding the pressure drops along the path S2-2. We can write

$$P_2 = P_{s1} + \Delta P_4 + \Delta P_2 \quad (5.20)$$

$$P_2 = P_{s2} + \Delta P_3 \quad (5.21)$$

Subtracting equation (5.21) from equation (5.10), we obtain

$$P_{s1} - P_{s2} + \Delta P_4 + \Delta P_2 - \Delta P_3 = 0 \quad (5.22)$$

Using the definition of pressure drop, we can define the quantity $(P_{S1}-P_{S2})$ as the pressure drop of an additional link originating from separator S1 and terminating at separator S2, as shown in Figure 5.16. This link has the following properties:

- a) The pressure drop of the link is constant and equals $P_{S1}-P_{S2}$
- b) The volumetric flowrates of oil, water and gas in link S1-S2 are zero
- c) This link cannot be selected as a chord and the corresponding flowrates of this link may not be used as tearing variables

Using this approach, the second boundary condition has been converted into a pseudo-loop equation simply by adding a no-flow pipeline, S1-S2. Should more separators exist, additional links can be added, provided they all originate from the same separator.

5.6 MODELING OF GAS INJECTION NETWORKS

Modeling of gas injection networks is similar to hydrocarbon production networks. The main difference lies in the presence of compressors and the fact that gas exits the network at the wellheads as opposed to streams of hydrocarbons entering the network. In gas network analysis, frictional losses are conventionally calculated using analytical equations (such as the Weymouth or Panhandle A & B equations) which relate the pressure drop with the gas rate, the outlet pressure and the gas and pipeline properties (Martinez-Romero, 2002). In the context of this dissertation, frictional losses are calculated using the pipeline model presented in Chapter 4, with the oil and water rates set equal to zero. The modeling of compressors can be implemented either by performing linear interpolation on manufacturer supplied compressor curves, or with the use of analytical equations which provide the polytropic head as a function of the horsepower, the gas rate and the suction temperature and pressure. Assuming adiabatic compression, the relationship between the compression ratio, horsepower and gas rate can be obtained from the following equation (Lee, 1996).

$$HP = \frac{1}{E} \frac{k}{k-1} \frac{p_{sc}}{T_{sc}} T_s Z_s \left[R_c^{\frac{k-1}{k}} - 1 \right] Q_{sc} = 0.75 \frac{1}{E} \frac{k}{k-1} T_s Z_s \left[R_c^{\frac{k-1}{k}} - 1 \right] Q_{sc} \quad (5.23)$$

Where:

HP: Compressor capacity in Horsepower (hp)

Q_{sc} : Gas rate in MMScf/Day

E: Compressor efficiency

k: Specific heat ratio

T_s : Suction temperature in F

Z_s : Compressibility factor at suction conditions

R_c : Compressor ratio, defined as $P_{\text{discharge}}/P_{\text{suction}}$

Since the pipeline model is isothermal, the compressor inlet temperature must be provided or obtained by a temperature sensor. The compressor is represented by a node, the pressure of which corresponds to the suction pressure. For a given compressor horsepower, the differential pressure is calculated from equation (5.22) and then added to the right-hand-side of the pressure equations, specifically to the pressure drop of the pipeline downstream of the compressor.

5.7 VALIDATION AND BENCHMARKING

In this section, the proposed network solver is validated using network solutions published in the literature, compared with field measurements from large scale gas distribution networks and benchmarked against commercial network solvers such as EPANET and PIPESIM.

5.7.1 Incompressible, Single-Phase Network Flows – Case 1

Firstly, the proposed model is validated against single-phase network solutions published in the textbook “Analysis of Flow in Pipe Networks” by Jeppson (1976). The skeletonized structure of the network under study is shown in Figure 5.17. The pipeline properties along with the external flowrates of water are shown in Tables 5.5 and Table 5.6, respectively. Additionally, the nodes are assumed to have equal elevations resulting in a friction-dominated network problem. Jeppson (1976) solved the node and loop equations using the Linear Theory Method and reported the flowrates for each pipeline in the network. Since the model presented herein requires a pressure boundary condition, we arbitrarily specify the pressure at node #7 at 60psi. The solution is expected to be insensitive to the boundary condition as both the density and viscosity of the water phase are independent of pressure.

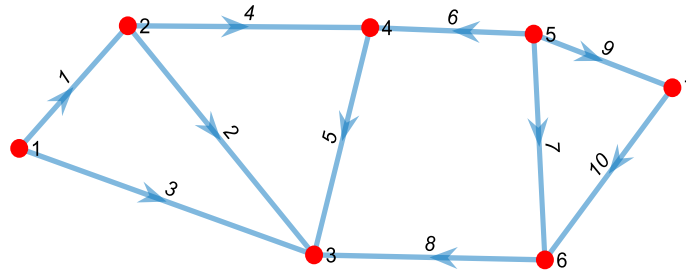


Figure 5.17 Network Topology of Validation Case 1 – Jeppson (1976)

Table 5.5 Pipeline Properties for Validation Case 1 - Jeppson (1976)

| Pipe Index | Length (ft) | Inside Diameter (in) | Wall Roughness (in) |
|------------|-------------|----------------------|---------------------|
| 1 | 1600 | 18 | 0.0102 |
| 2 | 2000 | 15 | 0.0102 |
| 3 | 2400 | 18 | 0.0102 |
| 4 | 1800 | 12 | 0.0102 |
| 5 | 1900 | 12 | 0.0102 |
| 6 | 1300 | 10 | 0.0090 |
| 7 | 1700 | 15 | 0.0102 |
| 8 | 2000 | 18 | 0.0090 |
| 9 | 1200 | 24 | 0.0102 |
| 10 | 1800 | 15 | 0.0102 |

Table 5.6 Sinks/Sources for Validation Case 1 – Jeppson (1976)

| Node Index | Supply/Demand (gpm) |
|------------|---------------------|
| 1 | 2000 |
| 2 | -300 |
| 3 | -900 |
| 4 | -500 |
| 5 | 1500 |
| 6 | -800 |
| 7 | 1000 |

For this validation case, the network comprises a single cluster containing a total of four linearly independent loops. The proposed model was deployed to solve for the pipeline flowrates and nodal pressures.

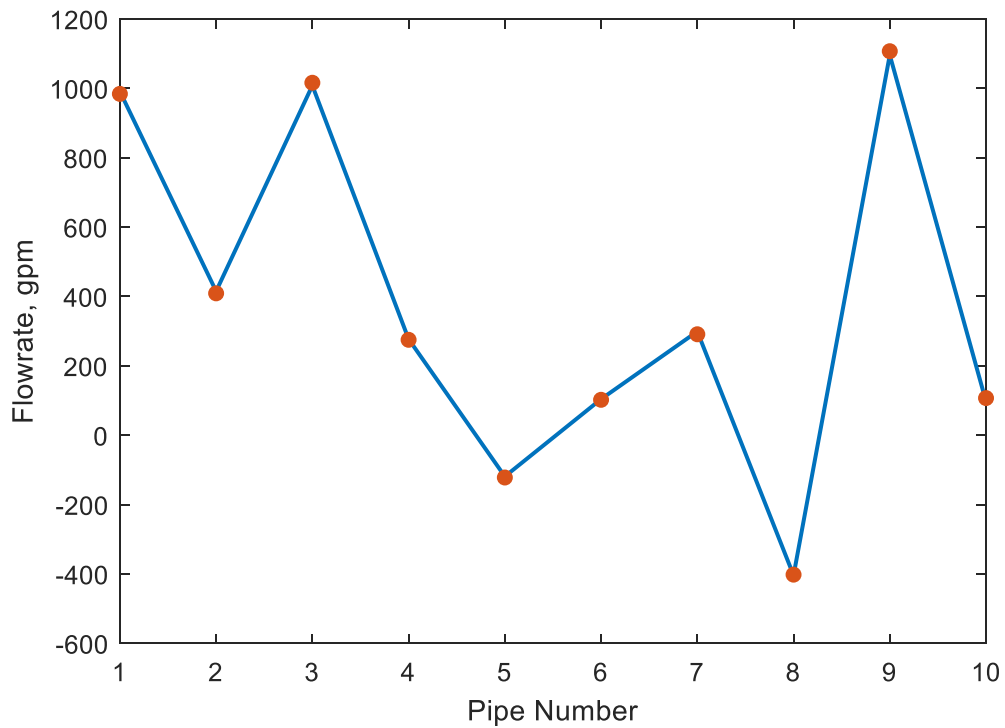


Figure 5.18 Comparison of model results with published network solution (Jeppson, 1976)

Figure 5.18 compares the flowrates obtained from the proposed model versus the flowrates reported by Jeppson (1976). We observe good agreement with an average absolute error of 0.3%, which validates the model for single-phase incompressible flows.

5.7.2 Incompressible, Single-Phase Network Flows – Case 2

In the second validation case, the output of the proposed model is compared against the results obtained using EPANET, a single-phase network solver developed by the Environmental Protection Agency to model water distribution systems with application in urban hydraulic works and water resources management. The results of the model are compared versus EPANET for the network topology shown in Figure 5.19.

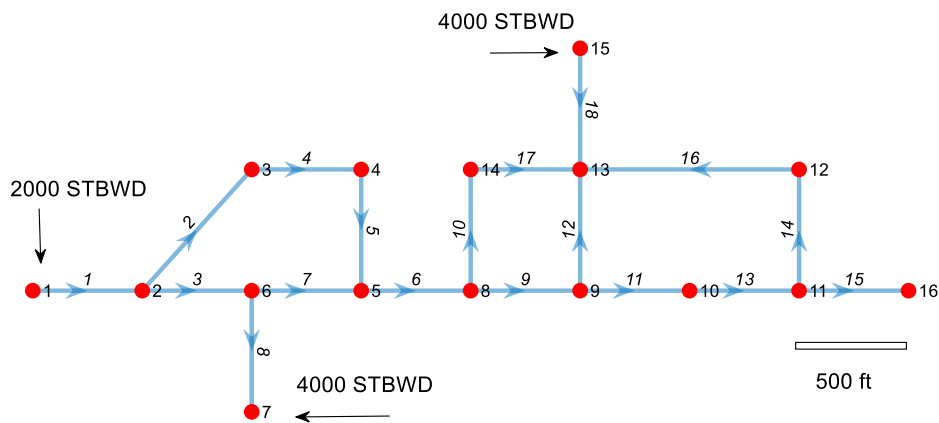


Figure 5.19 Network topology and external flows

The network comprises three linearly independent loops. Water streams enter the network at nodes #1, 7 and 15. Fluid exits the network at node #16 under a constant pressure of 63 psi, which constitutes the pressure boundary condition. All pipelines have an internal diameter of 4 inches, except pipeline #10 (2 inches) and pipeline #15 (5 inches). Additionally, all pipelines are assumed to be horizontal.

A significant difference between EPANET and the proposed model is the calculation of pressure drop: EPANET calculates the head loss along a pipeline using the Hazen-Williams equation given the material C-factor, where as our model requires the wall roughness. For a C-Factor of 100 (steel pipe), the hydraulic roughness was estimated to be 0.0035 inches by matching the pressure drop of both models for a *single pipeline segment*. Upon calibration of the pipeline model, the proposed network solver was used to obtain the pipeline flowrates and nodal pressures.

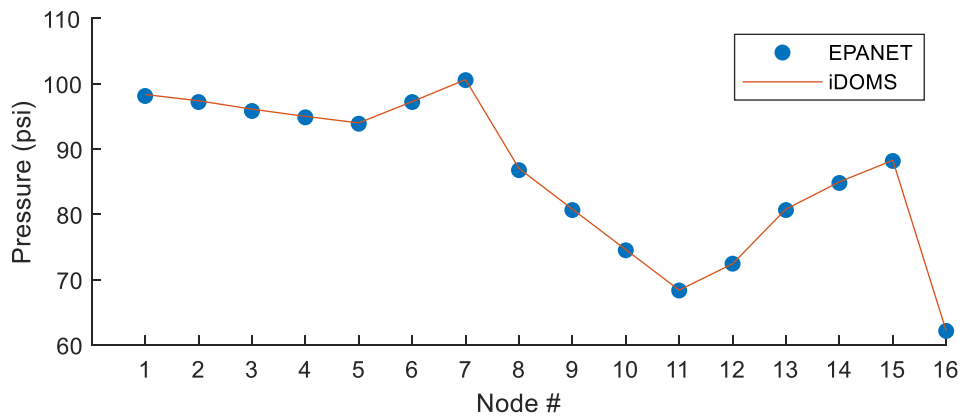


Figure 5.20 Comparison of nodal pressures with EPANET

Figure 5.20 compares the nodal pressures obtained from the proposed model (iDOMS) versus EPANET. The average error in pressures is 0.4% and that further validates the accuracy of the proposed model for incompressible networks.

5.7.3 Compressible, Single-Phase Network Flows

The results of the model are compared against field pressure measurements obtained by the gas distribution network of Consumer Powers Company, serving Lower Michigan (Stoner 1972; Zhou 1998). The topology of the gas transmission network is presented in Figure 5.21. The network consists of 17 nodes, 21 pipelines and a total of six linearly independent loops. In the

original network published by Stoner (1972), the path comprising nodes 11-17-12 was modeled using a single pipeline. Since the model presented herein requires that each pipeline is connected to a unique set of upstream and downstream nodes, the original topology was slightly modified by adding node 17 and splitting the original pipeline into two pipelines (11 & 17) of equal lengths.

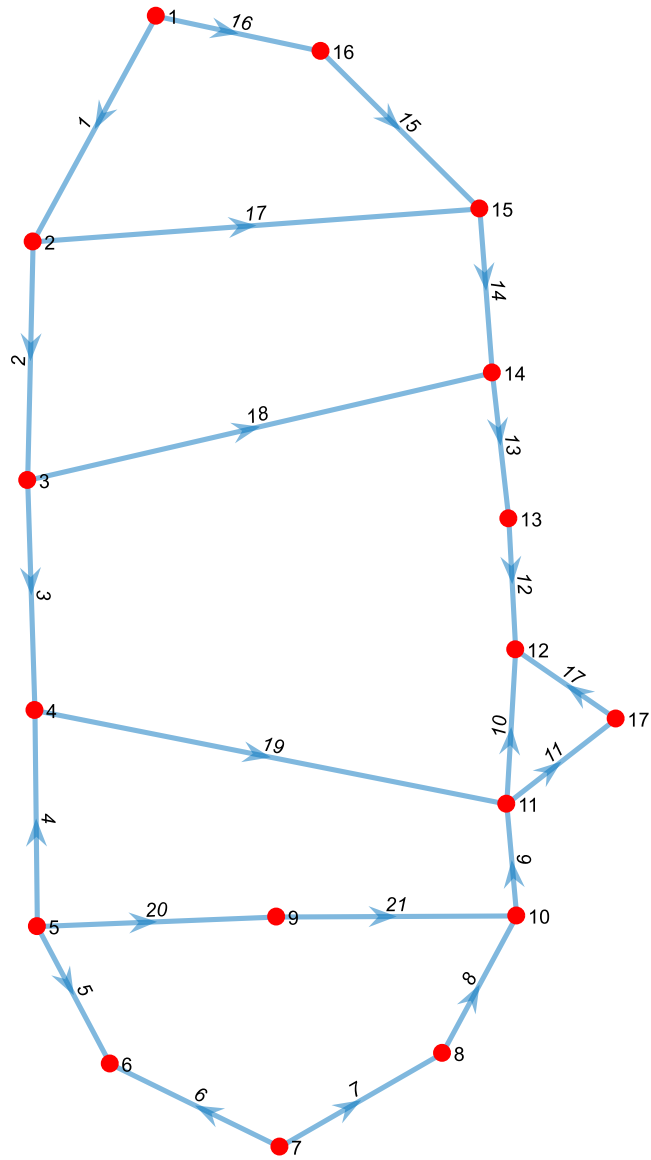


Figure 5.21 Network topology of Consumer Power Co. gas network (Stoner, 1972)

The pipeline properties (length, diameter and friction factors) are shown in Table 5.7. Since no elevation data is available, all pipelines are assumed horizontal. Table 5.8 presents the gas supply and demand along with pressure measurements for each node of the network. It is important to note that the reported pressure measurements have an accuracy of ± 5 psi. At node #1, gas is supplied into the network at a constant pressure of 547 psi which serves as the pressure boundary condition. The gas specific gravity, γ_g , is 0.60 and the average temperature of the gas transmission network is 35F.

Table 5.7 Pipelines Properties of Consumer Power Co. gas distribution network

| Pipe Index | Length (miles) | Inside Diameter (in) | Friction Factor |
|-------------------|-----------------------|-----------------------------|------------------------|
| 1 | 37.49 | 30.95 | 0.0200 |
| 2 | 13.88 | 33.35 | 0.0175 |
| 3 | 31.26 | 33.35 | 0.0175 |
| 4 | 9.13 | 31.65 | 0.0170 |
| 5 | 15.99 | 19.5 | 0.0102 |
| 6 | 35.52 | 19.5 | 0.0100 |
| 7 | 30.18 | 17.5 | 0.0105 |
| 8 | 13.32 | 15.5 | 0.0105 |
| 9 | 15.43 | 15.5 | 0.0125 |
| 10 | 10.31 | 14.18 | 0.0125 |
| 11* | 9.64 | 25.17 | 0.0125 |
| 12 | 21.47 | 12.25 | 0.0125 |
| 13 | 11.05 | 12.25 | 0.0125 |
| 14 | 5.70 | 12.25 | 0.0125 |
| 15 | 17.76 | 12.25 | 0.0125 |
| 16 | 46.36 | 12.25 | 0.0125 |
| 17 | 34.84 | 15.44 | 0.0125 |
| 18 | 30.59 | 25.47 | 0.0900 |
| 19 | 41.90 | 25.37 | 0.0105 |
| 20 | 16.55 | 23.44 | 0.0125 |
| 21 | 22.75 | 23.44 | 0.0125 |
| 22* | 9.64 | 25.17 | 0.0125 |

Table 5.8 Sink/Sources and field pressure measurements for Consumer Powers Co. gas network

| Node Index | Net Inflow (MMScfD) | Pressure Measurement (psia) |
|------------|---------------------|-----------------------------|
| 1 | 121.0 | 547 |
| 2 | -4.7 | 540 |
| 3 | -15.1 | |
| 4 | -8.9 | 530 |
| 5 | 151.8 | 535 |
| 6 | -20.1 | |
| 7 | 192.6 | 590 |
| 8 | -83.6 | |
| 9 | -11.2 | |
| 10 | -57.8 | 520 |
| 11 | -60.8 | 520 |
| 12 | -80.8 | |
| 13 | -18.6 | |
| 14 | -64.2 | |
| 15 | -50.7 | 515 |
| 16 | 0.0 | |
| 17 | 0.0 | |

In Table 5.7, the reported friction factors (Montoya, 2000) were calculated using Chen's equation:

$$\frac{1}{\sqrt{f_g}} = -2 \log \left\{ \frac{\frac{k_{wall}}{D}}{3.7065} - \frac{5.0452}{N_{Re}} \log \left[\frac{1}{2.8257} \left(\frac{k_{wall}}{D} \right)^{1.1098} + \frac{5.8506}{N_{Re}^{0.8981}} \right] \right\} \quad (5.24)$$

Since the pipe wall roughness, k_{wall} , was not provided in the original dataset, the network was modeled assuming various values for the roughness and then friction factors were back-calculated using equation (5.24). The wall roughness that minimized the average error in the calculated versus the reported friction factors is 0.0059 inches, and for this solution, the nodal pressures were compared against the field pressure measurements.

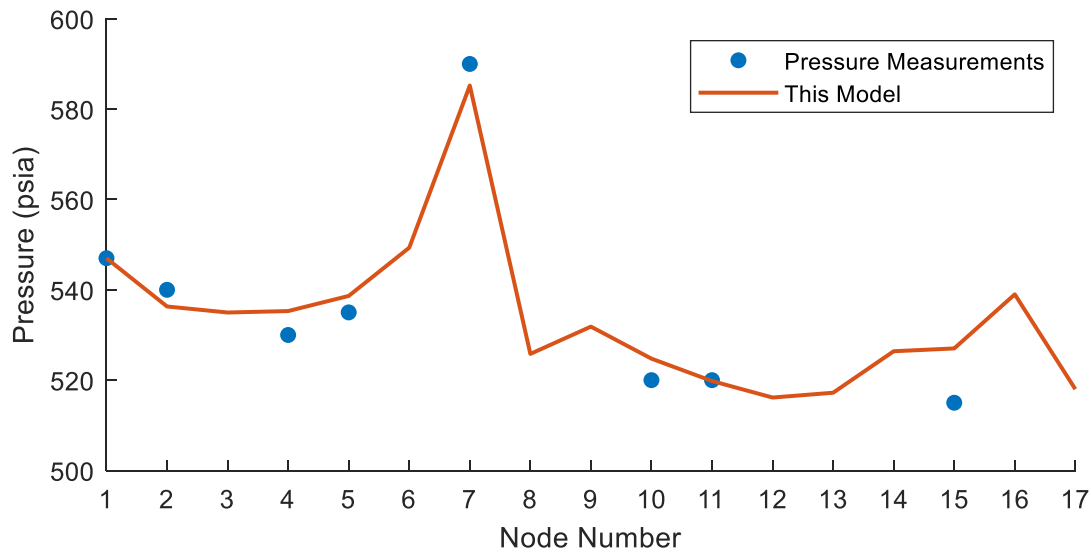


Figure 5.22 Comparison of model results (solid line) with pressure measurements (data points).

Figure 5.22 compares the nodal pressures obtained using the proposed model with the reported field measurements. The largest discrepancy between the calculated and measured data is observed for node #15 – possibly due to the absence of elevation data. The average error is approximately 3.9% which is well within engineering accuracy given the poor accuracy of pressure measurements (± 5 psi) and lack of elevation data.

5.7.4 Benchmarking – Three phase network flows

In this section, the proposed model is compared against PIPESIM (Schlumberger, 2005), a multiphase network solver that is widely used in the upstream oil and gas industry. Both network solvers handle phase continuity equations at standard conditions and utilize the same black-oil PVT correlations. However, a major difference between the two models is the way that network flows are solved. More specifically, PIPESIM solves the entire system of node and loop equations using iterative Newton-Raphson whereas, the proposed method minimizes cluster residuals using the principle of tearing variables. In addition, PIPESIM calculates pressure drops using empirical

or analytical equations (i.e. Baker Jardine , OLGA) whereas, the model presented herein, evaluates the frictional pressure losses using the explicit finite difference scheme presented in Chapter 4 along with the PVT correlations summarized in Appendix C. The results of the two models are compared for the network topology shown in Figure 5.23.

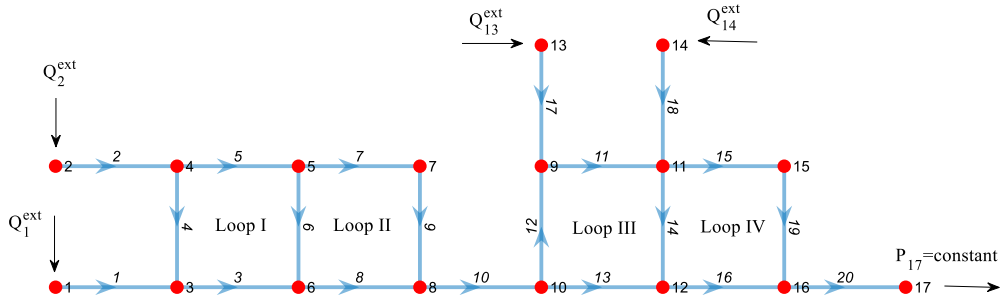


Figure 5.23 Network topology for comparing the proposed model with PIPESIM.

The pipeline properties for the network under study are presented in Table 5.9. The network was selected to be compact so that the results can easily be reproduced in future validation studies. Fluid enters the network at nodes 1, 2, 13 and 14 with the corresponding flowrate triplets (oil, water and gas rates) shown in in Table 5.10. Fluids exit the network at node 17 at a constant pressure of 200 psi.

The PIPESIM simulation was run using three different models for calculating the pressure drop along pipe segments: The Baker-Jardine equation, the UTFFP model and OLGA three-phase simulator. Table 5.11 presents the nodal pressures obtained using PIPESIM and the proposed model. We observe that nodal pressures deviate by less than 2%. In addition, Table 5.12 summarizes the calculated pipeline-based unknowns (flowrates and pressure drop).

Table 5.9 Pipeline properties

| Pipe Index | Length (ft) | Inside Diameter (in) | Pipe Roughness (in) |
|-------------------|--------------------|-----------------------------|----------------------------|
| 1 | 500 | 4 | 0.001 |
| 2 | 500 | 4 | 0.001 |
| 3 | 500 | 4 | 0.001 |
| 4 | 500 | 4 | 0.001 |
| 5 | 500 | 4 | 0.001 |
| 6 | 650 | 2 | 0.001 |
| 7 | 500 | 4 | 0.001 |
| 8 | 500 | 4 | 0.001 |
| 9 | 500 | 4 | 0.001 |
| 10 | 500 | 4 | 0.001 |
| 11 | 500 | 4 | 0.001 |
| 12 | 500 | 4 | 0.001 |
| 13 | 500 | 4 | 0.001 |
| 14 | 500 | 4 | 0.001 |
| 15 | 600 | 3 | 0.001 |
| 16 | 500 | 4 | 0.001 |
| 17 | 500 | 4 | 0.001 |
| 18 | 500 | 4 | 0.001 |
| 19 | 500 | 4 | 0.001 |
| 20 | 500 | 4 | 0.001 |

Table 5.10 External volumetric flowrates entering the network

| Node Index | Oil Influx (STBOD) | Water Influx (STBWD) | Gas Influx (MScfD) | GOR (SCF/STBO) | WOR |
|-------------------|---------------------------|-----------------------------|---------------------------|-----------------------|------------|
| 1 | 1600 | 400 | 400 | 250 | 0.25 |
| 2 | 700 | 300 | 175 | 242 | 0.43 |
| 13 | 800 | 200 | 200 | 250 | 0.25 |
| 14 | 1120 | 280 | 280 | 250 | 0.25 |

Table 5.11 Calculated nodal pressures using the proposed model and PIPESIM

| Node | Pressure (psi) | | | | |
|-----------|--|--------------------|-------------------|------------|---------------------------|
| | PIPESIM (Baker Jardine) | PIPESIM (UTFFP) | PIPESIM (OLGA) | This Model | Diff with PIPESIM OLGA |
| 1 | 326.54 | 320.90 | 295.53 | 300.61 | 1.72% |
| 2 | 333.25 | 326.09 | 300.29 | 305.97 | 1.89% |
| 3 | 324.19 | 319.27 | 294.09 | 290.90 | -1.08% |
| 4 | 325.06 | 320.30 | 294.81 | 299.67 | 1.65% |
| 5 | 320.42 | 317.64 | 292.28 | 296.54 | 1.46% |
| 6 | 318.24 | 316.28 | 290.40 | 294.42 | 1.38% |
| 7 | 310.63 | 312.02 | 283.05 | 288.00 | 1.75% |
| 8 | 307.94 | 309.04 | 283.70 | 286.79 | 1.09% |
| 9 | 288.87 | 290.52 | 271.27 | 271.75 | 0.18% |
| 10 | 290.41 | 291.90 | 272.53 | 272.91 | 0.14% |
| 11 | 282.03 | 284.89 | 267.24 | 266.36 | -0.33% |
| 12 | 279.34 | 283.05 | 265.62 | 264.54 | -0.41% |
| 13 | 291.51 | 292.47 | 272.77 | 273.67 | 0.33% |
| 14 | 286.80 | 287.85 | 270.20 | 270.65 | 0.17% |
| 15 | 271.52 | 247.18 | 260.26 | 257.41 | -1.10% |
| 16 | 259.46 | 264.06 | 252.11 | 248.27 | -1.52% |
| 17 | 200 (Pressure Boundary Condition) | | | | |

Table 5.12 Calculated pipeline flowrates and pressure drops using the proposed model and PIPESIM

| Pipe | PIPESIM (OLGA) | | | | This Model | | | |
|-----------|----------------|----------------|----------------|-------|----------------|----------------|----------------|--------|
| | q ^o | q ^w | q ^g | ΔP | q ^o | q ^w | q ^g | ΔP |
| | (STBOD) | (STBWD) | (MMScfD) | (psi) | (STBOD) | (STBWD) | (MMScfD) | (psi) |
| 1 | 700.00 | 300.00 | 0.18 | 1.44 | 700.00 | 300.00 | 0.18 | 1.705 |
| 2 | 1056.14 | 389.03 | 0.26 | 2.85 | 1238.43 | 380.89 | 0.32 | 4.282 |
| 3 | 1535.56 | 508.89 | 0.38 | 5.68 | 1679.55 | 517.66 | 0.43 | 7.629 |
| 4 | 356.14 | 89.03 | 0.09 | 0.85 | 538.43 | 80.89 | 0.14 | 0.798 |
| 5 | 479.42 | 119.85 | 0.12 | 1.89 | 441.12 | 136.77 | 0.11 | 2.114 |
| 6 | 764.45 | 191.11 | 0.19 | 0.65 | 620.45 | 182.34 | 0.15 | 1.207 |
| 7 | 1600.00 | 400.00 | 0.40 | 5.48 | 1600.00 | 400.00 | 0.40 | 6.269 |
| 8 | 1243.86 | 310.97 | 0.31 | 3.42 | 1061.57 | 319.11 | 0.26 | 3.157 |
| 9 | 764.45 | 191.11 | 0.19 | 9.23 | 620.45 | 182.34 | 0.15 | 8.537 |
| 10 | 2300.00 | 700.00 | 0.58 | 10.82 | 1061.91 | 700.00 | 0.58 | 13.884 |
| 11 | 1627.56 | 495.34 | 0.41 | 6.41 | 1726.78 | 490.07 | 0.44 | 8.289 |
| 12 | 2342.49 | 684.15 | 0.59 | 11.62 | 2421.26 | 677.02 | 0.61 | 15.769 |
| 13 | -672.44 | -204.66 | -0.17 | -1.30 | -573.22 | -209.93 | -0.13 | -1.163 |
| 14 | 714.93 | 188.81 | 0.18 | 1.62 | 694.48 | 176.95 | 0.16 | 1.814 |
| 15 | 1877.51 | 495.85 | 0.47 | 8.15 | 1798.74 | 502.98 | 0.45 | 9.153 |
| 16 | 1472.44 | 404.66 | 0.37 | 5.18 | 1373.22 | 409.93 | 0.33 | 5.399 |
| 17 | 1877.51 | 495.85 | 0.47 | 6.98 | 1798.74 | 502.98 | 0.45 | 8.957 |
| 18 | 800.00 | 200.00 | 0.20 | 1.50 | 800.00 | 200.00 | 0.20 | 1.924 |
| 19 | 1120.00 | 280.00 | 0.28 | 2.96 | 1120.00 | 280.00 | 0.28 | 4.292 |
| 20 | 4220.00 | 1180.00 | 1.06 | 52.11 | 4220.00 | 1180.00 | 1.06 | 48.268 |

Table 5.13 Comparison of Loop Residuals

| Loop | Cluster Residual | |
|------------|------------------|------------|
| | PIPESIM (OLGA) | This Model |
| I | 0.17 | 0.018 |
| II | 0.13 | 5E-5 |
| III | 0.11 | 5E-3 |
| IV | 0.06 | 0.014 |

Finally, Table 5.13 compares the loop residuals for both models, calculated using equation (5.11). We observe that the proposed model yields loop residuals which are significantly smaller (by at least an order of magnitude) compared to PIPESIM which solves the network equations using Newton's iterative Method.

5.8 SUMMARY

In this chapter, a systematic analysis was presented for modeling three-phase network flows. The proposed network model:

- a) Uses Fractional Flow theory for calculating pressure drops
- b) Explicitly calculates black-oil PVT properties
- c) Minimizes cluster residuals using the Fletcher-Reeves gradient-based method

The model assumes that PVT properties are the same for all incoming streams and that the flow of oil, water and gas is unidirectional in each pipeline of the network. In the proposed network solver, each cluster is solved individually, and cluster solutions are coupled, in an iterative manner, with the network pressure equations. The method was validated using published network solutions, compared versus gas field data and benchmarked against PIPESIM, a commercial multiphase network solver widely used by the oil and gas industry. In a comparative study, the model provided significantly lower loop residuals, by two orders of magnitude compared with PIPESIM. The network analysis presented herein has the following advantages:

- a) Significantly fewer unknowns compared to Newton's Method. More specifically, the model solves the network problem using $3(L-N+1)$ minimization variables as opposed to $3L+N-1$ variables required by Newton's iterative Method. This is translated to significant computational savings when it comes to the modeling of complex pipeline networks.

- b) The method does not require the derivatives of the pressure drop equations for out-of-loop pipelines, as is the case for the Newton-Raphson iterative method.
- c) The proposed method does not require an accurate initial guess for the entire network as each cluster is solved individually, obtaining the corresponding initial guess using the Linear Theory Method.
- d) In the proposed model, the residuals of the node equations are inherently zero since flow rates are obtained by solving the linear systems of the phase continuity equations. That limits the error propagation from the mass balance equations to the loop equations (and vice versa), resulting in more accurate network solutions.

In the next chapters we present an approach for coupling the surface network with well models in order to calculate field production for a given set of well and network controls.

5.9 NOMENCLATURE

| | | |
|-----------------------|---|--|
| $A_{MST,r}^{cluster}$ | = | The reduced (node-pipeline) local incidence matrix of the Minimum Spanning Tree (MST) of the cluster |
| A^{Loop} | = | The local oriented incidence matrix of the loop |
| a_{min} | = | minimum step length |
| $A_{MST,r}^{network}$ | = | Reduced (node-pipeline) incidence matrix of the minimum spanning tree of the network |
| A_r | = | reduced (node-pipeline) oriented incidence matrix |
| a_s | = | split coefficient |
| B_i^j | = | the external flowrate in standard conditions of phase j in node i |
| \mathbf{B}^j | = | is the column vector comprising the external flowrates, in standard conditions, of phase j, for each node i in the network |
| B_x^j | = | The column vector comprising the sum of j-phase external flowrates and j-phase tearing variables for each node in the cluster |
| D_i | = | Diameter of pipeline i |
| E | = | Compressor efficiency |
| f_g | = | gas-phase friction factor |
| HP | = | Compressor capacity in Horsepower (hp) |
| k | = | Specific heat ratio |
| K_i | = | Hydraulic resistivity of pipeline i |
| L | = | number of links (pipelines) |
| L_i | = | Length of pipeline i |
| N | = | number of nodes |
| N_{Loops} | = | number of loops |
| N_{Loops}^c | = | the number of linearly independent loops contained in a cluster |
| N_{RE} | = | Reynolds number |
| P_i | = | Pressure at node i |
| \mathbf{P}^{k+1} | = | the column vector comprising the nodal pressures at iteration k+1 |
| \mathbf{p}_k | = | search direction at iteration k |
| $q_i^{(k)}$ | = | single-phase flowrate in pipeline i at iteration k |
| $Q_{ext,n}^j$ | = | external flowrate of phase j in node n (expressed in standard conditions) |
| q_i^j | = | volumetric flowrate of phase j in pipeline i (expressed in standard conditions) |
| \mathbf{q}^j | = | is the column vector comprising the volumetric flowrates in standard conditions of phase j in pipeline i, q_i^j , for each pipeline in the network |
| \mathbf{q}_{MST}^j | = | The column vector comprising the flowrates of phase j for each pipeline in the Minimum Spanning Tree of the Cluster |
| Q_{sc} | = | Gas rate in MMScf/Day |
| R | = | the relative cluster residual |
| R_c | = | Compressor ratio, defined as $P_{discharge}/P_{suction}$ |
| R_{loop}^i | = | The relative residual of loop i |
| \mathbf{S} | = | the column vector contain the constants s_j for pipeline j in the loop |
| S_j^i | = | the sign constant for pipeline j in loop i, indicating clock-wise or anti-clock direction |
| s_j | = | A constant (-1 or +1) indicating whether the assigned positive direction of pipeline j is clockwise or anticlockwise |
| T_s | = | Suction temperature in F |
| \mathbf{x}_k | = | vector of tearing variables at iteration k |
| Z_s | = | Compressibility factor at suction conditions |
| a | = | step length |
| ΔP_i | = | pressure drop along pipeline i |
| $\Delta \mathbf{P}^k$ | = | the column vector comprising the pressure drop along each pipeline i at iteration k |
| ε | = | convergence tolerance |
| Ω_i | = | the set of pipelines contained in loop i |

Chapter 6: Integration of Well Models with Surface Facilities

6.1 INTRODUCTION

In traditional production engineering analysis, well deliverability analysis is performed under the assumption of constant Well-Head-Pressure (WHP). In the field, this assumption rarely holds true since any adjustment on the surface network can affect nodal pressures and hence individual well streams (Dempsey & Patterson, 1971). Nodal analysis in isolation to the surface network, necessitates data exchange between surface network and subsurface models and hence excessive communication overhead between surface and subsurface teams. In order to capture the effects of multi-well pressure interference, operators have adopted the approach of integrated production modeling which refers to the coupling the surface and subsurface models into a single computational domain by numerically eliminating physical boundary conditions. In recent years, asset teams have recognized the business impact of integrated production modeling as it provides a more accurate estimate of production rates and contributes towards achieving operational excellence of producing assets. More specifically, dynamic coupling of the surface and subsurface models can assist asset teams in performing the following tasks (Tingas 1998; Kurimov 2017; Stepanchok, 2018):

- Optimize well controls and lift-gas allocation
- Identify system active constraints and production bottlenecks
- Prioritize well intervention
- Assess current network capacity and the potential of future facility expansion
- Optimize network variables such as the separator pressure or valve controls
- Compare field operating strategies
- Compare the suitability of various artificial lift methods

- Plan the expansion of surface facilities
- Simulate network depressurization scenarios
- Establish shut-in criteria and procedures
- Assess the effect of upcoming facilities expansion
- Evaluate long term depletion strategies

The integration of surface and subsurface models can be accomplished using an explicit or implicit computational scheme. In implicit schemes, the reservoir, completion, wellbore and surface equations are formulated into a global matrix which is then solved simultaneously and iteratively for all unknowns present in the system (Shiralkar et al. 2005, Liang 2014). This is accomplished by discretizing the wellbore and surface components into “reservoir” cells and then appending these cells to the reservoir domain (Wang & Fleming, 2017). Implicit schemes are intrusive, in the sense that they require access to the source code of the reservoir simulation which may not always be granted. A major caveat of the implicit methods is that the modeling of production systems with multiple reservoir models could potentially result in a large system of equations/unknowns that would be impossible to solve within a reasonable amount of time. Another disadvantage of implicit methods is that they cannot handle complex surface networks such as topologies with closed-loop flow paths or multiple pressure boundary conditions (Litvak & Darlow, 1995). Implicit schemes have been proposed by (Startzman 1977; Emanuel & Ranney 1981; Litvak & Darlow 1995). Coats (2004) noticed that non-linear network equations require significantly more iterations which negatively impacts the solution of the entire system and proposed a preconditioning state to improve convergence.

On the other hand, explicit coupling methods, simulate the surface and subsurface models in a sequential and iterative manner where each model utilizes the results of its companion

simulator from the previous iteration (Heguler et al. 1997). Explicit schemes terminate when pressure and/or rates on the physical boundary are in agreement within a predetermined tolerance (Liang et al. 2014). Explicit methods are non-intrusive (i.e. they do not require the source code of the wellbore or reservoir simulator) and can incorporate black-box models for the subsurface or surface models. In other words, explicit schemes are highly modular as opposed to implicit schemes (Wang et al. 2013). Finally, explicit schemes are characterized by ease of coding however, the stability of the coupled model greatly depends on the numerical stability of its components. Explicit schemes have been applied in the field by Heguler (1997), Trick (1998) and Tingas (1998). It is important to note that these models are not commercially available, their internal structure is proprietary, and they can only handle single phase network flows, except for the model presented by Heguler (1997).

Even though integrated production models are perceived to have great potential in terms of production uplift, their implementation still faces many challenges. According to the proceedings of the SPE Workshop in “Smart Integration in Production System Modeling”, integrated asset modeling requires a significant amount of input parameters. Input parameters are required to accurately delineate the properties of each reservoir and wellbore in the system as well as the properties of the surface pipeline network. This can lead to a significant data gathering overhead, especially if one considers that many Oil and Gas companies have not yet established data standardization protocols. In addition, when data is provided to an integrated model, attention should be given to reference conditions. For example, in a production system comprising many wells, the along-well measure depth and wellhead elevation should be provided with respect to the same datum level (Kurimov et al. 2017). Another significant challenge mentioned by operators in the SPE workshop is the proper handling of PVT properties between the various components of the

system. For example, a wellbore model may use a different PVT model than the surface model in which case the integration scheme should handle the lumping or delumping of the PVT components at the physical boundary between the two systems. Finally, integrated production packages are typically associated with high deployment costs and require hundreds of hours of training. The high deployment costs tend to compete with the cost of drilling hence dissuading asset managers from decisively adopting new technology.

This chapter focuses on presenting an integration scheme for coupling the well models with the surface pipeline network. The proposed integrated scheme (forward model) allows the calculation of field production rate for a given set of network and well controls, both for naturally flowing wells and wells on artificial lift. To this end, a) the components of the system are defined b) the integration scheme is presented and c) the proposed model is applied to a synthetic field.

6.2 COMPONENTS OF THE INTEGRATED SYSTEM

The integrated model for coupling the surface and subsurface models comprises three major components:

- a) The well models
- b) The surface production network (or surface gathering network)
- c) The surface gas-injection network

The Well Models encompass the elements upstream of the wellheads and the subsurface (reservoir) models. The surface production network gathers the produced fluids to the separator and the gas-injection network distributes the allocated gas to the injection points.

6.2.1 Well Models

The term “Well Model” (WM) refers to the computational entity comprising the elements of the production system upstream of the wellhead. For example, in a naturally flowing well, the “well model” comprises the production choke, the wellbore, the completion and the reservoir. Similarly, for a well produced with an Electric Submersible Pump (ESP), the “Well Model” comprises the wellbore, the ESP, the completion and the reservoir. The WM conveniently represents the computational entity that performs nodal analysis and provides the well production rate, $Q_i^{o,w,g}$, at the current reservoir conditions, given the well controls and surface nodal pressure:

$$Q_i^{o,w,g} = WM_i(c_i, P_{n,i}) \quad (6.1)$$

Where:

$Q_i^{o,w,g}$: The oil, water and gas production rates in standard conditions from well i

c_i : The control variable for well i

$P_{n,i}$: the surface nodal pressure of well i

It is important to note that the surface nodal pressure, $P_{n,i}$, is defined as the flowline pressure downstream of the production choke as illustrated in Figure 6.1. The surface nodal pressure is not equal to the WHP which represents the pressure upstream of the choke.

By well controls we refer to the controls associated with well management. For example, in a naturally flowing well, the well controls refer to the choke sizes whereas for a well on gas-lift well, the well controls refer to the allocated gas injection rate. In the next paragraphs we discuss in detail the well models for naturally flowing wells and wells on artificial lift.

6.2.1.1 Naturally Flowing Wells

The “Well Model” (WM) of a naturally flowing well comprises the choke, the production tubing segments, the completion and the reservoir components as discussed in detail in Chapter 4. As opposed to chapter 4, and in the context of multi-well production system analysis, the wellbore component does not include the surface pipelines since they are a part of the surface gathering network. The concept of the “Well Model” for a naturally flowing well is show in Figure 6.1.

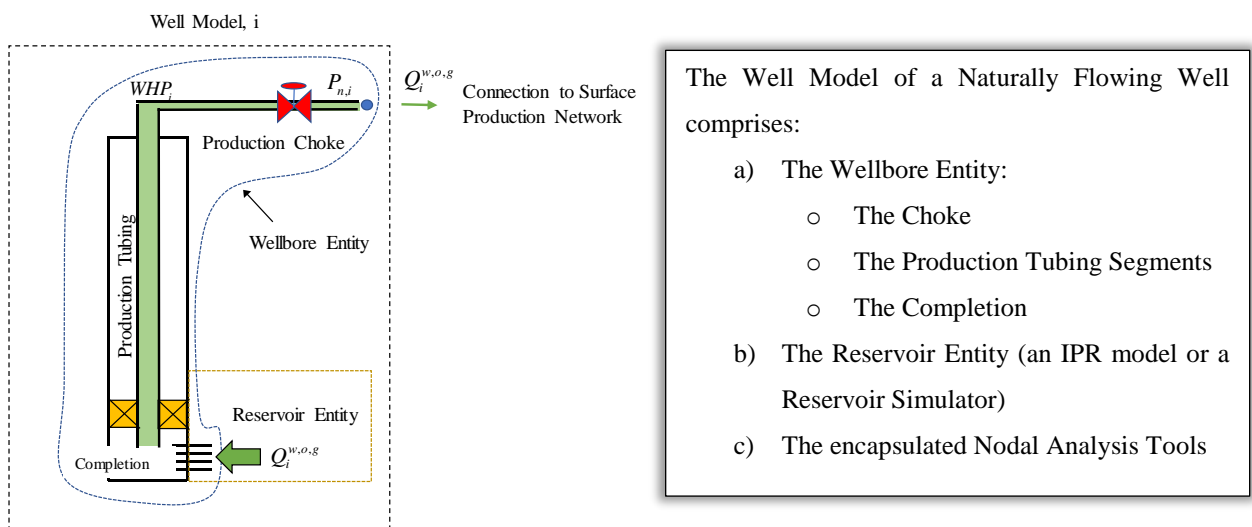
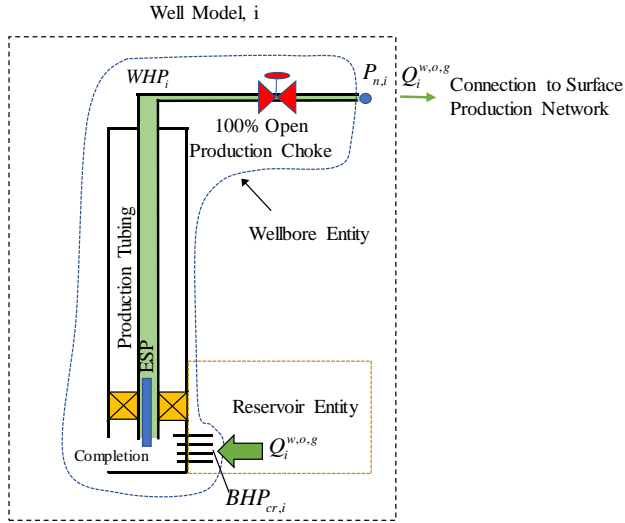


Figure 6.1 Concept of "Well Model" for naturally flowing wells

At the current reservoir conditions (average reservoir pressure and fluid saturations) and for a given well control, c_i (i.e. choke size) and surface nodal pressure, $P_{n,i}$, the WM returns the liquid production rates in standard conditions (SC), $Q_i^{o,w,g}$, by performing nodal analysis using the secant method discussed in Chapter 4.

6.2.1.2 Wells produced with an ESP

The “Well Model” (WM) of a well produced with an Electric Submersible Pump (ESP) comprises the ESP, the production tubing segments, the completion and the reservoir components as shown in Figure 6.2.



The Well Model of a well produced with an ESP comprises:

- d) The Wellbore Entity:
 - The ESP
 - The Production Tubing Segments
 - The Completion
- e) The Reservoir Entity (an IPR model or a Reservoir Simulator)
- f) The encapsulated Nodal Analysis Tools

Figure 6.2 Concept of "Well Model" for wells produced with an ESP

For wells produced with an ESP, the production choke is assumed completely open (or completely removed) since any pressure drop across the production choke compromises the performance of the artificial lift method. The Bottom-Hole-Pressure, p_{wf} , is calculated by adding the pressure drops of the various components of the production system starting from the surface nodal pressure and heading towards the completion-reservoir interface:

$$\begin{aligned}
 p_{wf}(f_{ESP}, Q, P_{n,i}) &= P_{n,i} + \Delta P_{tubing}(P_{n,i}, Q) - \Delta P_{ESP}(f_{ESP}, Q) + \\
 &= P_{n,i} + (P_{Discharge} - P_{n,i}) - (P_{Discharge} - P_{wf})
 \end{aligned}
 \tag{6.2}$$

Where:

$P_{n,i}$: the surface nodal pressure of well i

ΔP_{tubing} : the pressure drop in the tubing calculated from the pipeline model discussed in chapter 4

ΔP_{ESP} : the differential pressure provided by the ESP, defined as $P_{\text{Discharge}} - P_{\text{Intake}}$

$P_{\text{Discharge}}$: the ESP discharge pressure

P_{Intake} : the ESP intake (suction) pressure

In equation (6.2), the pump differential pressure is obtained by performing linear interpolation on the manufacturer supplied pump performance curves given the ESP frequency and liquid flowrate.

At the current reservoir conditions (average reservoir pressure and fluid saturations) and for a given well control (i.e. ESP frequency) and surface nodal pressure, the “Well Model” provides the equilibrium production rate in Standard Conditions, $Q_i^{o,w,g}$, by performing nodal analysis using the secant method discussed in chapter 4.

6.2.1.3 Gas-injected Oil Wells

The “Well Model” (WM) for a well on gas-lift comprises the production tubing segments, the Gas Lift Valves (GLVs) the completion and the reservoir components as shown in Figure 6.3.

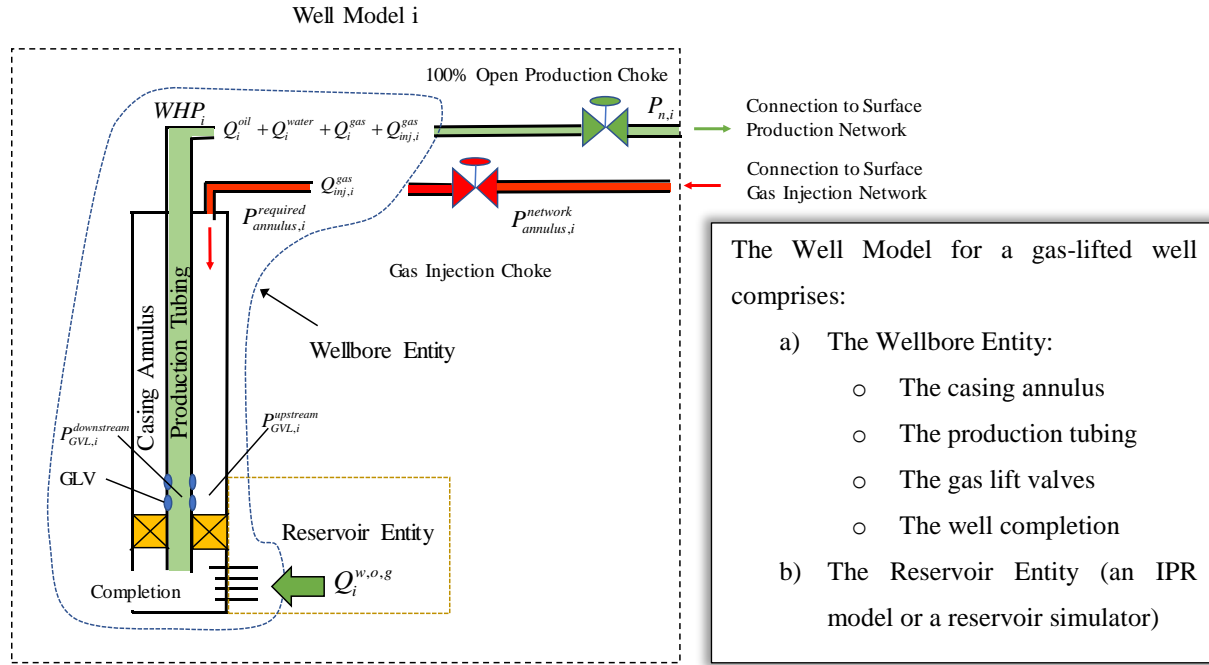


Figure 6.3 Concept of "Well Model" for gas-injected oil wells

The control variable for wells on gas lift is the allocated gas injection rate $Q_{inj,i}^{gas}$ provided through the surface gas injection network. For gas injected wells, the production choke is considered completely open (if not removed) since any pressure drop along the choke compromises the performance of the artificial lift method. For a selected gas-injection rate and surface nodal pressure, the “Well Model” returns the equilibrium production rate at the current reservoir conditions. For the solution obtained through nodal analysis, the wellbore model also calculates the required pressure in the annulus. The required injection pressure, $P_{annulus,i}^{required}$, is calculated using equation (6.3):

$$P_{annulus,i}^{required} = P_{GLV,i}^{downstream} + \Delta P_{GLV} + \Delta P_{annulus} \quad (6.3)$$

Where:

$P_{GLV,i}^{downstream}$: The pressure downstream of the gas lift valves (inside the production tubing)

ΔP_{GLV} : The differential opening pressure of the gas lift valve (GLV)

$\Delta P_{annulus}$: The pressure drop along the annulus space for the allocated gas injection rate, $Q_{inj,i}^{gas}$

The required gas injection pressure is the minimum annular pressure for which the GLV will open and the allocated gas will enter the production tubing in a *continuous* manner. Consequently, the gas injection network should deliver the allocated gas at a pressure $P_{annulus,i}^{network}$, which is at least equal to the required annular pressure:

$$P_{annulus,i}^{network} \geq P_{annulus,i}^{required} \quad (6.4)$$

Equation (6.4) represents the gas injectivity condition and serves as a means of coupling the production with the gas injection network that will be further discussed later in the chapter. It is important to note that if the annular pressure provided by the gas network is significantly higher than the required annular pressure the following issues arise:

- a) Because of pressure communication between the annulus and the production tubing, the pressure downstream of the gas lift valve increases significantly hence raising the BHP and reducing the influx of reservoir fluids into the wellbore.
- b) Excess compressor power is utilized resulting in higher field operating costs.

The issue of excessive annular pressure can be readily resolved by placing a gas injection choke (or pressure-reducing regulator) on the wellhead (see Figure 6.3). The purpose of the gas injection choke is to reduce the pressure provided from the gas injection network to a pressure

approximately equal to the required annular pressure, provided that the injectivity constraint is satisfied.

A selected gas injection rate corresponds to a unique VLP curve as shown in Figure 6.4. A plot of the liquid production at equilibrium conditions versus the allocated gas yields the Gas Lift Curve (GLC) under constant well-head-pressure (Figure 6.5). The gas lift attains a maximum liquid production when the gas rate equals $Q_{inj,*}^g$. For $Q_{inj}^g < Q_{inj,*}^g$, increasing the gas injection rate further reduces the effective density of the mixture which lowers the BHP and boosts production. On the contrary, increasing the gas injection rate above $Q_{inj,*}^g$ leads to higher compression costs and excessive frictional pressure losses in the tubing which comes at the cost of higher BHP and smaller production rates (Samier 2010, Borden et al. 2016).

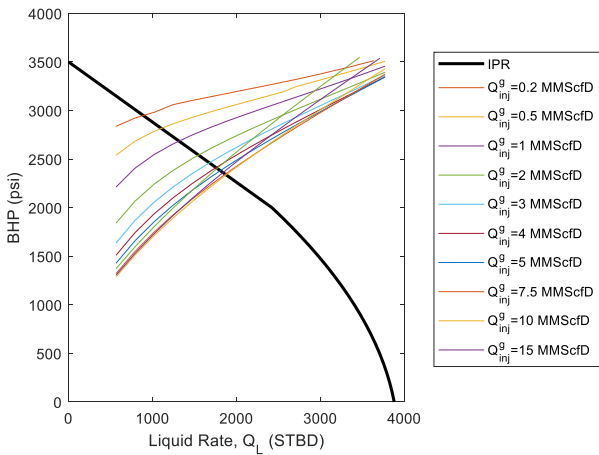


Figure 6.4 VLP curves for various gas injection rates

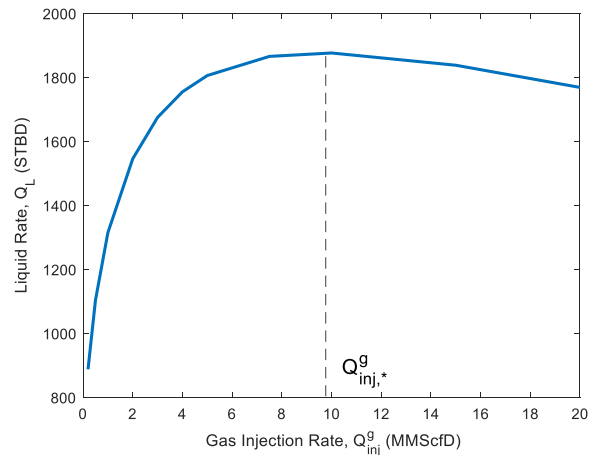


Figure 6.5 Gas Lift Curve (GLV) under constant WHP

It is important to note that the proposed “Well Model” evaluates the produced rates based on the current surface nodal pressure as opposed to other models which construct a Gas-Lift-Curve for a given WHP and then consider it static for further gas-lift analysis or production optimization.

6.2.2 The surface production and gas injection networks

The production from individual wells is fed into the surface production network which gathers the fluids to the separator or other distribution points. The gas injection network distributes the circulated gas from the separator to the gas-injected wells. Figure 6.6 depicts an oilfield comprising a production and a gas injection network.

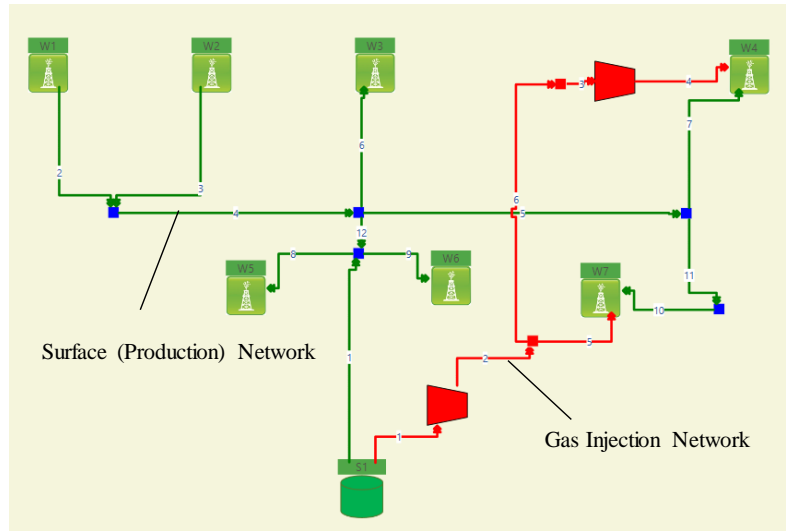


Figure 6.6 Superimposed surface production (green) and gas injection (red) surface networks.

In this dissertation, the production and gas injection surface networks are illustrated in green and red colors, respectively. From a topological perspective, the two networks have distinct incidence matrices, yet they share the surface nodes that represent a) the separator and b) the wells on gas lift. Additionally, the production network is in pressure communication with the outlet production choke for each of the producers in the field whereas, the gas injection network is in pressure communication with the gas injection chokes (or pressure regulators) of the gas-lifted wells (see Figure 6.3).

The surface production network utilizes the network solver presented in Chapter 5 to calculate the nodal pressures of the production network (and hence the pressures downstream of

the production chokes, $P_{n,i}$, for each well i) given the well production rates and the separator pressure. The numerical model for the surface production network can be written in the following compact form:

$$\overrightarrow{P_n} = \text{SurfaceNetwork}(\overrightarrow{Q^{w,o,g}}) \quad (6.5)$$

Where:

$\overrightarrow{P_n}$: the vector comprising the surface nodal pressure $P_{n,i}$ of each producer i in the field. This is the pressure downstream of the production choke.

$\overrightarrow{Q^{w,o,g}}$: the vector comprising the production rates of water, oil and gas in standard conditions, $Q_i^{o,w,g}$, for each producer i in the field

It is important to note that for wells on gas lift, the component of gas flowrate Q^g in the $\overrightarrow{Q^{w,o,g}}$ vector should also include the injected gas rate, since the total gas rate (produced and injected) is circulated back to the separator through the surface production network.

The gas injection network utilizes the network solver presented in Chapter 4 to calculate the nodal pressures of the gas injection network (and hence the pressure upstream of the pressure regulator $P_{annulus,i}^{network}$ for each well i on gas lift) for a given allocation of gas injection rates and compressor horsepower. Equation (6.6) conveniently represents the numerical model for the gas injection network:

$$\overrightarrow{P_{annulus}^{network}} = \text{GasNetwork}(\overrightarrow{Q_{inj}^g}) \quad (6.6)$$

Where:

$\overrightarrow{P_{annulus}^{network}}$: The vector comprising the pressures upstream of the gas injection choke (or regulator, $P_{annulus,i}^{network}$, for each well i on gas lift.

\overline{Q}_{inj}^g : The vector comprising the allocated gas injection rates in standard conditions $Q_{inj,i}^g$ for each well i on gas lift.

6.3 INTEGRATION SCHEME

In this section we present the explicit formulation for coupling the wells with the surface flowline network. The objective is to develop a forward model for estimating the total field production at a given time for a given set of well and network controls. The physical boundary between well models and the surface production network is the point downstream of the production choke, for all producers in the field (see Figure 6.1, 6.2, 6.3). Consequently, the coupling scheme needs to satisfy phase and pressure continuity at the surface nodes.

6.3.1 Coupling of the well models with the production network

In Chapter 4, iterative methods were deployed for performing well nodal analysis between the wellbore and the reservoir model. To this end, the Vertical Lift Performance curve (VLP) was constructed for a given Well-Head-Pressure (WHP) and well controls (for example choke size). The intersection of the VLP and the IPR curves provided the actual production rate. In a similar manner, we can perform nodal analysis between the Well Model and the surface production network. We adopt the term “Well Deliverability Curve” defined as the curve which provides the production rate for well i versus the surface nodal pressure, $P_{n,i}$, for a fixed well control (Lyons, 1995). The “well deliverability curve” can be obtained by performing nodal analysis on the “well model” for different values of the surface nodal pressure. Additionally, we define the term “Network Deliverability Curve” as the curve which provides the surface nodal pressure at node i , $P_{n,i}$, as a function of the production rate at well i , assuming constant influxes from the remaining producers. The Network Deliverability Curve can be constructed by solving the surface production

network for various well production rates. The intersection of the wellbore and network deliverability curves yields the actual flowrate entering the surface network from well i , as shown in Figure 6.7.

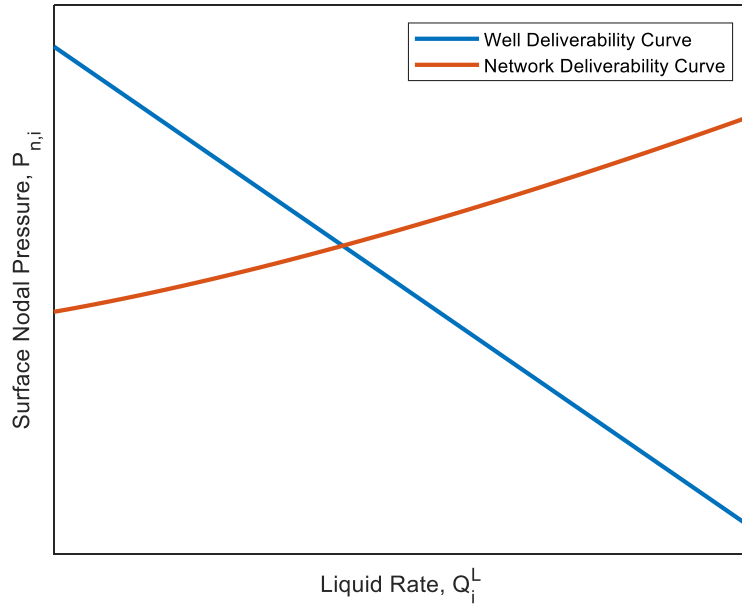


Figure 6.7 Concept of Surface Nodal Analysis for well i .

The slope of the Well Deliverability Curve depends greatly on the productivity index of the underlying reservoir model whereas the Network Deliverability curve depends on the network topology and pipeline properties of the surface network.

This notion can be extended to multi-point surface nodal analysis. As previously discussed, the network model can be conveniently represented by the following equation:

$$\vec{P}_n = \text{SurfaceNetwork}(\overline{Q^{o,w,g}}) \quad (6.7)$$

Where:

\vec{P}_n : The vector comprising the surface nodal pressures for each producer in the field.

$\vec{Q}^{w,o,g}$: The vector comprising the production rates of water, oil and gas in standard conditions for each producer in the field.

For a given set of well controls, each well model i , provides the oil, water and gas rates in standard conditions, $Q_i^{o,w,g}$, as a function of the corresponding nodal pressure, $P_{n,i}$:

$$Q_i^{o,w,g} = \text{WellModel}_i(P_{n,i}) \quad (6.8)$$

The set of well models for a producing field can be conveniently represented by the following equation:

$$\vec{Q}^{o,w,g} = \text{WellModels}(\vec{P}_n) \quad (6.9)$$

Substituting equation (6.9) into equation (6.7) yields

$$\vec{P}_n = \text{SurfaceNetwork}[\text{WellModels}(\vec{P}_n)] = f(\vec{P}_n) \quad (6.10)$$

Equation (6.10) has the form $x = f(x)$ and can be solved iteratively using fixed-point iteration:

$$\vec{P}_n^{(k+1)} = \text{SurfaceNetwork}[\text{WellModels}(\vec{P}_n^{(k)})] = f(\vec{P}_n^{(k)}) \quad (6.11)$$

Figure 6.8 illustrates the proposed iterative procedure for performing multi-point surface nodal analysis using fixed point iteration.

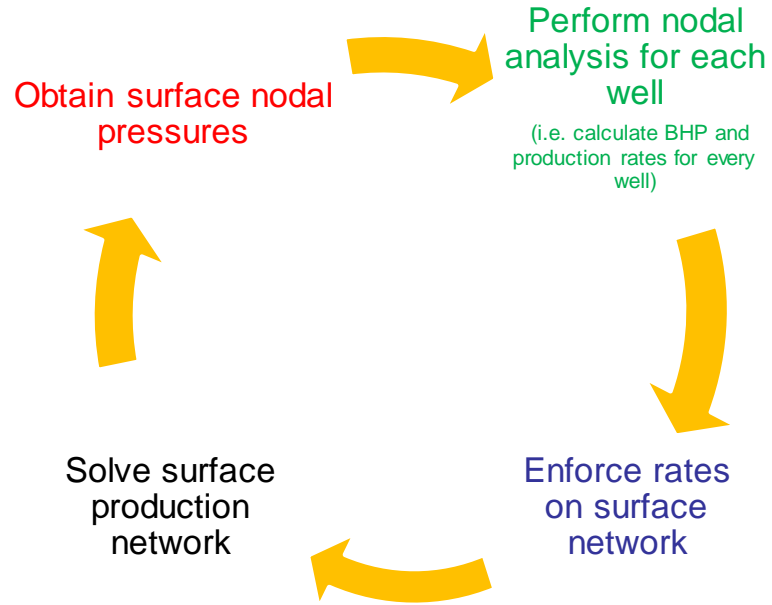


Figure 6.8 Iterative process for coupling the well models with the surface pipeline network.

The iteration starts by assuming a value for the surface nodal pressures (typically the value of the separator pressure). Using these values for the surface nodal pressures and the specified well controls, we obtain the flowrates for each well by performing nodal analysis using the secant method discussed in Chapter 4. The well rates are then enforced as external flowrates to the surface production network which is then solved and a new estimate for the surface nodal pressures is obtained. The process continues until convergence is achieved with respect to the vector of surface nodal pressures. The termination condition is provided in relative terms by equation (6.12).

$$\max_i \left| \frac{P_{n,i}^{(k+1)} - P_{n,i}^{(k)}}{P_{n,i}^{(k)}} \right| \leq \varepsilon \quad (6.12)$$

Where ε is selected to be equal to 10E-3, which is considered accurate for practical applications of production system analysis.

It is important to note that the proposed scheme converges except for the case where network deliverability curves are extremely steep, as was the case of small choke sizes in well nodal analysis. This behavior is observed when the network pipelines are characterized by high resistivity (i.e. small diameters and/or extremely long pipelines) When the iterative scheme is oscillating, relaxation factors are introduced (Chapra, 2010). In such cases the wellhead pressures at iteration $k+1$ are obtained from equation (6.13):

$$\bar{P}_n^{(k+1)} = \frac{1}{2}\bar{P}_n^{(k)} + \frac{1}{2}SurfaceNetwork[WellModels(\bar{P}_n^{(k)})] = \frac{1}{2}\bar{P}_n^{(k)} + \frac{1}{2}f(\bar{P}_n^{(k)}) \quad (6.13)$$

The use of relaxation factors increases the stability of the numerical scheme at the cost of convergence speed. The proposed iterative scheme was tested for a wide variety of surface network topologies and well properties and smoothly converged to a solution as opposed to the explicit method discussed by Litvak (1995). The explicit method proposed by Litvak (1995), considered the wellbore trajectories a component of the surface pipeline system and fixed-point iteration was deployed to couple the reservoirs models with the surface production system. In Chapter 4 we observed that fixed-point iteration diverges in cases of steep VLP curves, which justifies the occasional non-converging behavior of the model presented by Litvak (1995). To ensure convergence, the proposed model follows a different approach by utilizing a) the secant method to perform individual well nodal analysis and b) fixed-point iteration to couple the well models with the surface pipeline network.

The production system analysis presented by Samier (2010) assumes that the gas-lift curve is static and invariant of the WHP. This assumption is a commonplace in the field of gas-lift allocation optimization and has been shown to provide suboptimal solutions. On the contrary, the scheme proposed in this dissertation, calculates individual well production rates based on the latest

estimate of the WHP, taking into account back-pressure effects and multi-well pressure interference. This approach is expected to provide a more realistic estimate of the field production rates.

It is important to note that the proposed explicit scheme inherits the assumption of its components. For example, the use of the surface network model discussed in Chapter 5 imposes the assumption of steady-state conditions which is justified as reservoir transients are in general much slower compared to surface network transients (Shiralkar 2005; Hegguler 1995). Additionally, representing the reservoir model with the use of a steady-state IPR automatically imposes the entirety of assumptions associated with the material balance equation. Finally, in the formulation presented herein, the integration of the well models with the surface production system is performed by iteratively solving the surface network given the well rates that correspond to the surface nodal pressures of the previous iteration. This assumes that well rates are positive (i.e. fluid enters the surface network at the wellheads) and production wells may not turn into injectors. In the field, this can be prevented with the use of check valves in the wellhead vicinity.

6.3.2 Coupling the production with the gas injection network

The gas injection network needs to supply sufficient casing pressure so that the allocated gas can be injected in the annulus in continuous manner. This requirement may be imposed by satisfying the gas injectivity constraint for each well, i , on gas lift:

$$P_{annulus,i}^{network} \geq P_{annulus,i}^{required} \quad (6.14)$$

where

$P_{annulus,i}^{network}$: the actual pressure provided by the gas injection network (pressure upstream of the gas injection choke or pressure-reducing regulator – see Figure 6.3)

$P_{annulus,i}^{wellbore}$: the required casing pressure to ensure continuous gas injection

In the proposed model it is assumed that the casing pressure can be adjusted in order to closely match the required annular pressure. This can be achieved with a gas injection choke or a pressure-reducing regulator, provided that the injectivity constraint (equation 6.14) is satisfied.

6.4 APPLICATION OF THE COUPLING SCHEME

In this section, the proposed integration scheme is applied to a synthetic field. The purpose of this application is to a) to evaluate the convergence speed of the method b) illustrate the effect of multi-well pressure interference and c) suggest methods to mitigate back-pressure effects.

6.4.1 Description of Synthetic Field

The synthetic field under study comprises 10 wells, three reciprocal compressors (C1, C2 & C3), one gate valve (V1) and one separator (S1) as shown in Figure 6.9.

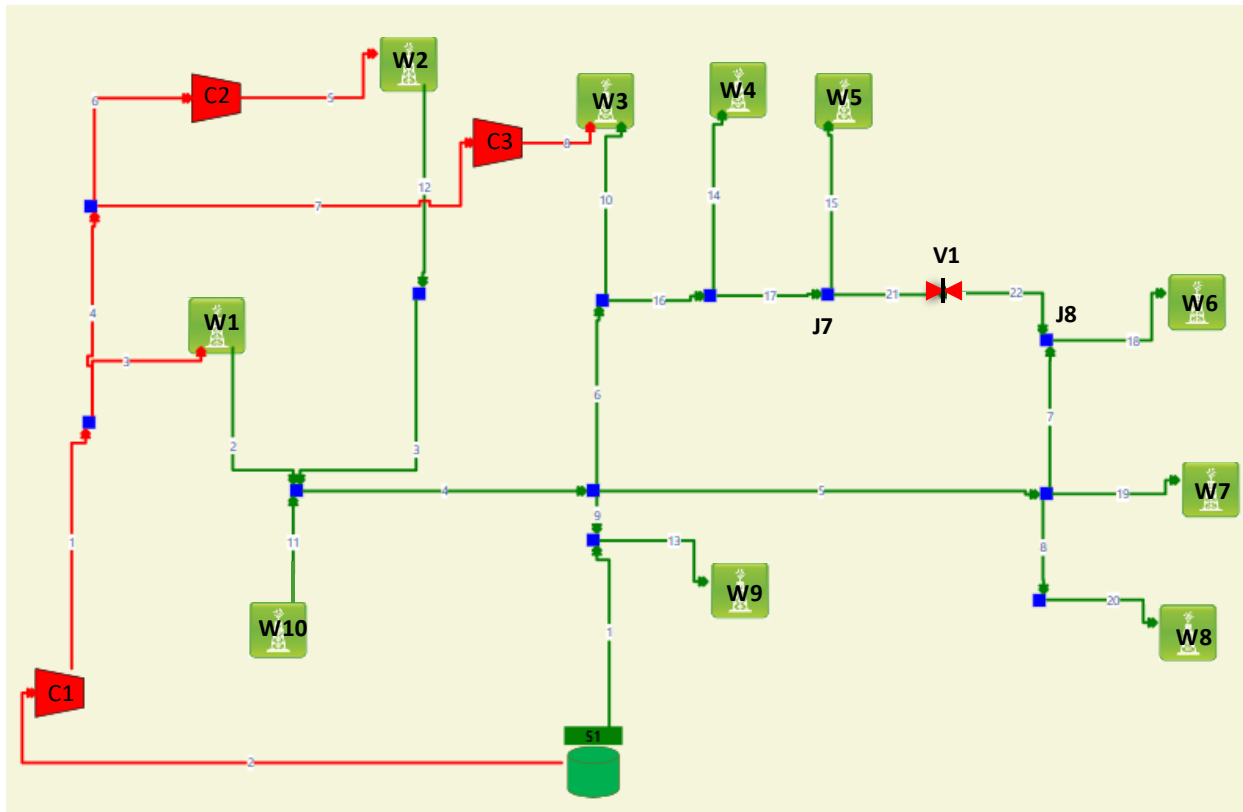


Figure 6.9 Synthetic Field: Schematic diagram of surface production and gas injection networks

Wells 1-3 are gas-lifted whereas Wells 4-10 are naturally flowing wells controlled with the use of a surface production choke. For this illustrative example, the wells are managed with the controls shown in Table 6.1 (Base Case scenario).

Table 6.1 Well controls for Base Case scenario

| | Well | W1 | W2 | W3 | W4 | W5 | W6 | W7 | W8 | W9 | W10 |
|-----------|---------------|-------------------|----|----|--------------|----|----|----|----|----|-----|
| | Control Units | Gas Lift (MMScfD) | | | Choke (/64") | | | | | | |
| Base Case | Controls | 10 | 5 | 10 | 16 | 20 | 16 | 22 | 18 | 20 | 12 |

The reservoir and wellbore properties for each well in the field are presented in Table 6.2. The separator pressure is set to 150 psi and the oil density and gas specific gravity are assumed equal to 30° API and 0.65, respectively.

Table 6.2 Reservoir and Wellbore properties for producing wells

| Well | Reservoir | | | | | Wellbore | |
|------|----------------------------|-----------------------|--------------------|------------|------|----------|-----------|
| | Average Reservoir Pressure | Productivity Index, J | Absolute Open Flow | GOR | WOR | TVD | Tubing ID |
| | (psi) | (STBOD/psi) | (STBLD/day) | (Scf/STBO) | | (ft) | (inch) |
| W1 | 6000 | 0.545 | 3650 | 500 | 0.1 | 12000 | 3.068 |
| W2 | 5800 | 0.545 | 3580 | 500 | 0.1 | 12000 | 3.068 |
| W3 | 5400 | 0.482 | 3170 | 500 | 0.25 | 12000 | 3.068 |
| W4 | 8000 | 0.582 | 8240 | 1000 | 0.4 | 9000 | 3.068 |
| W5 | 9000 | 0.364 | 8400 | 2500 | 0.25 | 8000 | 3.068 |
| W6 | 9000 | 0.473 | 7410 | 900 | 0.5 | 8500 | 3.068 |
| W7 | 7000 | 0.764 | 6800 | 1500 | 0.10 | 8000 | 3.068 |
| W8 | 7000 | 0.545 | 12600 | 1600 | 1.1 | 8000 | 3.068 |
| W9 | 9000 | 0.364 | 3800 | 500 | 0.10 | 12000 | 3.068 |
| W10 | 9000 | 0.60 | 11700 | 1500 | 0.50 | 11000 | 3.068 |

For the allocated lift-gas rates presented in Table 6.1 the horsepower for each compressor in the field is shown in Table 6.3.

Table 6.3 Allocated compressor power for base case

| Compressor | Operating Horsepower (HP) |
|------------|---------------------------|
| C1 | 1500 |
| C2 | 100 |
| C3 | 150 |

In the following paragraphs, the proposed model is deployed in order to couple the well models with the surface pipeline network.

6.4.2 Convergence Speed

For the base case configuration of surface controls, the integration scheme is deployed to couple the well models with the surface pipeline network. The initial guess for the nodal pressures is 200psi. In order to quantify the convergence speed, we define A_k as the ratio of the infinity norm of the error between successive iterations.

$$A_k = \frac{\left\| \overrightarrow{P}_n^{(k+1)} - \overrightarrow{P}_n^* \right\|_{\infty}}{\left\| \overrightarrow{P}_n^{(k)} - \overrightarrow{P}_n^* \right\|_{\infty}} \quad (6.15)$$

where

$\overrightarrow{P}_n^{(k)}$: the vector comprising the surface nodal pressure (pressure downstream of the production choke) for each well at iteration k

\overrightarrow{P}_n^* : the vector comprising the converged solution for the surface nodal pressures for each well

$\left\| \overrightarrow{x} \right\|_{\infty}$: the infinity norm, defined as $\max_{i=1,2,\dots,N} |x_i|$

The intermediate values of the surface nodal pressures per iteration k are shown in Table 6.4.

Table 6.4 Surface nodal pressure per iteration step, k

| Well Name | k: iteration | | | | | (Converged Solution) |
|-----------|--------------|----------|----------|----------|----------|----------------------|
| | k=1 | k=2 | k=3 | k=4 | k=5 | k=6 |
| Well W1 | 200 | 543.3999 | 514.9649 | 514.3305 | 514.3302 | 514.3304 |
| Well W2 | 200 | 522.7247 | 494.9739 | 494.3817 | 494.383 | 494.3832 |
| Well W3 | 200 | 481.2065 | 459.1416 | 458.6054 | 458.599 | 458.5988 |
| Well W4 | 200 | 582.4267 | 552.4944 | 551.8379 | 551.8272 | 551.8269 |
| Well W5 | 200 | 465.5998 | 445.705 | 445.2267 | 445.2199 | 445.2196 |
| Well W6 | 200 | 455.6212 | 436.2887 | 435.8205 | 435.8139 | 435.8136 |
| Well W7 | 200 | 541.6827 | 515.076 | 514.4718 | 514.4628 | 514.4625 |
| Well W8 | 200 | 493.2599 | 472.2745 | 471.7526 | 471.7434 | 471.743 |
| Well W9 | 200 | 330.5008 | 319.0606 | 318.7926 | 318.7898 | 318.7897 |
| Well W10 | 200 | 508.242 | 483.3136 | 482.7579 | 482.7564 | 482.7564 |

Adopting the definition of convergence (Singiresu, 2009), the integration scheme converges Q-linearly to the solution since there is a constant $r \in (0,1)$ for which equation (6.15) is satisfied for all k :

$$A_k = \frac{\|x_{k+1} - x^*\|_\infty}{\|x_k - x^*\|_\infty} \leq r \quad (6.16)$$

For this particular example, the constant r equals 0.10 which means that the distance to the solution decreases at each iteration by a factor bounded away from unity (Nocedal & Wright, 2006).

6.4.3 Understanding Well Interference

In order to understand the effects of back-pressure on individual well rates, the controls of the base case configuration are perturbed, one at a time, for a well on gas-lift and a naturally flowing well.

In the first case (Case A), the gas injection rate in Well “W2” is increased from 5 MMscfD to 7 MMScfD. This adjustment is not meant to provide the optimum field production but rather illustrate the effect multi-well pressure interference. Table 6.5 compares the controls and the individual well rates that correspond to the converged solution of the Base Case and Case A.

Table 6.5 Comparison of controls and production rates for Base Case and Case A.

| <i>Well Name</i> | <i>Case</i> Control Units | <i>Base Case</i> | | <i>Case A</i> | | ΔQ_{oil} |
|------------------|------------------------------|------------------|--------------|---------------|--------------|------------------|
| | | Control | Oil Rate | Control | Oil Rate | |
| W1 | MMScfD | 10 | 1487 | 10 | 1450 | -36.4 |
| W2 | MMScfD | 5 | 1202 | 7 | 1332 | 130.2 |
| W3 | MMScfD | 10 | 1135 | 10 | 1122 | -12.6 |
| W4 | /64" | 16 | 1672 | 16 | 1666 | -5.60 |
| W5 | /64" | 20 | 2014 | 20 | 2012 | -1.4 |
| W6 | /64" | 16 | 1731 | 16 | 1725 | -5.6 |
| W7 | /64" | 22 | 2445 | 22 | 2435 | -9.8 |
| W8 | /64" | 18 | 1759 | 18 | 1753 | -5.6 |
| W9 | /64" | 20 | 1603 | 20 | 1596 | -7.0 |
| W10 | /64" | 12 | 1327 | 12 | 1317 | -9.8 |
| V1 | open/closed | closed | - | closed | - | - |
| SUM | - | | 16375 | | 16441 | +36.4 |

Increasing the gas injection rate in Well W2 by 2 MMScfD results in increased oil production from W2 and decreased oil production from all other wells. More specifically, oil production from well W2 is increased by 130.2 STBOD and decreased by a total of -94.6STBOD from all other wells excluding W2. The net increase production is a mere 36.4STBOD. This is attributed to the fact that as the injection rate is increased, more gas is circulated into the surface production network resulting in elevated frictional pressure losses and hence higher WHPs. Keeping the controls of the other wells constant, higher WHPs result in reduced oil production from all other wells but well W2. The implication of this is that the net gain in production is significantly lower in a network of wells as would have been if well W2 had been produced individually. In addition, the current model evaluates the production in gas-injected wells by performing nodal analysis on the updated values of the WHP as opposed to other models which consider a constant-WHP gas lift curve. Should that be the case, the well rates for wells W1 and

W3 would be the same between the base case and Case A hence overestimating the net gain in production and possibly leading to suboptimal solutions.

In the second case (Case B), the choke size in Well “W6” is increased from 16/64” to 29/64”. The individual well rates for that correspond to the solution of the system for Case B are presented in in Table 6.6.

Table 6.6 Comparison of controls and production rates for Base Case and Case B

| <i>Well Name</i> | <i>Control Units</i> | <i>Base Case</i> | | <i>Case B</i> | | ΔQ_{oil} (STBOD) |
|------------------|----------------------|------------------|----------------------------|----------------|----------------------------|---|
| | | <i>Control</i> | <i>Oil Rate</i> (STBOD) | <i>Control</i> | <i>Oil Rate</i> (STBOD) | |
| W1 | MMScfD | 10 | 1487 | 10 | 1481 | -6.2 |
| W2 | MMScfD | 5 | 1202 | 5 | 1196 | -5.5 |
| W3 | MMScfD | 10 | 1135 | 10 | 1128 | -7 |
| W4 | /64” | 16 | 1672 | 16 | 1669 | -3.2 |
| W5 | /64” | 20 | 2014 | 20 | 2014 | -0.2 |
| W6 | /64” | 16 | 1731 | 29 | 2390 | 659.6 |
| W7 | /64” | 22 | 2445 | 22 | 2437 | -8.1 |
| W8 | /64” | 18 | 1759 | 18 | 1755 | -3.9 |
| W9 | /64” | 20 | 1603 | 20 | 1599 | -4.7 |
| W10 | /64” | 12 | 1327 | 12 | 1326 | -1.6 |
| VI | open/closed | closed | - | Closed | 16995 | - |
| SUM | - | - | 16375 | - | 16995 | +619.17 (net gain in production) |

Increasing the choke size in Well W6 increases oil production in W6 by 659 STBOD yet decreases oil production from all other wells. As more liquid flowrate enters the network from W6, higher frictional pressure losses are observed resulting in higher WHPs which tend to decrease oil production from all wells, except for Well W6. We observe that well W7 suffers the greatest reduction in produced oil rate which is justified by the fact that well W7 has the highest productivity index and hence the largest sensitivity to the surface nodal pressure. From cases A

and B we observe that the proposed model accurately captures the effects of back-pressure both in naturally flowing wells and wells on artificial lift.

The previous examples illustrate that multi-well pressure interference is attributed to the frictional pressure losses along the various components of the surface flowline network which influence WHPs whenever operational modifications are implemented. The effects of back-pressure can be mitigated by reducing or better managing the frictional pressure losses in the network. This could be achieved, for example, by replacing the surface pipelines with pipelines of larger diameter. Such an option, however, would not only be time consuming but also labor intensive. An alternative approach would be to properly adjust the operation of valves and manage the direction of flow in order to minimize WHPs. For the synthetic case under study, we consider Case C in which the well controls are the same as in Case B with the gate valve V1 opened instead of closed. Opening the gate valve V1, forms a closed network loop and enables flow along pipelines J7-V1 and V1-J8.

Table 6.7 Comparison of controls and production rates for Case B and Case C

| Well Name | Case | Case B | | | Case C | | |
|-----------|---------------|---------------|--------------|--------------------------|-------------|------------------|--|
| | Control Units | Control | Oil Rate | ΔQ_{oil} (STBOD) | Control | Oil Rate (STBOD) | ΔQ_{oil} (STBOD) |
| W1 | MMScfD | 10 | 1481 | -6.2 | 10 | 1483.4 | -3.8 |
| W2 | MMScfD | 5 | 1196 | -5.5 | 5 | 1198.1 | -3.4 |
| W3 | MMScfD | 10 | 1128 | -7 | 10 | 1130.7 | -4.3 |
| W4 | /64" | 16 | 1669 | -3.2 | 16 | 1670.2 | -2.0 |
| W5 | /64" | 20 | 2014 | -0.2 | 20 | 2014.1 | -0.1 |
| W6 | /64" | 29 | 2390 | 659.6 | 29 | 2442.99 | 702.59 |
| W7 | /64" | 22 | 2437 | -8.1 | 22 | 2440.1 | -5.0 |
| W8 | /64" | 18 | 1755 | -3.9 | 18 | 1756.5 | -2.4 |
| W9 | /64" | 20 | 1599 | -4.7 | 20 | 1600.8 | -2.9 |
| W10 | /64" | 12 | 1326 | -1.6 | 12 | 1326.6 | -1.0 |
| V1 | open/closed | Closed | - | - | Open | - | - |
| SUM | - | - | 16995 | 619.17 | | 17307 | 687.62 (net gain in production) |

Opening Valve V1 (Case C) increases the area available to flow, reduces the resistance of the surface network resulting in a higher net gain of production compared to Case B (see Table 6.7).

This example attests to the fact that modifying the network topology by properly adjusting the valve controls can mitigate well-interference effects and increase produced volumes. In the next chapter, the forward model is utilized to simultaneously optimize well and network controls for the purpose of maximizing hydrocarbon production on a daily basis.

6.4.4 Satisfying the gas injectivity condition

For the Base Case scenario, the allocated compressor horsepower is shown in Table 6.1. For each well on gas lift, the corresponding well model calculates the minimum casing pressure to

ensure continuous injection of the allocated gas. The actual pressure in the annulus is calculated from the surface gas injection network given the gas allocation rates and compressor horsepower. The actual versus the required annular pressure for each well on gas lift is shown in Table 6.8.

Table 6.8 Provided versus required gas injection pressure

| Well Name | $P_{annulus,i}^{required}$ (psi) | $P_{annulus,i}^{network}$ (psi) |
|------------------|----------------------------------|---------------------------------|
| Well W1 | 2174.7 | 2312 |
| Well W2 | 2425.6 | 2547 |
| Well W3 | 2071.3 | 2752 |

We observe that for the allocated compressor horsepower, the actual annular pressure is greater than the required annular pressure and hence the injectivity constraint is satisfied. For well W3, the actual pressure at the annulus is significantly higher compared to the required pressure, indicating excessive use of compressor power and elevated operating costs.

6.5 CONCLUSIONS

In this chapter, we introduced an explicit numerical scheme for coupling the well models with the surface pipeline network at each time step. To this end, the well model was integrated with the surface flowline network both for naturally flowing wells and wells on artificial lift. The idea underlying the coupling scheme is that nodal analysis and surface network modeling are performed in a sequential and iterative manner as dictated by fixed-point iteration. The production and gas injection networks are coupled using the injectivity constraint, ensuring continuous injection of the allocated gas.

The proposed method assumes steady-state conditions and for this reason, the application of the model is currently limited to naturally flowing wells and wells on continuous lift (i.e. ESP

and continuous gas lift). The model could potentially be used to model intermittent lift methods (such as intermittent gas lift or rod pumps) if the underlying well models provide time-averaged production flowrates. Additionally, the integration scheme assumes similar black-oil PVT properties for all producers in the field.

The application of the model in a synthetic field comprising 10 wells revealed the following:

- a) The proposed method converges Q-linearly to a solution, typically within 4-6 iterations.
- b) The proposed method accurately captures the back-pressure effects resulting from multi-well pressure interference through the surface network, both for naturally flowing wells and wells on artificial lift.
- c) The model provides a more realistic estimate of production rates as it uses a dynamic nodal analysis tool instead of a constant-WHP Gas Lift Curve for wells on gas lift.
- d) The model evaluates the residual of the injectivity constraints and infers whether the allocated compressor power is sufficient to ensure continuous gas injection.

The integration model presented herein (“the forward model”) can be used to calculate the total field production for a given set of well and network controls at the current reservoir conditions. In the following chapter the forward model is deployed to optimize well and network controls for the purpose of maximizing an asset’s daily operating income.

6.6 NOMENCLATURE

| | | |
|-----------------------------------|---|---|
| c_i | = | Control for well i |
| $p_{annulus,i}^{network}$ | = | Gas Injection pressure at well i, evaluated from the gas injection network |
| $\mathbf{P}_{annulus}^{network}$ | = | Vector comprising the gas injection pressure, $p_{annulus,i}^{network}$, for each well I on gas lift |
| $p_{annulus,i}^{required}$ | = | Minimum (required) gas injection pressure for well i |
| $\mathbf{P}_{annulus}^{required}$ | = | Vector comprising the required gas injection pressure, $p_{annulus,i}^{required}$, for each well I on gas lift |
| $P_{Discharge}$ | = | ESP Discharge Pressure |
| $P_{n,i}$ | = | Surface nodal pressure of well i. This is the pressure downstream of the production choke |
| $p_{n,i}^{(k)}$ | = | Surface nodal pressure of well i at iteration k. This is the pressure downstream of the production choke |
| $\mathbf{P}_n^{(k)}$ | = | Vector comprising the surface nodal pressures, $p_{n,i}^{(k)}$, for each well i at iteration k |
| Q_i^j | = | j-Phase production rate for well i, expressed in standard conditions |
| $Q_{inj,i}^{gas}$ | = | Gas injection rate for well i |
| \mathbf{Q}_{inj}^{gas} | = | Vector comprising the Gas injection rate, $Q_{inj,i}^{gas}$, for each well i on gas lift |
| $\Delta P_{annulus}$ | = | Pressure drop along the annular space |
| ΔP_{ESP} | = | Pump differential pressure |
| ΔP_{GLV} | = | Gas Lift Valve Pressure rating |
| ΔP_{tubing} | = | Pressure drop along the production tubing |

Chapter 7: Optimization of Well and Network Controls

7.1 INTRODUCTION

Optimization of oilfield controls has been a major topic of interest for oil and gas producers since it can improve oil recovery and reduce operating costs, ultimately increasing operating income and asset value. In addition, field-wide optimization of well and surface controls can assist operators identify the active constraints of the system and rebalance the production facilities in case of unpredicted events, such as unexpected reservoir behavior or compressor shutdown. Any approach to optimize the production system should take into consideration (i) inter-well pressure interference imposed through the surface pipeline network and (ii) the set of constraints placed on various components of the system. In Chapter 4, completion and reservoir constraints were introduced for the design of choke management strategies and flowback operations on an individual well basis. In a similar manner, completion and reservoir constraints may be imposed for each well in the field to mitigate the risk of completion failures and/or avoid costly workovers. Additional constraints include the gas injectivity constraints discussed in Chapter 6 and the constraints imposed from the surface facilities, such as:

- the installed compressor capacity
- the water handling capacity of the surface facilities such as separators, hydrocyclones and floatation units
- the total available lift-gas
- the maximum flared gas as dictated by state environmental regulations
- maximum pipeline fluid velocities to avoid erosion of the surface equipment
- minimum pipeline fluid velocities to prevent hydrate or wax formation

Operators have applied various optimization techniques for improving well management on a field-wide basis, ranging from linear programming to hybrid optimization workflows comprising derivative-free and gradient based methods. In most cases, especially when it comes to lift-gas allocation problems, proposed schemes typically, and incorrectly, neglect back-pressure effects due to common well tie backs in surface pipeline network. This assumption only holds true when the surface network is characterized by insignificant resistivity (large pipeline diameters) in which case the problem becomes a separable programming problem where the objective and constraint function are sums of functions comprising a single control (Wang, 2002) variable. In real fields, however, this assumption barely holds true and the application of such models tends to overestimate production rates, possibly leading to suboptimal solutions.

This chapter focuses on the problem of field-wide production optimization. To this end, the chapter (i) provides a review of the optimization methods that have been utilized to optimize well controls on a field-wide basis and (ii) applies a hybrid optimization workflows in a synthetic field using the integrated physics-based model presented in Chapter 6 along with the DAKOTA optimization framework by Sandia National Laboratories.

7.2 REVIEW OF OPTIMIZATION METHODS IN OILFIELD MANAGEMENT

Optimization of oilfield controls has been studied extensively both in the context of lift-gas allocation as well as in the broader definition of oilfield management which pertains to identifying the optimum controls of the entire production system, including chokes and lift-gas rates. Optimization of production management typically involves the definition of some economic objective function which accounts for liquids production and field operating costs. The classification of the studies should not be categorized based on the definition of the objective function, since this definition may vary significantly among researchers, but rather on the underlying assumptions and optimization workflows. Different methods have been applied, varying from linear or separable programming to complex optimization workflows involving evolutionary algorithms, gradient-based techniques and Mixed-Integer-Non-Linear-Problem (MINLP) formulations.

Early studies in gas-lift optimization (Simmons 1972, Kanu 1981) focused on single well analysis and gave rise to the incremental Gas-Oil-Ratio or “equal-slope” heuristic rule. According to the “equal-slope” principle, the optimum gas injection rate is not the rate at which production is maximized but rather the point where the incremental revenue equals the incremental cost of gas-injection. Redden (1974) expanded this notion for a set of wells and concluded that all wells tied to a common manifold should operate at the same incremental GOR. However, this recommendation was derived assuming that wells are tied to a fixed-pressure manifold, hence ignoring back-pressure effects. The “equal-slope” principle was later adopted by various authors to allocate the available lift gas among producers. For example, Chia and Hussain (1999) discretized the available gas and sequentially allocated it to high productivity wells. In addition to the equal slope solution, Nishikiori (1989) utilized a Quasi-Newton method for optimizing gas allocation and proposed guidelines for obtaining an initial estimate of the gas injection rates. Fang

and Lo (1996) and Handley-Schachler (2000) used Sequential Linear Programming (SLP) and approximated the gas-lift curves using piecewise linear functions. Using a two-well system tied to a common surface pipeline, Dutta-Roy (1997) observed that back-pressure effects can be significant and non-linear optimization tools should be used in order to obtain satisfactory results. The broader problem of oilfield management (both for naturally flowing wells and wells on gas lift) has also been addressed in the form of a Mixed-Integer-Linear-Problem (MILP) (Wang 2002; Kosmidis 2004; Guyaguler 2007) where the binary integer variables correspond to the well status (online/offline). It is important to note that none of the previously mentioned studies take into consideration back-pressure effects through the surface gathering network.

Optimization of well controls using surface network modeling and non-linear optimization methods has been proposed by Wang (2002) and Davidson (2003). To account for well interference, Wang (2002) and Davidson(2003) used a single-phase branched network model and optimized field controls (gas-injection rates and production rates) using Sequential Quadratic Programming (SQP). Field-scale production optimization using genetic algorithms has been reported for the Kuparuk River (Stoisits, 1999) and the Prudhoe Bay oilfields (Litvak, 2002) where production is vastly limited by compressor capacity and ambient temperatures. With regard to the Prudhoe Bay oilfield, Litvak (2002) suggested heuristic techniques to optimize well connections to manifolds, possibly leading to suboptimal solutions.

7.3 STATEMENT OF THE OPTIMIZATION PROBLEM

In this work, the objective function is defined as the operating income, f , (i.e. revenue minus operating expenses) generated over a short period of time, for the selected vector of control variables, \mathbf{x} :

$$f(\mathbf{x}) = r^{oil} Q_{field}^{oil}(\mathbf{x})\Delta t + r^{gas} Q_{field}^{gas}(\mathbf{x})\Delta t - r^{water} Q_{field}^{water}(\mathbf{x})\Delta t - r_{kWh} \sum_{i \in C} x_i \Delta t - r_{kWh} \sum_{i \in E} W_{ESP}(x_i)\Delta t \quad (7.1)$$

where

| | |
|---------------------|--|
| r^{oil} | Oil price (\$/STBO) |
| r^{gas} | Gas price (\$/MScf) |
| r^{water} | Cost of water disposal (\$/STBW) |
| Q_{field}^{oil} | Field oil production (STBO/day) |
| Q_{field}^{water} | Field water production (STBW/day) |
| Q_{field}^{gas} | Field gas production (MScf/day) |
| Δt | Timestep for calculating produced volumes (24h) |
| \mathbf{x} | The Vector of Control variables |
| N | The subset of control variables that correspond to Naturally Flowing Wells (choke sizes) |
| E | The subset of control variables that correspond to wells on ESP (ESP frequencies) |
| C | The subset of control variables that correspond to Compressors (operating horsepower) |
| W | The function for converting ESP frequency to horsepower using an ESP pump curve |

The term instantaneous implies that the operating income is calculated from the short-term production rates obtained from the steady-state solution of the production system, given a vector of control variables, \mathbf{x} . The volume of produced liquids is calculated over a short period, Δt , with a duration of 24 hours. This operating income should not be confused with the operating income generated over longer time periods (i.e. monthly or quarterly) in which case reservoir depletion can be significant. The reader should be aware that the term “control variables”, \mathbf{x} , encompasses a) the well controls (production choke sizes, ESP frequencies and gas injection rates) b) the allocated compressor horsepower and c) the valve controls in the surface network. The objective

of the optimization problem is to maximize the operating income, $f(x)$, or, equivalently, minimize the cost function defined as $-f(x)$. The field-wide optimization problem has the generic form shown in Table 7.1:

Table 7.1 Statement of the Field-Wide Production Optimization Problem

| | | |
|--|-----------------------------------|-------|
| $\min -f(x)$ | Objective Function | (7.2) |
| s.t. | | |
| $0 \leq x_i \leq UB_i, i = 1, 2, \dots, N$ | Bound Constraints | (7.3) |
| $g_j(x) \leq g_{j,\max}, j = 1, 2, \dots, m$ | Linear and Non-Linear Constraints | (7.4) |

Equations (7.3) represent the bound constraints which determine the feasible range for each of the control variables, x_i . The nature of the control variables necessitates that $x_i \geq 0$ since choke sizes, ESP frequencies, gas injection rates etc. should all be non-negative numbers. In addition, the control variables, x_i , are upper-bounded. For example, in naturally flowing wells, the choke sizes are upper bounded by the largest available choke size in the field. Table 7.2 illustrates the physical meaning of the Upper Bounds for each control variable in the production system.

Table 7.2 Description of upper bound values for control variables.

| Control Variable, x_i | Production Element | Variable Type | Upper Bound, UB_i |
|-------------------------|-------------------------|---------------|-----------------------------------|
| Choke Size | Naturally Flowing Wells | Continuous | Largest Available Choke Size |
| ESP Frequency | Wells on ESP | Continuous | Max frequency of Electric Current |
| Injected Gas | Wells on gas-lift | Continuous | Maximum gas injection rate |
| Compressor HP | Gas Compressor | Continuous | Horsepower rating |
| Valve Control | Surface Valve | Discrete | Number of Configuration Options |

The constraint equations (7.4) comprise both linear constraints (for example the total gas injection rate compared to the available lift-gas) and non-linear constraints. The non-linear constraints encompass the a) the wellbore, completion and reservoir constraints for each well in

the field, as discussed in detail in Chapter 4, b) the gas injectivity constraint for each well on gas-lift c) the constraints imposed by the surface facilities such as the water handling capacity.

In the absence of discrete control variables, the optimization problem is a Non-Linear Constrained Problem (NCP) whereas, in the presence of discrete control variables, the optimization problem is posed as a Mixed-Integer-Non-Linear Problem (MINLP).

7.4 OPTIMIZATION FRAMEWORK

7.4.1 The Dakota Framework

In this work we utilize the “Design Analysis Kit for Optimization and Terascale Applications” (abbreviated as “DAKOTA”) developed by Sandia National Laboratories. The DAKOTA project initiated in 1994 for the development of optimization tools intended primarily for structural analysis and aerospace engineering. A strong motivation for the DAKOTA project was the development of an archive of optimization methods that would eliminate the necessity for engineers to repeatedly develop new interfaces between engineering software and optimization routines (Adams et al. 2019). In its current form, DAKOTA is an open-source expandable framework which encompasses tools for optimization, parameter estimation, sensitivity analysis and statistical sampling. More specifically, DAKOTA contains routines for:

- a) *Parameter Studies* for assessing the characteristic of the response functions such as smoothness, nonlinearity, multi-modularity and understanding the effect of parameter sensitivity on the output of the simulation models
- b) *Design of Experiments (DoE)* for performing global sensitivity analysis and exploring the parameter space given a limited number of computer experiments (i.e.

simulation of the forward model). DoE methods include, for instance, Latin-Hypercube-Sampling and Orthogonal Sampling.

- c) *Uncertainty Quantification* for obtaining the probability distribution of the response function given the probability distribution functions for each of the input parameters. DAKOTA provides various methods for uncertainty quantification such as Monte-Carlo Sampling and reliability methods
- d) *Optimization* for minimizing or maximizing an objective function given a set of bound, equality and inequality constraints. The objective function can either be stated explicitly (i.e. with an algebraic or symbolic expression) or obtained through an external simulation model (i.e. a black-box function). DAKOTA encompasses gradient and non-gradient based methods along with the capability to handle both discrete and continuous variables.
- e) *Calibration* for estimating the value of parameters that minimize the discrepancy between simulation results and field (or experimental) data. Calibration models can also be used to solve inverse problems.

Among the analysis tools provided by DAKOTA, in this work we utilize the routines associated with a) global and local optimization and b) Design of Experiment (DoE). The major benefits of using DAKOTA over other optimization frameworks (such as Knitro, NOMAD, AIMS) are (a) the capability of Dakota to interface with external, “black-box” simulation models (b) the availability of both gradient-based and non-gradient based optimization methods and (iii) the capability of DAKOTA to internally coordinate parallel simulation of “black-box” objective functions among the logical processors, thus taking full advantage of the available computational resources.

Table 7.3 presents the Design or Experiment (DoE) and Optimization methods available in Dakota along with their capabilities with respect to a) internally handling non-linear inequality constraints and b) internally handling the parallel execution of the black-box objective function. From the methods available in Dakota, we only utilize those who support parallel execution of the forward model in order to alleviate computational expenditure.

Table 7.3 Sampling and Optimization routines available in the DAKOTA framework

| Method | Analysis | Input Parameters (Integer, Real, Mixed) | Gradient Based | Internally Handles Non- Linear Constraints | Supports Parallel Execution |
|------------------------------------|----------|---|-------------------------------------|---|-------------------------------------|
| Latin-Hypercube-Sampling | DoE | Real | <input type="checkbox"/> | <input type="checkbox"/> | <input checked="" type="checkbox"/> |
| Orthogonal Array Sampling | DoE | Real | <input type="checkbox"/> | <input type="checkbox"/> | <input checked="" type="checkbox"/> |
| Box-Behnken Design | DoE | Real | <input type="checkbox"/> | <input type="checkbox"/> | <input checked="" type="checkbox"/> |
| Central Composite Design | DoE | Real | <input type="checkbox"/> | <input type="checkbox"/> | <input checked="" type="checkbox"/> |
| Monte Carlo Design | DoE | Real | <input type="checkbox"/> | <input type="checkbox"/> | <input checked="" type="checkbox"/> |
| Genetic Algorithm (COLINY) | Global | R | <input type="checkbox"/> | <input type="checkbox"/> | <input checked="" type="checkbox"/> |
| Genetic Algorithm (SOGA) | Global | R | <input type="checkbox"/> | <input type="checkbox"/> | <input checked="" type="checkbox"/> |
| Division of Rectangles | Global | R | <input type="checkbox"/> | <input type="checkbox"/> | <input checked="" type="checkbox"/> |
| Branch & Bound | Global | M | <input checked="" type="checkbox"/> | <input checked="" type="checkbox"/> | <input checked="" type="checkbox"/> |
| Newton Method | Local | R | <input checked="" type="checkbox"/> | <input checked="" type="checkbox"/> | <input checked="" type="checkbox"/> |
| Quasi-Newton (BFGS) | Local | R | <input checked="" type="checkbox"/> | <input checked="" type="checkbox"/> | <input checked="" type="checkbox"/> |
| Conjugate Gradient Method | Local | R | <input checked="" type="checkbox"/> | <input checked="" type="checkbox"/> | <input checked="" type="checkbox"/> |
| Asynchronous Pattern Search | Local | R/I | <input checked="" type="checkbox"/> | <input type="checkbox"/> | <input checked="" type="checkbox"/> |
| Coliny Pattern Search | Local | R/I | <input type="checkbox"/> | <input checked="" type="checkbox"/> | <input checked="" type="checkbox"/> |
| Nelder-Mead Simplex Method | Local | R | <input type="checkbox"/> | <input type="checkbox"/> | <input type="checkbox"/> |
| Greedy Search Heuristic | Local | R | <input checked="" type="checkbox"/> | <input type="checkbox"/> | <input checked="" type="checkbox"/> |
| Augmented Langragian | Local | R | <input checked="" type="checkbox"/> | <input checked="" type="checkbox"/> | <input checked="" type="checkbox"/> |

7.4.2 Design of Experiment Methods (Sampling)

Design of Experiment (DoE) refers to the process of choosing a set of samples (i.e. a set of vectors \mathbf{x} , comprising variables $x_i, i=1,2,\dots,n$) from the n -dimensional parameter space in order to extract as much information as possible, given a limited number of simulations. DoE methods are also referred to as “space filling methods” and are categorized into classical and modern methods (Giunta et al. 2003).

Classical methods (such as Box-Behnken design, and Central Composite Design Sampling) tend to place most of the samples towards the boundaries of the parameter space, thus leaving the interior space vastly unexplored. Additionally, in classical DoE methods, the number of samples scales with the dimensionality of the problem, n , by approximately 2^n . Consequently, classical DoE methods are not suitable for computationally expensive simulations or problems characterized by high dimensionality (Myers & Montgomery, 1995).

Modern DoE methods such as Latin Hypercube Sampling and Orthogonal Array sampling, have significant advantages over classical DoE methods, namely their ability to provide a better coverage of the interior space for the same number of function evaluations (Adams et al. 2019). Pseudo-Monte Carlo sampling is the most commonly used modern DoE method: a sample is generated using random numbers that lie between the upper and lower bounds for each parameter. However, the use of MC sampling can still leave regions of the search space vastly unexplored (Figure 7.1a). Improved space fill design can be obtained using stratified MC sampling in which case the range of each variable is split into

s equally probable bins and one sample is selected within each bin, for a total of s^n samples (Figure 7.1b).

Given a limited number of computer experiments, Latin-Hyper-Sampling (LHS) has been shown to provide better space filling results compared to MC sampling with regard to evaluating the mean of the response function (Giunta et al. 2003). In LHS the number of samples, s , is specified and then the range of each parameter is divided in s -equally probable bins, as was the case in stratified MC sampling. The samples are then obtained by the following rules: a) each bin contains at most one sample and b) for all one-dimensional projections of the p samples and bins, there is exactly one sample per bin (Figure 7.1c).

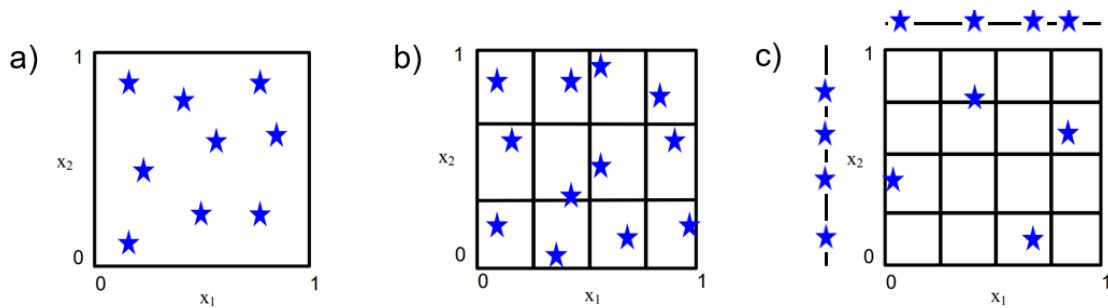


Figure 7.1 Sampling from a two-dimensional parameter space using a) Pseudo MC b) Stratified Monte-Carlo and c) Latin Hypercube Sampling (after Adams et al. 2019)

The orthogonal array sampling is a more generic case of the LHS that requires that exactly b samples are located within a bin in any t -dimensional projection (Figure 7.2). Constants t and b are referred to as the strength and index of the array, respectively.

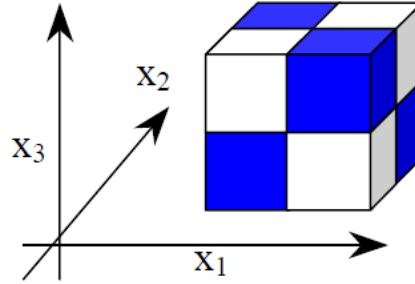


Figure 7.2 Orthogonal array sampling in a three-dimensional parameter space. There is exactly one sample per bin (index =1) in any two-dimensional projection (strength =2) (after Giunta et al. 2003)

For an OA design sampling, the number of samples, N_s , is obtained from the following equation:

$$N_s = bs^t \quad (7.5)$$

Where

- b : Index of the array
- s : Number of equally probable bins per parameters
- t : Strength of the array

The LHS is a specific case of the OA sampling, where $t=1$ and $b=1$.

7.4.3 Local Search Methods

Local optimization methods seek an improved solution in the vicinity of the current iteration. Local search methods are broadly categorized into gradient based and derivative free methods. In this paragraph we provide a quick overview of the local search methods that have been coupled with the physics-based model presented in this work.

7.4.3.1 Newton and Quasi-Newton Methods

Newton and Quasi-Newton methods are gradient-based, line search methods for unconstrained optimization. Line search methods iteratively determine a search direction, \mathbf{p}_k and then search along that direction to identify new iterates with a lower function value. The difference between the Newton and Quasi-Newton methods lies in the calculation of the search direction, \mathbf{p}_k (Nocedal, 2006).

Assuming that the function f is continuously twice differentiable, the second order Taylor series expansion about the current iterate, \mathbf{x}_k , yields:

$$f(x_k + p) \approx f(x_k) + p^T \nabla f(x_k) p + \frac{1}{2} p^T \nabla^2 f(x_k) p = m_k(p) \quad (7.6)$$

Assuming that $\nabla^2 f(x_k)$ is positive definite, the search direction \mathbf{p} can be obtained by setting the derivative of $m_k(p)$ equal to zero. Doing so, we obtain the Newton search direction:

$$p_k = -(\nabla^2 f(x_k))^{-1} \nabla f(x_k) \quad (7.7)$$

Where $\nabla^2 f(x_k)$ is the square matrix comprising second-order partial derivatives of function f (typically referred as the Hessian Matrix). The newton direction, \mathbf{p}_k , can then be used to perform a line search provided that (i) $\nabla^2 f(x_k)$ is positive definite, otherwise $(\nabla^2 f(x_k))^{-1}$ may not exist and (ii) the search direction \mathbf{p}_k satisfies the descent property $(\nabla f(x_k))^T \mathbf{p}_k < 0$ in which case, \mathbf{p}_k is a suitable search direction (Singiresu, 2009). In Newton's method (sometimes referred to as full-Newton method), the calculation of the second order partial derivatives in the Hessian matrix is performed using forward or central finite difference approximations. This can be a computationally expensive process, especially in problems of high dimensionality or in cases where the evaluation of the objective function value is computationally expensive. To overcome this, quasi-Newton methods require only the gradient of the objective function and provide an approximation of the inverse of Hessian Matrix, \mathbf{B}_k , by postulating that \mathbf{B}_k is (i) symmetric and (ii) positive definite (Nocedal, 2006). Quasi-Newton methods are characterized by superlinear convergence (as opposed to quadratic convergence of the full-Newton method) yet they can achieve improved overall performance as they require lesser function evaluations. Popular quasi-Newton methods are the BFGS (Broyden-Fletcher-Goldfarb-Shano) method (BFGS) and the DFP (Davidon, Fletcher, Powell) method. Details on the implementation of these methods can be found in Nocedal (2006).

The Dakota library offers the capability of using either the full-Newton or the BFGS quasi-Newton methods. The non-linear constraints are handled by augmenting the

objective function with a smooth penalty term, treating the optimization problem as an unconstrained problem.

7.4.3.2 Mesh Adaptive Direct Search

Mesh Adaptive Direct Search (MADS) is a derivative-free local search method. Derivative free methods are particularly useful when the objective function is non-smooth or in cases where gradient evaluation is either expensive or unreliable. MADS uses a stencil to navigate in the variable space in search of an improved solution. The stencil is defined by a set of polling directions and a polling step size. The center of the stencil is placed at the current iterate and a set of trial points is generated. The objective function value is evaluated for each of the trial points and compared with the value of the current iterate. If an improved solution is found, the stencil is moved to the new iterate, a new set of trial points is obtained, and the process continues. If the trial points yield no improvement, the polling step size is reduced (typically halved) and a new set of trial points is generated. The process terminates when the polling step size is reduced below a predetermined value (Isebor et al. 2014). Mesh-Adaptive-Direct-Search has the following advantages: a) it is guaranteed to converge to local optimum as supported by the local convergence theory b) is naturally parallelizable since the objective value of the trial points can be evaluated concurrently and c) supports both continuous and discrete variables (Audet et al. 2006). For the case of discrete variables, the corresponding step size is integer and larger or equal to unity. Finally, the application of MADS can be combined with the extreme barrier approach where the objective function value is set to infinity should at least one constraint

is violated (Singiresu, 2009). An illustrative example of MADS is shown in Figure 7.3 for the case of a two-dimensional space and a total of five search directions.

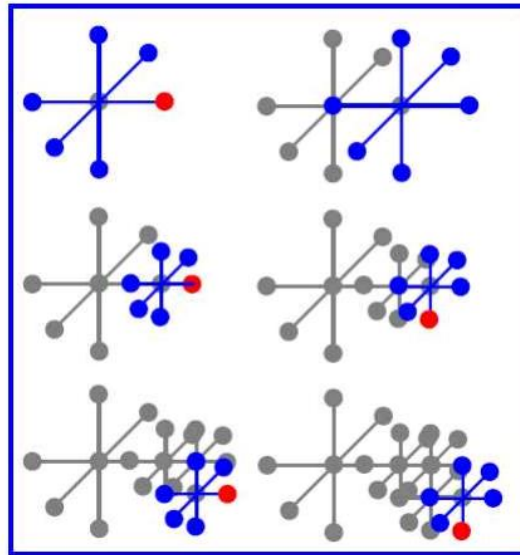


Figure 7.3 Pattern search methods for local optimization: The stencil undergoes operations of a) displacement and b) contraction in search of the local optimum (after Adams et al. 2018)

7.4.4 Global Search Methods

Global search methods comprise iterative, well-structured algorithms that can efficiently explore the design space. In this paragraph we discuss Evolutionary algorithms, Division of Rectangles and Surrogate Based Optimization.

7.4.4.1 Evolutionary Algorithms

Evolutionary algorithms were proposed in the early 1960's and they are inspired by Darwin's theory of evolution. A randomly generated population of sample points (genes)

undergoes operations of natural selection, mutation and cross-over in search of an improved solution per iteration step (or generation). The offsprings generated tend to replace the worst-performing genes while the top-performers (parents or elites) continue to exist in the next generation, ensuring that the performance of the Genetic Algorithm will not deteriorate in future generations (Singiresu, 2009). Evolutionary algorithms typically terminate when a maximum number of generations has been reached or a satisfactory objective value has been attained. The Dakota optimization framework offers two types of evolutionary algorithms, a Single Objective Genetic Algorithm (SOGA) and an Evolutionary Algorithm (EA).

7.4.4.2 Division of Rectangles

Division of rectangles (DIRECT) is a global search method that adaptively subdivides the feasible space in order to obtain trial points in the vicinity of a global minimum within a finite number of iterations. (Adams et al. 2018) The DIRECT iterative process for a two-dimensional parameter space is illustrated in Figure 7.4.

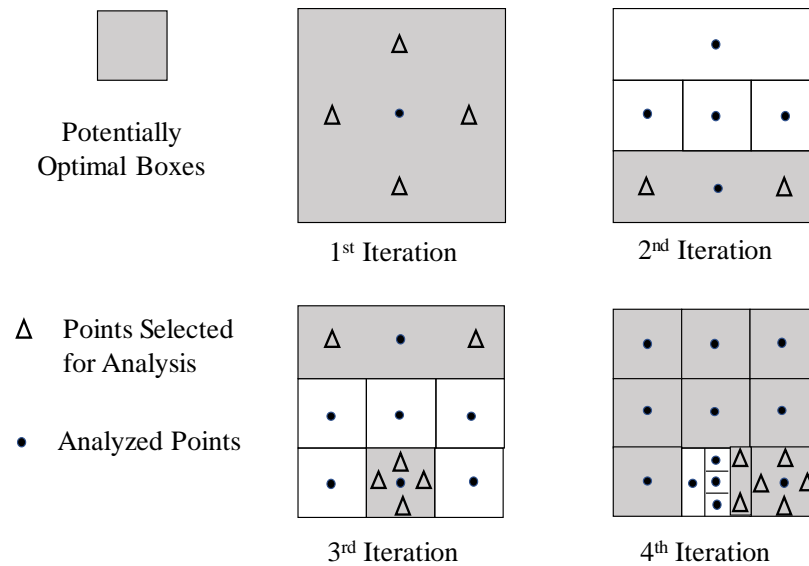


Figure 7.4 Illustrative example of Division of Rectangles in a two-dimensional variable space (adjusted from Adams et al. 2018).

7.4.4.3 Surrogate Based Optimization

Surrogate based methods provide an attractive alternative in optimization problems where the objective function is computationally expensive. A training set generated using the high-fidelity (true model) is used to approximate the objective function with a Gaussian Process (GP). The Gaussian Process can then be used to obtain a prediction of the objective function at any point in the search space along with the corresponding uncertainty. In each iteration, a new set of trial points is generated in order to a) minimize the objective value based on the current predictions of the GP and b) further explore regions of the search space characterized by high uncertainty (Adams et al. 2018). The true model is then deployed to obtain the actual objective values for the new set of trial points and the Gaussian Process is retrained. In the surrogate based optimization routine provided by

Dakota, the initial set of trial points is generated using Division of Rectangles and the non-linear constraints are handled using an augmented Lagrangian merit function.

7.5 OBJECTIVE FUNCTION AND CONSTRAINT EVALUATION

For a given vector of control variables, x , the value of the objective, $-f(x)$, is obtained using an encapsulated function (onwards referred to as “Black-Box”) which encompasses a) the integration scheme presented in Chapter 6 and b) post-processing tools. More specifically, for a given set of controls, the function evaluates the total field production using the forward model discussed in Chapter 6 and using the post-processing tools it further calculates (i) the value of the cost function, $-f$, and (ii) the normalized value for each of the inequality constraints. In equation (7.4), the non-linear constraints were expressed in the form:

$$g_j(x) \leq g_{j,\max}, j = 1, 2, \dots, m \quad (7.8)$$

The normalized form of the inequality constraints is defined as

$$\bar{g}_j = \frac{g_j(x)}{g_{j,\max}} - 1 \leq 0, j = 1, 2, \dots, m \quad (7.9)$$

Using this connotation, a positive value of a normalized inequality constraint indicates constraint violation. It is important to note that the black-box function does not evaluate the normalized value of the *bound* constraints since they are internally handled by all DAKOTA optimization methods. Additionally, the current optimization task (gradient

or derivative free) determines the specific output of the black-box function as discussed in the following paragraphs.

7.5.1 Evaluation of Objective Function for Gradient Based Optimization

Methods

When the encapsulated (black-box) function is called by a gradient based optimization method (such as Newton’s Method, Quasi-Newton, Augmented Lagrangian etc.) it returns both the value of the cost function (i.e. negative operating income), $-f(\mathbf{x})$, as well as the normalized value for each of the inequality constraints, g_i , as illustrated in Figure 7.5.

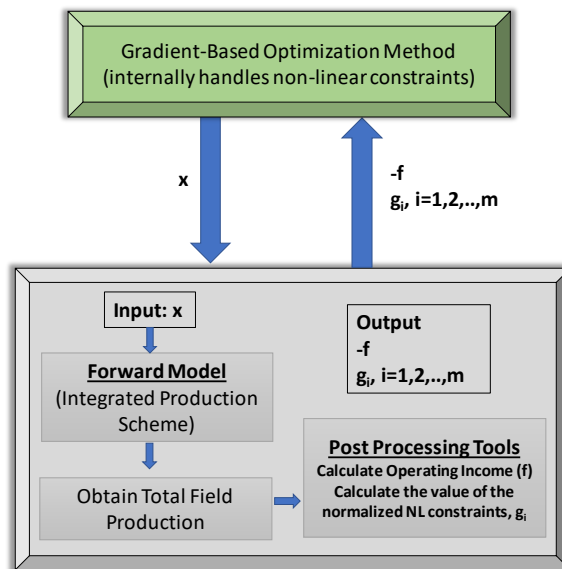


Figure 7.5 Objective function and constraint evaluation for gradient based methods.

The values of the normalized constraints are then used internally by the optimization routines to penalize the objective value using smooth penalty functions (Adams et al. 2008, Singiresu 2009).

7.5.2 Evaluation of Objective Function for Derivative-Free Optimization Methods

Design of Experiment Methods and some derivative-free optimization methods do not internally handle inequality constraints (see Table 7.3). In order to account for constraint violation, the calculation of the objective function is modified by adding an external penalty term $r \max\{0, g_i\}$, where r is the penalty parameter. The penalty parameter, r , is chosen to be relatively large (if not infinity) so that optimization algorithms can decisively disregard cases that violate the inequality constraints. Even though the use of a large penalty parameter causes discontinuities in the objective function, this does not compromise the performance of the optimization routines since no gradients are being evaluated. The internal structure of the encapsulated function is shown in Figure 7.6.

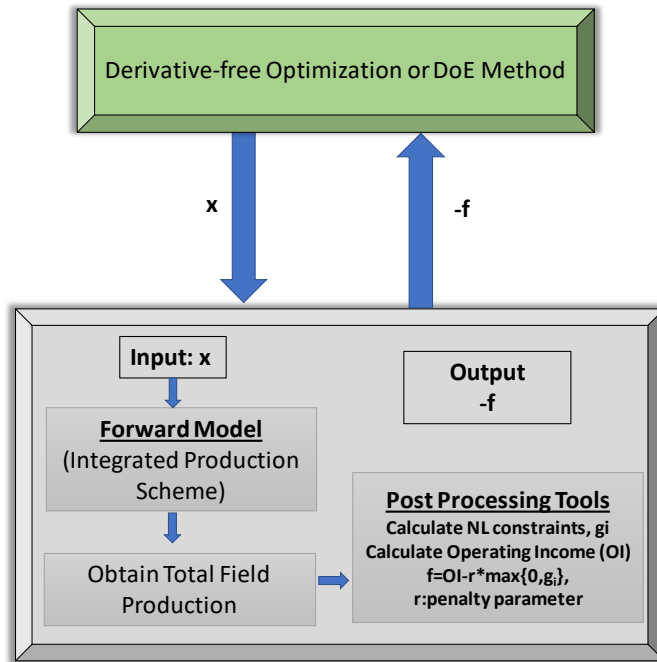


Figure 7.6 Objective function and constraint evaluation for derivative free methods

7.6 OPTIMIZATION WORKFLOWS

The wide range of optimization routines available in the Dakota framework allow us to define custom optimization workflows. The term “optimization workflow” refers to a series of optimization tasks which are executed sequentially. An optimization workflow may comprise a) sampling methods to explore the control variable space b) global search methods and c) local search methods. It is important to note that the optimization variables may vary among tasks. For example, a local optimization method may optimize for the entire set of control variables (well controls, compressor horsepower) or the well controls alone. The optimization workflow keeps track of the so-far optimal solution and the corresponding objective function value. At the end of the optimization workflow, the

production system is simulated for the optimal controls, providing the active constraints of the system and hence, the bottlenecks in production.

7.7 APPLICATION TO SYNTHETIC FIELD

In this section, the optimization framework is deployed to optimize the well and network controls of a synthetic field. The synthetic field under study comprises 7 naturally flowing wells, 5 wells on gas lift and 4 reciprocating gas compressors, for a total of 16 optimization variables. The topology of the surface pipeline network is illustrated in Figure 7.7. The wellbore and reservoir properties for each well in the field are presented in Table 7.4.

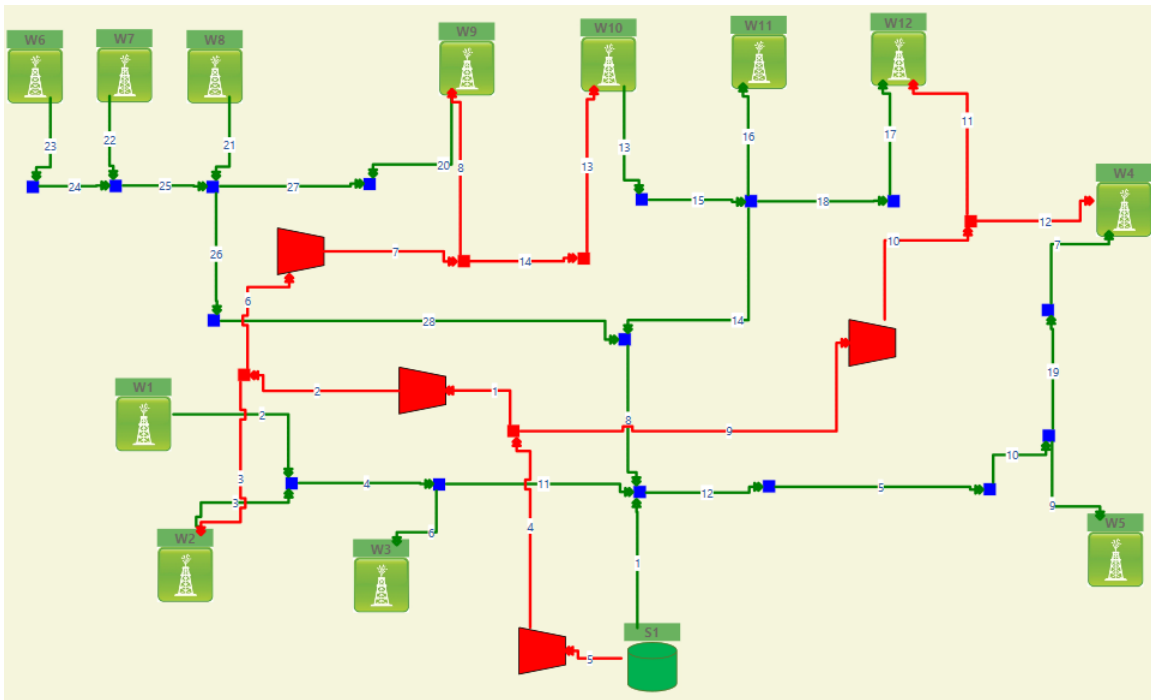


Figure 7.7 Network topology of synthetic field. Field comprises 12 wells and 4 compressors

The separator pressure is set to 150psi. The oil density is set to 30 degrees API and the gas specific gravity equal to 0.65. The system is optimized assuming an oil price of \$62, a water treatment cost of \$2/STBW and an electricity cost of \$0.07/KWh.

The system is subject to bound constraints for each of the optimization variables along with as set of inequality constraints applicable to:

- Maximum liquid rates for each well in the field
- Lift-gas availability constraint set to 100MMScfD
- Gas injectivity constraints for each well on gas lift and finally,
- The water handling capacity of the surface facilities set to 30MSTBW/day

The system is subject to 19 inequality constraints which outnumber the number of optimization variables. The upper and lower bounds for each of the control variables in the system are shown in Table 7.5.

Table 7.4 Reservoir and wellbore properties of synthetic field

| Well | Reservoir Pressure | Productivity Index (J) | GOR | WOR | TVD | Tubing ID |
|------|--------------------|------------------------|------------|------|-------|-----------|
| | (psi) | (STBOD/psi) | (Scf/STBO) | | (ft) | (inch) |
| W1 | 7000 | 4.364 | 500 | 3.00 | 12000 | 3.068 |
| W2 | 3900 | 5.455 | 500 | 1.41 | 12000 | 3.068 |
| W3 | 8000 | 5.455 | 500 | 1.50 | 8000 | 3.068 |
| W4 | 4000 | 5.273 | 500 | 0.65 | 12000 | 3.068 |
| W5 | 8700 | 5.810 | 500 | 0.20 | 12000 | 3.068 |
| W6 | 7000 | 2.909 | 500 | 0.10 | 12000 | 3.068 |
| W7 | 9000 | 3.636 | 500 | 0.10 | 12000 | 3.068 |
| W8 | 9000 | 5.273 | 500 | 0.50 | 10000 | 3.068 |
| W9 | 5100 | 3.810 | 500 | 0.40 | 11000 | 3.068 |
| W10 | 4300 | 5.090 | 500 | 0.60 | 12000 | 3.068 |
| W11 | 9000 | 4.470 | 500 | 0.10 | 12000 | 3.068 |
| W12 | 3700 | 5.273 | 500 | 1.10 | 12000 | 3.068 |

Table 7.5 Description and bounds for optimization variables

| Element | Description | Control | Control Units | Lower Bound | Upper Bound |
|-------------|------------------|--------------------|---------------|-------------|-------------|
| W1 | Well on Choke | Choke Size | /64" | 8 | 64 |
| W2 | Well on Gas Lift | Gas Injection Rate | MMScfD | 0 | 40 |
| W3 | Well on Choke | Choke Size Rate | /64" | 8 | 64 |
| W4 | Well on Gas Lift | Gas Injection Rate | MMScfD | 0 | 40 |
| W5 | Well on Choke | Choke Size | /64" | 8 | 64 |
| W6 | Well on Choke | Choke Size | /64" | 8 | 64 |
| W7 | Well on Choke | Choke Size | /64" | 8 | 64 |
| W8 | Well on Choke | Choke Size | /64" | 8 | 64 |
| W9 | Well on Gas Lift | Gas Injection Rate | MMScfD | 0 | 40 |
| W10 | Well on Gas Lift | Gas Injection Rate | MMScfD | 0 | 40 |
| W11 | Well on Choke | Choke Size | /64" | 8 | 64 |
| W12 | Well on Gas Lift | Gas Injection Rate | MMScfD | 0 | 40 |
| C1,C2,C3,C4 | Compressor | Horsepower | HP | 100 | 3000 |

The synthetic field under study is optimized using a hybrid optimization workflow comprising global and local search. Among the various global optimization methods, the Genetic Algorithm was selected as it has been shown to provide satisfactory results for gas-lift allocation optimization (Stoisits 1999, Litvak 2002). In order to efficiently sample the variable space, the population of the Genetic Algorithm was instantiated using Latin-Hypercube Sampling providing superior space filling design compared to other methods such as the quasi or stratified Monte-Carlo, for the same number of computer experiments (Adams et al. 2019, Guinta et al. 2003). For the Genetic Algorithm, all variables are treated as continuous variables with the upper and lower bounds shown in Table 7.5. With regard to local optimization, choke sizes are treated as discrete (integer) variables and compressor horsepower/ gas injection rates as continuous variables. The presence of both discrete and continuous variables necessitates the use of Asynchronous Pattern Search which is also

guaranteed to converge to local optima as proven by the local convergence theory (Audet et al. 2006). The implemented optimization workflow is presented in Table 7.6.

Table 7.6 Optimization workflow for synthetic field case

| Optimization Task | Variable Type | Function Evaluations |
|---|---------------|----------------------|
| Task I: Genetic Algorithm (Global Search) | Continuous | 800 |
| Task II: Asynchronous Pattern Search (Local Search) | Discrete | 600 |

For Task I, the genetic algorithm has a population of 50 and the population is instantiated using Latin Hypercube Sampling. For each of the subsequent generations, population members that do not satisfy the inequality constraints are replaced with new members using the same sampling approach. The genetic algorithm was run for total of 16 generations and the so-far optimal solution was used as the initial point for the local search. The evolution of the optimization process, in terms of the so-far (feasible) optimal solution is illustrated in Figure 7.8.

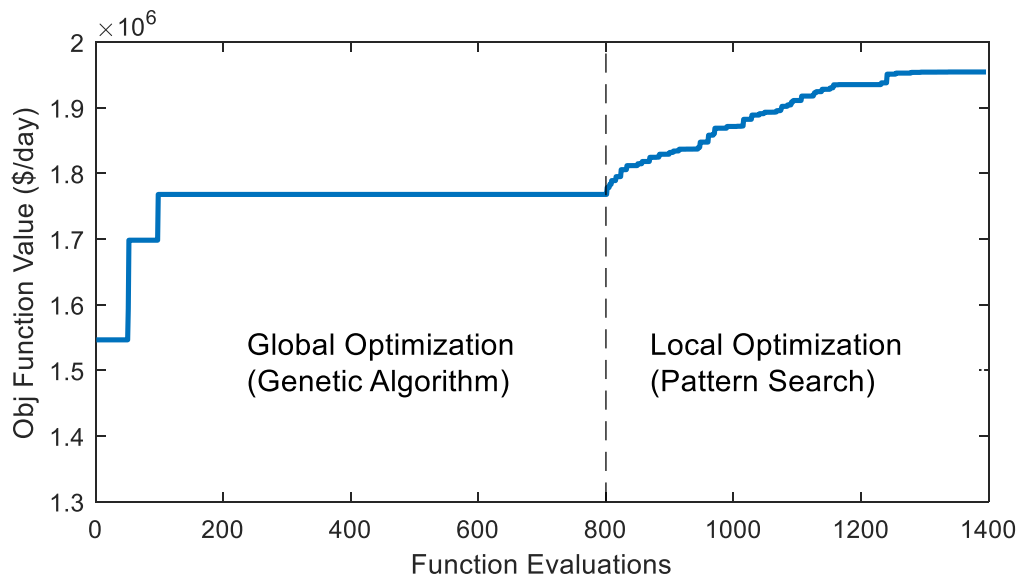


Figure 7.8 Evolution of optimal objective value versus function evaluations

We observe that the optimization process can provide significantly improvement in the operating income by up to 30%, depending on the initially selected vector of well controls. During the GA, and over a significant number of function evaluations (specifically over 600 function evaluations), no improvement is observed. Due to the high number of inequality constraints, the sampling method fails to pinpoint *feasible* solutions which can effectively be used in the mutation and crossover operations. In order to allow for a more efficient sampling, we examine the use of a reduced variable range for each of the system controls (well and network controls).

In order to confine the variable range, we utilize the observation made in Chapter 4, according to which the optimal well control is a function of the surface nodal pressure. More specifically, in Chapter 4 we noticed that as the surface pressure increases, more

back-pressure is applied from the surface facilities and a choke of larger aperture may be used. Consequently, obtaining an upper bound on the well surface nodal pressure can provide a proxy for the allowable value of controls (choke size or gas injection rate or ESP frequency). The upper bounds for surface nodal pressures can be assessed by simulating the field using the maximum value of well controls (i.e. the upper bounds shown in Table 7.5) which relate, for example, to the maximum choke sizes available in the field. This solution is expected to provide the flow potential of the field along with the corresponding upper bounds for the surface nodal pressures. Following this process and using the calculated upper bound values for surface nodal pressures we can perform individual well nodal analysis to identify the maximum value of well controls that satisfies the entire set of wellbore, completion and reservoir constraints, for each well in the field. This process effectively provides reduced upper bounds for each of the well controls and the resulting parameter range can be used to perform global or local optimization. Using the process described above, the upper bounds can be significantly reduced as shown in Table 7.7.

Table 7.7 Reduced upper bounds for well controls

| Element | Control | Control Units | Lower Bound | Upper Bound | Reduced Upper Bound |
|---------|------------------|---------------|-------------|-------------|---------------------|
| W1 | Well on Choke | Choke Size | 8 | 64 | 28 |
| W2 | Well on Gas Lift | Gas Injection | 0 | 40 | 24 |
| W3 | Well on Choke | Choke Size | 8 | 64 | 32 |
| W4 | Well on Gas Lift | Gas Injection | 0 | 64 | 24 |
| W5 | Well on Choke | Choke Size | 8 | 64 | 18 |
| W6 | Well on Choke | Choke Size | 8 | 64 | 31 |
| W7 | Well on Choke | Choke Size | 8 | 64 | 64 |
| W8 | Well on Choke | Choke Size | 8 | 64 | 29 |
| W9 | Well on Gas Lift | Gas Injection | 0 | 40 | 19 |
| W10 | Well on Gas Lift | Gas Injection | 0 | 40 | 18 |
| W11 | Well on Choke | Choke Size | 8 | 64 | 37 |
| W12 | Well on Gas Lift | Gas Injection | 0 | 40 | 19 |

The reduced parameter range was then deployed to perform global and local optimization, using the same optimization workflow (see Table 7.6). The performance of the optimization workflow, using both the full as well as the reduced variable range is shown in Figure 7.9. We observe that using the reduced parameter range, can significantly improve the efficiency of the global search however, the local search is still trapped in local minima within the reduced parameter range. Consequently, in order to accelerate the global optimization, the reduced parameter range may be utilized in lieu of the full parameter range which is defined, for example, by the maximum choke sizes available in the field.

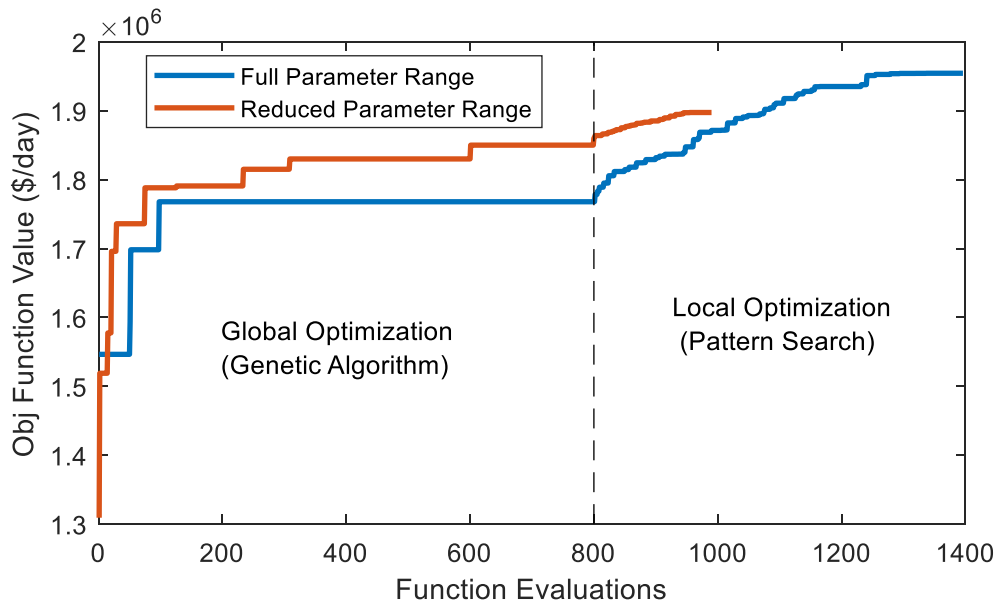


Figure 7.9 Evolution of optimal objective value versus function evaluations using a) full parameter range and b) reduced parameter range

Next, in order to quantify the impact of integrated production modeling, the synthetic field was optimized using static, instead of dynamic gas-lift curves. More specifically, for each well on gas-lift (Wells #2, #4, #9, #10, #12), the corresponding static gas-lift curve was generated assuming a surface nodal pressure of 300psi. The static Gas-Lift Curves for wells W2 and W9 are shown in Figure 7.10a and 7.10b, respectively.

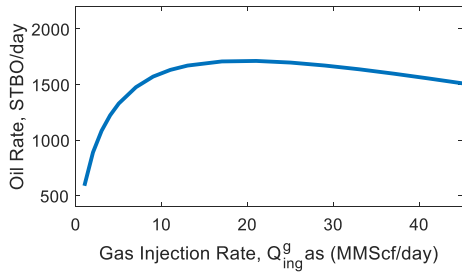


Figure 7.10a Static Gas-Lift Curve for Well W2

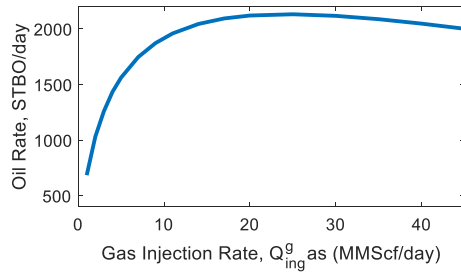


Figure 7.10b Static Gas-Lift Curve for Well W9

The static gas lift curves were then deployed to perform global and local optimization using the same optimization workflow (see Table 7.6). The resulting optimal control values were then used to evaluate the operating income using the high-fidelity forward model (i.e. using the integration scheme presented in Chapter 6 instead of the static gas-lift curves). The comparison of the optimal solutions using a) integrated production modeling (dynamic coupling) and b) static gas-lift curves is shown in Table 7.8.

Table 7.8 Comparison of optimal solutions using a) Static gas-lift curves and b) integrated production modeling

| Method | Objective Function Value in \$M/day |
|---|-------------------------------------|
| Optimization using Static Gas Lift Curves | 1.81 |
| Dynamic coupling | 1.96 |

We observe that the use of static-gas lift curves provides suboptimal solutions since the underlying objective function evaluation is a proxy model which fails to capture the effect of surface pressure on liquids production. More specifically, if the static gas-lift curves are generated using high values of surface nodal pressure then excessive lift-gas will be required in order to boost production from gas-injected wells. The circulation of the excessive gas in the gathering network will have an adverse effect on surface nodal pressures, impairing production from naturally flowing wells. On the contrary, if the assumed nodal pressure for the generation of gas-lift curves is significantly lower, that tends to underestimate liquids production from naturally flowing wells, ultimately yielding suboptimal solutions. This example illustrates the importance of integrated production modeling when it comes to optimizing well and network controls.

7.8 SUMMARY AND CONCLUSIONS

In this chapter, the proposed integration scheme presented in Chapter 6 was coupled with the Dakota open source library to optimize the well and network controls for a synthetic field. The synthetic field was optimized using a hybrid optimization workflow comprising a) global search using Genetic Algorithm and b) Pattern search. Optimization results indicate that operating income can be significantly improved, by up to 30% while at the same time satisfying the entire set of wellbore, completion and reservoir constraints placed on the system. In addition, an approach for improving the performance of global search methods was proposed, namely by defining a reduced variable range for the well control variables. Finally, the use of static gas-lift curves was shown to provide suboptimal

solutions, lower by approximately 7% in terms of daily operating income. The proposed framework can be used to compare and suggest efficient workflows for optimizing well and network controls on a field-wide basis.

7.9 NOMENCLATURE

| | | |
|---------------------|---|--|
| b | = | Index of Orthogonal array sampling |
| C | = | The subset of control variables that correspond to Compressors (operating horsepower) |
| E | = | The subset of control variables that correspond to wells on ESP (ESP frequencies) |
| $f(x)$ | = | Daily Operating Income |
| $\overline{g_j(x)}$ | = | Normalized inequality constraint function |
| $g_i(x)$ | = | Inequality constraint |
| LB_i | = | Lower Bound for control variable x_i |
| m | = | Number of inequality constraints |
| N | = | The subset of control variables that correspond to Naturally Flowing Wells (choke sizes) |
| N_s | = | Number of samples in Orthogonal array sampling |
| p_k | = | search direction at iteration k |
| Q_{field}^{gas} | = | Field gas production (MScf/day) |
| Q_{field}^{oil} | = | Field oil production (STBO/day) |
| Q_{field}^{water} | = | Field oil production (STBW/day) |
| r^{gas} | = | Gas price (\$/MScf) |
| r^{oil} | = | Oil price (\$/STBO) |
| r^{water} | = | Cost of water disposal (\$/STBW) |
| s | = | Number of equally probable bins per parameter |
| t | = | Strength of Orthogonal array sampling |
| UB_i | = | Upper Bound for control variable x_i |
| x | = | The Vector of Control variables |
| Δt | = | Timestep for calculating operating income (24h) |

Chapter 8: Summary, Key Findings and Future Work

This chapter summarizes the analysis presented in this dissertation, provides and the key findings of this work and suggests topics for future research.

8.1 SUMMARY

The research presented in this dissertation provides a systematic method for the design of choke management strategies and flowback operations. The proposed methodology was described in detailed and applied to individual wells (Chapters 2 to 4) as well as for optimizing well and network controls on a field-wide basis (Chapters 5 to 7).

More specifically:

- A. Drawdown strategies were studied with respect to their potential for reducing near-wellbore pressure gradients and fracture pressure gradients in conventional and hydraulically fractured wells, respectively.
- B. A coupled wellbore-reservoir model was developed for translating a set of wellbore, completion and reservoir constraints into a choke management schedule.
- C. A stress-rate dependence relationship was proposed for the design of flow-back operations in hydraulically fractured wells.
- D. A computationally efficient three-phase pipeline network solver was formulated, developed and validated using public network solutions and gas field pressure measurements. The proposed network solver utilizes the fractional flow theory and can model both branched and looped pipeline

networks. The major advantages of the network solver presented in this work are:

- a. There is no requirement for an accurate initial guess.
 - b. There is no need for calculating of partial derivatives on the pressure drop equations as is the case when using the iterative Newton-Raphson method.
- E. An explicit coupling scheme has been proposed for the integration of well models with the surface pipeline network. The numerical scheme deploys fixed point iteration in order to perform multi-point surface nodal analysis. The coupling scheme:
- a. Ensures rate and pressure continuity on the wellheads
 - b. Converges linearly to a solution, typically within 5-6 iterations
 - c. Efficiently captures multi-well pressure interference due to common well tie backs both for naturally flowing wells and wells on artificial lift
- F. The integration scheme has been combined with an optimization framework to optimize well and network controls using gradient based and derivative-free methods. The framework was deployed for optimizing well controls in a synthetic field comprising naturally flowing and gas-injected wells.

8.2 KEY FINDINGS

The key findings of this work can be summarized as follows:

1. In order to mitigate sand mobilization and hence sand production in conventional open-hole completions, no more than 70% overall drawdown should be applied in less than 20% of the ramp-up duration.
2. In conventional formations characterized by high diffusivity (i.e. high permeability gas formations) the Bottom-Hole-Pressure should be reduced linearly with time. This is attributed to the fact that in such formations, typical ramp-up durations are significantly longer than reservoir transients.
3. The proposed coupled wellbore-reservoir model can be used to order to translate a set of wellbore, completion and reservoir constraints into a sequence of choke sizes as a function of time. This approach establishes a systematic method for the design of choke management strategies and can be used both in conventional and unconventional wells.
4. The optimum choke management strategy depends on various parameters including the separator pressure, the tubing diameter, the water saturation in the SRV etc. Consequently, empirical guidelines on rate constraints or choke recommendations should not be applied universally as they will only guarantee a successful production ramp-up for a given set of well specifications.
5. The proposed rate-stress envelope can be used for the design of flowback operations in unconventional wells. This constraint effectively couples the

maximum allowable rate with the in-situ closure stress, allowing engineers to design ramp-up procedures that curtail excessive proppant flowback and mitigate the risk of fracture closure near the wellbore.

6. The application of the model for the design of flowback operations using the proposed rate-stress dependence constraint suggests drawdown rates in agreement with successful field practices reported in the literature (in the range of 5-10 psi/hour)
7. Optimization of well and network controls using integrated production modeling can significantly improve daily operating income. In addition, dynamic coupling of well models with the surface network can further improve operating income by up to 8% compared to the use of static gas-lift curves
8. When optimizing well controls on a field-wide basis, the performance of global optimization methods can be accelerated by using a reduced parameter range. This approach makes sampling more efficient in terms of identifying feasible solutions. The reduced parameter range for each of the control variables can be obtained by performing individual well nodal analysis using upper bound values on surface nodal pressures.

8.3 FUTURE WORK

There are still many challenges associated with integrated production modeling and optimization of field and network controls. The work presented in this study can be extended in order to study the following interesting topics:

1. Assess the effect of wellbore transients on the optimal design of ramp-up or flowback operations. Emphasis can be placed on transient liquid loading and unloading of gas condensate wells.
2. Using a transient wellbore model, deploy the proposed choke selection algorithm for the design of shut-in operations. For example, the concept of choke management could also be applied for addressing the effect of pressure fluctuations on the stability of the proppant pack in unconventional wells during a shut-in process.
3. Assess the impact of uncertainty on optimal choke control. For instance, evaluate the effect of geologic uncertainty on flow-back operations.
4. Establish stress dependent rate constraints for open-hole and cased-hole completions. These rate-stress dependence relationships can be derived using a coupled fluid flow-geomechanics simulator and then be used as additional constraints in the choke selection algorithm presented herein.
5. Extensively benchmark the performance of various optimization workflows. In the current work, the physics-based model has been coupled with DAKOTA, an optimization framework which encompasses various sampling, global and local search methods. This framework could be used

in order to propose efficient workflows for optimizing well and network controls.

Appendices

APPENDIX A1 - SOLUTION OF RADIAL-DIFFUSION EQUATION

Equation A-1 constitutes the dimensionless form of the transient radial-diffusion equation:

$$\frac{\partial^2 P_D}{\partial r_D^2} + \frac{1}{r_D} \frac{\partial P_D}{\partial r_D} = \frac{\partial P_D}{\partial t_D} \quad (\text{A.1})$$

For the case of a well producing from the center of a circular reservoir under constant BHP (P_{wf}), the dimensionless variables are defined as:

$$r_D = \frac{r}{r_w} \quad (\text{A.2})$$

$$t_D = \frac{kt}{\phi\mu cr_w^2} \quad (\text{A.3})$$

$$P_D(r_D, t_D) = \frac{P_i - P(r, t)}{P_i - P_{wf}} \quad (\text{A.4})$$

$$q_D = \frac{q\mu}{2\pi kh(P_i - P_{wf})} \quad (\text{A.5})$$

$$r_{eD} = \frac{r_e}{r_w} \quad (\text{A.6})$$

Where

| | |
|--|--|
| <p>r the radius</p> <p>r_w the wellbore radius</p> <p>k Formation permeability</p> <p>t time</p> <p>ϕ porosity</p> <p>s skin factor</p> | <p>μ Fluid viscosity</p> <p>c Total compressibility</p> <p>P_i Initial Reservoir Pressure</p> <p>P_{wf} Bottom-Hole-Pressure</p> <p>h Formation thickness</p> |
|--|--|

For infinite outer boundary the dimensionless pressure solution P_D and dimensionless production rate, q_D , can be obtained by numerically calculating the following inverse Laplace transformations:

$$P_D(r_D, t_D) = L^{-1}(K_0(r_D \sqrt{l}) / \{l[K_0(\sqrt{l}) + s\sqrt{l}K_1(\sqrt{l})]\}) \quad (\text{A.7})$$

$$q_D(r_D, t_D) = L^{-1}(K_1(\sqrt{l}) / \{\sqrt{l}[K_0(\sqrt{l}) + s\sqrt{l}K_1(\sqrt{l})]\}) \quad (\text{A.8})$$

In equations. A.6 and A.7, l represents the Laplace variable and K_0 and K_1 are the modified Bessel functions of the second kind of order zero and one, respectively.

For closed (no-flow) outer boundary, the dimensionless pressure solution P_D and dimensionless production rate, q_D , can be obtained by numerically calculating the following inverse Laplace transformations:

$$P_D(r_D, t_D) = L^{-1}([K_1(r_{eD} \sqrt{l})I_0(r_{eD} \sqrt{l}) + K_0(r_{eD} \sqrt{l})I_1(r_{eD} \sqrt{l})] / D_1) \quad (\text{A.9})$$

$$q_D(r_D, t_D) = L^{-1}([K_1(\sqrt{l})I_1(r_{eD} \sqrt{l}) - K_1(r_{eD} \sqrt{l})I_1(\sqrt{l})] / D_1) \quad (\text{A.10})$$

Where

$$D_1 = \sqrt{l}\{A+B\} \quad (\text{A.11})$$

$$A = [K_1(r_{eD} \sqrt{l})I_0(\sqrt{l}) + K_0(\sqrt{l})I_1(r_{eD} \sqrt{l})] \quad (\text{A.12})$$

$$B = -s\sqrt{l}[K_1(r_{eD} \sqrt{l})I_1(\sqrt{l}) - K_1(\sqrt{l})I_1(r_{eD} \sqrt{l})] \quad (\text{A.13})$$

In equations A.9 - A.13, l represents the Laplace variable and I_0 and I_1 are the modified Bessel functions of first kind of order zero and one, respectively. K_0 and K_1 are the modified Bessel functions of the second kind of order zero and one, respectively.

A thorough overview on the solution of the transient radial-diffusion equation is provided by Ehlig-Economides (1979).

APPENDIX A2 - TRANSIENT MODEL FOR HYDRAULICALLY FRACTURED WELLS

The transient reservoir model presented herein is a simplification of the model proposed by Cinco-Ley (1989). For the case of a vertical well intersected by a finite conductivity fracture, the end of formation linear flow can be approximated by:

$$t_{elf} = 1200 \frac{\phi \mu c_t}{k} x_f^2 \quad (\text{A.14})$$

where

- ϕ Matrix Porosity
- k Matrix permeability (md)
- x_f Fracture Half-length (ft)
- c_t Total compressibility (1/psi)
- μ Effective viscosity (cp)

For $t < t_{elf}$, transient flow occurs. The total liquid rate at transient conditions is obtained using the equation A.15:

$$Q_L(STBD) = \frac{N_f \cdot k(md) \cdot h(ft) \cdot (P_r - P_{wf})(psi)}{141.2 \cdot \mu(cp) \cdot \left(\frac{1}{q_D} \right)} \quad (A.15)$$

where

- k Matrix permeability (md)
- N_f Number of fractures
- P_r Reservoir pressure (psi)
- h Formation height (ft)
- μ Effective viscosity (cp)
- $1/q_D$ Reciprocal dimensionless rate

Where q_D is the dimensionless flowrate for wells operating under constant BHP. q_D is a function of the dimensionless fracture conductivity, F_{cd} and dimensionless time, t_d . The value of q_D is obtained from fracture type curves (Pratinko et al. 2003). The dimensionless time is calculated as:

$$t_d = \frac{t}{t_{elf}}$$

During the transient period, the produced liquid is proportional to the drawdown. Additionally, during the transient period the average reservoir pressure, P_r , is constant.

At the end of the transient period, we evaluate the productivity index J_{TPSS} using, the derivative of equation (A.15) for q_D evaluated at $t=t_{elf}$. This productivity index is used to

fit Vogel's equation for the pseudo-steady flow. During the pseudo-steady flow, the change in the flowrate is attributed to reservoir depletion which is taken into account by solving the material balance equation using a selected timestep Δt .

Figure A-1 illustrates the transient IPRs at various times. The productivity index is decreasing with time. Observe that the productivity at steady state (Vogel's equation for BHP above the Bubble point pressure) is equal to the productivity at the end of the transient period.

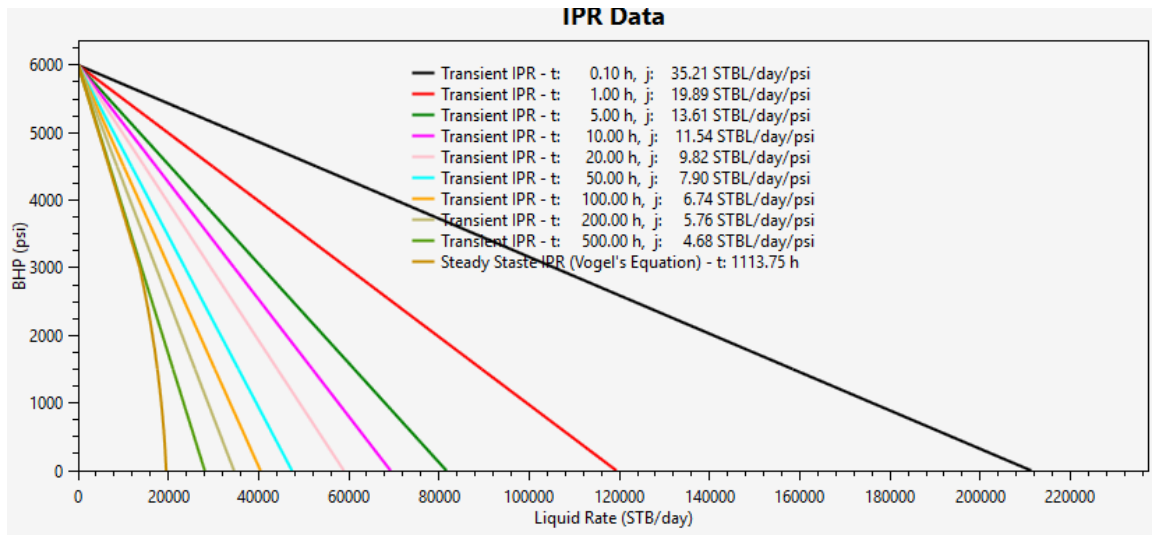


Figure A-1 Transient and Steady-State Inflow Performance Relationship

APPENDIX B – CHOKE MODELS

In this appendix we present the models for calculating the pressure drop through an orifice.

Single Phase Incompressible Liquid

Using the Bernoulli equation and a discharge coefficient (C) for quantifying the frictional pressure losses through the orifice, the relation between liquid rate and pressure drop is obtained from Miller (1983):

$$q = 8081.7C \frac{d_2^2}{\sqrt{1-\beta^4}} \sqrt{\frac{\Delta P}{\rho}} \quad (\text{B.1})$$

Where

q = liquid flowrate (bbl/day)

C = discharge coefficient

d_1 = upstream pipe internal diameter (inch)

d_2 = choke internal diameter (inch)

$$\beta = \frac{d_2}{d_1}$$

ΔP = pressure drop (psi)

ρ = liquid density (lbm/ft³)

The discharge coefficient can be calculated using equation (B.2)

$$C = 0.9975 - 6.53 \sqrt{\frac{\beta}{R_e}} \quad (\text{B.2})$$

Where

d_1 = upstream pipe internal diameter (inch)

d_2 = choke internal diameter (inch)

$$\beta = \frac{d_2}{d_1}$$

R_e = Reynolds number for fluid flow in the choke orifice

The Reynolds number, R_e , is evaluated using equation B.3

$$R_e = 1.478 \frac{q\rho}{d_2\mu} \quad (\text{B.3})$$

Where

q = liquid flowrate (bbl/day)

ρ = liquid density (lbm/ft³)

d_2 = choke internal diameter (inch)

μ = liquid viscosity (cp)

Single Phase Gas Flow

For single-phase gas flow (i.e. dry gas wells) the pressure drop (p_2-p_1) is evaluated using the Szilas (1960) equation:

$$q = 3.505aD_{64}^2 \frac{p_1}{p_2} \sqrt{\frac{\gamma}{\gamma_g T_1 (\gamma - 1)} \left[\left(\frac{p_2}{p_1} \right)^{\frac{2}{\gamma}} - \left(\frac{p_2}{p_1} \right)^{\frac{\gamma+1}{\gamma}} \right]} \quad (\text{B.4})$$

Where

q = the gas flowrate (MScfD)

a = discharge coefficient

D_{64} = choke internal diameter (64th inch)

μ = liquid viscosity (cp)

p_1 = pressure upstream of the choke (psi)

p_2 = pressure downstream of the choke (psi)

T_1 = temperature upstream of the choke (R)

γ = gas specific heat ratio

Equation (B.4) is valid for subcritical flow conditions. For supercritical flow, the pressure ratio equals the critical pressure ratio:

$$\left(\frac{p_2}{p_1}\right)_{crit} = \left(\frac{2}{\gamma + 1}\right)^{\frac{\gamma}{\gamma - 1}} \quad (\text{B.5})$$

Two Phase Flow

For two phase flow through a choke, we use the choke model suggested by Ros (1960):

$$q = \frac{p_1 D_{64}^2}{17.4 \sqrt{GLR}} \quad (\text{B.6})$$

Where

q = the liquid rate (bbl/day)

D_{64} = choke internal diameter (64th inch)

p_1 = pressure upstream of the choke (psi)

GLR = the gas-liquid ratio (Scf/bbl)

Two phase flow through an orifice can also be modeled using the equation by Bairamzadeh (2015):

$$q = \frac{p_1 D_{64}^{1.1731}}{7.8337 GLR^{0.3636}} \quad (\text{B.7})$$

Where

q = the liquid rate (bbl/day)

D_{64} = choke internal diameter (64th inch)

p_1 = pressure upstream of the choke (psi)

GLR = the gas-liquid ratio (Scf/bbl)

APPENDIX C – FLUID PROPERTIES

In this appendix we present the correlations used to calculate the oil and gas fluid properties as a function of pressure, P and temperature T. The correlations presented herein require the fluid properties shown in Table C.1

Table C.1 Input parameter for Black-Oil PVT Correlations

| <i>Required Black-Oil Properties</i> | <i>Symbol</i> |
|---|----------------|
| <i>Oil density (API degrees)</i> | γ_{API} |
| <i>Gas Specific Gravity ($\gamma_{air}=1$)</i> | γ_g |
| <i>Bubble point pressure (psi)</i> | P_{bubble} |

Gas Properties

At a given pressure P, and temperature, T, the following gas properties need to be calculated:

- The gas deviation (or compressibility) factor, z
- The gas density, ρ_g in lbm/ft³
- The gas formation volume factor, B_g in cf/Scf
- The viscosity of the gas, μ_g in centipoise (cp)

Calculation of the Gas Deviation Factor, z

To calculate the gas deviation factor, we first calculate the pseudo-critical pressure, P_{pc} and pseudo-critical temperature, T_{pc} using the Standing (1977) correlations:

$$T_{pc} (\text{Rankine}) = 168 + 325\gamma_g - 12.5\gamma_g^2 \quad (\text{C.1})$$

$$p_{pc} (\text{psia}) = 677 + 15.0\gamma_g - 37.5\gamma_g^2 \quad (\text{C.2})$$

The gas compressibility factor, z is then calculated using the Hall-Yarborough Method (1973):

$$z = \left[\frac{0.06125 p_{pr} t}{Y} \right] \exp[-1.2(1-t)^2] \quad (\text{C.3})$$

Where

- p_{pr} The pseudo-reduced pressure (i.e. P/p_{pc})
- t The reciprocal of the pseudo-reduced temperature (i.e. T_{pc}/T)
- Y The solution of equation C.4

The value of Y is obtained from equation:

$$F(Y) = x_1 + \frac{Y + Y^2 + Y^3 + Y^4}{(1-Y)^3} - x_2 Y^2 + x_3 Y^{x_4} = 0 \quad (\text{C.4})$$

Where

- x_1 $-0.06125 p_{pr} t \exp[-1.2(1-t)^2]$
- x_2 $14.76t - 9.76t^2 + 4.58t^3$
- x_3 $90.7t - 242t^2 + 42.4t^3$
- x_4 $2.18 + 2.82t$
- p_{pr} The pseudo-reduced pressure (i.e. P/p_{pc})
- t The reciprocal of the pseudo-reduced temperature (i.e. T_{pc}/T)

Equation (C.4) can be solved using iterative Newton-Raphson. A good initial guess for Y can be acquired from equation (C.5)

$$Y^0 = 0.0125 p_{pr} t \exp[-1.2(1-t)^2] \quad (C.5)$$

Calculation of Gas Density

The gas density, ρ_g , in lbm/ft³ is obtained from the following equation (Ahmed, 2006):

$$\rho_g = \frac{2.7 \gamma_g P}{(T + 460) z} \quad (C.6)$$

where

- γ_g The gas specific gravity
- P The pressure in psia
- T The temperature in Fahrenheit degrees
- z The gas compressibility factor

Calculation of the Gas-Formation-Volume factor

The gas formation volume factor, B_g in bbl/Scf is calculated the following equation (Ahmed, 2006):

$$B_g = 0.005035 \frac{z(T + 459.67)}{P} \quad (C.7)$$

where

- z The gas compressibility factor
- T The temperature in Fahrenheit degrees
- P The pressure in psia
- $X = 3.5 + 986/T + 0.01M$

$$Y = 2.4 - 0.2X$$

T The temperature in Rankine degrees

M The molecular weight of the gas (i.e. $29.4\gamma_g$)

ρ_g The gas density in lbm/cf³

Gas Viscosity

The gas viscosity is calculated using the correlation proposed by Lee-Gonzalez-Eaking (1966):

$$\mu_g = 10^{-4} K \exp \left[X \left(\frac{\rho_g}{62.4} \right)^Y \right] \quad (C.8)$$

where

$$K = \frac{(9.4 + 0.02M_a)T^{1.5}}{209 + 19M_a + T}$$

$$X = 3.5 + \frac{986}{T} + 0.01M_a$$

$$Y = 2.4 - 0.2X$$

ρ_g Gas density at reservoir pressure and temperature (lbm/ft³)

T Temperature in Rankine degrees

M_a Molecular weight of gas (i.e. $M_a=29.8\gamma_g$)

Oil Properties

In the following paragraphs, we present the correlations for evaluating the PVT properties of the oil phase. The properties of interest are:

- The Solution Gas-Oil Ratio, R_s in Scf/STBO
- The Oil-Formation-Volume Factor, B_o in bbl/STBO

- The compressibility of the oil, c_o in psi^{-1}
- The oil density, ρ_o in lbm/cf
- The viscosity of the oil, μ_o in centipoise (cp)

In the following paragraphs we present the correlations applicable for saturated and undersaturated conditions.

Calculation of the Solution Gas-Oil Ratio

The solution Gas-Oil Ratio, R_s in Scf/STB is calculated using the correlations by Vasquez and Beggs (1980). For undersaturated conditions (i.e. $P \geq P_{\text{bubble}}$), the R_s (Scf/STB) is independent of pressure and equal to:

$$R_s = C_1 \gamma_g (p_{\text{bubble}})^{C_2} \exp \left[C_3 \frac{\gamma_{API}}{T + 459.67} \right] \quad (\text{C.9})$$

For saturated conditions ($P \leq P_{\text{bubble}}$), the Solution Gas, R_s (Scf/STBO) is a function of pressure and equal to:

$$R_s = C_1 \gamma_g (p)^{C_2} \exp \left[C_3 \frac{\gamma_{API}}{T + 459.67} \right] \quad (\text{C.10})$$

where

| | |
|---------------------|---------------------------------------|
| C_1, C_2 | see Table C.2 |
| γ_g | The gas specific gravity |
| p_{bubble} | The bubble point pressure in psia |
| P | The pressure in psia |
| T | The temperature in Fahrenheit degrees |
| γ_{API} | The oil density in API units |

Table C.2 Coefficients for the calculation of solution gas (Vasquez and Beggs, 1980)

| Coefficient | $\gamma_{API} \leq 30^\circ API$ | $\gamma_{API} \leq 30^\circ API$ |
|----------------|----------------------------------|----------------------------------|
| C ₁ | 4.677E-4 | 4.67W-4 |
| C ₂ | 1.751E-5 | 1.100E-5 |
| C ₃ | -1.811E-8 | 1.377E-9 |
| A1 | 0.0362 | 0.0178 |
| A2 | 1.0937 | 1.1870 |
| A3 | 25.7240 | 23.9310 |

Calculation of the Oil compressibility, c_o

The oil compressibility is calculated using the correlations proposed by Vasquez and Beggs (1980). More specifically, for saturated conditions ($P \leq P_{bubble}$) the oil compressibility, c_o (bbl/STBO) is calculated using equation (C.11).

$$c_o = \frac{-1433 + 5R_{sb} + 17.2T - 1180\gamma_g + 12.62\gamma_{API}}{10^5 P} + \frac{\frac{B_g}{B_o} \frac{dR_s}{dP}}{5.6145835} \quad (C.11)$$

For undersaturated conditions (i.e. $P \geq P_{bubble}$) the oil compressibility, c_o (bbl/STBO) is calculated from the following equation.

$$c_o = \frac{-1433 + 5R_{sb} + 17.2T - 1180\gamma_g + 12.62\gamma_{API}}{10^5 P} \quad (C.12)$$

where

R_{sb} The solution gas-oil ratio at the bubble point pressure

| | |
|----------------|---------------------------------------|
| T | The temperature in Fahrenheit degrees |
| γ_g | The gas specific gravity |
| γ_{API} | The oil API density |
| P | The pressure in psia |

Calculation of the Oil formation Volume Factor

The Oil Formation Volume Factor, B_o , is calculated using the Vesquez and Beggs (1980) correlations. More specifically, for saturated conditions ($P \leq P_{bubble}$) the Oil-Formation-Volume factor, B_o (bbl/STBO) is calculated using the following equation:

$$B_o = 1 + A_1 R_s + A_2 (T - 60) \left(\frac{\gamma_{API}}{\gamma_g} \right) + A_3 R_s (T - 60) \left(\frac{\gamma_{API}}{\gamma_g} \right) \quad (C.13)$$

For undersaturated conditions (i.e. $P \geq P_{bubble}$) the Oil-Formation-Volume factor, B_o (bbl/STBO) is calculated using equation (C.14)

$$B_o = B_{ob} \exp \left[c_o (p_{bubble} - p) \right] \quad (C.14)$$

Where

| | |
|-----------------|---|
| A_1, A_2, A_3 | see Table C.2 |
| R_s | The solution gas oil ratio at P (Scf/STBO) |
| T | The temperature in Fahrenheit degrees |
| γ_g | The gas specific gravity |
| γ_{API} | The oil API density |
| B_{ob} | The oil formation volume factor at the Bubble-Point Pressure (bbl/STBO) |

Calculation of the Oil Density

For saturated conditions ($P \leq P_{bubble}$) the Oil density, ρ_o (lbm/ft³) is calculated from the following equation (Ahmed, 2006):

$$\rho_o = \frac{62.4\gamma_o + 0.0136R_s\gamma_g}{B_o} \quad (C.15)$$

Using the definition of oil compressibility, for undersaturated conditions (i.e. $P \geq P_{bubble}$) the Oil density, ρ_o (lbm/ft³) is calculated from equation C.16 (Ahmed, 2006):

$$\rho_o = \rho_{ob} \exp\left[c_o (P - P_{bubble})\right] \quad (C.16)$$

Where

- γ_o The oil specific gravity at stock-tank conditions (water=1)
- R_s The solution gas oil ratio at P Scf/STBO
- γ_g The gas specific gravity
- B_o The oil formation volume factor bbl/STBO
- ρ_{ob} The oil density at the bubble-point pressure in psia
- c_o The compressibility of the oil at the bubble-point-pressure in psi⁻¹
- P The pressure in psia
- P_{bubble} The bubble-point pressure in psia

Calculation of Oil Viscosity

The oil viscosity, μ_o , is calculated using the correlations by Beggs and Robinson (1975). The first step in the calculation of the oil viscosity is the evaluation of the dead oil viscosity, μ_{od} , in centipoise (cp):

$$\mu_{od} = 10^X - 1 \quad (\text{C.17})$$

where

$$X = Y(T - 460)^{1.163}$$

$$Y = 10^Z$$

$$Z = 3.0324 - 0.02023\gamma_{API}$$

For saturated oil conditions (i.e. $P \leq P_{bubble}$) the Oil viscosity, μ_o (cp) is calculated from Beggs and Robinson (1975):

$$\mu_o = a(\mu_{od})^b \quad (\text{C.18})$$

where

$$a = 10.715(R_s + 100)^{-0.515}$$

$$b = 5.44(R_s + 150)^{-0.338}$$

R_s The solution gas-oil Ratio is Scf/STBO

For undersaturated oil conditions (i.e. $P \geq P_{bubble}$) the Oil viscosity, μ_o (cp) is calculated using the correlation proposed by Vasquez and Beggs (1980)

$$\mu_o = \mu_{ob} \left(\frac{P}{P_{bubble}} \right)^m \quad (\text{C.19})$$

where

μ_{ob} The oil viscosity at the bubble point pressure evaluated using equation (C.18)

P The pressure in psia

P_{bubble} The bubble-point pressure in psia

$$m = 2.6P^{1.187}10^a$$

$$a = \frac{3.9}{10^5}P - 5$$

APPENDIX D – MATERIAL BALANCE EQUATION

In this appendix we present the material balance calculation for evaluating the new reservoir pressure, p , given the current reservoir pressure, p_i , and the volume of liquids removed from the reservoir.

In the description that follows we adopt the notations found in the textbook “Reservoir Engineer Handbook” by Ahmed (2006). We define the residual of the material balance equation at pressure p , $R_{MB}(p)$, as:

$$R_{MB}(p) = A(p) - B(p) = 0 \quad (D.1)$$

$$A(p) = N_p B_o + (G_p - N_p R_s) B_g - (W_e - W_p B_w) \quad (D.2)$$

$$B(p) = N \left\{ (B_o - B_{oi}) + (R_{si} - R_s) B_g + m B_{oi} \left[\frac{B_g(p)}{B_{gi}} - 1 \right] + B_{oi} (1+m) \left[\frac{S_{wi} c_w + c_t}{1 - S_{wi}} \right] (p - p_i) \right\} \quad (D.3)$$

Where:

$R(p)$ = the residual of the material balance equation

p = new reservoir pressure

p_i = initial reservoir pressure

N_p = cumulative oil produced (STB)

G_p = cumulative gas produced (scf)

W_p = cumulative water produced (STBW)

$B_o = B_o(p)$ = oil formation volume factor (bbl/STBO) at pressure p

$B_{oi} = B_o(p_i)$ = initial oil formation volume factor (bbl/STBO) at pressure p_i

R_{si} = Initial solution gas (i.e. solution gas at pressure p_i)

R_s = solution gas at pressure p

$B_{g(p)}$ = the gas formation volume factor at pressure p (bbl/scf)

W_e = cumulative water influx (bbl)

m = Ratio of initial gas-cap volume to initial reservoir oil volume

B_w = water formation volume factor (bbl/STBW)

c_w = water compressibility (psi^{-1})

c_f = rock compressibility (psi^{-1})

B_w = water formation volume factor (bbl/STBW)

S_{wi} = initial water saturation

To new reservoir pressure, p, is the pressure for which the residual of the material balance equation equals zero:

$$R_{MB}(p) = 0 \quad (\text{D.4})$$

Equation C.4 is solved using the secant method. The new guess for the reservoir pressure at iteration k, p^k , is obtained using equation (D.5):

$$p^k = p^{k-1} - R(p^{k-1}) \frac{p^{k-1} - p^{k-2}}{R(p^{k-1}) - R(p^{k-2})}, k \geq 2 \quad (\text{D.5})$$

The secant method is instantiated by selecting p^0 and p^1 in the vicinity of the initial reservoir pressure, p_i , with $p^0 \neq p^1$. The secant method terminates when

$$|p^{k+1} - p^k| \leq \varepsilon = 0.1 \text{psi} \quad (\text{D.6})$$

References

- Adams, B., Ebeida, M., Eldred, M., & Geraci, G. (2018). *Dakota, A Multilevel Parallel Object-Oriented Framework for Design Optimization, Parameter Estimation, Uncertainty Quantification and Sensitivity Analysis: Version 6.9 User's Manual*. Sandia National Laboratories.
- Ahmed, T. (2006). *Reservoir Engineering Handbook*. Burlington, MA: Elsevier Inc.
- Andrews, J., & Kjoholt, H. (1998). Rock Mechanical Principles help to predict proppant flowback from hydraulic fractures. Paper SPE 47382 presented at the SPE/ISRM Eurock, Trondheim, Norway, 8-10 July.
- Andrews, J., Kittlisen, P., Lahnne, T., & Antonsen, J. (2017). Optimizing Bean-up Procedure after Well Shut-in. Simple Rock Mechanical Aspects and Operation Guidelines. Paper SPE 185906 presented at the SPE Bergen One Day Seminar, Bergen, Norway, 5 April.
- Asgian, M. (1994). The Mechanical Stability of Propped Hydraulic Fractures: A Numerical Study. Paper SPE 28510 Presented at the SPE Annual Technical Conference and Exhibition, Dallas, 25-28 September.
- Audet, C., & Dennis, J. (2006). Mesh Adaptive Direct Search Algorithms for Constrained Optimization. *Society of Industrial and Applied Mathematics*, 17(1), 188-217.
- Azzopadi, B. (1999). Phase Separation at T junctions. *Multiphase Science and Technology*, 11(7), 229-329.
- Bairamzadeh, S., & Ghanaatpisheh, E. (2015). A New Choke Correlation to Predict Liquid Flow Rate. *Science International*, 27(1), 271-274.
- Barree, R., & Makherjee, H. (1995). Engineering Criteria for Fracture Flowback Procedures. Paper SPE 29600 presented at the SPE Rocky Mountain Regional/Low-Permeability Reservoirs Symposium, Denver, CO, 20-22 March.
- Beggs, H., & Robinson, J. (1975, September). Estimating the Viscosity of Crude Oil Systems. *JPT*, 27(09), 1140-1141.

- Bennett, C., Reynolds, A., Raghavan, R., & Elbel, J. (1986, August). Performance of Finite-Conductivity, Vertically Fractured Wells in Single Layer Reservoirs. *SPE Formation Evaluation*, 1(04), 399-412.
- Blyton, C., Gala, D., & Sharma, M. (2015). A Comprehensive Study of Proppant Transport in a Hydraulic Fracture. Paper SPE 174973 presented at the Annual Technical Conference and Exhibition, Houston, TX, 28-30 September.
- Borden, Z., El-Bakry, A., & Xu, P. (2016). Workflow Automation for Gas Lift Surveillance and Optimization, Guld of Mexico. Paper SPE 188506 presented at the SPE Intelligent Energy International Conference and Exhibition, Aberdeen, United Kingdom, 6-8 September.
- Cao, H., Samier, P., & Kalunga, H. (2015). A Fully Coupled Network Model, Practical Issues and Comprehensive Comparison with Other Integrated Models on Field Cases. Paper SPE 173251 presented at the SPE Reservoir Simulation Symposium, Houston, TX, 23-25 February.
- Chapra, S. (2010). *Numerical Methods for Engineers*. Jefferson City, MO.
- Chia, Y., & Hussain, S. (1999). Gas Lift Optimization Efforts and Challenges. Paper SPE 57513 presented at the SPE Asia Improved Oil Recovery Conference, Kuala Lumpur, Malaysia, 21-24 October.
- Cinco-Ley, H., & Samaniego, F. (1981). Transient Pressure Analysis for Fractured Wells. *Journal of Petroleum Technology*, 1749-1766.
- Crafton, J. (2008). Modeling Flowback Behavior of Flowback Equals "Slowback". Paper SPE 119894 presented at the SPE Shale Gas Production Conference, Fort Worth, TX, 16-18 November.
- Crafton, J., & Gunderson, D. (2007). Stimulation Flowback Management: Keeping a Good Completion Good. Paper SPE 110851 presented at the SPE Annual Technical Conference and Exhibition, Anaheim, CA, 11-14 November.
- Davidson, J., & Beckner, B. (2003). Integrated Optimization for Rate Allocation in Reservoir Simulation. Paper SPE 79701 presented at the Reservoir Simulation Symposium, Houston, TX, 3-5 February.

- Dempsey, J., & Patterson, J. (1971, September). An efficient Model for Evaluating Gas Field Gathering System Design. *Journal of Petroleum Technology*, 23(09), 1067-1077.
- Dolan, A., & Aldous, J. (1993). *Networks and Algorithms: an introductory approach*. West Sussex: John Wiley and Sons.
- Dutta-Roy, K., & Kattapuram, J. (1997). A New Approach to Gas-Lift Allocation Optimization. Paper SPE 38333 presented at the SPE Western Regional Meeting, LongBeach, CA, 25-27 June.
- Earlougher, R. (1977). *Advances in Well Test Analysis*. SPE Publications.
- Economides, C. (1979). Well Test Analysis for Wells Produced at a Constant Pressure. *PhD Thesis*, Stanford University.
- Economides, C., Tomic, & Economides, M. (2008). Foolproof Completions for High-Rate Production Wells. Paper SPE 111455 presented at the SPE International Symposium and Exhibition of Formation Damage Control, Lafayette, LA, February 13-15.
- Ely, J., Arnold, W., & Holditch, S. (1990). New Techniques and Quality Control Find Success in Enhancing Productivity and Minimizing Proppant Flowback. Paper SPE 20708 presented at the SPE Annual Technical Conference and Exhibition, New Orleans, LA, 23-26 September.
- Fang, Y., & Lo, K. (1996, May). A Generalized Well Management Scheme for Reservoir Simulation. *SPE Reservoir Engineering*, 11(02), 116-120.
- Gadde, P., & Sharma, M. (2005). The Impact of Proppant Retardation on Propped Fracture Lengths. Paper SPE 97106 presented at the SPE Annual Technical Conference and Exhibition, Dallas, TX, 9-12 October.
- Geilikman, M., Dria, D., Stewart, D., & Wong, G. (2005). Bean-up Guidelines for Sand Control Completions. Paper SPE 95870 presented at the SPE Annual Technical Conference and Exhibition, Dallas, TX, 9-12 October .

- Giunta, A., Wojtkiewicz, S., & Eldred, M. (2003). Overview of Modern Design of Experiments Methods for Computational Simulations. *American Institute of Aeronautics and Astronautics*, 21(06), 117-124.
- Guyaguler, B., & Byer, T. (2007). A New Production Allocation Optimization Framework. Paper SPE 105200 presented at the SPE Reservoir Simulation Symposium, Houston, YX, 26-28 February.
- Hall, K., & Yarborough, L. (1973). A New Equation-of-State for Z-factor Calculations. *Oil and Gas Journal*, June 18, 82-92.
- Handley-Schachler, S., McKie, C., & Quintero, N. (2000). New Mathematical Techniques for the Optimization of Oil and Gas Production Systems. Paper SPE 65161 presented at the SPE European Petroleum Conference, Paris, France, 24-25 October.
- Heguler, G., Barua, S., & Bard, W. (1997). Integration of a Field Surface and Production Network with a Reservoir Simulator. *SPE Computer Applications*, 9(03), 247-256.
- Isaa, E., & Oliveira, P. (1994). Numerical Prediction of Phase Separation in Two-Phase Flow Through T-Junctions. *Computer Fluids*, 23(02), 347-372.
- Isebor, O., Ciaurri, D., & Durlofsky, L. (2013). Generalized Field Development Optimization Using Derivative-Free Procedures. Paper SPE 169631 presented at the SPE Reservoir Symposium, Woodlands, TX, 18-20 February.
- Jeppson, R. (1977). *Analysis of Flow in Pipe Networks*. Ann Arbor: Ann Arbor Science.
- Junyang, Z., & Adewumi, M. (1998). Gas Pipeline Network Analysis Using an Analytical Steady-State Flow Equation. Paper SPE 51044 presented at the SPE Eastern Regional Meeting, Pittsburgh, PA, 9-11 November.
- Kanu, P., Mach, J., & Brown, E. (1891). Economic Approach to Oil Production and Gas Allocation in Continuous Gas Lift. *Journal of Petroleum Technology*, 33(10), 1887-1891.
- Karantinos. (2015). *A General Method for the Selection of the Optimum Choke Management Strategy*. Masters Report, The University of Texas at Austin.

- Karantinos, E., & Sharma, M. (2017). Choke Management under Wellbore, Completion and Reservoir Constraints. Paper SPE 187190 presented at the SPE Annual Technical Conference and Exhibition, San Antonio, TX, 9-11 October .
- Karantinos, E., Sharma, M., Ayoub, J., Parlar, M., & Chanpura, R. (2015). A General Method for the Selection of an Optimum Choke Management Strategy, Paper SPE 178973 presented at the SPE European Formation Damage Conference and Exhibition, Budapest, Hungary, 3-5 June.
- Karantinos, E., Sharma, M., Ayoub, J., Parlar, M., & Chanpura, R. (2016). Choke Management Strategies for Hydraulically Fractured Wells and Frac-Pack Completions in Vertical Wells. Paper SPE 178973 presented at the SPE International Conference and Exhibition on Formation Damage Control, Lafayette, LA, 24-26 February.
- Kosmidis, V., Perkins, J., & Pistikopoulos, E. (2004, March). Optimization of Well Oil Rate Allocations in Petroleum Fields. *Ind. Eng. Chem*, 43(14), 3513–3527.
- Kron, G. (1963). *Diakoptiks: The Piecewise Solution of Large-Scale Systems*. London, UK: Macdonald Publishing.
- Kurimov, D., Lim, K.-T., & Urazmukhambetov, B. (2017). Application and Challenges of Coupled Model with Complex Surface Network Connected to Multiple Reservoirs. Paper SPE 189023 presented at the SPE Annual Caspian Technical Conference and Exhibition, Baku, Azerbaijan, 1-3 November.
- Lee, A., Gonzalez, M., & Eakin, B. (August 1966). The Viscosity of Natural Gases. *JPT*, 997-1000.
- Lee, J. (1982). *Well Testing*. SPE Publications.
- Lee, J., & Wattanbarger, R. (1996). *Gas Reservoir Engineering*. Soc. of Petroleum Engineers.
- Liang, J., & Rubin, B. (2014). A Semi-Implicit Approach for Integrated Reservoir and Surface-Network Simulation. Paper SPE 163615 presented at the SPE Reservoir Simulation Symposium, The Woodlands, TX, 18-20 February.

- Litvak, M., & Darlow, B. (1995). Surface Network and Well Tubinghead Pressure Constraints in Compositional Simulation. Paper SPE 29125 presented at the SPE Symposium on Reservoir Simulation, San Antonio, TX, 12-15 February.
- Malhotra, S., & Sharma, M. (2014, January). Experimental Measurement of Settling Velocity of Spherical Particles in Unconfined and Confined Surfactant-Based Shear Thinning Viscoelastic Fluids. *Journal of Visualized Experiments.*, 11(83).
- Martin, D., & Peters, G. (1963). The Application of Newton's Method to Network Analysis by Digital Computers. *Journal of the Institution of Water Engineers and Scientists*, 17(06), 115-129.
- Martinez-Romero, N., Osorio-Peralta, O., & Santamaria-Vite, I. (2002). Natural Gas Network Optimization and Sensitivity Analysis. Paper SPE 74384 presented at the SPE International Petroleum Conference and Exhibition, Villahermosa, Mexico, 10-12 February.
- Milton-Taylor, D. (1992). Factors Affecting the Stability of Proppant in Propped Fractures. Paper SPE 24821 presented at the at the SPE Annual Technical Conference & Exhibition, Washington, D.C., 4-7 October.
- Mucharam, L., & Adewumi, M. (1990). A Compositional Two-Phase Flow Model for Analyzing and Designing Complex Pipeline Network Systems. *Society of Petroleum Engineers.*, 90 (18), 1-16.
- Mucharam, L., & Adewumi, M. (1990). A Compositional Two-Phase Flow Model for Analyzing and Designing Complex Pipeline Network Systems. Paper SPE 21562 presented at the International Technical Meeting of CIM and the Society of Petroleum Engineers, Calgary, Canada, 10-13 June.
- Muller, U., & Riemann, J. (1991). Redistribution of Two-Phase Flow in Branching Conduits: A Survey. *1st International Conference on Multiphase Flows*. Tsukuba, Japan.
- Myers, R., & Montgomery, D. (1995). *Response Surface Methodology: Process and Product Optimization Using Designed Experiments*. New York, NY: John Wiley & Sons Inc.

- Nagoo, A. (2013). *Pipe Fractional Flow Theory - Principles and Applications*. PhD Dissertation, The University of Texas at Austin.
- Nguyen, P., Stegent, N., & Ingram, S. (2006). Remediation of Production Loss Due to Proppant Flowback in Existing Wellbores. Paper SPE 102629 presented at the SPE Annual Technical Conference and Exhibition, San Antonio, TX, 24-27 September.
- Nishikiori, N., Redner, R., Doty, D., & Schmidt, Z. (1989). An Improved Method for Gas Lift Allocation Optimization. Paper SPE 19711 presented at the Annual Technical Conference and Exhibition, San Antonio, TX, October 8-11.
- Niven, R., Waldrip, S., Abel, M., & Schlegel, M. (2015). Maximum Entropy Analysis of Flow Networks with Nonlinear Constraints. Presented at the International Electronic Conference on Entropy and Its Applications. .
- Nocedal, J., & Wright, S. (2006). *Numerical Optimization*. Ithaca, NY: Springer Series in Operations Research.
- Nouri, A., Vaziri, H., Belhaj, H., & Islam, R. (2004). Sand-Production Prediction: A New Set of Criteria for Modeling Based on Large-Scale Transient Experiments and Numerical Investigation. Paper SPE 90273 presented at the 2004 SPE Annual Technical Conference and Exhibition, Houston, TX, September 26-29.
- Ong, S., Atlas, B., Ramos, R., & Zheng, Z. (2000). Sand Production Prediction in High Rate, Perforated and Open-hole Gas Wells. Paper SPE 58721 presented at the 2000 SPE International Symposium on Formation Damage Control, Lafayette, LA, 23-24 February.
- Patterson, J., & Coats, K. (1971). An Efficient Model for Evaluating Gas Field Gathering System Design. *Journal of Petroleum Technology*, 1067-1073.
- Pratinko, H., Rushing, J., & Blasingame, T. (2003). Decline Curve Analysis using Type Curves - Fractured Wells. Paper SPE 84287 presented at the SPE Annual Technical Conference and Exhibition, Denver, CO, 5-8 October.

- Robinson, B., Holditch, S., & Whitehead, W. (1998, June). Minimizing Damage to a Propped Fracure by Controlled Flowback Procedures. *Journal of Petroleum Technology*, 40(06), 753-759.
- Ros, J. (1960). An Analysis of Critical Simultaneous Gas-Liquid Flow Through a Restriction and Its Application to flow Metering. *Applied Science Research*, 1(03), 374-377.
- Saba, N., & Lahey, R. (1994). The Analysis of Phase Separation Phenomena in Branching Conduits. *International Journal of Multiphase Flow*, 10(1), 1-20.
- Samier, P. (2010). Comparisons of Various Algorithms for Gas-Lift Optimization in a Coupled Surface Network and Reservoir Simulator. Paper SPE 130912 presented at the SPE EUROPEC/EAGE Annual Technical Conference and Exhibition, Barcelona, Spain, 14-17 June.
- Schlumberger. (2005). *PIPESIM Suite, User Guide*.
- Shiralkar, G., & Watts, J. (2005). An Efficient Formulation for Simultaneous Solution of the Surface Network Equations. Paper SPE 93073 presented at the SPE Reservoir Symposium, Houston, TX, 31 January - 2 February.
- Shor, R., & Sharma, M. (2014). Reducing Proppant Flowback From Fractures: Factors Affecting the Maximum Flowback Rate. Paper SPE 168649 presented at the Hydraulic Fracturing Technology Conference, The Woodlands, TX, 4-6 February.
- Simmons, W. (1972). Optimizing Continuous Flow Gas Lift Wells. *Petroleum Engineer*, 45(08), 46-48.
- Singiresu, S. (2009). *Engineering Optimization*. Hoboken, NJ: Wiley.
- Standing, M. (1981). Volumetric and Phase Behavior of Oil Field Hydrocarbon Systems. *Dallas: Society of Petroleum Engineers*, 125-126.
- Stepanchuk, A. (2018). Application of Integrated Reservoir to Surface Network Coupling of Giant Oil Field, Kazakhstan. Paper SPE 192537 presented at the SPE Annual Caspian Technical Conference and Exhibition, Astana, Kazakhstan, 31 October -2 November.

- Stewart, J. (2015). *Pipe Fractional Flow through Branching Conduits*. MS Thesis. The University of Texas at Austin.
- Stoitsits, R., Crawford, K., MacAllister, D., & McCormack, M. (1999). Production Optimization at the Kuparak River. Paper SPE 52177 presented at the SPE Mid-Continent Operations Symposium, Oklahoma City, OK, 28-31 March.
- Stoner, A. M. (n.d.). Sensitivity Analysis Applied to a Steady-State Model of Natural Gas Transportation Systems. Paper SPE 3056 presented at the 45th Annual Fall Meeting, Houston, TX, 4-7 October.
- Stoner, A. M. (1968). *Analysis and Control of Steady of Unsteady Flows in Natural Gas Piping Systems*. PhD Dissertation, University of Michigan.
- Tiffin, D., Stein, M., & Wang, X. (2003). Drawdown Guidelines for Sand Control Completions. Paper SPE 84495 presented at the 2003 SPE Annual Technical Conference and Exhibition, Denver, CO, October 5-8.
- Tingas, J., & Liou, J. (1998). Integrated Reservoir and Subsurface Network Simulation in Reservoir Management of Southern North Sea Gas Reservoirs. Paper SPE 50635 presented at the SPE European Conference, The Hague, The Netherlands, 20-22 October.
- Trick, M. (1998). A Different Approach to Coupling a Reservoir Simulator with a Surface Facilities Model. Paper SPE 4001 presented at the SPE Gas Technology Symposium, Calgary, Alberta, Canada, 15-18 March.
- Tronvoll, J., Papamichos, E., Skjaerstein, A., & Sanfilippo, F. (1997). Sand Production in Ultra-Weak Sandstones: Is Sand Control Absolutely Necessary? Paper SPE 39042 presented at the Latin American and Caribbean Petroleum Engineering Conference, Rio de Janeiro, Brazil, 30 August - 3 September.
- Van Batenburg, D. (1999). Towards Proppant Back-Production Prediction. Paper SPE 54730 presented at the SPE European Formation Damage Conference, Hague, The Netherlands, 31 May - 1 June.
- Vasquez, M., & Beggs, D. (1980, June). Correlations for Fluid Physical Properties Prediction. *JPT*, 32(06), 968-970.

- Vaziri, H., Allam, R., Kidd, G., Bennett, C., Grose, T., Robison, P., & Malyn, J. (2004). Sanding: A Rigorous Examination of the Interplay Between Drawdown, Depletion, Start-up Frequency and Water Cut. Paper SPE 89795 presented at the SPE Annual Technical Conference and Exhibition, Houston, TX, 26-29 September.
- Vaziri, H., Barree, B., Xiao, Y., Palmer, I., & Kutas, M. (2002). What is the Magic of Water in Producing Sand? Paper SPE 77683 presented at the SPE Annual Technical Conference and Exhibition, San Antonio, TX, 29 September-2 October.
- Vaziri, H., Xiao, Y., & Palmer, I. (2002). Assessment of several sand prediction models with particular reference to HPHT wells. Paper SPE 78235 presented at the SPE/ISRM Rock Mechanics Conference, Irving, TX, 20-23 October.
- Waldrip, H., Niven, S., & Abel, R. (2016). Maximum Entropy Analysis of Hydraulic Pipe Flow Networks. *Journal of Hydraulic Engineering*, 142(09), 142-154.
- Walton, I. (2000). Optimum Underbalance for the Removal of Perforation Damage. Paper SPE 63108 presented at the SPE Annual Conference and Exhibition in Dallas, TX, 1- 4 October.
- Wang, P., Litvak, M., & Aziz, K. (2002). Optimization of Production Operations in Petroleum Fields. Paper SPE 77658 presented at the SPE Annual Technical Conference and Exhibition, San Antonio, TX, 29 September - 2 October.
- Wang, Q., & Fleming, G. (2017). An Improved Slack Variable Method to Determine Active Constraints in Large Surface Networks. Paper SPE 182640 presented at the SPE Reservoir Simulation Conference, Montgomery, TX, 20-22 February.
- Wang, Q., & Graham, F. (2013). A New Approach to Improve Linear Solver Performance for a Fully Implicit Coupled System of Reservoir and Surface Network . Paper SPE 163670 presented at the SPE Reservoir Simulation Symposium, The Woodlands, TX, 18-20 February.
- Weingarten, J., & Perkins, T. (1995). Prediction of Sand Production in Gas Wells: Methods and Gulf of Mexico Case Studies. *JPT*, 47(07), 596-600.

- Willberg, D., Steinsberger, N., Hoover, R., Card, R., & Queen, J. (1998). Optimization of Fracture Cleanup Using Flowback Analysis. Paper SPE 39920 presented at the Rocky Mountain Regional/Low Permeability Reservoirs Symposium and Exhibition, Denver, CO, 5-8 April.
- Wilson, K. (2015). Analysis of Drawdown Sensitivity in Shale Reservoirs Using Coupled-Geomechanics Models. Paper SPE 175029 presented at the Annual Technical Conference and Exhibition, Houston , TX, 28-30 September.
- Wilson, K. (2016). Geomechanical Modeling of Flowback Scenarios to Establish Best Practices in the Midland Basin Horizontal Program. Paper URTEC 2448089 presented at the Unconventional Resources Technology Conference held in San Antonio, TX, USA 1-3 August.
- Wong, G., Fair, P., Bland, K., & Sherwood, R. (2003). Balancing Act: Gulf of Mexico Sand Control Completions, Peak Rate Versus Risk of Sand Control Failure. Paper SPE 84497 presented at the 2003 SPE Annual Technical Conference and Exhibition, Denver, CO, October 5-8.
- Wood, D., & Charles, C. (1972). Hydraulic Network Analysis Using Linear Theory. *Journal of the Hydraulics Division*, 98(07), 1157-1170.